Insights into RNase P RNA structure and function by a retro-evolution approach

Dissertation

zur

Erlangung des Doktorgrades

der Naturwissenschaften

(Dr. rer. nat.)

dem Fachbereich

Pharmazeutische Chemie

der Philipps-Universität Marburg

vorgelegt von

Dan Li

aus Guizhou, China

Marburg/Lahn 2009

Vom Fachbereich Pharmazeutische Chemie
der Philipps-Universität Marburg als Dissertation am_____angenommen.

Erstgutachter: Prof. Dr. Roland K. Hartmann
Zweitgutachter: Prof. Dr. Albrecht Bindereif

Tag der mündlichen Prüfung am:_____

Table of Contents

1 Introduction

1.1 RNase P

Ribonuclease P (RNase P) is an endonuclease responsible for the specific removal of 5'-leader sequences from precursor transfer RNAs (ptRNA) in all organisms and organelles analyzed so far (Robertson *et al.* 1972; Schön 1999; Kazantsev and Pace 2006; Hartmann *et al.* 2009). The only known exception is *Nanoarchaeum equitans* in which tRNA gene promoters allow the synthesis of leaderless tRNAs (Randau *et al.* 2008). RNase P also cleaves other substrates, such as some viral RNAs (Mans *et al.* 1990; Hartmann *et al.* 1995), SRP (4.5S) RNA (Peck-Miller and Altman 1991), the precursor of tmRNA (Komine *et al.* 1994), a few mRNAs (Alifano *et al.* 1994; Li and Altman 2003) and some riboswitches (Altman *et al.* 2005). In addition, the enzyme has been reported to be a transcription factor (Reiner *et al.* 2006).

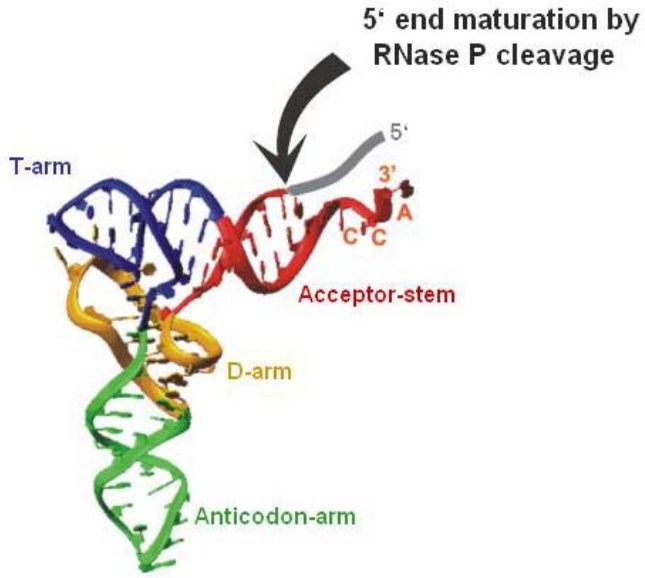

Fig. 1.1: The tertiary structure of ptRNA. The site of cleavage by RNase P is marked by the black arrow. The cleaved 5'-flank is depicted in grey, the acceptor-stem in red, the T-arm in blue, the D-arm in yellow and the anticodon-arm in green.

In ptRNA processing, RNase P typically recognizes the T-arm and acceptor-stem of ptRNA (Kirsebom and Vioque 1996), catalyses the hydrolysis of the phosphodiester between the last nucleotide of the 5'-flank and the first nucleotide of the acceptor-stem of ptRNA (Fig. 1.1), and produces 3'-hydroxyl and 5'-phosphate ends on the resultant RNA fragments. During the process, divalent metal ions, preferably Mg^{2+}, are required for specific folding of the RNA and its catalytic mechanism (Pan 1995). The catalysis reaction is thought to follow an S_N2-

like nucleophilic substitution mechanism (Smith and Pace 1993; Beebe and Fierke 1994; Persson *et al.* 2003; Cassano *et al.* 2004).

RNase P is usually composed of a single highly structured RNA subunit plus a variable number of protein subunits that increases from bacteria (one protein) over archaea (at least four proteins) to eukarya (nine to ten proteins) (Hartmann and Hartmann 2003). The RNA subunit (P RNA) and the protein subunits (P proteins) are both indispensable *in vivo* for cell viability. Some chloroplast and mitochondrial RNase P enzymes were proposed to be protein enzymes (Wang *et al.* 1988; Thomas *et al.* 1995; Salavati *et al.* 2001), and human mitochondrial RNase P without RNA was recently confirmed by biochemical experiments (Holzmann *et al.* 2008).

1.2 The RNA subunit of RNase P

In 1983, Sidney Altman's research group reported that the RNA moiety of bacterial RNase P was catalytically active in the absence of its protein cofactor (Guerrier-Takada *et al.* 1983), and because of this, S. Altman won the Nobel Prize in chemistry together with Thomas R. Cech in 1989 for their "discovery of catalytic properties of RNA". More recently, archaeal and eukaryal P RNAs were also found capable of mediating ptRNA cleavage without protein cofactors (Pannucci *et al.* 1999; Kikovska *et al.* 2007). Yet, only bacterial P RNA alone is substantially active without the protein, whereas archaeal and eukaryal P RNAs are more dependent on the contribution of their protein moieties and display only residual activity when these are absent.

1.2.1 Bacterial RNase P RNA

The RNA subunit of RNase P from bacteria, encoded by the *rnpB* gene, is typically 350-400 nucleotides long (Brown and Pace 1992). *In vitro*, high activity in the absence of its small protein subunit requires increased ionic strength (Guerrier-Takada *et al.* 1983).

Bacterial P RNAs can be divided into two structural classes (Fig. 1.2.1 a): type A, the ancestral type found in most bacteria, represented by *Escherichia coli* P RNA, and type B, present in the low GC content gram-positive bacteria, the prototype being *Bacillus subtilis* P RNA (Haas *et al.* 1996). An intermediate structure type C is found in green non-sulphur bacteria (Haas and Brown 1998).

Bacterial P RNA consists of two independently folding domains (Fig. 1.2.1 a), the specificity domain (S-domain) and the catalytic domain (C-domain) (Loria and Pan 1996). The S-domain is involved in substrate binding by contacting the T-arm of ptRNA, as demonstrated by

biochemical experiments (Pan 1995; Loria and Pan 1998) and photocrosslinking studies (Nolan *et al.* 1993; Chen *et al.* 1998). The C-domain includes most of the nucleotides conserved in P RNA. This domain, as its name suggests, is the part of the molecule that comprises the catalytic core. It recognizes ptRNA through interactions with the substrate's acceptor-stem and the CCA in the ptRNA's 3' flank, and contains all crucial structural elements for catalysis, including the protein subunit binding interface and catalytically important metal ion binding sites. The holoenzyme reconstituted from the C-domain of *E. coli* P RNA and the *E. coli* RNase P protein can cleave ptRNA *in vitro* (Green *et al.* 1996; Li *et al.* 2007).

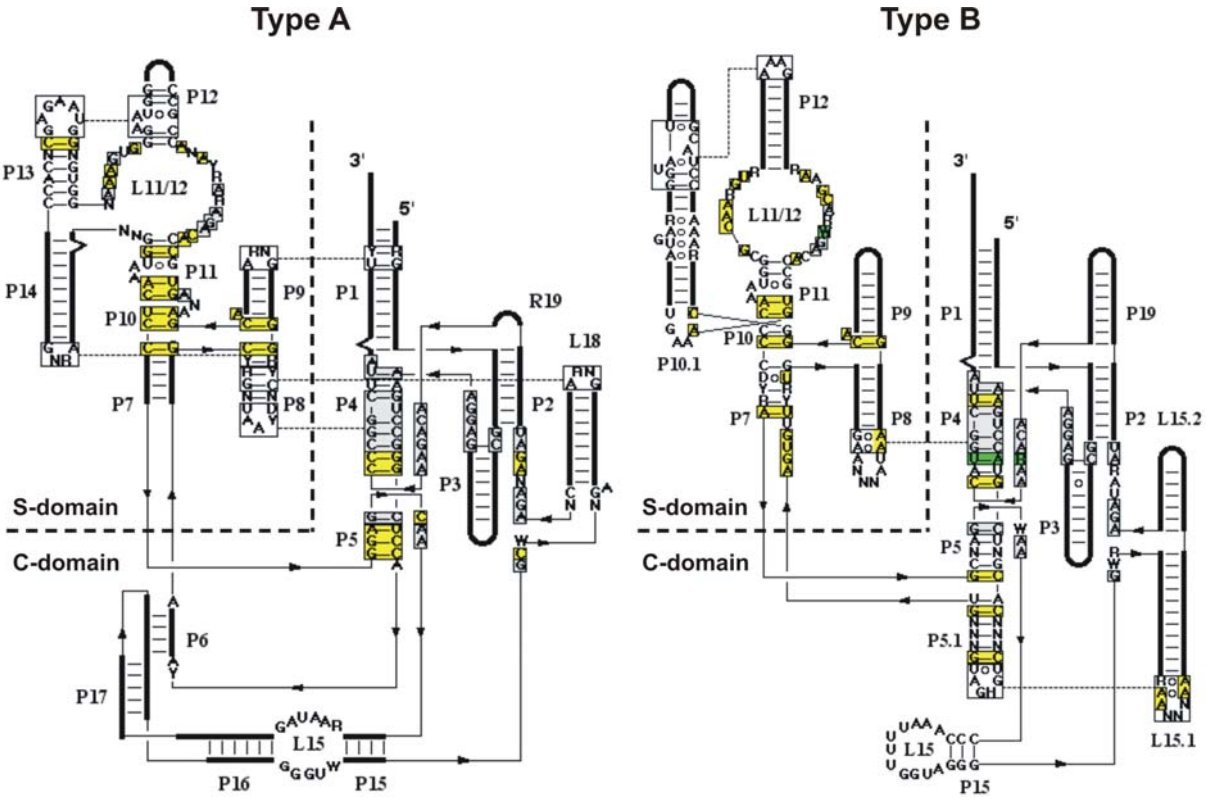

Fig. 1.2.1 a: The secondary structures and sequence consensus of bacterial RNase P RNAs (type A and B). In the scheme of the type A consensus (left), conserved nucleotides of type A RNase P RNAs are coloured in grey, semi-conserved nucleotides are in yellow. In the scheme of the type B consensus (right), nucleotides conserved in both type A and B RNase P RNAs are highlighted in grey, nucleotides solely conserved in type B are in yellow, those solely conserved in type A are in green. N: any nucleotide; R: A or G; Y: U or C; H: A, C or U; L: loop, P: helix.(Massire 1999)

Within the bacterial type A P RNA subunit (Fig. 1.2.1 a, left), the S-domain comprises helices P7-P14, and the C-domain is constituted of helices P1-P6 and P15-P18. Covariation analyses predicted three major long range interdomain interactions, between P1 and L9, P4 and L8, as

well as between P8 and L18, and two loop-helix interactions within the S-domain, between P8 and L14 and between P12 and L13 (Massire *et al.* 1998). As for the bacterial type B P RNA (Fig. 1.2.1 a, right), helices P7-P12 plus P10.1 construct the S-domain, and helices P1-P5, P5.1, P15, P15.1, P15.2 as well as P19 compose the C-domain. There is one major long range interdomain interaction between P4 and L8, and two intradomain interactions: P10.1/L12 in the S-domain and L15.1/L5.1 in the C-domain (Massire *et al.* 1998). The long range interdomain interactions bring the S- and C-domains together to form a functional architecture. The loop-helix intradomain interactions contribute substantially to domain stabilization. Although there are some significant differences in peripheral structural elements between type A and B, the two different types of P RNAs fold into globally similar three-dimensional structures (Massire *et al.* 1998; Kazantsev *et al.* 2005; Torres-Larios *et al.* 2005).

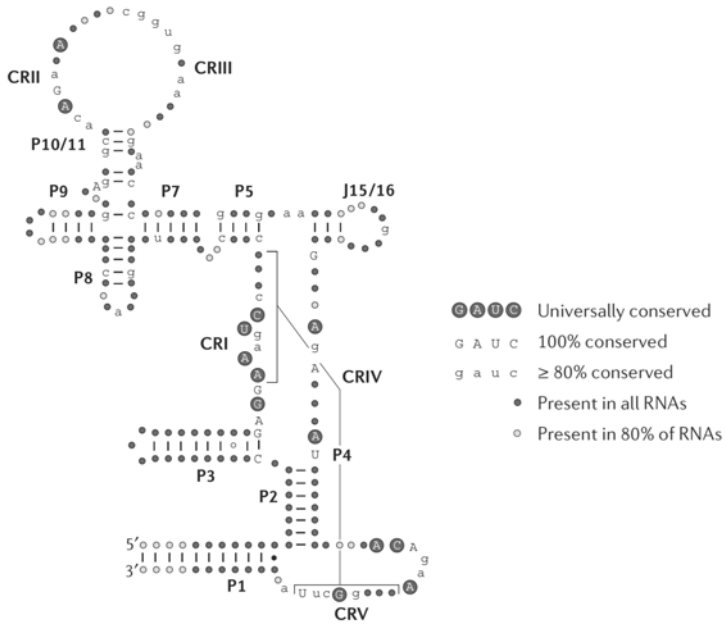

Fig. 1.2.1 b: Phylogenetic minimum-consensus bacterial RNase P RNA secondary structure. (Kazantsev and Pace 2006)

The overall consensus of bacterial P RNAs was revealed by comparative sequence analysis (Chen and Pace 1997; Massire 1999). Accordingly, the focus of conserved nucleotides lies in five regions, named as conserved region CRI-V (Fig. 1.2.1 b). These conserved regions are supposed to be closely associated with the enzyme's function.

The recently solved X-ray crystal structures improved our view of the tertiary structure of bacterial RNase P RNA: Two S-domain crystal structures were solved, of type A *Thermus thermophilus* P RNA (Krasilnikov *et al.* 2004) and type B *B. subtilis* P RNA (Krasilnikov *et al.* 2003), as well as two full-length crystal structures (Fig. 1.2.1 c) from type A *Thermotoga maritima* P RNA (Torres-Larios *et al.* 2005) and type B *Bacillus stearothermophilus* P RNA

(Kazantsev *et al.* 2005). Although the overall *T. maritima* structure is resolved at the relatively low resolution of 3.85 Å, and not the entire molecule (298 of the 417 nucleotides) of *B. stearothermophilus* P RNA is resolved, these structures have largely confirmed and further refined earlier three-dimensional models of P RNA (Massire *et al.* 1998).

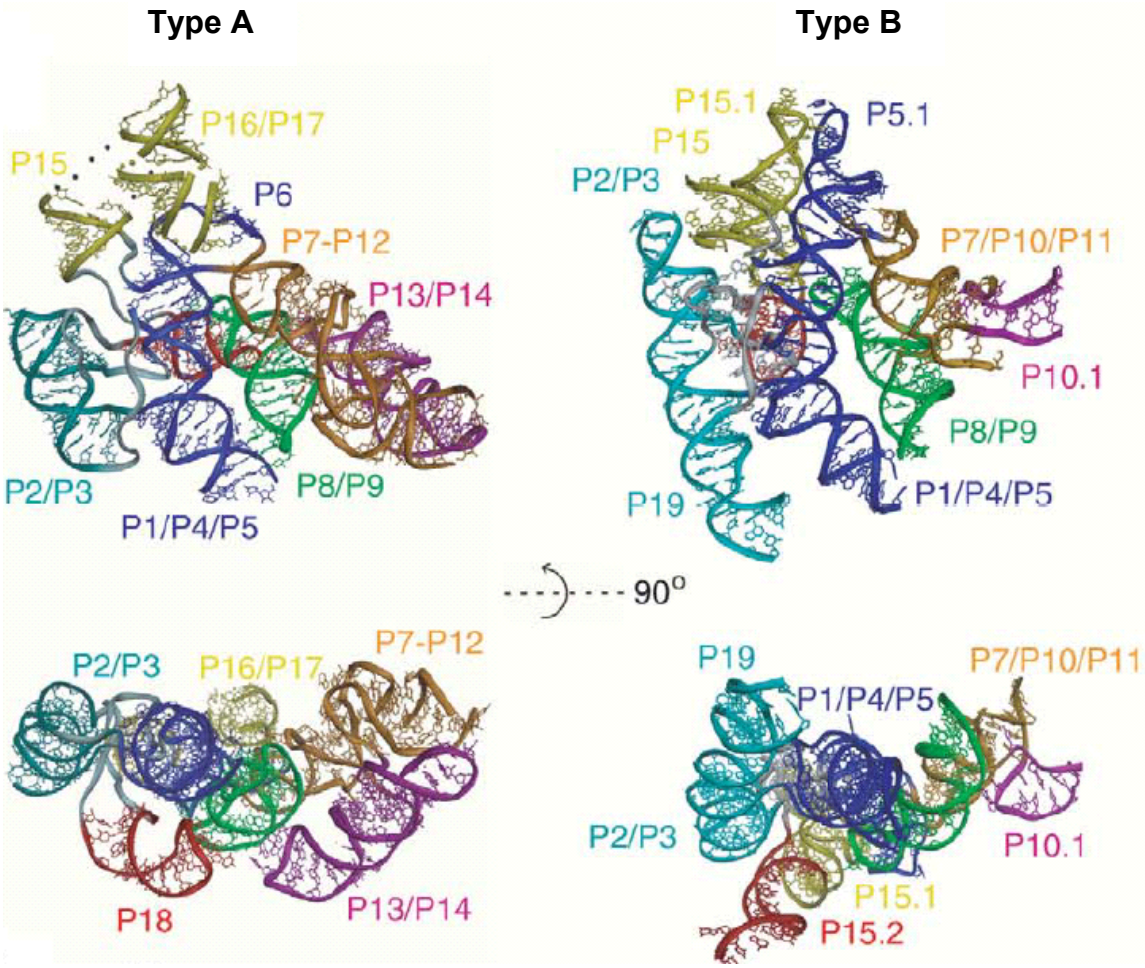

Fig. 1.2.1 c: The crystal structures of full-length bacterial type A (PDB code 2a2e) and type B (PDB code 2a64) RNase P RNAs in two orthogonal views (Kazantsev *et al.* 2005; Torres-Larios *et al.* 2005).

Comparision of the crystal structures of two S-domains revealed a conserved ptRNA binding interface (helices P9-11 and the joining regions J11/12-J12/11) (Krasilnikov *et al.* 2004).

The crystal structures of complete RNA subunits show that the entire RNA is generally a remarkably flat architecture formed by helical domains connected by long range tertiary interactions. The five universally conserved regions CRI-V are positioned on one face of the molecule and form two conserved modules in both types (Torres-Larios *et al.* 2006).

Type A RNA is built up of two layers of stacked helices. The larger layer contains the helices P1-P12, P15-P17, the junctions J5/15, J11/12-J12/11 and the loop L15 region. This layer thus contains most of the universally conserved regions, including the putative ptRNA binding

interface and the catalytic core. The second layer comprises helices P13, P14 and P18. Within this overall architecture, the S-domain structure is essentially identical to that crystallized without the associated C-domain (Krasilnikov *et al.* 2004), which illustrates its structural stability as an independent folding domain. The C-domain comprises several coaxially arranged helices: one helical stack is formed by P1/P4/P5, another by P2/P3. P18 protrudes almost perpendicularly from the two afore mentioned two helical stacks, linking P2/P3 to the P15/P17 stems and folding back onto the large layer by means of the P8/L18 interaction. Three interdomain interactions between helix and loop, P1/L9, P4/L8 and P8/L18, bridge S- and C-domain and orient them relative to each other, which is consistent with comparative analysis and biochemical data (Brown *et al.* 1996; Massire *et al.* 1997; Massire *et al.* 1998; Marszalkowski *et al.* 2008).

Type B RNA shares a common structural core with type A. This core structure comprises the coaxial stacks P1/P4/P5, P2/P3, P8/P9 and P15, and J11/12-J12/11 module (Torres-Larios *et al.* 2006). P19 coaxially stacks with P2/P3; P15.2 sticks out from the flat main structure. Further, the crystal structure confirms the two previously proposed long-range interactions between L15.1 and L5.1 and between P4 and L8.

However, the X-ray crystal structures do not provide specific information on how the ptRNA substrate and protein might interact with the RNA.

1.2.2 Archaeal RNase P RNA

Archaeal RNase P RNAs can be classified into two types (Fig. 1.2.2 a): type A and type M (Harris *et al.* 2001).

Type A is the major structural class among archaeal P RNAs, and is strikingly similar to bacterial type A P RNA. In general, archaeal type A P RNAs are distinguished from those of bacteria primarily by the loss of helices P13/P14 and P18. Since the P8/L18 interdomain contact is lacking, the archaeal P RNA may strongly depend on the P1/L9 contact for interdomain orientation of its type A architecture. Interestingly, a common motif of archaeal P1 elements is an A:A or C:A mismatch at identical position in both types of P RNA. These mismatched nucleotides have been proposed to interact with the third G residue of a conserved 5'-GAGA L9 tetraloop. A few archaeal type A RNAs are weakly catalytically active in the absence of protein under high salt conditions (Pannucci *et al.* 1999).

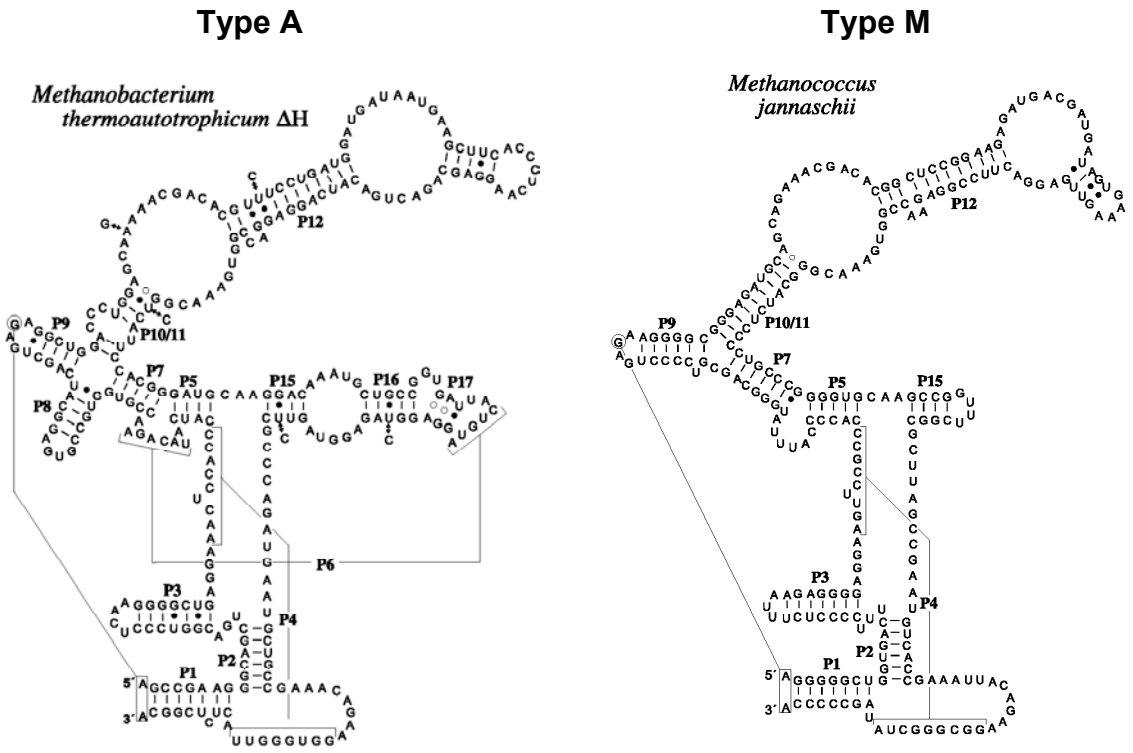

Fig. 1.2.2 a: Secondary structures of archaeal type A (*Methanobacterium thermoautotrophicum* ΔH) and type M (*Methanococcus jannaschii*) RNase P RNAs (Harris *et al.*, 2001). Note that according to more recent data, the P1 helices are 5 base pairs longer (Li *et al* 2009).

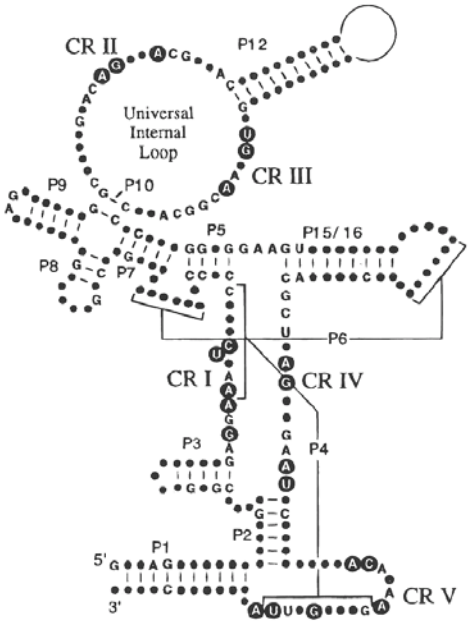

Fig. 1.2.2 b: Phylogenetic minimum-consensus archaeal RNase P RNA secondary structures (Chen and Pace 1997). Invariant nucleotides are indicated by letter (G, A, U, or C). Invariant nucleotides universally conserved in all three phylogenetic domains are highlighted by black background. Nucleotides universally present but varying in identity appear as black dots.

Type M RNAs have so far been found merely in *Methanococcus* and *Archaeoglobus fulgidus*. Compared with type A, they further miss the catalytically critical elements P8 and P16/P17, and they were reported to be catalytically inactive without protein (Pannucci *et al.* 1999). Nevertheless, recently a substrate-tethered archaeal type M P RNA, ptRNA-*M. jannaschi* P RNA, was shown to perform self-cleavage (Pulukkunat and Gopalan 2008).

As in bacteria, the five conserved regions CRI-V (Fig. 1.2.2 b) are preserved in archaeal P RNAs of type A and M (Chen and Pace 1997).

1.2.3 Eukaryal RNase P RNA

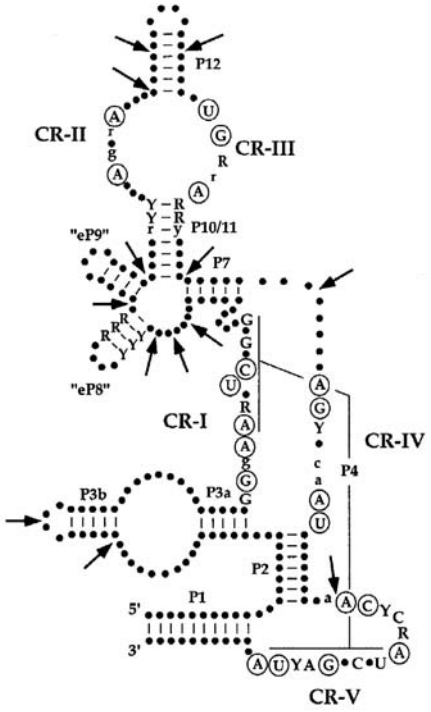

Fig. 1.2.3 a: Phylogenetic minimum-consensus secondary structures of eukaryal RNase P RNA (Frank *et al.* 2000). The nucleotides universally conserved in all three phylogenetic domains are circled. Invariant nucleotides within eukarya are shown in upper case, 90% conserved in lower case (R: purine, Y: pyrimidine). The nucleotides universally present but varying in identity appear as black dots. Arrows represent sites where variable helices are inserted in selected species.

A eukaryotic P RNA is typically around two-thirds the sequence length of a bacterial one. Phylogenetic comparative analysis of eukaryal P RNAs reveals that despite low sequence conservation among the eukaryal RNAs, the RNA subunits also contain the five conserved regions CRI-V (Fig. 1.2.3 a) found in bacterial and archaeal P RNAs (Frank *et al.* 2000).

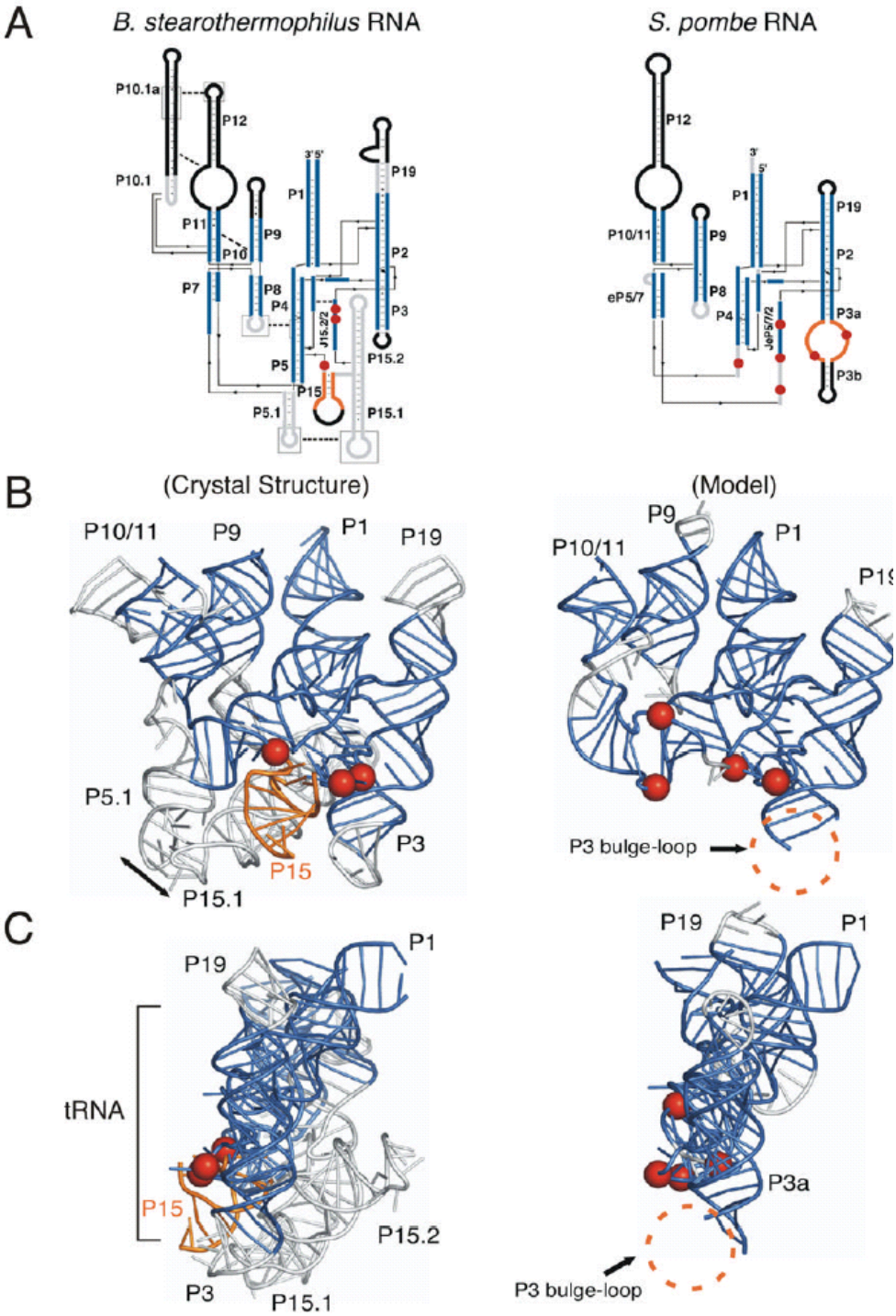

Fig. 1.2.3 b: Commonalities in structure and function between the crystal structure of bacterial RNase P RNA and modelled eukaryal RNase P RNA (Marquez *et al*. 2006). Homologous structures are in blue. Sites of 5' tRNA crosslinking are represented as red spheres. The main sites of 3' tRNA crosslinking are indicated in gold.

In contrast to bacterial P RNAs (Fig. 1.2.3 b), the eukaryal homologues have a large bulge loop in P3, and often a larger P12 like some archaeal P RNAs, further they lack a few structural elements, P5, P6, and P15-18, thought to be critical for both substrate binding and catalysis. Crosslinking experiments indicate that eukaryal P RNAs fold into a functional

structure and specifically bind tRNA even in the absence of protein subunits (Marquez *et al.* 2006). A tertiary structure model of eukaryal P RNA was created on the basis of crosslinking results and crystal structures of bacterial P RNAs (Marquez *et al*. 2006). It suggests that the eukaryal P RNA contains a core structure similar to that of bacterial P RNA, but lacks some structural elements that contribute to catalysis and global stability of tertiary structure.

For a long time, eukaryal RNase P was considered to be inactive without its protein subunits. Recently however, RNase P RNAs from human and the lower eukaryote *Giardia lamblia* were found to have residual catalytic activity *in vitro* when analyzed on a substrate ^{32}P-labeled with very high specific activity and at pH 6.0 to reduce metal ion-induced RNA fragmentation (Kikovska *et al.* 2007). The concept that the catalytic core of RNase P resides in the RNA subunit thus also holds for the eukaryal enzyme, in line with the nucleotide conservation in the parts of the molecule considered to build the catalytic core.

1.3 The RNase P protein subunit

The protein component is not directly involved in the cleavage mechanism, but both RNA and protein subunits of RNase P are essential under physiological salt concentrations and *in vivo* (Kole *et al.* 1980; Guerrier-Takada *et al.* 1983; Reich *et al.* 1988; Kurz *et al.* 1998) except for those few cases where no RNase P exists or where the enzyme is a protein enzyme without RNA component.

1.3.1 The bacterial RNase P protein

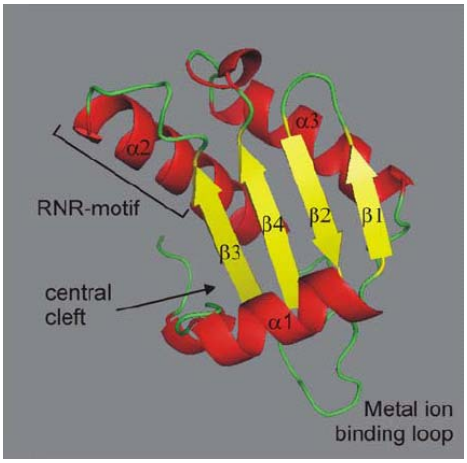

Fig. 1.3.1: 3D structure of the *B. subtilis* RNase P protein. The α-helices (red) and the β-sheet (yellow) are numbered sequentially from the N- to the C- terminus. The RNR-motif, the metal ion binding loop and the central cleft formed by helix α1 and the β-sheet were proposed as RNA-binding sites (Stams *et al.* 1998; Niranjanakumari *et al.* 2007).

Bacterial RNase P holoenzymes contain only a single small basic P protein subunit (ca. 13 kDa, encoded by the *rnpA* gene), which contributes about 10% to the molecular mass of the holoenzyme. The structures of bacterial P protein subunits from *Bacillus subtilis* (Stams *et al.* 1998), *Staphylococcus aureus* (Spitzfaden *et al.* 2000) and *Thermotoga maritima* (Kazantsev *et al.* 2003) have been determined by X-ray crystallography or NMR. All protein structures display extremely similar 3D shapes although they share only 20-30% identical amino acids. Accordingly, it has been proved that Type A and B P protein subunits are interchangeable *in vitro* (Guerrier-Takada *et al.* 1983) and also *in vivo* (Wegscheid *et al.* 2006; Gössringer and Hartmann 2007).

The protein has two conserved RNA-binding sites (Fig. 1.3.1): an unusual left-handed βαβ crossover connection and a large central cleft. Additionally, a third potential RNA-binding site is comprised in the metal binding loop. The Arg-Asn-Arg (RNR) motif within the βαβ crossover is universally conserved in bacterial P proteins. The topology of the unusual βαβ crossover was also found in the RNA-binding regions of ribosomal protein S5 and ribosomal elongation factor G (Stams *et al.* 1998).

The roles of the bacterial P protein are not fully understood, but are generally proposed to be (1) stabilization of the catalytically active conformation of P RNA (Kim *et al.* 1997), (2) preferential binding of ptRNA versus tRNA through interactions with the 5' flank of ptRNA (Kurz *et al.* 1998; Stams *et al.* 1998; Rueda *et al.* 2005), (3) increasing the affinity of functionally important metal ions (Kurz and Fierke 2002), and (4) possibly mediation of holoenzyme dimerization (Fang *et al.* 2001). The bacterial protein also relaxes the substrate specificity of the enzyme (Liu and Altman 1994), thus explaining the *in vivo* activity on non-tRNA substrates. In addition, a role in offsetting differences in ptRNA structures was reported (Sun *et al.* 2006).

1.3.2 The archaeal and eukaryal RNase P proteins

Unlike bacterial RNase P, archaeal and eukaryal RNase P enzymes contain multiple protein subunits, making up about 50% of the molecular mass of the enzyme in archaea (at least 4 protein subunits) (Hall and Brown 2002; Hartmann and Hartmann 2003), and at least 70% in eukarya (9-10 protein subunits) (Jarrous 2002; Xiao *et al.* 2002). Eukarya have homologues to all four protein subunits (Pop4, Rpp1, Pop5 and Rpr2; see Fig. 1.3.2 a) present in the majority of archaea. Pop4 is the only RNase P protein subunit identifiable in all eukarya and archaea with available genome sequences. There is no evidence for an evolutionary relation of the bacterial P protein to any of the archaeal and eukaryotic RNase P proteins. Non-bacterial

RNase P proteins failed to replace the *B. subtilis* P protein *in vivo* (Gössringer and Hartmann 2007), supporting the notion that archaeal/eukaryal P proteins indeed are evolutionary unrelated to the bacterial P protein.

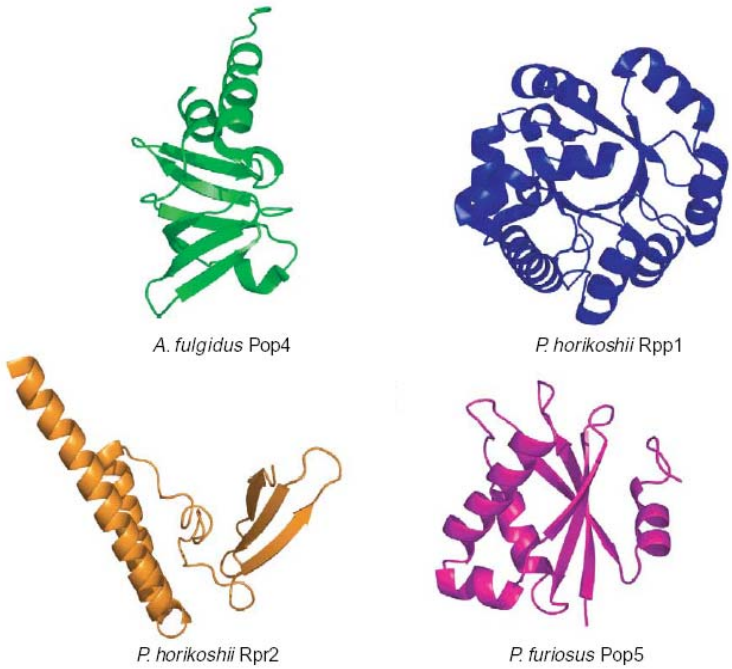

Fig. 1.3.2 a: 3D structures of four archaeal RNase P proteins: Pop4 (the homologue of Rpp29, PDB code: 1ts9), Rpp1 (the homologue of Rpp30, PDB code: 1v77), Rpr2 (the homologue of Rpp21, PDB code: 1x0t) and Pop5 (PDB code: 2av5).

Considering the decreased functionality of their RNase P RNAs, as inferred from the reduced catalytic activity of the RNAs alone, the protein moieties of archaeal and eukaryal RNase P appear to make a larger contribution to the enzyme's function than the bacterial P protein. The specific functions of archaeal and eukaryal P proteins are not clearly known. Besides the roles proposed for the bacterial P protein (1.3.1), evidence has been provided for roles in intracellular localization (Jarrous *et al.* 1999), precursor P RNA processing (Holzmann *et al.* 2008), active site architecture (True and Celander 1998), as well as substrate binding (Jarrous *et al.* 2001; Pulukkunat and Gopalan 2008).

Much effort has been put into the study of protein-protein interaction and active enzyme reconstitution. Either of the two protein pairs, Rpp21 (Rpr2)/Rpp29 (Pop4) and Pop5/Rpp30 (Rpp1), is sufficient to reconstitute functional enzymes with archaeal *Pyrococcus furiosus* P RNA (Pulukkunat and Gopalan 2008). Together with the human P RNA subunit, the human homologues Rpp21 and Rpp29 were shown to form an RNase P enzyme with substantial activity (Mann *et al.* 2003). These two protein subunits were proposed to play a crucial role in the stabilization of an active conformation of P RNA. The crystal structure of a Rpp21/29

heterodimer from *Pyrococcus horikoshii* (Fig. 1.3.1.2 b) has been recently determined (Honda *et al.* 2008). It shows a positively charged cluster on its upper face, suggesting a possible RNA-binding surface.

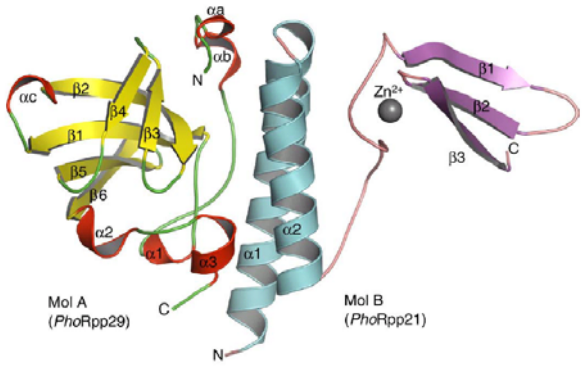

Fig. 1.3.2 b: Crystal structure of the *Pho*Rpp21-*Pho*Rpp29 heterodimeric complex. (Honda *et al.* 2008)

However, so far it has not been possible to obtain a coherent map of proteins contact on the RNA, and the data of interaction between the many eukaryotic proteins are still not fully conclusive.

1.4 Holoenzyme models of bacterial RNase P

P RNA, P protein and ptRNA, the three components of the bacterial RNase P system, have been crystallographically solved individually, but no high-resolution structures of a holoenzyme or a substrate-bound complex have been solved to date. Nevertheless, on the basis of chemical experiments and individual crystal structures, several bacterial models have been built for *E. coli* (type A) (Westhof and Altman 1994; Tsai *et al.* 2003), *B. stearothermophilus* (type B) (Buck *et al.* 2005), and *B. subtilis* (type B) (Tsai *et al.* 2003; Niranjanakumari *et al.* 2007) RNase P. In these models, the overall topology of the P RNA is either identical or similar to the X-ray structures.

In the ternary complex model of *E. coli* RNase P (type A, Fig. 1.4 a), the P protein is accommodated in a cavity formed by P3, P4, P5 and P15 of *E. coli* P RNA. The 3' terminus of the ptRNA substrate base pairs with the loop L15 of the P RNA; the T stem-loop of the ptRNA contacts the paired regions P9 and P11. The 5' leader of ptRNA locates to the cleft of the P protein. The two highly conserved residues A248 and A249 lie in the shallow groove of the acceptor stem, close to the cleavage site. More recent data from in-gel phosphorothioate-iodine structure probing (Buck *et al.* 2005) showed that the residues of *E. coli* P RNA protected by the P protein are located within P2, P3, P4, J3/4 and J2/18 (marked by the grey broken circle in Fig. 1.4 a). This suggests that not only P3, but also P2 of *E. coli* P RNA is

involved in P protein binding, which is in line with data from our mutational analyses (Li *et al.* 2009).

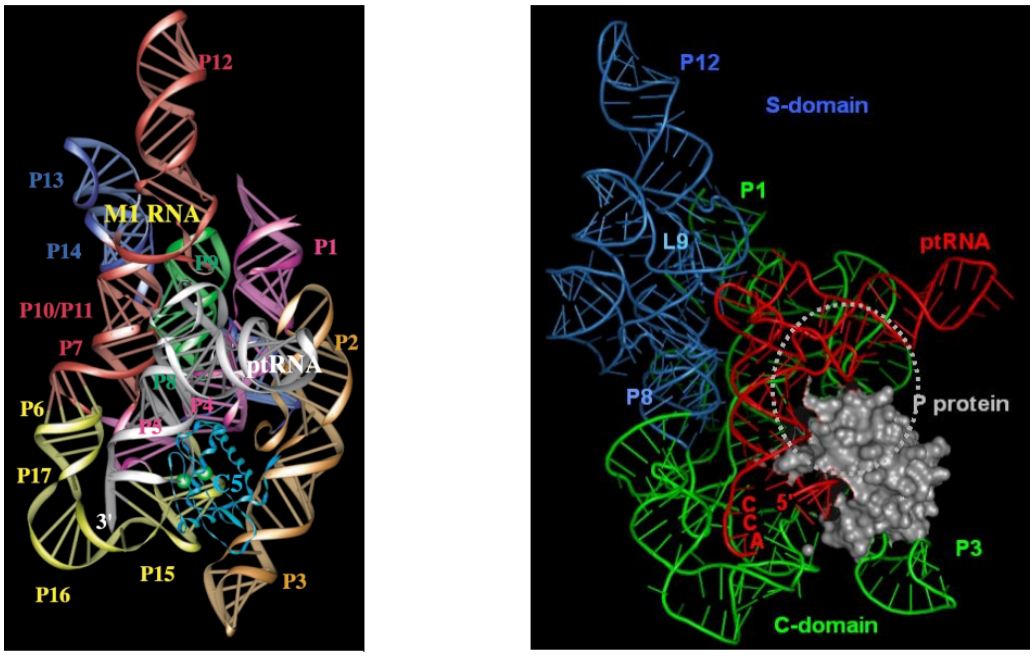

Fig. 1.4 a: *E. coli* RNase P ternary complex model. In the view on the left, the *E. coli* P protein and the ptRNA substrate are depicted in cyan and silver, respectively (Tsai *et al.* 2003). On the right, another view of the same model (downloaded from (http://www-ibmc.u-strasbg.fr/upr9002/westhof/) was coloured to depict the S-domain (blue) and the C-domain (green), with the P protein in grey, and the ptRNA substrate in red. The P protein binding area predicted by in-gel phosphorothioate-iodine structure probing (Buck *et al.* 2005) is marked with the grey broken circle.

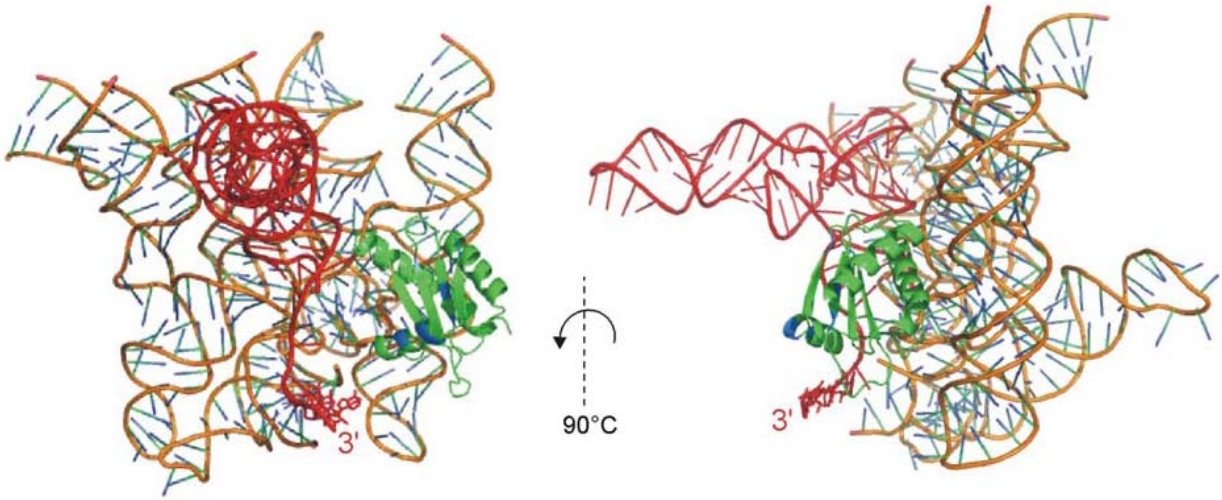

Fig. 1.4 b: *B. stearothermophilus* RNase P ternary complex model in two orthogonal views. The RNase P RNA is represented in gold, the P protein in green, and the tRNA substrate in red. (Buck *et al.* 2005)

The ternary complex model of *B. stearothermophilus* RNase P (type B, Fig. 1.4 b), which takes into account in-gel probing data (Buck *et al.* 2005), places the P protein in the P2-3

region and at the periphery of P4. The protein is adjacent to the active site and influences the conformation of the RNA near the tRNA-binding site. The T-stem of the tRNA lies in the S-domain ptRNA binding interface, the 5'-end of the tRNA lies close to the P4/P5 region and to the protein, and the acceptor-stem sits on the flat groove formed by the concave C-domain.

1.5 RNase P: an ideal natural model to study the transition from the RNA world to the protein world

For several decades, catalysis within cellular compartments was thought to be mediated exclusively by protein enzymes. Only in 1983, this concept was shattered by the discovery of catalytic activity of RNase P RNA (Guerrier-Takada *et al.* 1983). Soon after, the term "RNA world" was coined (Gilbert 1986; North 1987): The RNA world hypothesis proposes that RNA, equipped with the capacity to store information, like DNA, as well as being able to act as an enzyme, might have been the class of molecule at the basis of the very beginning of life. Accordingly, only during later evolution this early RNA world gradually changed into the protein world of today. Several pieces of evidence have been found in the last twenty years to support the hypothesis, such as the discovery of other ribozymes and the observation that also in the ribosome the catalytically active part is RNA. Ultimately, the RNA world hypothesis results in a further fundamental question regarding the evolution of life: how, during the subsequent stages of evolution, did proteins take over the job of RNA?

When dealing with this question, RNase P is of special interest because this enzyme might be regarded as a molecular fossil of the RNA world, for several reasons: (1) It is the only known RNA enzyme naturally devoted to act *in trans*, aside from the ribosome which, however, is more a macromolecular machine rather than a classical enzyme. (2) RNase P exists throughout all three kingdoms of life, where it consists of a single RNA subunit and a varying number of protein subunits (Fig. 1.4). Regarding the RNA subunit, phylogenetic-comparative analysis showed the five conserved regions CRI-V of P RNAs to be universally preserved throughout all three kingdoms of life (Chen and Pace 1997; Frank *et al.* 2000), and all extant P RNAs contain the P4 region in their structural core, including a pattern of conserved base identities (Hartmann and Hartmann 2003). This indicates that all RNase P RNAs stem from a common ancestor. Regarding the protein subunits, most eukarya have homologues to all four protein subunits (Pop4, Rpp1, Pop5 and Rpr2) present in the majority of archaea, and there is no structural homology between bacterial and archaeal/eukaryal RNase P proteins. The simplest interpretation is that RNase P has an "RNA-alone" origin, and that progenitors of bacteria and archaea diverged very early in evolution to then pursue completely different

strategies in the recruitment of protein subunits during the transition period from the "RNA-alone" to the "RNA-Protein" state of the enzyme. (3) Kinetics assays *in vitro* indicate that bacterial P RNA alone is highly active at elevated metal ion concentrations, while archaeal/eukaryal P RNAs show only residual catalytic activity and are more dependent on their protein moieties for efficient catalytic function, with archaeal P RNA alone being more active than eukaryal P RNA. The gain in protein content of RNase P enzymes thus is paralleled by a loss of function on the side of the RNA subunit.

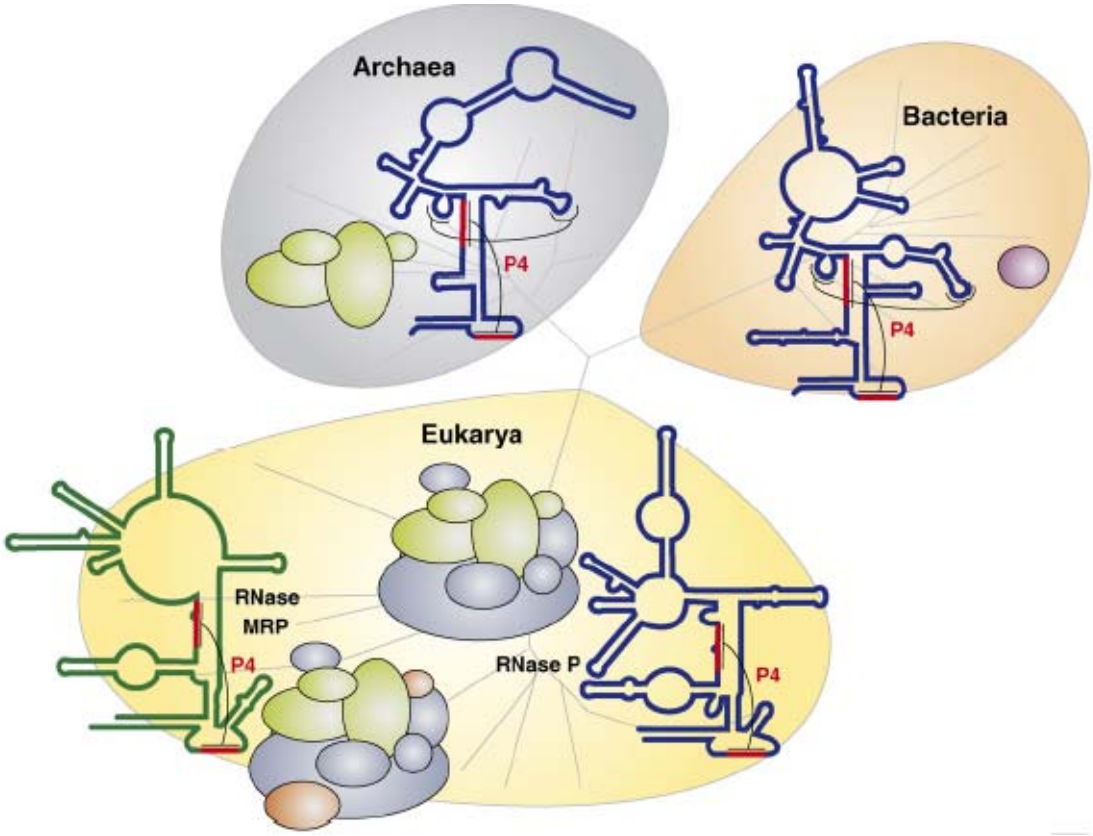

Fig. 1.5: RNase P holoenzymes from Bacteria, Archaea and Eukarya. The RNA subunits are shown as blue lines. The single protein subunit from bacteria is indicated by a purple oval. Archaeal proteins are shown in green and eukaryal ones in green (homologs of archaeal P proteins) and gray. All RNAs share conserved nucleotides in helix P4 (indicated in red). In Eukarya there is a sibling of RNase P, RNase MRP (dark green), which is involved in processing of precursor rRNAs and shares the majority of its protein subunits with eukaryal RNase P. In addition, the core of its RNA subunit is structurally related to eukaryal P RNA (Willkomm and Hartmann 2007).

The diversity of RNase P in the different life domains of lifes thus may be considered to reflect different stages of molecular evolution, which makes this RNA enzyme an ideal natural model to study the transition from the RNA world to the protein world. Detailed and comprehensive study of RNase P from not only bacteria but also archaea and eukarya therefore is of key importance to reveal some of the enigma of the evolution of life.

1.6 References

Alifano, P., Rivellini, F., Piscitelli, C., Arraiano, C.M., Bruni, C.B., and Carlomagno, M.S. 1994. Ribonuclease E provides substrates for ribonuclease P-dependent processing of a polycistronic mRNA. *Gene Dev.* **8:** 3021-3031.

Altman, S., Wesolowski, D., Guerrier-Takada, C., and Li, Y. 2005. RNase P cleaves transient structures in some riboswitches. *Proc. Nat. Acad. Sci. U.S.A.* **102:** 11284-11289.

Beebe, J.A. and Fierke, C.A. 1994. A kinetic mechanism for cleavage of precursor tRNA(Asp) catalyzed by the RNA component of *Bacillus subtilis* ribonuclease P. *Biochemistry-US* **33:** 10294-10304.

Brown, J.W., Nolan, J.M., Haas, E.S., Rubio, M.A., Major, F., and Pace, N.R. 1996. Comparative analysis of ribonuclease P RNA using gene sequences from natural microbial populations reveals tertiary structural elements. *Proc. Nat. Acad. Sci. U.S.A.* **93:** 3001-3006.

Brown, J.W. and Pace, N.R. 1992. Ribonuclease P RNA and protein subunits from bacteria. *Nucleic Acids Res.* **20:** 1451-1456.

Buck, A.H., Kazantsev, A.V., Dalby, A.B., and Pace, N.R. 2005. Structural perspective on the activation of RNAse P RNA by protein. *Nat. Struct. Mol. Biol.* **12:** 958-964.

Cassano, A.G., Anderson, V.E., and Harris, M.E. 2004. Analysis of solvent nucleophile isotope effects: evidence for concerted mechanisms and nucleophilic activation by metal coordination in nonenzymatic and ribozyme-catalyzed phosphodiester hydrolysis. *Biochemistry-US* **43:** 10547-10559.

Chen, J.L. and Pace, N.R. 1997. Identification of the universally conserved core of ribonuclease P RNA. *RNA* **3:** 557-560.

Kurz, J.C. and Fierke C.A. 2002. The affinity of magnesium binding sites in the *Bacillus subtilis* RNase P x pre-tRNA complex is enhanced by the protein subunit. *Biochemistry-US* **41:**9545-9558.

Fang, X.W., Yang, X.J., Littrell, K., Niranjanakumari, S., Thiyagarajan, P., Fierke, C.A., Sosnick, T.R., and Pan, T. 2001. The *Bacillus subtilis* RNase P holoenzyme contains two RNase P RNA and two RNase P protein subunits. *RNA* **7:** 233-241.

Frank, D.N., Adamidi, C., Ehringer, M.A., Pitulle, C., and Pace, N.R. 2000. Phylogenetic-comparative analysis of the eukaryal ribonuclease P RNA. *RNA* **6:** 1895-1904.

Gilbert, W. 1986. Origin of life - the RNA world. *Nature* **319:** 618-618.

Gössringer, M. and Hartmann, R.K. 2007. Function of heterologous and truncated RNase P proteins in Bacillus subtilis. *Mol. Microbiol.* **66:** 801-813.

Green, C.J., Rivera-Leon, R., and Vold, B.S. 1996. The catalytic core of RNase P. *Nucleic Acids Res.* **24:** 1497-1503.

Guerrier-Takada, C., Gardiner, K., Marsh, T., Pace, N., and Altman, S. 1983. The RNA moiety of ribonuclease P is the catalytic subunit of the enzyme. *Cell* **35:** 849-857.

Haas, E.S., Banta, A.B., Harris, J.K., Pace, N.R., and Brown, J.W. 1996. Structure and evolution of ribonuclease P RNA in Gram-positive bacteria. *Nucleic Acids Res.* **24:** 4775-4782.

Haas, E.S. and Brown, J.W. 1998. Evolutionary variation in bacterial RNase P RNAs. *Nucleic Acids Res.* **26:** 4093-4099.

Harris, J.K., Haas, E.S., Williams, D., Frank, D.N., and Brown, J.W. 2001. New insight into RNase P RNA structure from comparative analysis of the archaeal RNA. *RNA* **7:** 220-232.

Hartmann, E. and Hartmann, R.K. 2003. The enigma of ribonuclease P evolution. *Trends Genet.* **19:** 561-569.

Hartmann, R.K., Gössringer, M., Späth, B., Fischer, S., and Marchfelder, A. 2009. Chapter 8 The Making of tRNAs and more - RNase P and tRNase Z. *Prog. Nucleic Acid Res. Mol. Biol.* **85C:** 319-368.

Hartmann, R.K., Heinrich, J., Schlegl, J., and Schuster, H. 1995. Precursor of C4 antisense RNA of bacteriophages P1 and P7 is a substrate for RNase P of *Escherichia coli*. *Proc. Nat. Acad. Sci. U.S.A.* **92:** 5822-5826.

Holzmann, J., Frank, P., Loffler, E., Bennett, K.L., Gerner, C., and Rossmanith, W. 2008. RNase P without RNA: identification and functional reconstitution of the human mitochondrial tRNA processing enzyme. *Cell* **135:** 462-474.

Honda, T., Kakuta, Y., Kimura, K., Saho, J., and Kimura, M. 2008. Structure of an archaeal homolog of the human protein complex Rpp21-Rpp29 that is a key core component for the assembly of active ribonuclease P. *J. Mol. Biol.* **384:** 652-662.

Jarrous, N. 2002. Human ribonuclease P: Subunits, function, and intranuclear localization. *RNA* **8:** 1-7.

Jarrous, N., Wolenski, J.S., Wesolowski, D., Lee, C., and Altman, S. 1999. Localization in the nucleolus and coiled bodies of protein subunits of the ribonucleoprotein ribonuclease P. *J. Cell Biol.* **146:** 559-571.

Kazantsev, A.V., Krivenko, A.A., Harrington, D.J., Carter, R.J., Holbrook, S.R., Adams, P.D., and Pace, N.R. 2003. High-resolution structure of RNase P protein from Thermotoga maritima. *Proc. Nat. Acad. Sci. U.S.A.* **100:** 7497-7502.

Kazantsev, A.V., Krivenko, A.A., Harrington, D.J., Holbrook, S.R., Adams, P.D., and Pace, N.R. 2005. Crystal structure of a bacterial ribonuclease P RNA. *Proc. Nat. Acad. Sci. U.S.A.* **102:** 13392-13397.

Kazantsev, A.V. and Pace, N.R. 2006. Bacterial RNase P: a new view of an ancient enzyme. *Nat. Rev. Microbiol.* **4:** 729-740.

Kikovska, E., Svard, S.G., and Kirsebom, L.A. 2007. Eukaryotic RNase P RNA mediates cleavage in the absence of protein. *Proc. Nat. Acad. Sci. U.S.A.* **104:** 2062-2067.

Kim, J.J., Kilani, A.F., Zhan, X.Y., Altman, S., and Liu, F.Y. 1997. The protein cofactor allows the sequence of an RNase P ribozyme to diversify by maintaining the catalytically active structure of the enzyme. *RNA* **3:** 613-623.

Kirsebom, L.A. and Vioque, A. 1996. RNase P from bacteria. Substrate recognition and function of the protein subunit. *Mol. Biol. Rep.* **22:** 99-109.

Kole, R., Baer, M.F., Stark, B.C., and Altman, S. 1980. E. coli RNAase P has a required RNA component. *Cell* **19:** 881-887.

Komine, Y., Kitabatake, M., Yokogawa, T., Nishikawa, K., and Inokuchi, H. 1994. A tRNA-like structure is present in 10Sa RNA, a small stable RNA from *Escherichia coli*. *Proc. Nat. Acad. Sci. U.S.A.* **91:** 9223-9227.

Krasilnikov, A.S., Xiao, Y., Pan, T., and Mondragon, A. 2004. Basis for structural diversity in homologous RNAs. *Science* **306:** 104-107.

Krasilnikov, A.S., Yang, X., Pan, T., and Mondragon, A. 2003. Crystal structure of the specificity domain of ribonuclease P. *Nature* **421:** 760-764.

Kurz, J.C., Niranjanakumari, S., and Fierke, C.A. 1998. Protein component of *Bacillus subtilis* RNase P specifically enhances the affinity for precursor-tRNAAsp. *Biochemistry-US* **37:** 2393-2400.

Li, D., Willkomm, D.K., and Hartmann, R.K. 2009. Minor changes largely restore catalytic activity of archaeal RNase P RNA from Methanothermobacter thermoautotrophicus. *Nucleic Acids Res.* **37:** 231-242.

Li, D., Willkomm, D.K., Schon, A., and Hartmann, R.K. 2007. RNase P of the Cyanophora paradoxa cyanelle: a plastid ribozyme. *Biochimie* **89:** 1528-1538.

Li, Y. and Altman, S. 2003. A specific endoribonuclease, RNase P, affects gene expression of polycistronic operon mRNAs. *Proc. Nat. Acad. Sci. U.S.A.* **100:** 13213-13218.

Liu, F.Y. and Altman, S. 1994. Differential evolution of substrates for an RNA enzyme in the presence and absence of its protein cofactor. *Cell* **77:** 1093-1100.

Loria, A. and Pan, T. 1996. Domain structure of the ribozyme from eubacterial ribonuclease P. *RNA* **2:** 551-563.

-. 1998. Recognition of the 5' leader and the acceptor stem of a pre-tRNA substrate by the ribozyme from *Bacillus subtilis* RNase P. *Biochemistry-US* **37:** 10126-10133.

Mann, H., Ben-Asouli, Y., Schein, A., Moussa, S., and Jarrous, N. 2003. Eukaryotic RNase P: role of RNA and protein subunits of a primordial catalytic ribonucleoprotein in RNA-based catalysis. *Mol. Cell* **12:** 925-935.

Mans, R.M., Guerrier-Takada, C., Altman, S., and Pleij, C.W. 1990. Interaction of RNase P from *Escherichia coli* with pseudoknotted structures in viral RNAs. *Nucleic Acids Res.* **18:** 3479-3487.

Marquez, S.M., Chen, J.L., Evans, D., and Pace, N.R. 2006. Structure and function of eukaryotic ribonuclease P RNA. *Mol. Cell* **24:** 445-456.

Marszalkowski, M., Willkomm, D.K., and Hartmann, R.K. 2008. Structural basis of a ribozyme's thermostability: P1-L9 interdomain interaction in RNase P RNA. *RNA* **14:** 127-133.

Massire, C. 1999. Ph. D. thesis. In *Institut de Biologie Moléculaire et Cellulaire du CNRS*, Strasbourg.

Massire, C., Jaeger, L., and Westhof, E. 1997. Phylogenetic evidence for a new tertiary interaction in bacterial RNase P RNAs. *RNA* **3:** 553-556.

-. 1998. Derivation of the three-dimensional architecture of bacterial ribonuclease P RNAs from comparative sequence analysis. *J. Mol. Biol.* **279:** 773-793.

Niranjanakumari, S., Day-Storms, J.J., Ahmed, M., Hsieh, J., Zahler, N.H., Venters, R.A., and Fierke, C.A. 2007. Probing the architecture of the B. subtilis RNase P holoenzyme active site by cross-linking and affinity cleavage. *RNA* **13:** 521-535.

North, G. 1987. Back to the RNA World and Beyond. *Nature* **328:** 18-19.

Pan, T. 1995. Higher order folding and domain analysis of the ribozyme from *Bacillus subtilis* ribonuclease P. *Biochemistry-US* **34:** 902-909.

Pannucci, J.A., Haas, E.S., Hall, T.A., Harris, J.K., and Brown, J.W. 1999. RNase P RNAs from some Archaea are catalytically active. *Proc. Nat. Acad. Sci. U.S.A.* **96:** 7803-7808.

Peck-Miller, K.A. and Altman, S. 1991. Kinetics of the processing of the precursor to 4.5 S RNA, a naturally occurring substrate for RNase P from *Escherichia coli*. *J. Mol. Biol.* **221:** 1-5.

Persson, T., Cuzic, S., and Hartmann, R.K. 2003. Catalysis by RNase P RNA: unique features and unprecedented active site plasticity. *J. Biol. Chem.* **278:** 43394-43401.

Pulukkunat, D.K. and Gopalan, V. 2008. Studies on Methanocaldococcus jannaschii RNase P reveal insights into the roles of RNA and protein cofactors in RNase P catalysis. *Nucleic Acids Res.* **36:** 4172-4180.

Randau, L., Schroder, I., and Soll, D. 2008. Life without RNase P. *Nature* **453:** 120-123.

Reich, C., Olsen, G.J., Pace, B., and Pace, N.R. 1988. Role of the protein moiety of ribonuclease P, a ribonucleoprotein enzyme. *Science* **239:** 178-181.

Reiner, R., Ben-Asouli, Y., Krilovetzky, I., and Jarrous, N. 2006. A role for the catalytic ribonucleoprotein RNase P in RNA polymerase III transcription. *Gene Dev.* **20:** 1621-1635.

Robertson, H.D., Altman, S., and Smith, J.D. 1972. Purification and properties of a specific *Escherichia coli* ribonuclease which cleaves a tyrosine transfer ribonucleic acid presursor. *J. Biol. Chem.* **247:** 5243-5251.

Rueda, D., Hsieh, J., Day-Storms, J.J., Fierke, C.A., and Walter, N.G. 2005. The 5 ' leader of precursor tRNA(Asp) bound to the *Bacillus subtilis* RNase P holoenzyme has an extended conformation. *Biochemistry-US* **44:** 16130-16139.

Salavati, R., Panigrahi, A.K., and Stuart, K.D. 2001. Mitochondrial ribonuclease P activity of *Trypanosoma brucei*. *Mol. Biochem. Parasit.* **115:** 109-117.

Schön, A. 1999. Ribonuclease P: the diversity of a ubiquitous RNA processing enzyme. *FEMS Microbiol. Rev.* **23:** 391-406.

Smith, D. and Pace, N.R. 1993. Multiple magnesium ions in the ribonuclease P reaction mechanism. *Biochemistry-US* **32:** 5273-5281.

Spitzfaden, C., Nicholson, N., Jones, J.J., Guth, S., Lehr, R., Prescott, C.D., Hegg, L.A., and Eggleston, D.S. 2000. The structure of ribonuclease P protein from Staphylococcus aureus reveals a unique binding site for single-stranded RNA. *J. Mol. Biol.* **295:** 105-115.

Stams, T., Niranjanakumari, S., Fierke, C.A., and Christianson, D.W. 1998. Ribonuclease P protein structure: evolutionary origins in the translational apparatus. *Science* **280:** 752-755.

Sun, L., Campbell, F.E., Zahler, N.H., and Harris, M.E. 2006. Evidence that substrate-specific effects of C5 protein lead to uniformity in binding and catalysis by RNase P. *EMBO J.* **25:** 3998-4007.

Thomas, B.C., Gao, L., Stomp, D., Li, X., and Gegenheimer, P.A. 1995. Spinach chloroplast RNase P: a putative protein enzyme. *Nucleic Acids Symp. Ser.***:** 95-98.

Torres-Larios, A., Swinger, K.K., Krasilnikov, A.S., Pan, T., and Mondragon, A. 2005. Crystal structure of the RNA component of bacterial ribonuclease P. *Nature* **437:** 584-587.

Torres-Larios, A., Swinger, K.K., Pan, T., and Mondragon, A. 2006. Structure of ribonuclease P--a universal ribozyme. *Curr. Opin. Struct. Biol.* **16:** 327-335.

True, H.L. and Celander, D.W. 1998. Protein components contribute to active site architecture for eukaryotic ribonuclease P. *J. Biol. Chem.* **273:** 7193-7196.

Tsai, H.Y., Masquida, B., Biswas, R., Westhof, E., and Gopalan, V. 2003. Molecular modeling of the three-dimensional structure of the bacterial RNase P holoenzyme. *J. Mol. Biol.* **325:** 661-675.

Wang, M.Y., Chien, L.F., and Pan, R.L. 1988. Radiation inactivation analysis of chloroplast CF0-CF1 ATPase. *J. Biol. Chem.* **263:** 8838-8843.

Wegscheid, B., Condon, C., and Hartmann, R.K. 2006. Type A and B RNase P RNAs are interchangeable *in vivo* despite substantial biophysical differences. *EMBO Rep.* **7:** 411-417.

Westhof, E. and Altman, S. 1994. 3-Dimensional working model of M1 RNA, the catalytic RNA subunit of ribonuclease-P from Escherichia-Coli. *Proc. Nat. Acad. Sci. U.S.A.* **91:** 5133-5137.

Willkomm, D.K. and Hartmann, R.K. 2007. An important piece of the RNase P jigsaw solved. *Trends Biochem Sci* **32:** 247-250.

Xiao, S.H., Scott, F., Fierke, C.A., and Engelke, D.R. 2002. Eukaryotic ribonuclease P: A plurality of ribonucleoprotein enzymes. *Annu. Rev. Biochem.* **71:** 165-189.

2 Goal of the Project

RNase P catalyzes tRNA 5'-end maturation in all organisms and organelles. The enzyme is composed of a single RNA subunit plus a varying number of proteins that increases from bacteria (one protein) over archaea (at least four proteins) to eukarya (nine to ten proteins) (Hartmann and Hartmann 2003). Conserved base identities indicate that the RNase P RNA subunits (P RNAs) from all three kingdoms of life stem from a common ancestor. Yet, only in bacteria the P RNA alone is substantially active *in vitro* without the protein, whereas archaeal and eukaryal P RNAs are more dependent on the contribution of their protein moieties and display only residual activity when these are absent. RNase P thus represents a natural model system to study the transition from a ribozyme to a ribonucleoprotein enzyme, generally accepted to have occurred during natural evolution of the RNA world to the protein world.

To get a deeper understanding of the principles of ribozyme evolution and of the structural requirements of P ribozyme function, attempts have been made to "retro-evolve" non-bacterial P RNAs to bacterial-like P RNA ribozymes. The previous efforts, however, were not successful (Harris *et al.* 2001; Wagner *et al.* 2001). In this project, we pursued a rational design approach where we changed domains, subdomains, modules and nucleotides within non-bacterial P RNAs into the bacterial P RNA consensus. The chimeras were tested *in vitro* for ptRNA processing activity in RNA-alone and holoenzyme reactions and *in vivo* for complementation of a bacterial P RNA knockdown strain. The variants showing improved catalytic activities were then further characterized by a series of other biochemical and biophysical assays along with the native RNase P ribozyme from *E. coli*. A detailed comparative analysis of the structural differences occurring in the transition from the inactive to the "reactivated" state offers the potential to understand the structural basis for P ribozyme function, which has been the major objective of the thesis project. The non-bacterial P RNAs studied were an organellar P RNA from *Cyanophora paradoxa*, an archaeal one from *Methanothermobacter thermoautotrophicus*, and a eukaryal one from *Homo sapiens*. The first one contains essentially all structural elements of bacterial P RNAs, but has been reported to be inactive (Baum *et al.* 1996). The others display only residual RNA-alone activity at very high salt concentration (Pannucci *et al.* 1999; Kikovska *et al.* 2007).

This study was intended to help answering the following questions:

(1) Can we retro-evolve ribozyme activity?

(2) Which structural changes are required to convert a non-bacterial P RNA to a bacterial-like P RNA ribozyme?

(3) What are the requirements for specific P RNA ribozyme function in terms of conformational flexibility and stability?

(4) Which structural elements of archaeal/eukaryal P RNA primarily determine the loss of the RNA's catalytic capacity, and which exert their effect on holoenzyme function via impaired interaction with the bacterial P protein?

(5) Are the P RNA ribozymes selected *in vitro* functional *in vivo*, as inferred from their ability to complement bacterial mutant strains in which *rnpB* gene expression is suppressed?

References

Baum, M., Cordier, A., and Schön, A. 1996. RNase P from a photosynthetic organelle contains an RNA homologous to the cyanobacterial counterpart. *J. Mol. Biol.* **257:** 43-52.

Harris, J.K., Haas, E.S., Williams, D., Frank, D.N., and Brown, J.W. 2001. New insight into RNase P RNA structure from comparative analysis of the archaeal RNA. *RNA* **7:** 220-232.

Hartmann, E. and Hartmann, R.K. 2003. The enigma of ribonuclease P evolution. *Trends Genet.* **19:** 561-569.

Kikovska, E., Svard, S.G., and Kirsebom, L.A. 2007. Eukaryotic RNase P RNA mediates cleavage in the absence of protein. *Proc. Nat. Acad. Sci. U.S.A.* **104:** 2062-2067.

Pannucci, J.A., Haas, E.S., Hall, T.A., Harris, J.K., and Brown, J.W. 1999. RNase P RNAs from some Archaea are catalytically active. *Proc. Nat. Acad. Sci. U.S.A.* **96:** 7803-7808.

Wagner, M., Fingerhut, C., Gross, H.J., and Schön, A. 2001. The first phytoplasma RNase P RNA provides new insights into the sequence requirements of this ribozyme. *Nucleic Acids Res.* **29:** 2661-2665.

3 Methods

3.1 General nucleic acids techniques

3.1.1 Isolation of plasmid DNA from bacteria

Plasmid DNA was generally prepared from bacterial cultures supplemented with antibiotics as selective agent. Isolation was normally done with commercial kits in small scale (miniprep; µg yields), medium scale (midiprep) and large scale (maxiprep; mg yields): NucleoSpin® plasmid miniprep and maxiprep kit (MACHEREY-NAGEL), QIAGEN® Plasmid Midi kit (QIAGEN) and GeneJET™ plasmid Miniprep Kit (Fermentas).

3.1.1.1 Growth of bacterial cultures

For cell growth in liquid media, an appropriate volume of LB (Luria Bertani) medium was inoculated with a single colony freshly developed on an agar plate. Usually, 3 ml of bacterial culture was used for a plasmid miniprep, 100 ml for a midiprep and 100-500 ml for a maxiprep. If not stated otherwise, the cultures were grown in the presence of 100 µg/ml ampicillin for 6-16 h at 37°C while shaking at 180-250 rpm. As a rule, all glassware and solutions were previously autoclaved or sterile filtrated; the work bench was previously cleaned with 70% ethanol; all glassware is fire flamed when transferring cells. Antibiotics were added just before inoculation.

1 liter LB (Luria Bertani) medium

Peptone	10 g
Yeast extract	5 g
NaCl	10 g
Dissolved in double-distilled water to 1 litre	

*12 g of agar were added for preparation of solid media. Antibiotics and chemicals were added after melted LB agar solution had cooled down to 55°C or below.

3.1.1.2 Isolation

Basically, a modified alkaline/SDS lysis method was employed (Birnboim and Doly 1979; Birnboim 1983). After lysis of bacteria under alkaline conditions, at defined salt and pH conditions, the lysate was applied to an anion-exchange resin in a column. Plasmid DNA selectively bound to the resin and was eluted after a wash step which efficiently removes RNA fragments, proteins and other cellular contaminants. The eluted plasmid DNA can

immediately be used in most downstream applications except for run-off T7 transcription *in vitro* due to residual RNase A from the miniprep.

3.1.2 Gel electrophoresis

Nucleic acids are negatively charged because of the phosphate groups in their backbones. In an electric field, nucleic acids move toward the positive pole of the electrophoresis chamber. Gel electrophoresis uses electricity to separate different sizes of nucleic acids as they migrate through a porous, sponge-like gel matrix. Small molecules move faster and migrate further than big ones. The technique is used for the purpose of analysis or preparation. Two popular gel matrix materials are agarose and polyacrylamide.

3.1.2.1 Agarose gel electrophoresis

Agarose is a polysaccharide made from highly purified seaweed. To prepare an agarose gel, agarose powder was mixed with TBE buffer and completely melted in a microwave oven, and then poured into a preset chamber with comb. Gels are ready to use when completely solidified. By adjusting the agarose concentration, variant pore sizes of gel matrix can be obtained. Nucleic acid molecules ranging from several hundreds to over 10,000 nucleotides in length can be separated. A loading buffer containing two dyes was used to monitor the progression of electrophoresis. In order to visualize samples, ethidium bromide or crystal violet was added after the agarose had melted in TBE buffer.

5 x TBE buffer

Tris	445 mM
Boric acid	445 mM
EDTA	10 mM

5 x DNA loading buffer

Tris/HCl pH 7.4	10 mM
EDTA	1 mM
Glycerol	70% (w/v)
Bromophenol blue (BPB)	0.05% (w/v)
Xylene cyanol blue (XCB)	0.05% (w/v)

Ethidium bromide

Ethidium bromide is able to intercalate into nucleic acids. When illuminated with ultraviolet light, it fluoresces orange. A final concentration of 40 µg/ml ethidium bromide was used. Mostly, the dye was applied for nucleic acids analysis and purification especially of shorter DNA fragments (100-1000 bp).

Crystal violet

Exposure to UV light may damage nucleic acids. Crystal violet does not require excitation by UV light and was therefore used to visualize large DNA fragments or long PCR products to be purified. The disadvantage of crystal violet is a much lower sensitivity compared with ethidium bromide. To be visible, a minimum 200 ng DNA is required. A white background helps to improve visibility. The final concentration of the stain, in the gel as well as in the running buffer, was 10 µg/ml.

% **agarose (w/v)**	**separable DNA fragment size (kbp)**
0.5	1.0-30
0.7	0.8-12
1.0	0.5-7
1.2	0.4-6.0
1.5	0.2-3.0
2.0	0.1-2.0

3.1.2.2 Polyacrylamide gel electrophoresis (PAGE)

Polyacrylamide (PAA) is a polymer of acrylamide. The polymerisation of acrylamide (AA) can be driven by addition of ammonium persulfate ($(NH_4)_2S_2O_8$, APS) and N, N, N', N',-tetramethyl-ethylendiamin (TEMED). Native PAA gels were applied to study RNA folding (see section 3.7). For denaturing PAGE, a stock solution of 20% acrylamide (8 M urea) was prepared and diluted to the required percentage using a solution of 8 M urea, both solutions containing 1 x TBE. To start polymerization, 1/100 volume of 10% APS and 1/1000 volume of TEMED were added. Then the solution was quickly poured between two assembled glass plates. After a comb had been inserted, the gel was left to polymerize for at least 15 min. Acrylamide is toxic and therefore must not be discarded as normal liquid waste until polymerized (PAA). By adjusting the acrylamide concentration, variant pore sizes of gel matrix can be obtained. Usually 8% PAA gels were employed for purification of RNAs

between 50-400 nucleotides, 15% PAA gels for structural probing, and 20% PAA gels for separation of RNase P cleavage products. In the activity assays of human RNase P RNA (H1 RNA), gels of 22% PAA (7 M urea) were used. For gel loading, an equal volume of 2 x PPF buffer was added to the samples.

Visualization

Preparative gels were illuminated directly using UV light. With the gel placed on a fluorescent silica gel plate, nucleic acids were detected by the shadow caused on the plate due to the UV light being absorbed by the nucleic acid (UV shadowing). Gels for analysis of small amounts of RNA were entirely soaked in ethidium bromide solution (3.1.2.1) while shaking, and about 500 ng of material was sufficient to appear as a prominent band. When ^{32}P-labeled RNAs were resolved, they were visualized by radioluminography: The gels were wrapped with transparent plastic foil and a phosphoimager plate was placed on top for exposure. Scanning of the plate for RNA detection was performed with a Bio-Imaging Analyser FLA 3000-2R (Raytest, Fuji Film) using the software PC-BAS. Evaluation was performed with the software AIDA (version 3.42, Raytest Isotopenmessgeräte GmbH). Exposure times depended on the amount of radioactivity. For instance, 2000 cpm of radioactive RNA could be visualized well after about 7 hours of exposure. In this case image plates were normally exposed over night. In contrast, for gels loaded with labeling reactions containing very high radioactivity, 1-2 min of exposure time was sufficient.

20% acrylamide (8 M urea) stock, 1 liter

Urea	480 g
50% Acrylamide	400 ml
5 x TBE (3.1.2.1)	200 ml
Add double-distilled water to 1 liter	

8 M urea solution, 1 liter

Urea	480 g
5 x TBE (3.1.2.1)	200 ml
Add double-distilled water to 1 liter	

22% acrylamide (7 M urea) stock, 1 liter	
Urea	450 g
50% Acrylamide	440 ml
5 x TBE (3.1.2.1)	200 ml
Add double-distilled water to 1 liter	

2 x PPF buffer	
Bromophenol blue (BPB)	0.02% (w/v)
Xylene cyanol blue (XCB)	0.02% (w/v)
Urea	2.6 M
Formamide	66% (v/v)
TBE buffer	2 x

3.1.3 Concentration determination

Nucleic acid concentration was determined by UV spectrophotometry using cuvettes with a path length of 1 cm. Samples to be measured were diluted with double-distilled water; absorbance was reliably measured between 0.1-1.0 A_{260} (the absorbance value at 260 nm). A_{260} values were used to calculate the concentration of nucleic acids on the basis of the Lambert-Beer law. The applied equation is described below.

$$c\ [ng/\mu l] = A_{260} \times \text{equivalent of 1.0 } A_{260} \times D$$

where c = concentration in ng/µl
A_{260} = absorbance value measured at 260 nm
equivalent of 1.0 A_{260} = concentration constant for an A_{260} value of 1.0
D = dilution factor of the measured sample

1.0 A_{260} dsDNA = 50 µg/ml, 1.0 A_{260} ssRNA = 37 µg/ml. If molar concentration was required, mass concentration was converted to molar concentration with a nucleotide average molecular weight of 340 g/mol. To check nucleic acid purity, the ratio of A_{260}/A_{280} was determined. In aqueous solution, pure DNA yields an A_{260}/A_{280} ratio of 1.8, and pure RNA yields A_{260}/A_{280} ratios of 2.0. If the absorbance ratio is fundamentally less than the above values, the nucleic acid is most likely contaminated with protein or phenol. Afterwards, the nucleic acids were analyzed on agarose or PAA gels with defined nucleic acids as standards.

3.1.4 Polymerase chain reaction (PCR)

PCR (Saiki *et al.* 1985) permits to produce millions of copies of a specific DNA sequence in a relatively short time. In our study, the enzyme preferentially employed for PCR was *Pfu* DNA polymerase (Promega, MBI Fermentas and our lab). It is a highly thermostable DNA polymerase from the hyperthermophilic archaeon *Pyrococcus furiosus* which remains 95% active after 2 hours of incubation at 95°C. The enzyme catalyzes the template-dependent polymerization of nucleotides into duplex DNA in the 5'=>3' direction and generates blunt-end PCR products. It also exhibits 3'=>5' exonuclease (proofreading) activity, which enables the polymerase to correct nucleotide incorporation errors. For "inside-out" PCR (3.2.2.3), VentR® (exo-) DNA polymerase (New England Biolabs) was sometimes used to ensure intact 3' ends. In other cases (e.g., TOPO TA cloning®, Invitrogen), dA was required at the ends of the PCR product, and *Taq* DNA polymerase (MBI Fermentas and our lab) was applied. *Taq* DNA polymerase (2800 nt/min, accuracy 4.5×10^4) generates PCR products with 3'-dA overhangs, and is five times faster and eight times less accurate than *Pfu* DNA polymerase (550 nt/min, accuracy 3.8×10^5).

A PCR reaction consists of three major steps: denaturation, annealing and extension. These are repeated for around 30 cycles in an automated thermal cycler.

(1) **Denaturation** (at about 95°C) is required to melt double-stranded DNA to single-stranded DNA.

(2) **Annealing** (ca. 50-65°C): Hydrogen bonds are constantly formed and broken between the single-stranded primer and single-stranded template. Under suitable conditions, designed primers bind to the template tightly enough for the DNA polymerase to attach and start copying the template. Too strict conditions cause low yield of the PCR, and too relaxed conditions result in side products. To optimize conditions for a specific PCR, temperature gradient PCRs were run, and Mg^{2+} concentration as well as DNA template concentration were titrated.

(3) **Extension** (at 68-72°C): This is the ideal working temperature for the thermostable DNA polymerase. Starting from the 3' end of the primer, dNTPs are attached stepwise to the nascent DNA strand in a template-dependent manner.

The setup of a standard PCR is given below (next page):

50 µl of PCR

DNA template	x µl	- single bacterial colony (3.1.4.1) or - 2-10 µl of bacterial suspension (3.1.4.1) or - ~ 10 ng of plasmid DNA or - ~ 500 ng genomic DNA
10 x PCR buffer[a]	5 µl	
25 mM Mg^{2+}	4-8 µl	
25 mM dNTPs	1 µl	
100 µM Primer forward	0.5 µl	
100 µM Primer reverse	0.5 µl	
Double-distilled water	to 49.5 µl	
5 U/µl DNA polymerase	0.5 µl	

a**:** 10 x *Taq* Buffer with KCl contains 100 mM Tris-HCl (pH 8.8 at 25°C), 500 mM KCl, 0.8% (v/v) Nonidet P40. 10 x *Taq* Buffer with $(NH_4)_2SO_4$ includes 750 mM Tris-HCl (pH 8.8 at 25°C), 200 mM $(NH_4)_2SO_4$, 0.1% (v/v) Tween 20. The latter allows for PCR at a wide range of magnesium concentrations. 10 x *Pfu* Buffer is composed of 200 mM Tris-HCl (pH 8.8 at 25°C), 100 mM $(NH_4)_2SO_4$, 100 mM KCl, 1% (v/v) Triton X-100, 1 mg/ml BSA.

Running program

1	Initial denaturation	95°C	5 min
2	Denaturation	95°C	1 min
3	Annealing	50-65°C	1.5 min
4	Extension	68-72°C	30 s-6.5 min[a] →2 # 30
5	Final extension	68-72°C	5 min

a: The running time is determined by the elongation rate of the DNA polymerase and the length of DNA sequence to be copied; "→2 # 30" means going back to step 2 and repeating this cycle 30 times.

3.1.4.1 Colony PCR

Colony PCR uses a bacterial colony as DNA template to quickly check transformants. A single colony was either directly transferred from the agar plate into the PCR reaction by tooth stick or pipette tip, or it was suspended in 15-20 µl of LB medium, of which 2-10 µl were transferred into 50 µl of PCR reaction. For one cloning experiment, 20-30 individual colonies were analyzed. A patch plate was prepared to preserve colonies for further assays.

3.1.5 Ethanol precipitation

Ethanol precipitation is a very common method to recover and concentrate nucleic acids from aqueous solutions. Ethanol displaces the hydration shell from nucleic acids and exposes negatively charged phosphate groups. Counter ions such as Na^+ bind to the phosphates and reduce the repulsive forces between the polynucleotide chains to the point where a precipitate can form. To precipitate nucleic acids, either 1/10 volume of 3 M NaOAc pH 5.0 or 1/5 volume of 2 M NH_4OAc pH 7.0, plus 2-3 volumes of ethanol were gently but thoroughly mixed with the aqueous nucleic acid solution. In the case of low amounts of nucleic acid material, glycogen was added as a carrier to a final concentration of 0.05-1 µg/µl. The mixture was then incubated at –20°C for at least 1 h, or at -80°C for 10 min, or in liquid nitrogen for 3 min. Finally, the nucleic acids were pelleted at 10,000-13,000 rpm for at least 20 min at 4°C in a tabletop centrifuge. The supernatant was discarded. The pellet was washed with 70% ethanol by centrifugation at room temperature for 2 min, air-dried and dissolved in a proper amount of double-distilled water.

For precipitation of small volumes of RNAs after a chemical or enzymatic reaction, e.g. 4 µl aliquots withdrawn from kinetics assays, a mix P (see below) was added (46 µl mix P per 4 µl reaction solution) to immediately stop the reaction, and ethanol was added later. In this case, precipitation was performed overnight at –20°C. Then the nucleic acid was pelleted by centrifugation, and, after removing the supernatant, dissolved directly in PPF buffer for PAGE analysis.

Mix P

RNase-free water	45 ml
3 M NaOAc pH 5.0	5 ml
20 mg/ml glycogen	2 ml

3.1.6 Phenol/ chloroform extraction

Phenol/ chloroform extraction is a standard procedure to remove protein from nucleic acid solutions. To extract nucleic acids from a protein enzyme reaction solution, an equal volume of phenol was added to the solution, followed by vigorous mixing on a vortex and centrifugation at 13,000 rpm for 2 min or at 11,000 rpm for 5 min in a tabletop centrifuge. During the procedure, proteins accumulate in the organic phase (the bottom layer) and interphase, and nucleic acids remain in the aqueous phase (the upper layer). After phase separation, the aqueous phase was transferred to another clean tube and traces of remaining phenol were removed by washing with chloroform twice. The wash procedures were the same

as for the phenol extraction: addition of an equal amount of chloroform, centrifugation and separation. Removing all phenol is necessary because phenol is a strong inhibitor for many enzymes. The entire procedure was performed at room temperature. In addition, chloroform could be replaced here by a mixture of chloroform and isoamylalcohol in a proportion 24:1, which facilitates phase separation as compared to pure chloroform.

3.2 Cloning

3.2.1 Construction of recombinant plasmids

For introducing an entirely new insert into a vector, vector and insert were cut with identical restriction enzymes or with restriction enzymes that produced identical or compatible ends, and vector and insert were then ligated with T4 DNA ligase.

3.2.1.1 Restriction enzyme digest

If the restriction enzyme sites required were not available within a vector, these were built in by site-directed mutagenesis (3.2.2.1). The restriction enzyme sites of inserts were normally introduced by the primers used for PCR amplification of the insert. Depending on the restriction enzyme, such primers were designed to contain two or more additional nucleotides 5' of the restriction enzyme site to ensure efficient restriction enzyme digestion. Two digestion reactions of one DNA species were done simultaneously (double digestion) if the two restriction enzymes were active at the same temperature and in a common reaction buffer. In some cases, there were several sites capable of being cut by a single restriction enzyme in a DNA strand, while only one site was required to be cut. Partial digestion was accomplished by diluting the enzyme, a shorter reaction time, or both.

A digestion reaction for vector/insert preparation, 100 µl

DNA	1 µg
10 x buffer	10 µl
Double-distilled water	to 99 µl
10 U/µl restriction enzyme	1 µl
Incubation at 37°C for at least 1 h	

3.2.1.2 Vector preparation

The vectors mostly used in this project were pSP64, pHY300 and pUC19. After restriction enzyme digestion, the linear vectors were often treated by Calf Intestinal Alkaline

Phosphatase (CIAP, MBI Fermentas) to remove 5' phosphates, which subsequently reduces self ligation. The modifying enzyme CIAP is active in many restriction enzyme reaction buffers and was directly added in many cases. When the restriction enzyme reaction buffer was not suitable for CIAP, ethanol precipitation was done prior to dephosphorylation. Finally, the linear vector was purified on agarose gels and extracted either with the QIAquick® Gel Extraction Kit (QIAGEN) or Wizard®SV Gel and PCR Clean-Up System (Promega).

CIAP treatment, 50 µl

DNA solution	1 µg
10 x CIAP buffer[a]	5 µl
Double-distilled water	to 49 µl
1U/µl CIAP	1 µl
Incubation at 37°C for 30 min	

a: 10 x CIAP buffer contains 100 mM Tris-HCl (pH 8.0 at 37°C), 50 mM $MgCl_2$, 1 M KCl, 0.2% Triton X-100, 10 mM 2-mercaptoethanol and 1 mg/ml BSA.

3.2.1.3 Insert preparation

Inserts were either cut from plasmid DNA or prepared by PCR. For inserts consisting of several parts from different sources, a series of PCRs were involved. In general, the modes of insert construction were diverse. Details are described in section 3.2.5. Procedures following PCR were restriction enzyme digestion and gel purification as performed for the vector. To purify and concentrate PCR products before restriction enzyme digestion or a second PCR, ethanol precipitation and commercial kits such as the QIAquick® PCR Purification Kit (QIAGEN) or Wizard®SV Gel and PCR Clean-Up System (Promega) were used.

3.2.1.4 DNA Ligation

	Ligation 1	Ligation 2	control
5 x T4 DNA ligase buffer[a]	2 µl	2 µl	2 µl
50 ng/µl vector	1 µl	1 µl	1 µl
25 ng/µl insert	1 µl	3 µl	-
Double-distilled water	5 µl	3 µl	6 µl
1U/µl T4 DNA ligase	1 µl	1 µl	1 µl
Incubation at room temperature for 1 h (for sticky ends) or at 14°C for 16 h (for blunt ends)			

a: 5 x T4 DNA ligase buffer: 250 mM Tris-HCl (pH 7.6), 50 mM $MgCl_2$, 50 mM ATP, 50 mM DTT, 25% (w/v) polyethylene glycol-800.

For vectors in the size range of 3-5 kbp, 50 ng of vector DNA were used in one ligation reaction. A bigger amount of vector was required for vectors larger than 5 kbp. Usually, two ligation reactions were done as part of one cloning experiment. In one reaction, the molar ratio of vector/insert was 1/3. In the other one, it was 1/6. To assess the efficiency of the ligation, in some cases 4 µl of the reaction solution were resolved on an agarose gel.

3.2.2 Plasmid mutants

3.2.2.1 Site-directed mutagenesis

Site mutation is often required for the study of structure and function of biological macromolecules. To generate single nucleotide exchanges, a pair of mutually complementary primers was used that included the mutation in the middle and around 20 nucleotides complementary to the template plasmid on each side. PCR amplification then generated a double-stranded mutant plasmid with a nick in each strand. Subsequently, the restriction endonuclease *Dpn* I, specific for the methylated or hemimethylated DNA target sequence 5'-Gm^6ATC-3', was used to digest native (non-mutated) parental DNA template. After *Dpn* I digestion, 1-5 µl of PCR products were directly used for transformation of competent cells (Scheme 3.2.2.1 a).

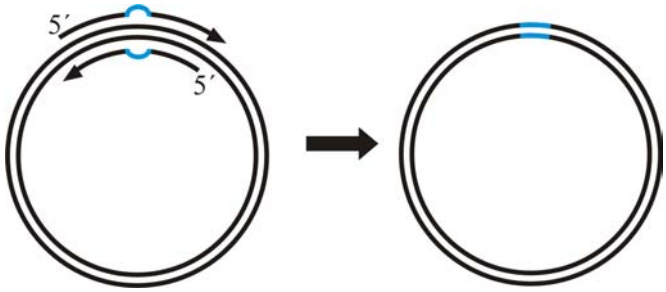

Scheme 3.2.2.1 a: Site-directed mutagenesis. The mutated site is in blue. Template sequences are in black.

50 µl of PCR for site-directed mutagenesis

	mutagenesis	control
50 ng DNA template	x µl	x µl
10 x PCR buffer (3.1.4)	5 µl	5 µl
25 mM Mg^{2+}	6 µl	6 µl
25 mM dNTPs	1 µl	1 µl
100 µM Primer forward	0.5 µl	0.5 µl
100 µM Primer reverse	0.5 µl	0.5 µl
Double-distilled water	to 49 µl	to 50 µl
5 U/µl *Pfu* DNA polymerase	1 µl	-

Running program

1	Initial denaturation	95°C	30 s
2	Denaturation	95°C	30 s
3	Annealing	50-65°C	1 min
4	Extension	68°C	6.5 min →2 # 15
5	Final extension	68°C	10 min

"→2 # 15" means going back to step 2 and repeating this cycle 15 times.

3.2.2.2 Megaprimer mutagenesis

Megaprimer mutagenesis (Scheme 3.2.2.2) allows exchanging a long sequence stretch within a plasmid. This method was employed to generate domain swap mutants. In a first step, megaprimers were prepared by standard PCR and purified by agarose gel electrophoresis. Both primers used in the PCR for megaprimer preparation were composed of two different sequence stretches: The 3' part of the primer was complementary to the template plasmid 1 (in blue). In a second step, the gel-purified double-stranded megaprimer was used as a pair of primers in a mutagenesis PCR reaction using plasmid 2 as template. Again the restriction endonuclease *Dpn* I served to digest the parental plasmids and to select for newly synthesized mutant plamids as in site-directed mutagenesis.

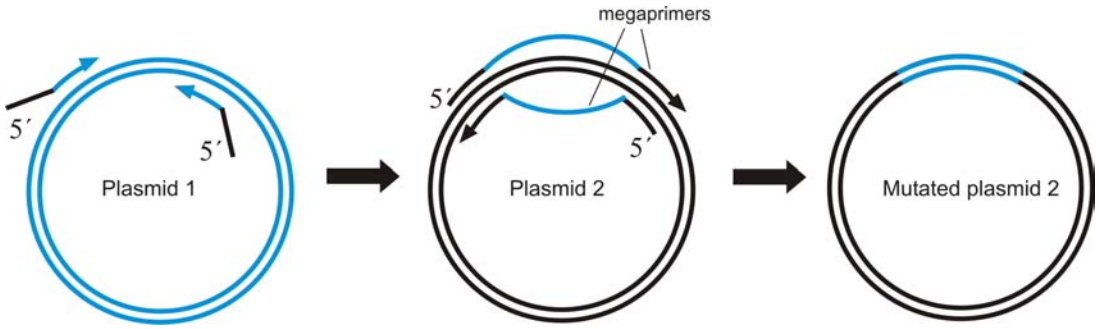

Scheme 3.2.2.2: Megaprimer mutagenesis. Plasmid 1 (the template for megaprimer preparation) and mutated area are in blue. The original sequence streches of plasmid 2 are in black.

50 µl of PCR for megaprimer mutagenesis

	mutagenesis	control
50 ng DNA template	x µl	x µl
10 x PCR buffer (3.1.4)	5 µl	5 µl
25 mM Mg^{2+}	6 µl	6 µl
25 mM dNTPs	1 µl	1 µl
350 ng Megaprimer	y µl	y µl
Double-distilled water	to 49 µl	to 50 µl
5 U/µl *Pfu* DNA polymerase	1 µl	-

Running program

1	Initial denaturation	95°C	30 s
2	Denaturation	95°C	30 s
3	Annealing	55°C	1 min
4	Extension	68°C	6.5 min →2 # 15
5	Final extension	68°C	10 min

"→2 # 15" means going back to step 2 and repeating this cycle 15 times.

3.2.2.3 "Inside-out"-PCR mutagenesis

"Inside-out"-PCR mutagenesis was used to introduce all kinds of mutations into our target genes. Mutations ranging from 1 to about 60 nucleotides were successfully introduced. Unlike a normal PCR, "inside-out" PCR amplifies the entire template plasmid "inside to outside" (Scheme 3.2.2.3); the primers hybridize 5' end to 5'end on opposite strands of the template. Here, each primer consists of two parts of DNA sequences. The 5' part contains the mutation to be introduced (in grey), and the 3' part (in black) is complementary to the original plasmid. The pair of primers was 5'-phosphorylated with polynucleotide kinase (PNK) prior to the PCR, so that the PCR products could converted to circular plasmids by DNA ligation. Following phosphorylation, the reaction solution was incubated at 70°C for 5 min to inactivate the kinase. Then 2.5 µl of each phosphorylated primer solution was used in the PCR. The methylation-sensitive endonuclease *Dpn* I served to digest the parental plasmids and to select for linear newly-synthesized plamids, as in site-directed mutagenesis. Then the linear PCR products were purified by agarose gel electrophoresis or commercial kits as in 3.2.1, circularized by T4 DNA ligase (Gibco BRL, Invitrogen or MBI Fermentas) and used for transformation. When nucleotides introduced by the 5' ends of the primers were missing in the plasmid obtained, VentR® (exo-) DNA polymerase was used instead of *Pfu* DNA polymerase.

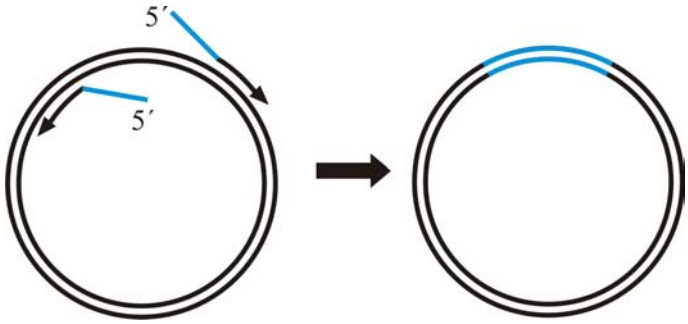

Scheme 3.2.2.3: "Inside-out" PCR mutagenesis. The mutated area is in grey. The sequence of the original plasmid is in black.

Phosphorylation of primers, 25 µl

100 µM Primer	5 µl
10 x Reaction Buffer A[a]	2.5 µl
10 mM ATP	2.5 µl
Double-distilled water	14 µl
10 U/µl T4 PNK	1 µl
Incubation at 37°C for 1 h	

a: The 10 x reaction Buffer A is for the forward reaction and includes 500 mM Tris-HCl (pH 7.6 at 25°C), 100 mM $MgCl_2$, 50 mM DTT, 1 mM spermidine and 1 mM EDTA.

50 µl of "inside-out" PCR

	mutagenesis	control
50 ng DNA template	x µl	x µl
10 x PCR buffer (3.1.4)	5 µl	5 µl
25 mM Mg^{2+}	6 µl	6 µl
25 mM dNTPs	1 µl	1 µl
20 µM Primer forward, kinased	2.5 µl	2.5 µl
20 µM Primer reverse, kinased	2.5 µl	2.5 µl
Double-distilled water	to 49 µl	to 50 µl
5 U/µl DNA polymerase	1 µl	-

Running program

1	Initial denaturation	95°C	5 min
2	Denaturation	95°C	1 min
3	Annealing	50-65°C	1.5 min
4	Extension	72°C	6.5 min →2 # 15
5	Final extension	72°C	10 min

"→2 # 15" means going back to step 2 and repeating this cycle 15 times.

Ligation

	Ligation	control
5 x T4 DNA ligase buffer (3.2.1.4)	2 µl	2 µl
~10 ng linear plasmid	x µl	x µl
Double-distilled water	to 9 µl	to 10 µl
1 U/µl T4 DNA ligase	1 µl	-
Incubation at room temperature for 1 h or at 14°C for 16 h		

3.2.3 Transformation

The uptake of naked exogenous DNA by cells that alters the phenotype or genetic trait of a cell is called transformation. In this study, plasmid DNA was usually transferred into competent bacterial cells which were pretreated to permit DNA uptake with high efficiency. Some bacterial strains used in this study, such as *B. subtilis* SSB318, are naturally capable of taking up DNA. Other strains, for example DH5α, DW2 and BW were passively made competent by $CaCl_2$ treatment (chemical competence) or by electroporation (electro-competence), which required special preparation of the cells. In this chapter, only the preparation and transformation of chemically competent DH5α cells are introduced. The competent cells SSB318, DW2 and BW are introduced in detail in section 3.3.

3.2.3.1 Preparation of chemically competent *E. coli* cells (DH5α)

To prepare chemically competent *E. coli* DH5α cells, the calcium chloride method was used. This chemical treatment requires no special equipment and gives 10^5-10^6 transformants per microgram DNA. As the strain DH5α is devoid of any antibiotic resistance, cells were handled with particular care during this procedure to avoid contamination.

Procedure

DH5α cells were first spread from a glycerol stock stored at -80°C onto an LB agar plate and incubated at 37°C for around 16 h. A single freshly developed colony was inoculated into 3 ml of LB medium and was grown at 37°C overnight or for at least 6 h in a shaking incubator. Afterwards, 2.5 ml of the culture were transferred into 500 ml of fresh LB medium and further grown until the OD_{578} reached 0.5-0.6, which took about 4 h. Cells were transferred into two centrifuge bottles and, after cooling on ice for 10 min, harvested at 4,000 rpm (Eppendorf 5810R centrifuge) for 15 min at 4°C. Each cell pellet was suspended in 50 ml of ice-cold 100 mM $CaCl_2$ solution and transferred into two 50 ml tubes kept on ice. Cells were

pelleted once more at 7,000 rpm (Eppendorf 5810R) for 10 min at 4°C. Each cell pellet was suspended in 7 ml of ice-cold $CaCl_2$ solution (75 mM, 25% (v/v) glycerol). Finally, aliquots were prepared in vials placed on ice, frozen in liquid nitrogen and stored at -80°C. The frozen competent cells could be stored for up to 1 year without substantial loss of transformation efficiency.

3.2.3.2 Transformation of chemically competent *E. coli* cells (DH5α)

Frozen competent cells were incubated on ice until completely thawed. Then 1-5 µl of circular plasmid (5-20 ng) were gently mixed with 50 µl of competent cells by tapping the side of the tube with the fingers. The mixture was placed on ice for 30 min, and the cells were briefly heat shocked at 42°C for 45 s to promote cellular DNA uptake. Afterwards the cells were put back on ice and cooled for 2 min. After addition of 800 µl of LB medium, the cells were placed in a heat block at 37°C for 1 h while intensively shaking. The cells were pelleted at 13,000 rpm in a tabletop centrifuge for 15 seconds, resuspended in 100 µl of the supernatant by pipetting up and down, and finally spread on selective LB agar plates for growth at 37°C.

3.2.3.3 Selection of objective transformant

In order to select genuine transformants, LB agar plates were supplemented with antibiotics, normally 100 µg/ml ampicillin. After overnight growth at 37°C, a few colonies were picked from the plate and individually inoculated into 3 ml LB medium to be grown for 6-16 h at 37°C in a shaking incubator. Finally, the plasmid DNA was isolated and checked by restriction enzyme digestion and sequencing (Eurofins MWG Operon).

Restriction enzyme digestion for analysis of plasmid DNA

Miniprep plasmid DNA (50-100 ng)	2-4 µl
10 x buffer	1 µl
Double-distilled water	to total of 10 µl
10 U/µl restriction enzyme	0.2-1 µl
Incubation at 37°C for at least 1 h	

3.2.4 TOPO cloning

The TOPO TA Cloning® kit (Invitrogen) provides a highly efficient cloning strategy by which PCR products amplified with *Taq* polymerase can be easily inserted into a TOPO plasmid vector. The vector pCR®2.1-TOPO® is designed to have single 3'-thymidine (T) overhangs as well as topoisomerase I at both ends of the linear vector to efficiently ligate PCR products with single 3'-adenine (A) overhangs. The topoisomerase I is attached to the linear vector by a covalent bond. The bond can be attacked by the 5' hydroxyl group of the PCR product, ligating the PCR product with the vector and releasing the enzyme. Neither ligase nor digestion of the PCR product is required. Further, the vector contains the *lacZα* gene, which is disrupted by integration of the insert and thus allows for blue/white screening: The *lacZα* gene encodes part of the reporter protein β-galactosidase which cleaves colourless X-Gal into galactose and a blue insoluble product. When a DNA fragment is inserted into the *lacZα* reading frame, synthesis and assembly of a functional β-galactosidase is usually prevented. Therefore, colonies harbouring a recombinant plasmid are in most cases white on X-Gal plates and can thus be easily identified.

In practice, we basically followed the protocol of the manufacturer. The inserts were prepared by PCR with *Taq* DNA polymerase and were then directly mixed with pCR®2.1-TOPO® vector if there was almost no side product in the PCR; otherwise PCR products were purified by agarose gel electrophoresis (3.1.2.1) prior to ligation. 2 µl of ligation reaction solution were gently mixed with 25 µl of competent One Shot® cells for transformation. LB agar plates were supplemented with 100 µg/ml of ampicillin and 80 µM IPTG. For blue/white screening, 40 µl of 4% X-Gal were spread on each plate and the plates were preincubated at 37°C for half an hour before use. White colonies were usually analyzed by colony PCR to amplify the inserted DNA (3.1.3). Candidate colonies were further cultured, analyzed by restriction enzyme digestion and sent for sequencing.

3.2.5 Plasmids generated throughout this study

Below is a list of recombinant plasmids generated throughout this study. Abbreviations used are: Cpa: *Cyanophora paradoxa* P RNA gene, Hsa: *Homo sapiens* P RNA gene, MM: *Methanothermobacter thermoautotrophicus* P RNA gene, EE: *Escherichia coli* P RNA gene, ME: the chimeric P RNA gene composed of *M. thermoautotrophicus* C-domain and *E. coli rnpB* S-domain etc. The cloning strategies are given and all primers involved are listed. Mutations introduced by the primer sequences are underlined, with Δ indicating where the primers brought about a deletion. Restriction enzyme cleavage sites are highlighted in italics.

The T7 promoter for transcription is indicated by lower case letters, as is the extra G (for better transcription yields) behind T7 promoters. The *cis*-hammerhead ribozyme cassette is in bold.

3.2.5.1 Plasmids for complementation assays

Plasmids used for complementation assays contain a P RNA gene, or a P RNA gene plus a P protein gene, as well as their promoters and sometimes also terminators. In general, these plasmids are derivatives of pSP64 (Promega), pHY300 (Ishiwa and Shibaharasone 1986), pBsrnpAnHis (also called pB.s.[*rnpA-NH+rnpB*]) (Gössringer *et al.* 2006) and pACYCmitEcm1ApaI (also named pACYC177 E. coli rnpBwt) (Wegscheid and Hartmann 2006).

pSP64 variants

The pSP64 variants were constructed for RNase P RNA complementation assays in *E. coli* strain DW2.

● pSP64-Cpa rnpB-ApaI

The vector pSP64 was prepared by cutting pSP64_ecoli_m1_ApaI with *Apa* I and *BamH* I. In plasmid pSP64_ecoli_m1_ApaI, the *E. coli rnpB* gene was under the control of the native *E. coli rnpB* promoter as described (Hardt and Hartmann 1996). The *C. paradoxa* P RNA gene was amplified from pUC19-Cpa wt, also called pT7G3CyRPR (Cordier and Schön 1999), with primers 5\'ApaI Cyp rnpB and 3\'Cyp rnpB BamHI; the PCR product was cut by *Apa* I and *BamH* I and then ligated into the vector using T4 DNA ligase. The *C. paradoxa* P RNA gene thus replaced *E. coli rnpB*, and was still under the control of the native *E. coli rnpB* promoter.

5\'ApaI Cyp rnpB

5'-CCA*GGGCCC*GCAAACCCTCTATACTGCGCGCCAAACGAATTTAATTAATGATT

3\'Cyp rnpB BamHI

5'-GCG*GGATCC*AAACGAACTTAATTTTAAGC

● pSP64-Cpa rnpB C57/G213-ApaI

The same cloning strategy was used as for pSP64-Cpa rnpB-ApaI. The *C. paradoxa* P RNA gene mutant C57/G213 was amplified from pT7G3CyRPR-C57/G213 (Cordier and Schön 1999) with primers 5\'ApaI Cyp rnpB and 3\'Cyp rnpB BamHI and introduced into pSP64_ecoli_m1_ApaI instead of *E. coli rnpB*.

● pSP64-Cpa rnpB C57/G213/G22-ApaI

Again the same cloning strategy was used as for pSP64-Cpa rnpB-ApaI. The *C. paradoxa* P RNA gene mutant C57/G213/G22 was amplified from pT7G3CyRPR-C57/G213/G22 (Cordier and Schön 1999) using primers 5\'ApaI Cyp rnpB and 3\'Cyp rnpB BamHI and introduced into the pSP64 vector instead of *E. coli* rnpB.

● pSP64-Mth rnpB-ApaI

The cloning strategy was as for pSP64-Cpa rnpB-ApaI. The *M. thermoautotrophicus* P RNA gene was amplified from pUC119_T7_M.th._rnpB (Jim Brown, North Carolina State University) using primers 5\'ApaI Mth rnpB and 5\'Mth rnpB BamHI and introduced into the pSP64 vector instead of *E. coli rnpB*.

5\'ApaI Mth rnpB

5'-CCA*GGGCCC*GCAAACCCTCTATACTGCGCGCCAGCCGAAGGGCAGCTGA

5\'Mth rnpB BamHI

5'-GCG*GGATCC*TGCCGAGAGTAACCCACCT

pHY300 variants

The shuttle vector pHY300 can replicate in *E. coli* cells and also *B. subtilis* cells. In the pHY300 derivatives used in this study, variants of P RNA genes were inserted into pHY300 for RNase P RNA complementation assays in the *B. subtilis* strain SSB318.

● pHY300-EE

The plasmid pHY300 was cut by *Xba* I and *Hind* III. The *E. coli rnpB* gene and its promoter were cut from pSP64_ecoli_m1_ApaI by *Nhe* I and *Hind* III and inserted in pHY300 via ligation by T4 DNA ligase.

● pHY300-Cpa rnpB wt

The same cloning strategy as for pHY300-EE was applied. The *C. paradoxa* P RNA gene and its promoter were cut from pSP64-Cpa rnpB-ApaI by *Nhe* I and *Hind* III and inserted in pHY300.

● pHY300-Cpa rnpB C57/G213

As above, The *C. paradoxa* P RNA gene mutant C57/G213 and its promoter were cut from pSP64-Cpa rnpB C57/G213-ApaI by *Nhe* I and *Hind* III and inserted in pHY300.

● pHY300-Cpa rnpB C57/G213/G22

Site-directed mutagenesis was performed to introduce G22 (underlined) into pHY300-Cpa rnpB C57/G213 with primers G22-Cyp-rnpB1 and G22-Cyp-rnpB2.

G22-Cyp-rnpB1

5'-CGAATTTAATTAATGATTGCAGATTTATTCAATCTGAGG

G22-Cyp-rnpB2

5'-CCTCAGATTGAATAAATCTGCAATCATTAATTAAATTCG

● pHY300-EC

A megaprimer mutagenesis was done to change the S-domain coding region of *E. coli rnpB* into that of *C. paradoxa* as encoded on pHY300-Cpa rnpB wt. The megaprimer was generated from pHY300-EE with primers 119 and 120.

119 C. p. specificity s

5'-GTCCGGGCTCCATAGGGCAGAATTGCTGGGTAATTCCCAG

120 C. p. specificity as

5'-CCTATTTGGCCTTGCTCCGAACGGGGTTTACTAAGTAT

● pHY300-CE

First two PCR fragments were produced from the *C. paradoxa rnpB* gene. One was generated with primers 113 and 114 and contained the 5'-part of the *C. paradoxa* C-domain. The other was obtained with primers 115 and 116 and contained the C-domain's 3'-part. The primers introduced additional restriction enzyme cleavage sites, a T7 promoter and nucleotides matching the 5'- or 3'- termini of the *E. coli rnpB* S-domain. After gel purification the two PCR products were used as primers for amplification of the *E. coli rnpB* S-domain. Then the final PCR product was cloned into pUC19 via *BamH* I and *EcoR* I restriction sites. A site-directed mutagenesis was done to complete the preparation of the chimeric *rnpB* gene CE with primers 143 and 144, which was amplified with primers 5\'ApaI Cyp rnpB plus 140 and inserted into pHY300-Cpa rnpB wt cut by *Xba* I and *Apa* I.

113

5'-GCGGGATCCtaatacgactcactatagCGAATTTAATTAATGATTACAG

114

5’-CAGGCGTTACCTGGCACCCTAACCTTATAGGAGCC

115

5’-GTGGCACGGTAAACTCCACCCAGGAGCAAAGTTTAGCG

116

5’-GCGGAATTCAAAACGAACTTAATTTTAAGCC

143 M Cypcat-Ecolispec s

5’-CCTGGCACCCTAACCTTTAAGGAGCCCGGACTTTCC

144 M Cypcat-Ecolispec as

5’-GGAAAGTCCGGGCTCCTTAAAGGTTAGGGTGCCAGG

5\’ ApaI Cyp rnpB

5’-CCA*GGGCCC*GCAAACCCTCTATACTGCGCGCCAAACGAATTTAATTAATGATT

140 XbaI-Cpy cat

5’-GCG*TCTAGA*GGATCCAAACGAACTTAATTTTAAGC

● pHY300-MM

Cloning was similar to pHY300-EE. The *M. thermoautotrophicus* P RNA gene and its promoter were excised from pSP64-Mth rnpB-ApaI by *Nhe* I and *Hind* III and inserted into pHY300.

● pHY300-EM

This plasmid was constructed by megaprimer mutagenesis on the basis of pHY300-EE. The megaprimer was generated by several PCRs. PCR I was performed to amplify the S-domain of the *M. thermoautotrophicus* P RNA gene with primers 125 plus 126 and template pHY300-MM. Then PCR II was done to combine the 5’ part of the *E. coli rnpB* C-domain with the S-domain of *M. thermoautotrophicus* P RNA gene, using templates pHY300-EE and the PCR I product for overlap extension and primers 100 and 126 for amplification of the product. In parallel, the combination of the *M. thermoautotrophicus* S-domain with the 3’ part of the C-domain of *E. coli rnpB* was obtained by PCR III using templates pHY300-EE and PCR I product for overlap extension and primers $99_{\text{BWegscheid}}$ plus 125 for amplification of the product. Then the PCR II and III products were combined for overlap extension, and the extension product was amplified with primers 100 and $99_{\text{BWegscheid}}$ to produce the megaprimer.

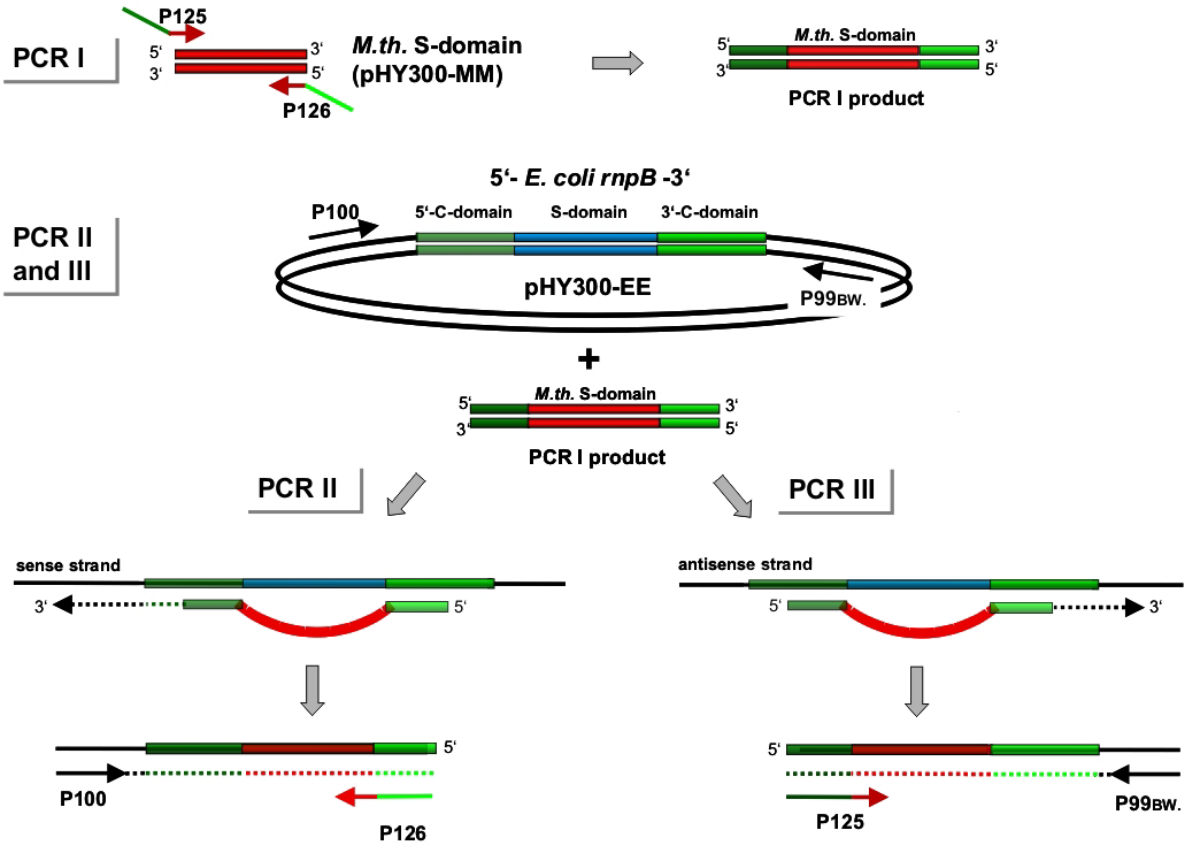

125 M.th. specificity s

5'-GTCCGGGCTCCATAGGGCACCGTGGTGCCGTGAGGCAT

126 M.th. specificity as

5'-CCTATTTGGCCTTGCTCCCCGTGGAATGGCCGTTTCAC

100 3 Chim-XbaI 2

5'-CGACCTGCAGATCTCTAGATTGCTGCTCAAGAACAGC

99 BWegscheid

5'-GCCAGGGGGAAACGCC

• pHY300-ME

First the S-domain of *E. coli rnpB* was amplified from pHY300-EE with primers 123 and 124 (PCR I). Then two PCRs were separately done to produce (i) the 5' part of the *M. thermoautotrophicus* C-domain plus *E. coli* S-domain (primers: 100 and124; templates: pHY300-MM and PCR I product) and (ii) *E. coli* S-domain plus the 3' part of the *M. thermoautotrophicus* C-domain (primers: 123 and $99_{BWegscheid}$; templates: pHY300-MM and PCR I product). With primers 100 plus $99_{BWegscheid}$ and the latter two PCR products as overlap extension templates, the large DNA segment containing the chimeric P RNA gene ME was

generated. Vector pHY300 and this large DNA segment were both cut with *Xba* I and then ligated to yield the recombinant plasmid. Because of an additional C accidently introduced in the middle of primer 124, a further site-directed mutagenesis with primers 138 and 139 was performed to delete the C residue.

123 M.th. catalytic s

5'-ACTCCACCCATCATACAGAAGGGTGCCAGGTAACGCCTG

124 M.th. catalytic as

5'-CAGCATTTGTCCTTGCATC**C**GGGTGGAGTTTACCGTGCCA

100 3 Chim-XbaI 2

5'-CGACCTGCAGATCTCTAGATTGCTGCTCAAGAACAGC

$99_{BWegscheid}$

5'-GCCAGGGGGAAACGCC

138 Mth cat as (124 new)

5'-CAGCAT TTGTCCTTGCATC<u>Δ</u>GGGTGGAGTTTACCGTGCCA

139 s138

5'-TGGCACGGTAAACTCCACCC<u>Δ</u>GATGCAAGGACAAATGCTG

● pHY300-Ecat

Using pHY300-EE as template, an "inside-out"-PCR mutagenesis was done to remove the S-domain of *E. coli* P RNA with primers 145 and 146. Helix P7 of the S-domain was retained within this construct and was capped with a GAAA tetraloop (underlined).

145 Ecoli cat alone s

5'-<u>GAAA</u>CACCCGGAGCAAGGCCA

146 Ecoli cat alone as

5'-CACCCTGCCCTATGGAGCC

pBsrnpAnHis derivative

pBsrnpAnHis, also called pB.s.[*rnpA-NH+rnpB*] (Gössringer et al. 2006), contains a *B. subtilis rnpA* gene, encoding the RNase P protein, and a *B. subtilis rnpB* gene. Its derivative was produced for RNase P holoenzyme complementation assays also in *B. subtilis* strain SSB318.

● pBsrnpAnHis_ME-mJ15/18/2/3/P2/nP1

This plasmid was constructed by replacing the *B. subtilis rnpB* in pBsrnpAnHis with the mutant chimeric ME-J15/18/2/3/P2/nP1 P RNA gene. The first PCR was done to amplify the

mutated *M. thermoautotrophicus* P RNA gene from pUC19-ME-mJ15/18/2/3/P2/nP1 with primers 275 and Mth-nP1-3. The second PCR copied the *B. subtilis* native Rho-independent *rnpB* terminator from pBsrnpAnHis with primers $45_{BWegscheid}$ and 276. Then the two PCR products were combined for overlap extension in a third PCR using primers 275 and 276 for amplification to generate a fusion of the mutated *M. thermoautotrophicus* P RNA gene and the *B. subtilis rnpB* terminator. The final PCR product was digested with *Hind* III and ligated into pBsrnpAnHis cut with *Hind* III and *Swa* I. A fortuitous mutation was corrected by site-directed mutagenesis with primers 285 and 286.

275 HindIII-ME

5'-CAGC*AAGCTT*CCGGGCAAGCCGAAGGGCAG

Mth-nP1-3 (designed by M. Gössringer)

5'-GCTTGTTTTCATCATTTTAAATGTCCGGGCATGCCGAGAGTAACCCACCTTCTG

$45_{BWegscheid}$

5'-ACATTTAAAATGATGAAAACAAGC

276 terminator B

5'-AAATTCTTTTCAAGATAAAAGCTC

285 A-G a

5'-CGAAACAGAAGGTGGGTTACTCTCGGCATGCCCGGACATTTAAAATG

286 A-G b

5'-CATTTTAAATGTCCGGGCATGCCGAGAGTAACCCACCTTCTGTTTCG

• pACYC-ME-mJ15/18/2/3/P2/nP1

A derivative of pACYCmitEcm1ApaI, also named pACYC177 E. coli rnpBwt (Wegscheid and Hartmann 2006), was generated for RNase P holoenzyme complementation assays in *E. coli* strain BW. Towards this goal, the mutant ME-mJ15/18/2/3/P2/nP1 P RNA gene was amplified from pUC19-ME-mJ15/18/2/3/P2/nP1 with primers 277 plus 278 and ligated into pACYCmitEcm1ApaI, cut with *Apa* I and *Xba* I.

277 ApaI-ME

5'-CGC*GGGCCC*GCAAACCCTCTATACTGCGCGCCCCGGGCAAGCCGAAGGGCAG

278 XbaI-ME

5'-CGC*TCTAGA*GGATCCCCGGGCATGCCGAGAGTAACCCACCTTCTG

3.2.5.2 Plasmids for RNA preparation

These plasmids served as templates for run-off transcription with bacteriophage T7 RNA polymerase. Most of them were composed of vector pUC19 and an insert with a T7 promoter preceding a P RNA gene, inserted via *Bam* HI and *EcoR* I restriction sites. Exceptions were plasmids for transcription of *C. paradoxa* P RNA variants, where a *Fok* I recognition site was located behind the P RNA gene, and plasmids for transcription of some *M. thermoautotrophicus* P RNA variants. For the latter, the P RNA genes were cloned into pUC119 and had a *Bsa* I recognition site downstream. To prepare a set of variants of the same P RNA, an initial plasmid was first constructed, and derivatives were subsequently obtained by mutagenesis. In the case of P RNA genes tailed by a *cis*-hammerhead ribozyme cassette, a PCR product was directly used as template for T7 transcription.

● pUC19-Cpa-mP15-17/P6

Using pUC19-Cpa wt, also called pT7G3CyRPR (Cordier and Schön 1999), as template, an "inside-out"-PCR mutagenesis was done with primers 229 and 230 to insert the P15-17 module of *E. coli* P RNA. The generated plasmid, pUC19-Cpa-mP15-17, served as a template in a second "inside-out"-PCR mutagenesis with primers 231 and 232, which additionally introduced the P6 element of *E. coli* P RNA P6.

229 CC-mP15-17 A

5'-GCCGTACCTTATGAACCCCTATTTGGCCTTGCTCCTGAACGGGGTTTA

230 CC-mP15-17 B

5'-CGTACTGAACCCGGGTAGGCTGCTAGAAAAATTGAGTAATTAATTTTGAAGACAG

231 CC-mP6 A

5'-CCAAGGAGCCCGGACTTTCCTCAGATTG

232 CC-mP6 B

5'-GCAGAATTGCTGGGTAATTCCCAGTACG

● pUC19-Cpa-mP15-17/P5-6

Site-directed mutagenesis I was carried out to delete one nucleotide in P5 of pUC19-Cpa-mP15-17/P6 with primers 237 and 238. With the first mutagenesis product (pUC19-Cpa-mP15-17/P5-6 A) as template, site-directed mutagenesis II was performed to insert ATA in P5 with primers 235 and 236.

237 CC- P17-15/P5/P6 C

5’-CTATACTTAGTAAACCCCGTTCΔGGAGCAAGGCCAAATAGGGGTTC

238 CC- P17-15/P5/P6 D

5’-GAACCCCTATTTGGCCTTGCTCCΔGAACGGGGTTTACTAAGTATAG

235 CC-P17-15/P5/P6 A

5’-GAAAGTCCGGGCTCCATAGGGCAGAATTGCTG

236 CC- P17-15/P5/P6 B

5’-CAGCAATTCTGCCCTATGGAGCCCGGACTTTC

● pUC19-Cpa-mP15-17/P5-7

Based on the plasmid pUC19-Cpa-mP15-17/P5-6, one nucleotide was mutated in P7 by site-directed mutagenesis with primers 239 and 240.

239 CC- P17-15/P5/P6/P7 A

5’-CGGGCTCCATAGGGCAGAACGCTGGGTAATTCCCAGTACG

240 CC- P17-15/P5/P6/P7 B

5’-CGTACTGGGAATTACCCAGCGTTCTGCCCTATGGAGCCCG

● pUC19-Ecat

The gene for Ecat, the catalytic domain of *E. coli* P RNA, was amplified from pHY300-Ecat with primers 136 and 149, digested by *Bam* HI and *EcoR* I, and then cloned into pUC19 cut with the same enzymes.

136 BamHI-T7-Ecoli rnpB

5’-GCG*GGATCC*taatacgactcactatagGAAGCTGACCAGACAGT

149 137 new

5’-CGC*GAATTC*AGGTGAAACTGACCGAT

● pUC19-EC

The cloning strategy was the same as for pUC19-Ecat. The chimeric P RNA gene EC was amplified from pHY300-EC with primers 136 and 149, cut with *Bam* HI and *EcoR* I, and then inserted into pUC19 digested with the same enzymes.

136 BamHI-T7-Ecoli rnpB

5’-GCG*GGATCC*taatacgactcactatagGAAGCTGACCAGACAGT

149 137 new

5’-CGC*GAATTC*AGGTGAAACTGACCGAT

● pUC19-CE

Similar to cloning of pUC19-Ecat, the chimeric P RNA gene CE was amplified from pHY300-CE with primers 134 and 148, cut with *Bam* HI and *EcoR* I, and then inserted into pUC19 digested with the same enzymes.

134 BamHI-T7- Cyp rnpB

5'-GCG*GGATCC*taatacgactcactatagGAAACGAATTTAATTAATGA

148 135 new

5'-CGC*GAATTC*AAACGAACTTAATTTTAAG

● pUC19-EE

The cloning followed the above strategy for pUC19-Ecat. The insert containing *E. coli rnpB* was produced by digesting the product of a PCR (primers: 136 and 149; template: pHY300-EE) with *Bam* HI and *EcoR* I. Afterwards the insert was ligated into pUC19 cut with the same enzymes.

136 BamHI-T7-Ecoli rnpB

5'-GCG*GGATCC*taatacgactcactatagGAAGCTGACCAGACAGT

149 137 new

5'-CGC*GAATTC*AGGTGAAACTGACCGAT

● pUC19-ME

Likewise, the chimeric P RNA gene ME was amplified from pHY300-ME with primers 132 and 147, cut with *Bam* HI and *EcoR* I, and then inserted into pUC19 linearized with *Bam* HI and *EcoR* I.

132 BamHI-T7-Mth rnpB

5'-GCG*GGATCC*taatacgactcactataggAGCCGAAGGGCAGCTGACG

147 133 new

5'-CGC*GAATTC* TGCCGAGAGTAACCCACCTTCT

● pUC19-EM

As for construction of pUC19-Ecat, the chimeric P RNA gene EM was amplified from pHY300-ME with primers 136 and 149, cut with *Bam* HI and *EcoR* I, and then cloned into pUC19 digested with the same enzymes.

136 BamHI-T7-Ecoli rnpB

5'-GCG*GGATCC*taatacgactcactatagGAAGCTGACCAGACAGT

149 137 new
5’-CGC*GAATTC*AGGTGAAACTGACCGAT

● pUC19-ME-mP1

As a first step, a PCR was performed with pUC19-ME as template and a pair of long primers (156 and 157). Both primers comprised a sequence stretch encoding *E. coli* P1 at their 5’ ends. Second, the plasmid pHY300-ME-mP1 was constructed by ligation of the above PCR product (ME-mP1) into pHY300-Cpa rnpB wt, after plasmid as well as the PCR product had been digested with *Apa* I and *Xba* I. Third, the ME-mP1 insert of plasmid pHY300-ME-mP1 was amplified with the primer pair 149/179 and inserted into pUC19 via *BamH* I and *EcoR* I restriction sites.

156 P1 A
5’-CGC*GGGCCC*GCAAACCCTCTATACTGCGCGCCGAAGCTGACCAGGCAGCTGA
CGGTCCCTCA
157 P1 B
5’-GCG*AGATCT*CTAGAGGATCCAGGTGAAACTGACCGATAACCCACCTTCTGTTT
CGGCT
149 137 new
5’-CGC*GAATTC*AGGTGAAACTGACCGAT
179 BamHI-T7-ME-P1
5’-GCG*GGATCC*taatacgactcactatagGAAGCTGACCAGGCAGCT

● pUC19-ME-mP2

Using pUC19-ME as initial template, two “inside-out”-PCR mutageneses were done to achieve a base pair insertion in P2 (underlined nucleotides), the first PCR with primers 188 and 189, the second with primers 190 and 191.

188 ME-mP2ins A
5’-TCTGACGGTCCCTCAAGGGGCTGA
189 ME-mP2ins B
5’-CTGCCCTTCGGCTCCTATAGTGAGTCGTATTAG
190 ME-mP2ins C
5’-ACTGCCGAAACAGAAGGTGGGTTAC
191 ME-mP2ins D
5’-CATTCATCTGGGCGGACTACCTC

● pUC19-ME-mP4

The cloning strategy was the same as for pUC19-ME-mP2. Using pUC19-ME as the initial template, two consecutive "inside-out"-PCR mutageneses were performed to mutate three base pairs in P4 with primer pairs 166 and 168, as well as 180 and 181.

166 ME-P4 A

5'-GGCATCATACAGAAGGGTGCCAGGT

168 ME-P4 B

5'-CGGAGTTTCCTCAGCCCCTTGAG

180 ME - P4 C

5'-CGGGTTACTCTCGGCAGAATTCAC

181 ME - P4 D

5'-GGTTCTGTTTCGGCAGCATTCATCTG

● pUC19-ME-mP5

Similar as for pUC19-ME-mP2, pUC19-ME was used as the initial template and two "inside-out"-PCR mutageneses were performed to mutate two base pairs in P5, the first with primers 169 and 170, the second with primers 171 and 172.

169 ME-P5 A

5'-CCATACAGAAGGGTGCCAGGTAAC

170 ME-P5 B

5'-AGGGTGGAGTTTCCTCAGCCCCT

171 ME-P5 C

5'-AGCAAGGACAAATGCTGCCGGT

172 ME-P5 D

5'-CCGGGTGGAGTTTACCGTGCCA

● pUC19-ME-mP17

In analogy to the cloning strategy for pUC19-ME-mP2, pUC19-ME was used as the initial template and two subsequent "inside-out"-PCR mutageneses were carried out to substitute *E. coli* P16-17 for *M. thermoautotrophicus* P16 with primers 173 and 174, and to then substitute *E. coli* P6 for the original P6 with primers 175 and 176.

173 ME-P16-17 A

5'-CCGTACTGAACCCAGGTAGTCCGCCCAGATGAATGCT

174 ME-P16-17 B

5’-GCCGTACCTTATGAACCCCATTTGTCCTTGCATCGGGTGGA

175 ME-P6 A

5’-GCAAGGGTGCCAGGTAACGC

176 ME-P6 B

5’-CCTGATGGGTGGAGTTTCCTCA

● pUC19-ME-mP18

In the first step, the plasmid pHY300-ME-mP18 was constructed by “inside-out”-PCR mutagenesis with primers 154/155 and pHY300-ME as template. In the second step, the mutated P RNA gene ME-mP18 was amplified from pHY300-ME-mP18 with primers 132 plus 147, and inserted into pUC19 cut with *BamH* I and *EcoR* I.

154 P 18 A

5’-TGGCCTAGATGAATGCTGCCGAAACAGAAG

155 P 18 B

5’-GCAATCGCTCACTGGCTCGGGCGGACTACCTCTGCCT

132 BamHI-T7-Mth rnpB

5’-GCG*GGATCC*taatacgactcactataggAGCCGAAGGGCAGCTGACG

147 133 new

5’-CGC*GAATTC* TGCCGAGAGTAACCCACCTTCT

● pUC19-ME-mJ2/3

An “inside-out”-PCR mutagenesis was performed to generate mutation J2/3 with primers 164 and 165. The template was plasmid pUC19-ME.

164 ME-J2/3 A

5’-CGGTCCCTCAAGGGGCTGAG

165 ME-J2/3 B

5’-ΔCΔGCTGCCCTTCGGCTCTATAG

● pUC19-ME-mJ15/18

Based on pUC19-ME, an “inside-out”-PCR mutagenesis with primers 177 and 178 was carried out to generate the mutation J15/18 (underlined).

177 ME-J15/18 A

5’-CAGATGAATGCTGCCGAAACAGA

178 ME-J15/18 B
5’-AGCGGACTACCTCTGCCTCCT

● pUC19-ME-mJ15/18/P1

Using pUC19-ME-mP1 as template, the mutation J15/18 was created by “inside-out”-PCR mutagenesis with primers 177 and 178.

177 ME-J15/18 A
5’-CAGATGAATGCTGCCGAAACAGA
178 ME-J15/18 B
5’-AGCGGACTACCTCTGCCTCCT

● pUC19-ME-mJ15/18/P2

The mutation J15/18 was built into pUC19-ME-mP2 by “inside-out”-PCR mutagenesis with primers 198 and 178.

198 ME-P2-J15/18 A
5’-CAGATGAATGACTGCCGAAACAGA
178 ME-J15/18 B
5’-AGCGGACTACCTCTGCCTCCT

● pUC19-ME-mJ15/18/P4

By “inside-out” PCR mutagenesis, the mutation J15/18 was introduced into pUC19-ME-mP4 with primers 177 and 178.

177 ME-J15/18 A
5’-CAGATGAATGCTGCCGAAACAGA
178 ME-J15/18 B
5’-AGCGGACTACCTCTGCCTCCT

● pUC19-ME-mJ15/18/P5

The mutation J15/18 was introduced into pUC19-ME-mP5 by “inside-out”-PCR mutagenesis with primers 177 and 178.

177 ME-J15/18 A
5’-CAGATGAATGCTGCCGAAACAGA
178 ME-J15/18 B
5’-AGCGGACTACCTCTGCCTCCT

● pUC19-ME-mJ15/18/P17

Using pUC19-ME-mP17 as a template, mutation J15/18 was introduced by "inside-out"-PCR mutagenesis with primers 177 and 183.

177 ME-J15/18 A

5'-CAGATGAATGCTGCCGAAACAGA

183 ME -J15/18-P17 B

5'-AGCGGACTACCTGGGTTCAGTACG

● pUC19-ME-mJ15/18/P18

With primers 182 and 178, the mutation J15/18 was built into pUC19-ME-mP18 by "inside-out" PCR mutagenesis.

182 ME -J15/18-P18 A

5'-CGAGCCAGTGAGCGATTGC

178 ME-J15/18 B

5'-AGCGGACTACCTCTGCCTCCT

● pUC19-ME-mJ15/18/2/3

The combination of the mutations J15/18 and J2/3 was obtained by "inside-out"-PCR mutagenesis with primers 177 plus 178 on the basis of pUC19-ME-mJ2/3.

177 ME-J15/18 A

5'-CAGATGAATGCTGCCGAAACAGA

178 ME-J15/18 B

5'-AGCGGACTACCTCTGCCTCCT

● pUC19-ME-mJ2/3/P2

The mutation J2/3 was introduced into pUC19-ME-mP2 by "inside-out"-PCR mutagenesis with primers 192 and 189.

192 ME-mJ2/3//J15/18//P2ins A

5'-TCΔGΔCGGTCCCTCAAGGGGCT

189 ME-mP2ins B

5'-CTGCCCTTCGGCTCCTATAGTGAGTCGTATTAG

● pUC19-ME-mJ15/18/2/3/P2

Two consecutive "inside-out"-PCR mutageneses were carried out on pUC19-ME-mJ15/18/2/3 to insert an extra base pair (underlined) into P2, the first PCR with primers 192 and 189, the second with 190 and 193.

192 ME-mJ2/3//J15/18//P2ins A

5'-TCGCGGTCCCTCAAGGGGCT

189 ME-mP2ins B

5'-CTGCCCTTCGGCTCCTATAGTGAGTCGTATTAG

190 ME-mP2ins C

5'-ACTGCCGAAACAGAAGGTGGGTTAC

193 ME-mJ2/3//J15/18//P2ins D

5'-CATTCATCTGAGCGGACTACCTCTGC

● pUC19-ME-mJ15/18/2/3/P2/nP1

The initial template was pUC19-ME-mJ15/18/2/3/P2. Two "inside-out"-PCR mutageneses were done to extend P1, first at the 3'-end (primers 186 and 187) and then at the 5'-end (primers 197 and 185).

186 MM-mP1extend C

5'-TGCCCGGGAATTCACTGGCCGTCGTTTTACAACGTC

187 MM-mP1extend D

5'-TGCCGAGAGTAACCCACCTTCTGTTTCG

197 ME-mJ15/18/2/3/P2-P1 extend A

5'-CCGGGCAAGCCGAAGGGCAGTCGC

185 MM-mP1extend B

5'-CCTATAGTGAGTCGTATTAGGATCCTCTAGAGT

● pUC119-MM-nP1

Two "inside-out"-PCR mutageneses were done to extend P1 of pUC119-MM, first at the 5' end (primers 184 and 185) and then at the 3'-end (primers 186 and 187).

184 MM-mP1extend A

5'-CCGGGCAAGCCGAAGGGCAGCTGA

185 MM-mP1extend B

5'-CCTATAGTGAGTCGTATTAGGATCCTCTAGAGT

186 MM-mP1extend C
5’-TGCCCGGGAATTCACTGGCCGTCGTTTTACAACGTC
187 MM-mP1extend D
5’-TGCCGAGAGTAACCCACCTTCTGTTTCG

● pUC19-MM-mJ15/18/P18

By megaprimer mutagenesis, the S-domain of *E. coli* in pUC19-ME-mJ15/18/P18 was replaced with the S-domain of *M. thermoautotrophicus.* The megaprimers were prepared with primers 194 plus 195 and template pUC119-MM.
194 ME-MM A
5’-AGGGGCTGAGGAAACTCCACCCATCATACAGAACCGTGGTGCCGTGAGGCAT
195 ME-MM B
5’-TACAGTAATCACCGGCAGCATTTGTCCTTGCATCCCGTGGAATGGCCGTTTCAC
C

● pUC19-MM-mJ2/3/P2

The cloning strategy was the same as for pUC19-MM-mJ15/18/P18. A megaprimer mutagenesis was done to replace the P RNA S-domain of *E. coli* within pUC19-ME-mJ2/3/P2 with that of *M. thermoautotrophicus.* The megaprimers were amplified from pUC119-MM with primers 194 and 195.
194 ME-MM A
5’-AGGGGCTGAGGAAACTCCACCCATCATACAGAACCGTGGTGCCGTGAGGCAT
195 ME-MM B
5’-TACAGTAATCACCGGCAGCATTTGTCCTTGCATCCCGTGGAATGGCCGTTTCAC
C

● pUC19-MM-mJ15/18/2/3/P2

Following the same cloning strategy as for pUC19-MM-mJ15/18/P18, the S-domain from *E. coli* within pUC19-ME-mJ15/18/2/3/P2 was replaced with that of *M. thermoautotrophicus* by megaprimer mutagenesis. The megaprimers were amplified from pUC119-MM with primers 194 and 195.
194 ME-MM A
5’-AGGGGCTGAGGAAACTCCACCCATCATACAGAACCGTGGTGCCGTGAGGCAT

195 ME-MM B

5’-TACAGTAATCACCGGCAGCATTTGTCCTTGCATCCCGTGGAATGGCCGTTTCAC
C

● pUC19-MM- mJ15/18/2/3/P2/nP1

As for pUC19-MM-mJ15/18/P18, a megaprimer mutagenesis was employed to substitute the S-domain of *M. thermoautotrophicus* for the *E. coli* counterpart in pUC19-ME-mJ15/18/2/3/P2/nP1 to the S-domain of *M. thermoautotrophicus*. The megaprimers were amplified from pUC119-MM with primers 194 and 195.

194 ME-MM A

5’-AGGGGCTGAGGAAACTCCACCCATCATACAGAACCGTGGTGCCGTGAGGCAT

195 ME-MM B

5’-TACAGTAATCACCGGCAGCATTTGTCCTTGCATCCCGTGGAATGGCCGTTTCAC
C

● pUC19-ME-mJ2/3/P2-2

Two successive site-directed mutageneses were performed. The first one deleted an A residue in J2/3 of pUC19-ME-mJ2/3/P2 with primers 199 and 200. Based on the first mutagenesis product, the second mutagenesis inserted an A into P2 with primers 201 and 202.

199 ME-J2/3-D A

5’-GCCGAAGGGCAGCTGΔCGGTCCCTCAAGGGGC

200 ME-J2/3-D B

5’-GCCCCTTGAGGGACCGΔCAGCTGCCCTTCGGC

201 ME-P2-I A

5’-GGTAGTCCGCCCAGATGAATAGCTGCCGAAACAGAAGGTGG

202 ME-P2-I B

5’-CCACCTTCTGTTTCGGCAGCTATTCATCTGGGCGGACTACC

● pUC19-MM-mJ2/3/P2-2

Similar as for pUC19-MM-mJ15/18/P18, a megaprimer mutagenesis was done to replace the *E. coli* S-domain in pUC19-ME-mJ2/3/P2-2 with the S-domain of *M. thermoautotrophicus*. The megaprimers were made with primers 194 plus 195 and template pUC119-MM.

194 ME-MM A

5’-AGGGGCTGAGGAAACTCCACCCATCATACAGAACCGTGGTGCCGTGAGGCAT

195 ME-MM B
5’-TACAGTAATCACCGGCAGCATTTGTCCTTGCATCCCGTGGAATGGCCGTTTCAC
C

● pUC19-MM-Marburg

Genomic DNA of *M. thermoautotrophicus* strain Marburg was extracted with the QIAGEN DNeasy® kit, and then used as a template to amplify the P RNA gene of this strain with primers 203 and 204. The P RNA gene was subsequently ligated into pUC19 via *BamH* I and *EcoR* I.

203 MM-Marburg A
5’-CGC*GGATCC*taatacgactcactatagAGCCGAAGGGCAGCTGAC
204 MM-Marburg B
5’-CGC*GAATTC*TGCCGAGAGTAACCCACCTTC

● pUC19-MM-Marburg-nP1(AU)

The cloning strategy was identical to that for pUC19-MM-Marburg. The extracted genomic DNA from *M. thermoautotrophicus* strain Marburg was used as template to amplify the P RNA gene of this strain with primers 205 and 206. The P RNA gene was then ligated into pUC19 after digestion of vector and PCR product with *BamH* I and *EcoR* I. The two primers introduced a sequence stretch encoding a longer P1 at the 5’ end.

205 MM-Marburg-nP1 A
5’-CGC*GGATCC*taatacgactcactatagACCGGGCAAGCCGAAGGGCAG
206 MM-Marburg-nP1 B
5’-CGC*GAATTC*ACCGGGCATGCCGAGAGTAACCCAC

● pUC19-MM-Marburg-nnP1

Likewise, genomic DNA from *M. thermoautotrophicus* strain Marburg was used as template to amplifiy the P RNA gene with primers 222 and 223, resulting in P1 ends as determined by RACE. Again, the PCR product containing the P RNA gene was subsequently ligated into pUC19 via *BamH* I and *EcoR* I restriction sites.

222 MM-Marburg-nP1 C
5’-CGC*GGATCC*taatacgactcactatagCGGGCAAGCCGGAGGGCAG
223 MM-Marburg-nP1 D
5’-CGC*GAATTC*AGGGCATGCCGGGAGTAACCCAC

● ME-HH

To produce transcripts with homogenous 3' ends, the PCR product ME-HH, containing the ME P RNA gene plus a *cis*-hammerhead ribozyme cassette immediately downstream, was used as a template for T7 transcription. To construct ME-HH, a PCR was performed with template pUC19-ME and primers 132 and 287. The coding sequence for the *cis*-hammerhead ribozyme was included at the 5'-end of the reverse primer (in bold).

132 BamHI-T7-Mth rnpB

5'-GCG*GGATCC*taatacgactcactataggAGCCGAAGGGCAGCTGACG

287 HH

5'-**TATTACGTTTCGTCCTCACGGACTCATCAAACCGGAAAGCACATCCGGT GACG**TGCCGAGAGTAACCCAC

● ME-mJ15/18/2/3/P2-HH

As for ME-HH, the transcription template ME-mJ15/18/2/3/P2-HH was prepared by PCR with template pUC19-ME-mJ15/18/2/3/P2 and primers 288 and 287.

288 BamHI-T7-Mth rnpB-J2/3/P2

5'-taatacgactcactataggAGCCGAAGGGCAGTCGCG

287 HH

5'-**TATTACGTTTCGTCCTCACGGACTCATCAAACCGGAAAGCACATCCGGT GACG**TGCCGAGAGTAACCCAC

● pUC19-Hsa

In order to ensure an accurate *H. sapiens* P RNA gene sequence for our downstream experiments, the gene was first cloned into a TOPO vector to determine its sequence: The gene was amplified from Hela genomic DNA with primers 224 and 225 and ligated into PCR2.1-TOPO vector with the TOPO TA cloning kit (Invitrogen). The pair of primers 233 and 234, comprising parts of the P RNA gene sequence, were then designed according to the sequencing result and used to amplify the *H. sapiens* P RNA gene from the plasmid. Subsequently, the amplified P RNA gene was cloned into pUC19 via digestion of PCR product and vector with *BamH* I and *EcoR* I.

224 H1RNA end A

5'-CTGTATGAGACCACTCTTTCCC

225 H1RNA end B

5'-CGGTTTCGTTTTGTTTTTTTTTTTTTTTTTTTTTTCCAAA

233 BamHI-T7-H1

5’-GCG*GGATCC*taatacgactcactataggATAGGGCGGAGGGAAGCTC

234 H1-EcoRI

5’-CGC*GAATTC*AATGGGCGGAGGAGAGTAGTCT

● pUC19-Hsa-mΔ298C325

The two single nucleotide mutations Δ298 and C325 were built into the human P RNA gene by two subsequent site-directed mutageneses. One introduced the mutation C325 into the plasmid pUC19-Hsa with primers 241 and 242. The other deleted G298 of the first mutagenesis product with primers 243 and 244.

241 H1-C A

5’-GACCTCATAACCCAATTCAGACCACTCTCCTCCGCCCATTTTTG

242 H1-C B

5’-CAAAAATGGGCGGAGGAGAGTGGTCTGAATTGGGTTATGAGGTC

243 H1-P19 A

5’-GCTGAGGTGAGGTACCCCGΔAGGGGACCTCATAACCCAATTC

244 H1-P19 B

5’-GAATTGGGTTATGAGGTCCCCTΔCGGGGTACCTCACCTCAGC

● pUC19-Hsa-mΔ298C325-P5/P15

A two-step cloning strategy was used. In the first step, one part of the mutation P5/P15 was inserted by “inside-out”-PCR mutagenesis with primers 245 plus 246 and template pUC19-Hsa-mΔ298C325. In the second step that used the first mutagenesis product as a template, another “inside-out”-PCR mutagenesis inserted the other part of the mutation P5/P15 with primers 247 and 248.

245 H1-P5/P15 A

5’-ATGGTAGGGGCTCAGATCAATGGCTGAGGTGAGGTAC

246 H1-P5/P15 B

5’-CATTTGGGTTΔGCTCCGGCCGTGAGTCTGTTCCAAGC

247 H1-P5/P15 C

5’-CACTAGGGCCAGAGGCGGCCCTAAC

248 H1-P5/P15 D

5’-GAGCTCAGACCTTCCCAAGGGACATG

● pUC19-Hsa-mΔ298C325-P2-3/J3/4

Using pUC19-Hsa-mΔ298C325 as a template, mutation P2-3/J3/4 was created by "inside-out"-PCR mutagenesis with primers 251 and 252.

251 H1-P2-3 A

5'-CTGTCACTCCACTCCCATGTCCCTTGAGGAAGGTCTGAGACTAGGGCCA

252 H1- P2-3 B

5'-GACGCACTCAGCTCGTGGCCCCTGCGGCTGAGCTTCCCTCCGCCCT

● pUC19-Hsa-mΔ298C325-P4/J4/19

By "inside-out" PCR mutagenesis, the mutation P4/J4/19 was introduced into pUC19-Hsa-mΔ298C325 with primers 257 and 256.

257 249 new

5'-CAGΔCCTACTCTCCTCCGCCCATTGAATTCA

256 250 new

5'-AGTTCTGTTATGAGGTCCCCTCGGGGTA

● pUC19-Hsa-mΔ298C325-P2-4/J4/19

This plasmid combined the mutations P4/J4/19 and P2-3/J3/4. On the basis of plasmid pUC19-Hsa-mΔ298C325-P2-3/J3/4, the mutation P4/J4/19 (underlined nucleotides) was introduced by "inside-out"-PCR mutagenesis with primers 257 and 256.

257 249 new

5'-CAGΔCCTACTCTCCTCCGCCCATTGAATTCA

256 250 new

5'-AGTTCTGTTATGAGGTCCCCTCGGGGTA

● pUC19-Hsa-mΔ298C325-P1/P9

Based on the plasmid pUC19-Hsa-mΔ298C325, a DNA sequence encoding *Thermus thermophilus* P9 was introduced by "inside-out"-PCR mutagenesis with primers 258 and 254. The single nucleotide mutation (one A missing in L9) in the plasmid obtained was corrected by site-directed mutagenesis with primers 279 and 280. Then the corrected pUC19-Hsa-mΔ298C325-P9 was used as a template to amplify the new P RNA gene Hsa-mΔ298C325-P1/P9 with primers 271 and 272 including DNA encoding *T. th.* P1. Afterwards, the new P RNA gene was cloned into pUC19 via *BamH* I and *EcoR* I.

258 253new

5’-ACCCGACGTGAGTTCCCAGAGAACG

254 H1-P9 B

5’-TACCCCGCAGCCCTGTTAGGGCCGC

279 insert A a

5’-GCCCTAACAGGGCTGCGGGGTAACCCGACGTGAGTTCCCAGAG

280 insert A b

5’-CTCTGGGAACTCACGTCGGGTTACCCCGCAGCCCTGTTAGGGC

271 P1 A

5’-CGC*GGATCC*taatacgactcactatagGGGAATTCCGGGACGAGGGCTCATCAGTGGGGC CAC

272 P1 B

5’-CGC*GAATTC*GCCTCCGGGACGAGGCGTGGTCTGAATTGGGTTATGA

● pUC19-Hsa-mΔ298C325-P3

A sequence stretch encoding P3 of *Bacillus stearothermophilus* P RNA was inserted into pUC19-Hsa-mΔ298C325 by “inside-out”-PCR mutagenesis with primers 273 and 274 to replace human P3. Simultaneously, the mutations of mutant P2-3/J3/4 (underlined nucleotides) were built in.

273 P3 A

P3- part Hsa

5’-CGGTTTCGGCCGTAGAGGAAGGTCTGAGACTAGGGCCAGA

274 P3 B

5’-GCCGCAGCGGCTGAGCTTCCCTCCGCCCTAT

● pUC19-Hsa-mΔ298C325-pATSerUG-5

In the T7 transcript obtained from this plasmid (see Fig. 4.3.6), a pATSerUG substrate is covalently tethered to the new 5’-end (between P7 and P2) of a circularly permuted H1 RNA 1 with its helix P1 capped by loop. The permuted enzyme-substrate conjugate was constructed in several PCR steps. First, three PCRs were done separately to amplify the segments of the pATSerUG substrate coding region (primers: 261 and 262; template: pUC19-pATSerUG-PstI), the 5’ part of the H1 RNA gene (primers: 263 and 264; template: pUC19-Hsa-mΔ298C325) as well as the 3’ part of the H1 RNA gene (primers 265 and 266; template: pUC19-Hsa-mΔ298C325). PCR products 1 and 2, and 2 and 3 overlapped with each other.

The three segments were purified by agarose gel electrophoresis and then employed as templates of a new PCR. In this PCR, primers 261 and 266 amplified the final product, which was digested with *EcoR* I and *BamH* I and cloned into pUC19 to yield plasmid pUC19-Hsa-mΔ298C325-pATSerUG-5. Accidental mutations in the substrate portion were corrected with primers 283 and 284 by "inside-out"-PCR mutagenesis.

261 BamHI-T7-pATSer

5'-CGC*GGATCC*taatacgactcactatagGATCTGAATGGAGAGAGGGGGT

262 Hsa-pATSer A

5'-GCCATTGAACTCACTACCGGATCCTGGCGGA

263 pATSer-Hsa A

5'-GATCCGGTAGTGAGTTCAATGGCTGAGGTGAGGT

264 link-Hsa-3

5'-GATCGAGTAAATCAGGTGAAAATGGGCGGAGGAGAGTGGGT

265 link-Hsa-5

5'-TTCACCTGATTTACTCGATCATAGGGCGGAGGGAAGCTCATCAG

266 EcoRI-Hsa

5'-CGC*GAATTC*TTCGCTGGCCGTGAGTCTGTT

283 corr mut 5 A

5'-TCTCCGCCAGCATGCGGTAGTGAGTTCAATGGCTGAGGTG

284 corr mut 5 B

5'-GAGGGGGATTTGAACCCCCTCTCTCCATTCAGATCCTATAG

● pUC19-Hsa-mΔ298C325-pATSerUG-3

Here, the pATSer substrate was tethered to the new 3'-end of the circularly permuted H1 RNA 1 (see Fig. 4.3.6). The cloning strategy was the same as for pUC19-Hsa-mΔ298C325-pATSerUG-5. The 5' part of the H1 RNA gene (primers: 267 and 264; template: pUC19-Hsa-mΔ298C325), the 3' part of the H1 RNA gene (primers: 265 and 268; template: pUC19-Hsa-mΔ298C325) as well as the pATSerUG coding region (primers: 269 and 270; template: pUC19-pATSerUG-PstI) were amplified separately. Using the three gel-purified PCR fragments as templates, overlap extension PCR with primers 267 and 270 amplified the full-length construct that was subsequently cloned into pUC19. Finally, a coincidental mutation was corrected by "inside-out"-PCR mutagenesis using primers 281 and 282.

267 BamHI-T7-G-Hsa

5'-CGC*GGATCC*taatacgactcactataggAATGGCTGAGGTGAGGTACCCCG

264 link-Hsa-3

5’-GATCGAGTAAATCAGGTGAAAATGGGCGGAGGAGAGTGGGT

265 link-Hsa-5

5’-TTCACCTGATTTACTCGATCATAGGGCGGAGGGAAGCTCATCAG

268 pATSer-Hsa B

5’-GATCGCCATAACTCACTTCGCTGGCCGTG

269 Hsa-pATSer B

5’-GAAGTGAGTTATGGCGATCTGAATGGAGAG

270 EcoRI -pATSer

5’-CGC*GAATTC*TGGCGGAGAGAGGGGGAT

281 D-seg A

5’-ΔGAGGGGGTTCAAATCCCCCTCT

282 D-seg B

5’-TCTCCATTCAGATCGCCATAACTCA

● pUC19-Hsa-mΔ298C325-P15-pATSerUG-5

To prepare the RNA fragment of H1 RNA 1-P15-pATSerUG-5 (see Fig. 4.3.6), two “inside-out”-PCR mutageneses inserted a sequence stretch encoding a designed P15 into pUC19-Hsa-mΔ298C325-pATSerUG-5, while the linker between the P RNA and substrate moieties was shortened. DNA encoding the 3’ part of P15 was introduced by the first mutagenesis with primers 291 and 292. The sequence encoding the 5’ part of P15 was subsequently introduced by the second mutagenesis with primers 289 and 290. Primers 293 and 294 were used to correct an incidental mutation by site-directed mutagenesis.

291 P5-5 C

5’-AGAATTCACTGGCCGTCGTTTTAC

292 P5-5 D

5’-ATTTCGGCTTCGCTGGCCGTGAGTCTGTTC

289 P5-5 A

5’-ATCGGCGTGAGTTCAATGGCTGAGGT

290 P5-5 B

5’-ACGGAGAGAGGGGGATTTGA

293 P5-5 m A

5’-GTTCAAATCCCCCTCTCTCCGTATCGGCGTGAGTTCAATGGCTGAGG

294 P5-5 m B

5’-CCTCAGCCATTGAACTCACGCCGATACGGAGAGAGGGGGATTTGAAC

● pUC19-HE

A megaprimer mutagenesis was employed to replace the S-domain of *H. sapiens* with the S-domain of *E. coli* in pUC19-Hsa-mΔ298C325. The megaprimer was amplified from pHY300-EE with primers 295 and 296.

295 H.sa. catalytic s

5’-CTCCCATGTCCCTTGGGAAGGTCTGAGACTAGGGGTGCCAGGTAACGCCTG

296 H.sa. catalytic as

5’-GTACCTCACCTCAGCCATTGAACTCACTTCGCTGGGTGGAGTTTACCGTGCCA

● pUC19-HE-P4/J4/19

By the same cloning strategy as for pUC19-HE, a megaprimer mutagenesis was performed to replace the S-domain of *H. sapiens* with that of *E. coli* in pUC19-Hsa-mΔ298C325-P4/J4/19. The megaprimer was amplified from pHY300-EE with primers 295 and 296.

295 H.sa. catalytic s

5’-CTCCCATGTCCCTTGGGAAGGTCTGAGACTAGGGGTGCCAGGTAACGCCTG

296 H.sa. catalytic as

5’-GTACCTCACCTCAGCCATTGAACTCACTTCGCTGGGTGGAGTTTACCGTGCCA

● pUC19-HE-P2-4/J4/19

The cloning strategy was similar to that for pUC19-HE. A megaprimer mutagenesis was done to replace the S-domain of *H. sapiens* with the S-domain of *E. coli* in pUC19-Hsa-mΔ298C325-P2-4/J4/19. The megaprimer was amplified from pHY300-EE with primers 301 and 296.

301 24419-H.sa. cat s

5’-CTCCCATGTCCCTTGAGGAAGGTCTGAGACTAGGGGTGCCAGGTAACGCCTG

296 H.sa. catalytic as

5’-GTACCTCACCTCAGCCATTGAACTCACTTCGCTGGGTGGAGTTTACCGTGCCA

● pUC19-HE-P2-5/P15/J4/19

As for construction of pUC19-HE, a megaprimer mutagenesis was employed to replace the S-domain of *H. sapiens* with that of *E. coli* in pUC19-Hsa-mΔ298C325-P2-5/P15/J4/19. The megaprimer was amplified from pHY300-EE with primers 302 and 303.

302 2515419-H.sa. cat s

5’-CTCCCATGTCCCTTGAGGAAGGTCTGAGCTCCACTAGGGGTGCCAGGTAACGCCTG

303 2515419-H.sa. cat as

5’-GCCATTGATCTGAGCCCCTACCATCATTTGGGTTΔGCTCCGGGTGGAGTTTACCGTGCCA

● HE-HH

A *cis*-hammerhead ribozyme encoded within this PCR-derived transcription template permitted to produce chimeric P RNA transcripts with homogenous 3’ ends. The ribozyme cassette was included in the 5’ end of the reverse primer (in bold), resulting in a PCR fragment with the ribozyme cassette behind the P RNA gene. The PCR fragment HE-HH was prepared with primers 233 plus 304 and template pUC19-HE.

233 BamHI-T7-H1

5’-GCG*GGATCC*taatacgactcactataggATAGGGCGGAGGGAAGCTC

304 HH a

5’-**TATTACGTTTCGTCCTCACGGACTCATCAAACCGGAAAGCACATCCGGTGACG**AATGGGCGGAGGAGAGTAGTCT

● HE-P4/J4/19-HH

Likewise, the PCR fragment of HE-P4/J4/19-HH was prepared with primers 233 plus 305 and template pUC19-HE-P4/J4/19.

233 BamHI-T7-H1

5’-GCG*GGATCC*taatacgactcactataggATAGGGCGGAGGGAAGCTC

305 HH b

5’-**TATTACGTTTCGTCCTCACGGACTCATCAAACCGGAAAGCACATCCGGTGACG**AATGGGCGGAGGAGAGTAGGCT

● H1 RNA-mΔ298C325-HH

In the same way as for HE-HH, the PCR fragment of H1 RNA-mΔ298C325-HH was amplified with primers 233 and 304 and template pUC19-Hsa-mΔ298C325.

233 BamHI-T7-H1

5’-GCG*GGATCC*taatacgactcactataggATAGGGCGGAGGGAAGCTC

304 HH a

5’-**TATTACGTTTCGTCCTCACGGACTCATCAAACCGGAAAGCACATCCGGTGACG**AATGGGCGGAGGAGAGTAGTCT

3.3 Complementation assays

3.3.1 Complementation assays with DW2 strain

DW2 (Waugh and Pace 1990) is an *E. coli* RNase P mutant strain in which the chromosomal *rnpB* gene was replaced with a chloramphenicol acetyltransferase gene. The *rnpB* gene essential for cell survival is provided on a plasmid, pDW160, which confers kanamycin resistance and is temperature-sensitive for replication, causing the plasmid-harboring strain (DW2/pDW160) not to be viable at 42°C. The conditionally lethal phenotype at 42°C can be suppressed by the expression of a functional P RNA gene from a second compatible plasmid. Accordingly, P RNA genes to be tested for complementation were provided on a plasmid, and cell growth at 42°C was monitored. The disadvantage of the strain is an unstable phenotype, sometimes leading to ambiguous results.

3.3.1.1 Preparation of electrocompetent *E. coli* cells (DW2)

DW2 was first spread on an LB agar plate from a glycerol stock (-80°C) and incubated at 30°C for about 16 h. Then one freshly developed colony was inoculated into 3 ml of LB medium and growth was continued overnight or for at least 6 h while shaking. Afterwards, the culture was transferred into 500 ml of fresh LB medium to continue growth until an OD_{578} of 0.5-0.6 was reached (about 4 h). All LB media and agar plates were supplemented with 30 µg/ml chloramphenicol. The cells were transferred into two centrifuge bottles and, after cooling on ice for 10 min, harvested at 4,000 rpm (Eppendorf 5810R) for 15 min at 4°C. The supernatant was discarded. Cells were washed three times, first with 500 ml, then with 250 ml, and finally with 20 ml of ice-cold 10% (v/v) glycerol by suspension-centrifugation cycles. Finally, the cells were pelleted and resuspended in 2 ml of ice-cold 10% (v/v) glycerol. Small aliquots were prepared in 1.5 ml vials on ice, frozen in liquid nitrogen and stored at -80°C. Concerning transformation efficiency, electrocompetent cells are usually superior to chemically competent cells.

3.3.1.2 Electroporation with electrocompetent *E. coli* cells (DW2)

Electroporation, or electropermeabilization, is a technique that uses a pulsed electrical field to significantly increase the electrical conductivity and permeability of the cell envelope for nucleic acid transformation or transfection. For bacterial transformation, 10 ng of plasmid DNA were gently mixed with 30 µl of electrocompetent cells. The mixture was transferred into a 1 mm gap cuvette and left on ice for 30-60 s. An electroporator (BIO-RAD, GenePulser Xcell^{TM}) was preset to 1,800 V, 25 µF and 200 Ω. After drying the outer surface, the cuvette

was placed into the slot of the electroporator. The transformation was initiated by pressing the button “pulse”. When the bell of the electroporator rang, 1 ml of LB medium was immediately added into the cuvette and thoroughly mixed with the cells. Then the diluted cells were quickly transferred into a 2 ml vial and shaken at 30°C for 1 h for recovery.

3.3.1.3 Observation of phenotype (DW2)

Following 1 h of shaking at 30°C, the DW2 cells were initially diluted 1:500 with LB medium. Afterward, the diluted DW2 cells were diluted once more 1:350. The second dilution of cells was spread on an LB agar plate (80 µl/plate). As DW2 can tolerate chloramphenicol and test plasmids usually included an ampicillin resistance gene, agar plates were supplemented with 100 µg/ml ampicillin and 30 µg/ml chloramphenicol to select for DW2 cells containing a test plasmid. For each plasmid to be tested, an aliquot of transformed cells was plated on two plates in parallel, to be incubated overnight at 30°C and 42°C, respectively. If too few or too many colonies had grown on the plate incubated at 30°C, a few single colonies were picked and resuspended individually in 500 µl of LB medium. Amounts of cells plated were varied by serial dilution to obtain sufficiently large, but countable numbers of colonies on the 30°C plate. With optimal amounts of cells plated, the comparison of colony numbers (CN) between the plates at 30°C and 42°C indicated the extent of complementation caused by the plasmid-encoded P RNA gene: The bigger the value of $CN_{42°C}/CN_{30°C}$, the more proficient was the tested P RNA gene in functionally replacing the native P RNA. Incubation at 42°C was sometimes prolonged to 48 h to check for retarded growth.

3.3.2 Complementation assays with SSB318 strain

The strain SSB318 (Wegscheid *et al.* 2006) is a *B. subtilis* mutant strain. Its native chromosomal *rnpB* gene is under the control of the IPTG-dependent *spac* promoter. In the absence of IPTG, cell growth relies on the efficient expression of an exogenous P RNA gene provided on a plasmid. A P RNA gene to be tested was normally cloned into a *B. subtilis* plasmid and then transferred into SSB318. If the test P RNA gene is capable of complementation, growth of SSB318 should be observed without IPTG. The strain SSB318 turned out to have a more stable phenotype than DW2.

3.3.2.1 Preparation of naturally competent *B. subtilis* cells (SSB318)

Preparation of competent *B. subtilis* cells was based on a modified two-step procedure (Dubnau and Davidoff.R 1971). In SpC medium, *B. subtilis* cells become naturally competent

when the cells enter stationary growth phase. An SSB318 glycerol stock (-80°C) was first spread on an LB agar plate and incubated at 37°C for about 16 h. One freshly developed colony was then inoculated into 3 ml of SpC medium and grown at 37°C overnight or for at least 6 h while shaking.

SpC medium

T-Base	20 ml
42% (w/v) Glucose	0.24 ml
1.2% (w/v) $MgSO_4 \cdot 7\ H_2O$	0.3 ml
10% (w/v) Yeast extract	0.4 ml

1 liter T-Base

$(NH_4)_2SO_4$	2 g
$K_2HPO_4 \cdot 3H_2O$	18.3 g
KH_2PO_4	6 g
$Na_3Citrat \cdot 2\ H_2O$	1 g
Dissolved in double-distilled water to 1 liter	

Afterwards, the overnight culture was transferred into 20 ml of fresh SpC medium to continue growth until the OD_{578} remained unchanged for 20-30 min (OD_{578} of about 2 for SSB318; if cells are harvested earlier, transformation efficiencies are lower, if harvested later, cells start sporulation). Cells were diluted 1:10 with prewarmed SpII medium and grown for another 1.5 h at 37°C, followed by harvesting at 6,000 rpm (Eppendorf 5810R) for 15 min at 4°C. Cell pellets were resuspended in 20 ml of a mixture (90 % (v/v) supernatant plus 10 % (v/v) glycerol). Using the culture's supernatant for resuspension is crucial, because it contains factors required for transformation. Small aliquots were prepared in 1.5 ml vials on ice, frozen in liquid nitrogen and stored at -80°C. SpC and SpII medium were freshly prepared from sterile stock solutions. For growth of the strain SSB318, 1 mM IPTG, 12.5 µg/ml lincomycin and 0.5 µg/ml erythromycin were supplemented.

SpII medium

T-Base	200 ml
42% (w/v) Glucose	2.4 ml
1.2% (w/v) $MgSO_4 \cdot 7\ H_2O$	14 ml
10% (w/v) Yeast extract	2 ml
0.1 M $CaCl_2$	1 ml

3.3.2.2 Transformation with naturally competent *B. subtilis* cells (SSB318)

Naturally competent cells can take up exogenous DNA without heat or electric force, but are less efficient than electrocompetent and chemically competent cells in transformation. For naturally competent SSB318 cells, 5 µl of miniprep DNA (roughly corresponding to 750 ng) of the test plasmid were used. The DNA to be transformed was mixed with 110 µl of SSB318 competent cells, and then the mixture was incubated at 37°C for 2 h while vigorously shaking.

3.3.2.3 Observation of phenotype (SSB318)

After intensive shaking for 2 h, 50 µl of each cell suspension were spread in parallel on two LB agar plates supplemented with 12.5 µg/ml lincomycin and 0.5 µg/ml erythromycin, one plate with and one without 1 mM IPTG. To screen for cells harbouring the test plasmid, 30 µg/ml tetracyclin was supplemented for pHY300 derivatives, and 20 µg/ml kanamycin for pBsrnpAnHis derivatives. If there had too few or too many colonies grown on the plate containing IPTG after overnight incubation at 37°C, a few single colonies were picked and resuspended in 500 µl of LB medium each. Dilutions for plating were varied such that optimum numbers of colonies were obtained for evaluation, with 50 µl of a 1:50 dilution usually yielding good results. Comparison of colony numbers (CN) between plates with and without IPTG indicated the extent of complementation by the plasmidal P RNA gene, with complementation being the more effective, the larger the ratio of CN_{-IPTG}/CN_{+IPTG}. Colony numbers were usually assessed after 24 h. Incubation was sometimes extended to 48 h to check for retarded growth.

3.3.3 Complementation assays with BW strain

BW is an *E. coli* RNase P mutant strain in which the chromosomal *rnpB* region has been replaced with a cassette called catRExBAD. CatRExBAD is composed of a chloramphenicol resistance gene *cat*, a gene encoding an arabinose operon regulatory protein, *araC*, and an *rnpB* gene under control of the arabinose-inducible pBAD promoter. In this mutant strain, expression of the native *rnpB* gene depends on the presence of the inducer arabinose. The other factor to activate the pBAD promoter is cAMP. It stimulates *araC* and indirectly activates the pBAD promoter. Addition of glucose, which leads to a decrease in cAMP levels, therefore represses basal expression levels of the native *rnpB* gene. To monitor *in vivo* complementation by a P RNA of interest, BW cells were transformed with a plasmid containing a respective gene. Growth on glucose plates, where the native *rnpB* gene is not expressed, indicated the *in vivo* functionality of the P RNA expressed from the plasmid.

3.3.3.1 Preparation of electrocompetent *E. coli* cells (BW)

The mutant strain BW (Wegscheid and Hartmann 2006) was made electrocompetent following the same protocol as for DW2 (3.3.1.1).

3.3.3.2 Electroporation with electrocompetent *E. coli* cells (BW)

Two types of low-copy plasmids were used to assess *in vivo* complementation by *rnpB* genes: derivatives of the plasmid pACYCmitEcm1ApaI harbouring the P RNA gene to be tested; in some cases, plasmid pBR322 pTrc *E. coli rnpA* containing an *E. coli rnpA* gene was co-transformed to overexpress the P protein in order to compensate affinity losses of the plasmid-encoded P RNA for the protein cofactor. Transformation with pBR322 pTrc *E. coli rnpA* and pACYCmitEcm1ApaI (containing wild-type *E. coli rnpB*) was performed in parallel as a positive control.

The protocol was basically the same as for DW2 (3.3.1.2). For BW, 15 ng of each plasmid (pBR322 pTrc *E. coli rnpA* and pACYCmitEcm1ApaI derivative) were mixed with 30 µl of competent cells for electroporation. For *in vivo* complementation assays, the strain BW was grown at 37°C and produced highly reproducible results.

3.3.3.3 Observation of phenotype (BW)

Following electroporation and 1 h of subsequent shaking at 37°C, the BW cells were initially diluted 1:500 with LB medium, followed by a second 1:350 dilution. 80 µl of this second dilution was then spread on an LB agar plate. After overnight incubation, if there were too few or too many colonies growing on the glucose plate, a few single colonies were resuspended in 500 µl of LB medium each and variant dilutions were replated to obtain a satisfactory number of colonies per plate. Colony numbers (CN) on the plates of test *rnpB* and *E. coli rnpB* were compared to assess the complementation efficiency of the test P RNA gene. The closer the ratio of $CN_{test}/CN_{E.coli}$ approached 1, the more efficient was the tested P RNA gene in complementation. As with the other mutant strains, incubation at 37°C was prolonged to 48 h to check for retarded growth.

The plasmid pBR322 pTrc *E. coli rnpA* carries a tetracycline resistance gene; its ampicillin resistance gene has been destroyed by inserting the *E. coli rnpA* gene between the restriction enzyme sites of *Pst* I and *EcoR* I. The *rnpA* gene is expressed under the control of the pTrc promoter and the *rrnB*t1t2 terminator from pTrc99a *E. coli rnpA*. Derivatives of pACYCmitEcm1ApaI carry an ampicillin resistance gene, a native *E. coli rnpB* promoter and

no terminator. Therefore, the LB agar plates were supplemented with 10 µg/ml tetracycline, 100 µg/ml ampicillin, 25 µg/ml chloramphenicol, 1 mM IPTG and 0.5 % (w/v) glucose. Tetracycline and ampicillin were used to select for cells harbouring plasmid pBR322 pTrc *E. coli rnpA* and pACYCmitEcm1ApaI derivatives. Chloramphenicol was required for the BW strain itself. IPTG was needed to induce expression of the *rnpA* gene. Glucose was added to repress the basal expression of the chromosomal *E. coli rnpB*.

3.4 RNA preparation

When working with RNA, special caution needs to be taken because of the high stability and ubiquity of ribonucleases, making RNA vulnerable to degradation and more difficult to handle than DNA. Disposable plastic ware was used wherever possible and gloves were worn for all RNA experiments.

3.4.1 Total RNA extraction

The RNeasy® mini kit (QIAGEN) was used to extract total RNAs from *M. thermoautotrophicus* strain Marburg following the manufacturer's protocol for isolation of total RNA from Gram-positive bacteria. 30 mg of wet cell pellet were first lysed and homogenized in a highly denaturing guanidine-thiocyanate-containing buffer that instantly inactivated RNases. Lysates were then adjusted to appropriate conditions by addition of ethanol and loaded onto an RNeasy Mini spin column. After three washing steps, the fraction of total RNA molecules larger than 200 nucleotides was finally eluted with water. Total RNA thus prepared could be applied to many downstream experiments such as RT-PCR, cDNA synthesis and primer extension.

3.4.2 *In vitro* run-off T7 transcription

3.4.2.1 Transcription

DNA-dependent phage RNA polymerases can transcribe double-stranded as well as single-stranded DNA (Milligan and Uhlenbeck 1989). RNAs in this project were principally prepared by *in vitro* run-off T7 transcription because of its relatively low price and high efficiency. T7 RNA polymerase starts transcribing immediately after its specific promoter 5'-TAATACGACTCACTATA in the 5'=>3' direction. A G nucleotide at position +1 behind the T7 promoter, the first nucleotide to be transcribed, is critically required for reasonably efficient transcription. The DNA template can be either plasmid DNA digested with a restriction enzyme or a purified PCR product. When a PCR product was used, as little as 200

ng of DNA sufficed for successful transcription in 50 µl reactions. Linear plasmid DNA was used straightforward, while PCR products were purified by the QIAquick® PCR Purification Kit (QIAGEN) or Wizard®SV Gel and PCR Clean-Up System (Promega). Typically, a small scale test transcription (50 µl) was done first and analyzed on a PAA gel. If product length and yields were satisfactory, a large scale preparative transcription (1 ml or 2 ml) was subsequently performed.

Digestion of plasmid for run-off T7 transcription, 500 µl

Plasmid DNA (Maxiprep or midiprep)	100 µg
10 x restriction enzyme buffer	50 µl
Double-distilled water	to 495 µl
10 U/µl restriction enzyme[a]	5 µl
Incubation at 37°C for at least 4 h[b]	

a: Additional enzyme was added at a later timepoint during incubation, normally after 2 h, for restriction enzymes with short half-lives. b: Incubation time was often extended to overnight.

Run-off T7 transcription in different scales

	50 µl	**1 ml**	**2 ml**
RNase-free water	28.8 µl	576 µl	1152 µl
1 M HEPES pH 7.5	4 µl	80 µl	160 µl
100 mM DTT	2.5 µl	50 µl	100 µl
2 M $MgCl_2$	0.55 µl	11 µl	22 µl
100 mM Spermidine	0.5 µl	10 µl	20 µl
20 mg/ml BSA	0.3 µl	6 µl	12 µl
1 mg/ml Pyrophosphatase	0.25 µl	5 µl	10 µl
25 mM NTPs	7.6 µl	152 µl	304 µl
200 ng/µl Linear plasmid DNA	5 µl	100 µl	200 µl
200 U/µl T7 RNA polymerase	0.5µl	10 µl	20 µl
Incubation at 37°C for at least 2h			

Transcription reactions were generally pipetted at room temperature. T7 RNA polymerase was added last to start the reaction and the mixture was briefly vortexed. Following 2 h of incubation at 37°C, more T7 RNA polymerase could be added and incubation could be prolonged for several hours, or even carried out overnight. After transcription, RNA products

were in most cases purified by denaturing PAA gels and occasionally by gel filtration using Sephadex columns.

To synthesize RNA to be used for 5'-end ^{32}P-labeling, guanosine was added in excess to the transcription reaction mixture so that the 5' terminal nucleotide of newly synthesized RNA would be guanosine instead of guanosine 5' triphosphate (GTP). Guanosine required to be dissolved at 75°C prior to being added to the reaction mixture, otherwise the protocol was the same as above.

Transcription for RNA to be 5'-end ^{32}P-labeled, 1 ml

RNase-free water	262.5 µl
1 M HEPES pH 7.5	80 µl
100 mM DTT	50 µl
2 M $MgCl_2$	16.5 µl
100 mM Spermidine	10 µl
20 mg/ml BSA	6 µl
1 mg/ml Pyrophosphatase	5 µl
25 mM NTPs	150 µl
200 ng/µl linear plasmid DNA	100 µl
30 mM guanosine (kept at 75°C)	300 µl
200 U/µl T7 RNA polymerase	20 µl
Incubation at 37°C for at least 2h	

3.4.2.2 RNA purification with denaturing PAA gels

In general, phenol/chloroform extraction (3.1.6) was carried out first to remove proteins from the transcripts. Then the transcripts were concentrated by ethanol precipitation (3.1.5) and loaded on a denaturing PAA gel (3.1.2.2) to separate expected products from side products, salts, DNA templates as well as mononucleotides. Wanted bands were visualized by UV shadowing and excised from the gel. Elution of RNA products from the gel pieces was normally done by shaking at 4°C overnight in a volume of elution buffer just sufficient to cover the gel pieces. Buffers used were 1 M NaOAc pH 5.0 and sometimes RNA elution buffer (200 mM Tris/HCl pH 7.0, 1 mM EDTA, 0.1 % SDS). 1 M NH_4OAc pH 7.0 was employed when phosphorothioate-modified RNA was purified. The next day, the supernatant, containing eluted RNA, was subjected to ethanol precipitation, and RNA pellets were finally dissolved in 20-60 µl of RNase-free water.

3.4.2.3 RNA purification with Sephadex columns

In some cases, self-prepared Sephadex columns were used to purify RNA products by gel filtration chromatography. Before loading onto the column, transcripts were concentrated by ethanol precipitation and DNA template was degraded by digestion with DNase (RQ1 DNase, Promega; Turbo DNase, Ambion). A salt-tolerant DNase was favourable in this case. The Sephadex column then retained salts and single nucleotides, as well as small DNA fragments. To be used as a matrix, Sephadex was swelled and then washed three times with double-distilled water. The volume of water was finally adjusted to obtain slurry still able to flow, but very slowly. To prepare a column, the plunger of a 2.5 ml syringe was pulled out. The wide side of the syringe was covered with a piece of microfilter (Whatman®), and then the plunger was pushed back into the syringe. Alternatively, a round Whatman paper perfectly fitting the inner diameter of the syringe could be prepared and deposited on the bottom of the syringe The plunger was then removed carefully to keep the microfilter or Whatman paper in position. Then the syringe was filled with fully preswelled Sephadex™ G-50 slurry, capped with parafilm and packed by centrifugation in a WIFUG X1 centrifuge (6 min, speed No.6). The column was then ready to use. 200 µl of DNase-digested transcription products were slowly pipetted onto the matrix, and the column was centrifuged once again as above. The flow-through contained the purified RNA solution. Enzymes in the solution were removed by phenol/chloroform. Afterwards the RNA was concentrated by ethanol precipitation and dissolved eventually in 10 µl of RNase-free water.

DNase digestion in different scales

	200 µl	**50 µl**
Transcription reaction	170 µl	43 µl
10 x DNase buffer	20 µl	5 µl
2 U/µl DNase	10 µl	2 µl
Incubation at 37°C for at least 30 min		

In some cases, *in vitro* transcription was highly efficient and yielded few side products; also products would be subsequently used for ^{32}P labeling. A small scale transcription (50 µl) was done, followed by DNase digestion and then purification (Sephadex™ G-75 column). 800 µl of preswelled Sephadex (2.5 g/50 ml) slurry was loaded into empty 1 ml commercial columns (Microspin™ columns, Amersham Pharmacia) and then packed at 4000 rpm for 1 min in a tabletop centrifuge. 50 µl of transcription reaction were gently loaded on the center of the

matrix and centrifuged at 4000 rpm for 1 min. The following procedures were the same as above.

3.4.3 RNA with homogeneous 3'-ends

The RNA products synthesized by run-off T7 transcription are in most cases heterogeneous because T7 RNA polymerase tends to add extra non-coded nucleotides to the trannscripts' 3' ends. For some applications such as structural probing, uniform transcripts are required to produce clear results. In this case, electrophoretic separation on denaturing PAA gels is not sufficient to purify RNA from its 3'-end variants, especially for relatively large RNAs like RNase P RNA. In order to eliminate 3'-end heterogeneity, an elegant approach is the use of a self-cleaving hammerhead ribozyme tethered to the 3' end of the RNA of interest (Figure 3.4.3). After transcription termination by the polymerase, the hammerhead ribozyme folds into an active conformation and self-cleaves to release the upstream portion of the transcripts with homogeneous 3'-ends.

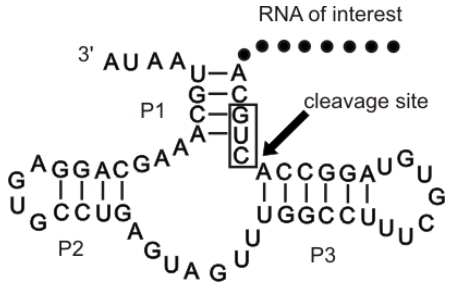

Figure 3.4.3: Self-cleaving hammerhead ribozyme. The RNA of interest is indicated as black dots. The self-cleavage site is marked with an arrow. The trinucleotide sequence GUC (boxed) is optimal for efficient catalysis. The two nucleotides upstream of GUC are variable, as long as helix P1 integrity is maintained by complementary changes in the 3' part of P1.

The DNA templates for such ribozyme-tethered RNA transcripts were produced by PCR. The T7 promoter was brought in through the sense primer, and the gene encoding the *cis*-hammerhead ribozyme through the antisense primer. Under conditions of standard transcription reactions, self-cleavage was usually close to completion by the time the transcription reaction was stopped. If *cis*-cleavage was inefficient, Mg^{2+} concentrations were increased and the incubation time was prolonged.

RNA transcripts cleaved by a hammerhead ribozyme have a 2', 3'-cyclic phosphate at their 3' end, which needs to be removed for downstream applications that require 3'-hydroxyl termini. To hydrolyze 2', 3'-cyclic phosphates, T4 polynucleotide kinase (T4 PNK, MBI Fermentas) was employed as a 3'-phosphatase. Following Sephadex^{TM} G-75 gel filtration (3.4.2.3),

transcripts pelleted from a 50 µl transcription reaction were dissolved in 78 µl of RNase-free water and further mixed with 5 x buffer P as well as T4 PNK. After incubation at 37°C for 2 h, additional T4 PNK was added and the reaction was incubated for another 1 h. It needs to be mentioned that the reaction was performed at pH 6.5 despite the optimum being pH 6.0 for the phosphatase activity of T4 PNK. However, RNA carrying randomly distributed phosphorothioates is sensitive to acid condition, so pH 6.5 was chosen to ensure reasonably efficient 3'-end dephosphorylation as well as RNA stability.

5 x Buffer P

MES pH 6.5 (37°C)	250 mM
$MgCl_2$	500 mM

Hydrolysis of 2', 3'-cyclic phosphate, 100 µl

Purified transcripts	78 µl
5 x Buffer P	20 µl
10 U/µl T4 PNK	2 µl
Incubation at 37°C for 2 h	
Addition of 1 µl of T4 PNK	
Incubation at 37°C for 1 h	

3.4.4 RNA carrying randomly distributed phosphorothioate analogues

Hydrolysis of RNA carrying randomly distributed phosphorothioates by iodine was utilized to generate size ladders for RNA structural probing. The *in vitro* run-off transcription was carried out with a self-prepared Y639F mutant T7 RNA polymerase in the presence of *S*p-ITPαS. In contrast to the wild-type polymerase, the Y639F enzyme shows increased tolerance to modified functional groups in the minor groove. *S*p-ITPαS is an NTP analogue in which sulfur replaces one of the non-bridging phosphate oxygens. The configuration at the phosphorus atom is inverted to *R* during polymerisation, so that *R*p-phosphorothioate-modified RNAs are the final products.

Transcription of *Rp*-phosphorothioate-modified RNA, 50 µl

RNase-free water	2.2 µl
1 M HEPES pH 7.5	4 µl
100 mM DTT	7.5 µl
2 M $MgCl_2$	0.8 µl
100 mM Spermidine	0.5 µl
5 mM *Sp*-ITPαS	1 µl
1 mg/ml Pyrophosphatase	0.5 µl
25 mM NTPs	7.5 µl
200 ng/µl linear plasmid DNA	10 µl
30 mM guanosine (kept at 75°C)	15 µl
200 U/µl T7 RNA polymerase	1 µl
Incubation at 37°C for at least 2 h	

50 µl of transcription was set up and afterwards purified by Sephadex™ G-75 columns (3.4.2.3) or PAGE (3.1.2.2). Because phosphorothioate-modified RNA is acid-labile, 1 M NH_4OAc pH 7.0 was used for gel elution (3.4.2.2) and 1/5 volume of 2 M NH_4OAc pH 7.0 for ethanol precipitation (3.1.5) instead of the usual 1 M NaOAc pH 5.0 for gel elution and 1/10 volume of 3 M NaOAc pH 5.0 for EtOH precipitation. The composition of the transcription reaction mixture was optimized to generate RNAs in which each RNase P RNA molecule carries about one modification.

3.4.5 Biotin-labeled RNA

Biotin-labeled RNA was used in downstream experiments where RNA was coupled to streptavidin-coated magnetic beads, such as in a cooperation project with M. Meyer and M. Keusgen (Pharmazeutische Chemie, Marburg) where we used beads-labeled RNA for affinity measurements based on the fact that when positioned in an excitation coil, paramagnetic beads influence the magnetic field.

Gel-purified RNA was used as starting material. In a first step, the RNA was oxidized by KIO_4 to generate a dialdehyde susceptible to nucleophilic attack at the RNA's 3' end. In a second step, this dialdehyde reacted with a nucleophilic biotin hydrazide derivative. The new compound was finally stabilized by borohydride reduction. (Hansske and Cramer 1979; Vonahsen and Noller 1995)

Oxidation of RNA, 100 µl	
RNA	3-4 nmol
50 mM KIO_4[a]	80 µl
RNase-free water	to 100 µl
Incubation at room temperature for 1 h in the dark	

a: KIO_4 was dissolved in RNase-free water by adjusting to pH 7.0 with 10 M NaOH. Higher pH increases solubility, but decreases reaction yield.

The oxidation reaction was stopped by mixing with 100 µl of 50 % ethylene glycol and subsequent ethanol precipitation. Then the 3'-terminally oxidized RNA was dissolved in 100 µl of 10 mM (+)-biotinamidohexanoic acid hydrazide and incubated at 37°C for 2 h to attach the biotin tag to the RNA. As a final step, 100 µl of 0.2 M $NaHB_4$ and 200 µl of 1 M Tris/HCl pH 8.2 were added. The reaction was placed on ice for 30 min in the dark. Downstream purification was done by sephadex columns (3.4.2.3) to remove salts and coupling reagents. When purity was not sufficient, further purification was done by the RNeasy® mini kit (QIAGEN). When preparing the solutions required, incubating the biotinamidohexanoic acid hydrazide at 95°C for 2 min helped dissolving it, as it has low solubility in water. Also, the 0.2 M $NaBH_4$ solution was freshly prepared in small portions as it releases free hydrogen.

Quality assessment of biotinylated RNA was performed by incubation with 0.2-2 µg streptavidin in a buffer of 10 mM Tris/HCl pH 7.4, 2.5 mM $MgCl_2$ and 100 mM NaCl. Biotinylated RNA displays slow migration on agarose gel due to its bigger size after binding to streptavidin. In most cases, almost all RNA was biotin-labeled, with no band corresponding to unlabeled RNA being visible on the test gel.

3.5 *E. coli* RNase P protein preparation

For RNase P holoenzyme analysis, mostly recombinant *E. coli* RNase P protein (around 13 kDa) was used in conjunction with *in vitro* transcribed P RNA.

3.5.1 Protein preparation

E. coli RNase P protein carrying an N-terminal His-tag (His-tagged peptide leader: MRGSHHHHHHGS, encoded in plasmid pQE-30 in *E. coli* JM109) was expressed essentially as described (Rivera-Leon *et al.* 1995). First, 25 ml of LB medium supplemented with 100 µg/ml ampicillin were inoculated with a glycerol stock and grown overnight at 37°C

under vigorous shaking. The next morning, 10 ml of the cells were transferred into 500 ml of LB medium containing 100 µg/ml ampicillin and growth was continued to an OD_{578} of 0.6 (2-3 h). Then IPTG was added to a final concentration of 1 mM to induce P protein expression. The cells were harvested after 3 h (OD_{578} ~ 2.5) at 4,000 rpm (Eppendorf 5810R) for 15 min at 4°C. The following steps were performed at 4°C or on ice if not stated otherwise, and all buffers contained 40 µg/ml of the protease inhibitor phenylmethylsulfonyl fluoride (PMSF, stock in isopropanol). The cells were then resuspended in 10 to 15 ml of sonication buffer SB (50 mM Tris-HCl, pH 8.0, 0. 3 M NaCl, 0.1 % triton X-100, 1 M NH_4Cl). Before sonication, lysozyme was added and the sample was incubated at room temperature for 10 min to help release proteins. During sonication (Branson Sonifier 250, output 20, duty cycle 50 %, 15 min on ice-water mixture), care was taken not to heat the sample, as the *E. coli* P protein is extremely sensitive to heat. Successful sonication resulted in a solution slightly cleared as compared to the unsonicated lysate. After sonication, the sample was centrifuged for 30 min (4°C, 14500 x g), and the supernatant, containing proteins, was mixed with Ni-NTA agarose (400 µl for 2 liters of cell culture) which had been prewashed twice with 10 ml SB buffer. The sample was incubated for 1 to 2 h at 4°C under gentle mixing or rotating to catch P protein tethered with a His-tag. The Ni-NTA agarose slurry was washed three times (centrifugation-suspension cycles; centrifugation at 4°C and 4,000 rpm in a tabletop centrifuge) with ice-cold washing buffer (30 mM imidazol, 50 mM Tris-HCl, pH 8.0, 8 M urea, 0.1 % triton X-100). The RNase P protein started to precipitate during this procedure; the supernatant after each washing step was therefore removed carefully to avoid release of protein aggregates from the matrix. The protein was then eluted with 500 µl of elution buffer (50 mM Tris-HCl, pH 7.0, 10 % glycerol, 7 M urea, 20 mM EDTA, and 0.3 M imidazol) for 45 min at 4°C under gentle shaking. The eluate was dialyzed twice for 1 h and subsequently overnight against 500 ml of dialysis buffer (50 mM Tris-HCl, pH 7.0, 0.1 M NaCl, 10 % glycerol; dialysis bags: Roth, molecular weight cut off 12-14 kDa). During dialysis, a white precipitate sometimes formed. The content of the dialysis bags was transferred to a 2 ml tube and centrifuged for 20 min at 4°C and 12,000 rpm in a tabletop centrifuge. The supernatant contained RNase P protein devoid of any P RNA contamination, whereas the pellet included traces of P RNA and was hence discarded. All purification steps were monitored by 15 % SDS-PAGE to assess the purity and concentration of RNase P protein.

3.5.2 Methods used in protein preparation

3.5.2.1 SDS-PAGE

SDS-PAGE stands for a polyacrylamide gel electrophoresis (3.1.2.2) using sodium dodecyl sulfate. The method is used to separate proteins according to their sizes. SDS is an anionic detergent which fulfills the roles of releasing proteins from cells, denaturing the proteins to their primary linear shape, and coating them with a number of negative charges proportional to the proteins' lengths.

Typically, samples were incubated at 95°C for a few minutes with an SDS solution and then loaded on a PAA gel composed of a stacking gel on the top and a separation gel at the bottom. For the analysis of recombinant RNase P protein, a Mini Protean. 3 cell chamber system (BioRad) was used. To prepare the gel, a 15 % separation gel solution was first prepared. After adding APS and TEMED, the solution was immediately poured between two assembled gel plates with a 1 ml pipette and sealed with 1 ml of isopropanol to obtain an even surface and expel air bubbles. After the separation gel had become solid, the isopropanol was poured off and the gel was left for several minutes to completely evaporate residual isopropanol. Then a 4 % stacking gel solution to which APS and TEMED had been added was cast on the top of the separation gel and a 0.75 mm thick comb was inserted. After polymerization, the glass plates containing the gel were fixed in the electrophoresis apparatus and the chamber was filled with 1 x running buffer (diluted from Rotiphorese® 10 x SDS-PAGE, ROTH). The proteins to be checked were respectively mixed with 5 x protein loading buffer, heated for 5 min at 95°C, and were then instantly loaded on the gel. Aliquots of cell suspension taken prior to IPTG induction and harvesting (normally 1 ml) were centrifuged for 5 min at 10,000 rpm in a tabletop centrifuge, and then the sediment was resuspended in an appropriate volume of double-distilled water. For example, if a cell suspension aliquot (1 ml) was withdrawn at an OD_{578} of 0.6, the aliquot was suspended in 60 µl of water; if the OD_{578} had been 2.5, the aliquot was resuspended in 250 µl of water. 10 µl sample were mixed with 2.5 µl of 5 x protein loading buffer, heated for 5 min at 95°C and immediately loaded on the gel. A prestained protein marker, covering a broad range of molecular weights (6 to 175 kDa; New England Biolabs), was loaded adjacent to the samples. The gel was run at 35 V until the dye BPB had migrated into the separation gel, whereafter voltage was switched to 90 V. Coomassie Brilliant Blue was used to stain and distilled water to destain the gel. For staining, the gel was soaked in gel staining solution and incubated at room temperature for 30 min while shaking. For destaining, the stained gel was transferred into a 250 ml beaker, covered with 150 ml of distilled water and shaken overnight at room temperature. Exchanging distilled

water during destaining improved efficiency. Further, heating the gel to be destained in water in a microwave oven until boiling substantially speeded up destaining, although at the cost of quality of the gel image.

4 x Separation gel buffer

Tris-HCl pH 8.8	1.5 M
SDS	0.6 % (w/v)

4 x Stacking gel buffer

Tris-HCl pH 6.8	0.5 M
SDS	0.6 % (w/v)

Gel solution (for 2 small gels)

	Separation gel	**Stacking gel**
	15 %	4 %
30 % Acrylamide stock (ROTH)	8 ml	1 ml
4 x Separation gel buffer	4 ml	-
4 x Stacking gel buffer	-	1.8 ml
Double-distilled water	4 ml	4.7 ml
10 % APS	80 µl	24 µl
TEMED	20 µl	9 µl

5 x Protein loading buffer

Tris-HCl pH 6.8	160 mM
SDS	2 % (w/v)
2-Mercaptoethanol	5 % (v/v)
Glycerol	40 % (v/v)
Bromophenol blue (BPB)	0.1 % (w/v)

Gel staining solution

Methanol	40 % (v/v)
Acetic acid	10 % (v/v)
Coomassie Brilliant Blue G25	0.5 % (w/v)

3.5.2.2 Dialysis

Dialysis is a common approach to adapt the salt and buffer conditions of macromolecular (often proteins, DNA, or polysaccharides) solutions. The underlying principle is diffusion of solutes across a semi-permeable membrane. Normally, the sample to be purified is loaded in a dialysis tube or bag such as a porous cellulose membrane. The container is then sealed and placed in an excess amount of solution with the identity and concentration of solutes being that ultimately aimed at for the sample to be dialysed. After adequate dialysis, the solutions inside and outside of the dialysis container are identical except for molecules significantly larger than the pores. Accordingly, the selection of dialysis membrane depends on the size of macromolecules to be purified.

To purify the eluate containing *E. coli* RNase P protein, the desired size of dialysis bag (Roth, molecular weight cut off: 12-14,000) was chopped off, boiled for 5 min at 100°C in 400 ml of distilled water, and then transferred into 500 ml of dialysis buffer cooled to 4°C. One edge of the bag was closed with a clip. The eluate was gently pipetted into the bag. Then the other edge of the bag was sealed with a second clip, expelling air bubbles from the dialysis tube for effective dialysis. Finally, the dialysis bag loaded with the eluate was allowed to float in the dialysis buffer at 4°C overnight while softly stirring with a magnetic stirrer. The dialysis buffer was exchanged usually twice during dialysis.

3.5.2.3 Concentration determination of protein

The Bio-Rad protein assay kit and the spectrophotometer Biomate3 (Thermo Spectronic, Rochester NY USA) was used to determine the concentration of RNase P protein. The Bio-Rad protein assay is based on the method of Bradford. An acidic solution of Coomassie® Brilliant Blue G-250 dye is added to the protein solution. The absorbance maximum of the mixture shifts from 465 nm to 595 nm when the dye binds to the protein. Hence a differential colour change of the dye occurs in response to various concentrations of protein.

The program “Bradford-Standard” on Biomate3 was utilized. In a first step, variant concentrations of the standard protein bovine serum albumin (BSA) were measured, by which a standard curve was generated. The components of standard samples 1-6 are listed below. In the second step, the test protein was measured. The program “Bradford-Standard” calculated its concentration automatically. As a rule, a test protein was measured in different concentrations for a few times and an average value was calculated. The samples to be measured were mixed very well using a pipette, avoiding bubbles. Afterward they were incubated at room temperature for 5 min to achieve thorough attachment of the dye to protein.

Preparation of standard protein samples

Standard sample	1	2	3	4	5	6
Double-distilled water	800 µl	780 µl	760 µl	720 µl	700 µl	650 µl
100 µg/ml BSA	-	20 µl	40 µl	80 µl	100 µl	150 µl
Dye reagent concentrate	200 µl	200 µl	200 µl	200 µl	200 µl	200 µl

Preparation of test protein samples

Test sample	1	2
Double-distilled water	798 µl	796 µl
Test protein	2 µl	4 µl
Dye reagent concentrate	200 µl	200 µl

In the last step, measured protein was analyzed by SDS-PAGE next to a protein of known concentration in order to confirm the concentration measurement.

3.5.3 Quality assessment of RNase P protein

SDS-PAGE is capable of detecting the proportion of major side products in protein preparations, but this alone was not sufficient to assess the quality of RNase P protein preparations: Here it was additionally important to verify that the protein preparation was completely void of P RNA contamination and that the P protein was sufficiently active in holoenzyme catalysis. A new preparation of P protein was therefore checked in a series of activity assays with or without *E. coli* P RNA, where no traces of ptRNA cleavage should occur in the absence of P RNA, whereas cleavage rates of reconstituted RNase P holoenzyme should be within the range of those obtained with previous P protein preparations.

3.6 Kinetic assays

In this study, kinetic assays were performed to study cleavage of precursor tRNA (ptRNA) by RNase P, following the reaction scheme below:

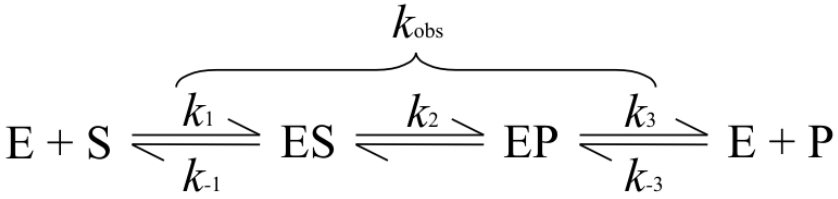

where E = Enzyme (RNase P holoenzyme or RNase P RNA subunit)
S = Substrate (ptRNA)
P = Product (tRNA)
k = Rate constant

Such assays were performed under two different types of conditions:

In **single turnover reactions**, the enzyme concentration is in far excess over that of the substrate ([E]>>[S]). Each enzyme molecule therefore goes through a reaction cycle at most once. Product release thus does not affect the velocity of the reaction, so that the speed of substrate conversion depends on substrate binding (k_1, k_{-1}) or on the rate of the chemical step (k_2).

In **multiple turnover reactions**, the substrate concentration is much higher than the enzyme concentration ([S]>>[E]), so that each enzyme molecule catalyzes the conversion of more than one substrate molecule. This setup is closer to the physiological situation and was applied to the study of holoenzyme reactions. Results of multiple turnover kinetics assays reflect the overall catalytic reaction, and thus may reveal information on substrate binding, enzyme folding, catalysis, product release, and interaction between holoenzyme subunits.

Quantification was done by evaluating the intensity of each band on the gel image scanned from a phosphoimager plate with the program "Aida" (version 3.42, Raytest Isotopenmessgeräte GmbH). The amount of cleaved ptRNA (processed tRNA) equals that of the 5'-flank, so that the proportion of cleaved substrate to total substrate can be determined as $I_{5'\text{-flank}}/(I_{5'\text{-flank}} + I_{\text{uncleaved ptRNA}})$, where I means intensity.

The **single turnover kinetic parameters** k_{obs}, $K_{m(sto)}$ and k_{react} were calculated with the data analysis and graphics program "GraFit" (version 3.04).

k_{obs} is the rate constant observed for a reaction, computed by fitting data to the 1st order rate equation.

$K_{m(sto)}$ is defined as the enzymeor substrate concentration at half-maximal cleavage rate. To assess $K_{m(sto)}$, cleavage rates at several concentrations of P RNA were determined.

k_{react} is the rate constant corresponding to the highest possible reaction velocity where enzyme concentration becomes saturating. Like K_m, k_{react} is calculated from cleavage rates at a set of enzyme concentrations.

For holoenzyme reactions, k_{obs} was determined as above. For reactions containing an excess of substrate over enzyme, k_{obs} values were multiplied with the molar ratio of substrate to enzyme.

3.6.1 5'-endlabeling of substrate with γ-^{32}P-ATP

The γ-phosphate of γ -^{32}P-ATP was transferred to the 5'-hydroxyl terminus of ptRNA or a P RNA-ptRNA conjugate with T4 polynucleotide kinase (T4 PNK, MBI Fermentas). The kinase is inhibited by high levels of salt (50% inhibition by 150 mM NaCl), phosphate (50% inhibition by 7 mM phosphate) and ammonium ions (75% inhibited by 7 mM $(NH_4)_2SO_4$). Hence, the RNA to be labeled should be purified beforehand by denaturing PAGE (3.4.2.2) or gel filtration (3.4.2.3) to remove salts, single nucleotides and small RNA fragments carrying 5'-hydroxyl groups. In addition, the oxidation of dithiothreitol (DTT) in T4 PNK buffer occurs naturally during long term storage and is accelerated by repeated freeze-thaw cycles and excessive heating. Therefore, a small amount of fresh DTT was always added to labeling reactions.

5'-^{32}P -endlabeling reaction, 15 µl

RNA	30 pmol
RNase-free water	to total of 15 µl
10 x T4 PNK buffer A (forward)	1.5 µl
25 mM DTT	1.5 µl
γ-^{32}P-ATP (3000 Ci/mmol, 10 µCi/µl)	3-5 µl
10 U/µl T4 PNK	1.5 or 2 µl
Incubation 37°C for 1-2 h	

Following incubation at 37°C, the labeled RNA was purified on thin gels (0.5 mm thick, 6-8 % denaturing PAGE). Depending on the sizes of the RNA and the chamber, the gel was run at

8-20 mA for 2-3 h to separate labeled full-length RNA from degraded material and, if still present, transcription side products. Then one of the glass plates was removed and the other one with the polyacrylamide gel was wrapped in plastic film. To determine the location of the band of labeled RNA to be excised, three radioactive stickers were affixed to the film and a second sheet of plastic film was put on top. An imaging plate was placed on the gel side of the pack, exposed for 1-2 min and scanned by the phosphoimager. The image, with signals for the RNA bands and the stickers, was printed in 100 % size, and the printout was placed under the gel, using the three stickers for precise orientation. The gel piece with the labeled RNA of interest was then excised according to the position on the printout. Subsequent elution was usually performed with 500 µl of 1 M NaOAc pH 5 for most RNAs, and with 1 M NH_4OAc pH 7.0 for *R*p-phosphorothioate-modified RNA. The labeled RNA was precipitated from the eluate with ethanol and dissolved in 10 µl of RNase-free water.
Before further use in kinetics assays, every batch of labeled ptRNA was tested in a standard reaction for cleavage rates to be similar to those obtained for previous batches.

Dephosphorylation of RNA prior to 5'-labeling increases labeling efficiency and accordingly leads to higher specific radioactivity of labeled material. Such pretreatment was required for substrates used in cleavage assays with H1 RNA variants, where extremely weak catalytic activities needed to be detected. The enzyme used for dephosphorylation was Calf Intestine Alkaline Phosphatase (CIAP, MBI Fermentas). The CIAP enzyme was subsequently removed by extraction with phenol/chloroform and the RNA was concentrated by ethanol precipitation.

5'-end dephosphorylation of RNA, 500 µl

RNA	200 pmol
RNase-free water	to 440 µl
10 x CIAP buffer	50 µl
1 U/µl CIAP	10 µl
Incubation at 37°C for 1 h	

3.6.2 P RNA alone kinetic assays

All P RNA alone kinetic assays in this study were performed under single turnover conditions, employing an excess of P RNA over ptRNA substrate and measuring 5'-end processing. Reaction buffers were designed according to the different types of P RNAs: For bacterial and archaeal P RNAs, the assay buffer contained 50 mM MES pH 6.0 (37°C), 2 mM

EDTA, 100 mM NH_4OAc, and 100 mM $Mg(OAc)_2$. For eukaryotic P RNA, buffer C (50 mM MES pH 6.0 (37°C), 800 mM NH_4OAc) supplemented with 160 mM $Mg(OAc)_2$ was used. The tables below describe an example of a P RNA alone catalytic reaction. P RNA and ptRNA solution were preincubated separately and then combined to start the cleavage reaction. For y reactions analyzed in parallel, 4 x (y + 0.5) µl of ptRNA solution were prepared, of which 4 µl would be added to each 18 µl of P RNA solution. The total volume per reaction was 22 µl, and aliquots of 4 µl each were withdrawn at 5 consecutive time points. For single time point reactions, 10-14 µl of reaction mixture (8 or 10 µl of enzyme solution combined with 2 or 4 µl of substrate solution) was prepared. The samples withdrawn were either immediately mixed with PPF buffer, or precipitated with ethanol, or extracted with phenol/chloroform to stop the cleavage reaction, and then mixed with PPF buffer. Finally, they were resolved on denaturing PAA gels (3.1.2.2). Ethanol precipitation and phenol/chloroform extraction improved gel resolution to some extent.

P RNA mix, 18 µl

P RNA[a]	10 x 22 pmol
5 x Reaction buffer	3.6 µl
2 M $Mg(OAc)_2$	0.9 µl
RNase-free water	to 18 µl
Incubation at 55°C for 5 min and then at 37°C for 35 min	

a: The final concentration of P RNA is 10 µM.

ptRNA mix, 4 µl

ptRNA (^{32}P-labeled)	5.5 x 2000 cpm
5 x Reaction buffer	0.8 µl
2 M $Mg(OAc)_2$	0.2 µl
RNase-free water	to 4 µl
Incubation at 55°C for 5 min and then at 37°C for 25 min	

In order to assess the catalytic activities of H1 RNA variants, 40,000-50,000 cpm radioactive substrate were used for each sample (each lane on the PAA gel) to be resolved.

3.6.3 Holoenzyme kinetic assays

All holoenzyme kinetic assays were performed in KN buffer (20 mM Hepes pH 7.4 (37°C), 150 mM NH_4OAc, 2 mM spermidine, 0.05 mM spermine, and 4 mM β-mercaptoethanol) supplemented with low concentrations of Mg^{2+}. Holoenzyme was reconstituted from P RNA and recombinant P protein in a molar ratio of 1:5. Depending on the enzyme analyzed, amounts of substrate were trace amounts or, in some cases, a ten times molar excess of substrate over enzyme. Solutions of P RNA and ptRNA were preincubated separately. P protein was added to the P RNA solution 5 min before the cleavage reaction was initiated by adding the substrate ptRNA. The total volume of one reaction was 22 µl; samples of 4 µl each were withdrawn at different time points and resolved by denaturing PAGE (3.1.2.2). In each experiment, reactions containing only one enzyme subunit (P protein or P RNA) were run as controls. The setup of an example of a multiple turnover holoenzyme reaction is listed in the two following tables.

Holoenzyme mix, 18 µl

P RNA[a]	0.22 pmol
5 x KN buffer	3.6 µl
45 mM $Mg(OAc)_2$[a]	1.8 µl
RNase-free water	to (18-a) µl
Incubation at 55°C for 5 min and then 37°C for 30 min	
Addition of a µl P protein[a]	
Incubation at 37°C for another 5 min	

a: The final concentrations in 22 µl of reaction: [P RNA] = 10 nM, [P protein] = 50 nM , [Mg^{2+}] = 4.5 mM. P protein was stored in 1.5 µl aliquots at –20°C and was always freshly diluted to the suitable concentration in RNase-free water shortly before use.

ptRNA mix, 4 µl

ptRNA (^{32}P-labeled)	5.5 x 2000 cpm
ptRNA (unlabeled)[a]	2.2 pmol
5 x KN buffer	0.8 µl
45 mM $Mg(OAc)_2$	0.4 µl
RNase-free water	to 4 µl
Incubation at 55°C for 5 min and then at 37°C for 25 min	

a: The final ptRNA concentration in 22 µl of reaction is 100 nM.

For enzymes with low catalytic activity, for instance H1 RNA and its variants, holoenzyme reconstituted from 200 nM P RNA and 1 µM recombinant P protein was analyzed with trace amounts of substrate. Here, substrate labeled to very high specific radioactivity (40,000-50,000 cpm per sample) was used.

3.6.4 *Cis*-cleavage of substrate-RNase P RNA conjugates

Substrate-RNase P RNA conjugates were designed to reduce the effect of substrate binding defects on cleavage. When analyzing cleavage efficiency of such tethered constructs, calcium instead of magnesium ions were usually contained in the preincubation buffer to prevent self-cleavage during preincubation: Magnesium ions help RNA folding and are required for RNase P catalysis, whereas calcium ions equally support folding, but not catalysis. Following preincubation, the reaction was triggered to *cis*-cleave by addition of Mg^{2+}.

In the case of H1 RNA 1-pATSerUG conjugates, the presence of Ca^{2+} instead of Mg^{2+} during preincubation was unnecessary owing to extremely weak catalytic activity of H1 RNA 1. Thus, Mg^{2+} was used throughout the analysis. The conjugates (^{32}P-labeled, 40,000-50,000 cpm) were incubated in buffer C (50 mM MES pH 6.0 (37°C), 800 mM $NH_4(OAc)$ supplemented with 160 mM $Mg(OAc)_2$. A reaction without Mg^{2+} was set up as control. The reaction solution was heated at 55°C for 5 min and afterwards incubated at 37°C for 22 h. Finally the samples were mixed with PPF buffer and resolved on denaturing PAA gels (3.1.2.2).

3.7 Folding analysis by native PAGE

Native PAGE is a type of polyacrylamide gel electrophoresis (3.1.2.2) run under near-physiological conditions, i.e. no denaturing agents such as urea or SDS are involved. During native PAGE, RNAs keep their native secondary/tertiary structure, so that this method can be applied to study RNA folding.

3'-endlabeled RNase P RNAs (20,000 cpm) were incubated in KN buffer (3.6.3) plus 4.5 mM Mg^{2+} at 55°C for 5 min and then 37°C for 50 min to allow RNA folding. As a control, an identical RNA mix was placed at 4°C. Afterwards the samples were adjusted to room temperature, mixed with one volume of 2 x native loading buffer and immediately loaded on a native PAA gel.

2 x Native loading buffer

Glycerol	10 % (v/v)
$MgCl_2$	4.5 mM
Bromophenol blue (BPB)	0.025 % (w/v)
Xylene cyanol blue (XCB)	0.025 % (w/v)

3.7.1 3'-endlabeling of RNA with [5'-^{32}P]pCp

P RNAs to be analyzed for folding by native PAGE were usually radiolabeled at their 3'-ends with [5'-^{32}P]pCp. The labeling reaction was catalyzed by T4 RNA ligase (MBI Fermentas). The purification procedure was the same as for 5'-endlabeled RNA (3.6.1).

3'-^{32}P-endlabeling reaction

RNA	10 pmol	15 pmol
RNase-free water	to total of 6.4 µl	to total of 7.5 µl
10 x T4 RNA ligase buffer[a]	0.64 µl	0.75 µl
2 mM ATP	1 µl	1.2 µl
[5'-^{32}P]pCp (3000 Ci/mmol, 10 µCi/µl)	3 µl	1.5 µl
10 U/µl T4 RNA ligase	1 µl	2 µl
Incubation at room temperature for 2 h and then 4°C overnight		

a: 10 x T4 RNA ligase buffer contains 500 mM HEPES-NaOH (pH 8.0 at 25°C), 100 mM $MgCl_2$, 100 mM DTT.

3.7.2 Native PAGE for analysis of RNA folding

In addition to being non-denaturing, buffer conditions of native PAGE were adjusted to stabilize RNA structure. Under such conditions, different conformers from a single RNA species could be identified by electrophoresis due to a conformation-dependent difference in electrophoretic mobility. In general, the procedure was the same as for denaturing PAGE (3.1.2.2). An 11.25 % thin gel (0.5 mm) was used for better resolution. THE buffer supplemented with 100 mM NH_4OAc and 4.5 mM $MgCl_2$ was used for gel preparation and running. The gel was run in a cold room (4°C) to avoid RNA structure disruption caused by overheating. Ice packs were used to cool the gel when necessary. The gel was run for around 6-7 h until xylene cyanol had migrated 11.5 cm from the pockets. Longer running times tended to give rise to smeary bands. In some cases, gels were dried on a slab gel dryer to improve the quality of the image.

10 x THE buffer

Tris	330 mM
Hepes	660 mM
EDTA	1 mM

PAA gel solution

	60 ml	C_{end}
10 x THE buffer	6 ml	1 x THE buffer
2 M NH_4OAc	3 ml	100 mM
2 M $MgCl_2$	135 µl	4.5 mM
50 % Acrylamide	13.5 ml	11.25 %
Double-distilled water	to 60 ml	

Running buffer

	2 liters	C_{end}
10 x THE buffer	200 ml	1 x THE buffer
2 M NH_4OAc	100 ml	100 mM
2 M $MgCl_2$	4.5 ml	4.5 mM
Double-distilled water	to 2 liters	

3.7.2.1 Drying gels with a slab gel dryer

Gels were dried with a slab gel dryer (Model 483, Bio-rad). Before drying, gels needed to be completely separated from the glass plates, which is difficult for a 0.5 mm thin gel. After removal of one glass plate, two alternative methods were used: (1) The gel was covered with a piece of gel blotting paper (Whatman paper, Roth). As the gel sticks to the paper, the other glass plate could be easily taken off after the stack had been flipped over, and the gel was finally covered with a plastic film. (2) The gel was covered first with a plastic film and then a rigid plastic sheet on top. The rigid sheet was utilized to hold the gel so that the gel could be turned over and the other glass plate could be removed. On this side, 2-3 pieces of gel blotting paper were placed on top of the gel. The gel, layered between plastic foil and blotting paper, was placed on the slab gel dryer with the paper side facing the heated slab. The gel was subsequently sealed with the soft slab of the dryer. After closing the dryer, the pump was switched on to draw vapour. The dryer was set to 60°C for 30 min, and the gel was subsequently cooled down to room temperature for 30 min with the pump still on.

3.8 Rapid amplification of cDNA ends (RACE)

The ends of *M. thermoautotrophicus* (strain Marburg, DSM 2133, *syn. M. marburgensis*) RNase P RNA were mapped by the RACE method. This method is fast and accurate, requires only small amounts of total cellular RNA, and, unlike primer extension analysis, is non-radioactive. Another prominent advantage of RACE over primer extension analysis is that, when combined with tobacco acid pyrophosphatase (TAP) treatment, RACE can distinguish between primary transcripts and processed RNA: Processed RNAs are directly accessible to RACE, whereas primary transcripts, due to their 5' triphosphate, are accessible only after the phosphodiester bond between their α- and β- phosphate groups has been hydrolyzed by TAP.
Total cellular RNAs were extracted from *M. th.* strain Marburg (3.4.1). DNase I (Ambion) was employed to digest possible traces of DNA. Afterwards total RNAs were purified from the digestion reaction by phenol/chloroform extraction and then ethanol precipitation. The purified total RNA was used for both 5'- and 3'-end mapping.

3.8.1 5'-end mapping of RNA

The adapter primer 5'-GTCAGCAATCCCTAAGGAG (GAG: ribonucleotides) was ligated to total RNA by T4 RNA ligase (MBI Fermentas). The RNA was subsequently purified by phenol/chloroform extraction followed by ethanol precipitation. 2 µg of total RNA were used and ultimately dissolved in 10 µl of RNase-free water.

Adapter ligation

Total RNA	2 µg
100 µM 5' adapter primer	2 µl
10 x T4 RNA ligase buffer	2 µl
0.1 % BSA	2 µl
10 mM ATP	2 µl
40 U/µl RNase inhibitor	1 µl
10 U/µl T4 RNA ligase	1 µl
RNase-free water	to 20 µl
4°C overnight plus room temperature 3 h	

The purified adapter-attached RNA was then used to generate the first strand of cDNA by ThermoScript™ RNase H-Reverse Transcriptase (Invitrogen) with a gene-specific reverse primer.

Reverse transcription

Adapter-attached RNA	4.5 µl
100 µM Reverse gene-specific primer	0.5 µl
Denaturing at 65°C for 5 min → ice	
RT-mix 1	5 µl
→ thermocycler	
42°C	5 min
55°C	20 min
60°C	20 min
65°C	20 min
85°C	5 min

*→: transfer to

RT-mix 1, 20 µl

5 x ThermoScript™ RNase H-Reverse Transcriptase buffer	8 µl
25 mM dNTPs	1.6 µl
0.1 M DTT	2 µl
40 U/µl RNase inhibitor (IBM Fermentas)	1 µl
15 U/µl ThermoScript™ RNase H-Reverse Transcriptase (Invitrogen)	2 µl
RNase-free water	5.4 µl

The cDNA was amplified by PCR with the gene-specific primer and primer 5'-GTCAGCAATCCCTAAG, identical in sequence to the 5' part of the adapter primer. PCR products were analyzed by agarose gel electrophoresis. Products of suitable size were excised from the gel, purified with kits (3.2.1.2), and inserted into the PCR®2.1-TOPO® vector (3.2.4) for sequencing.

3.8.2 3'-end mapping of RNA

A series of cytosines were added to the 3' end of total RNA by poly(A) polymerase (Invitrogen). The RNA was then purified by phenol/chloroform extraction and ethanol precipitation. 2 µg of total RNAs were initially used and finally dissolved in 10 µl of RNase-free water.

C-tailing

Total RNA	2 µg
25 mM $MgCl_2$	4 µl
10 x C-tailing buffer	5 µl
25 mM $MnCl_2$	4 µl
10 mM CTP	3 µl
40 U/µl RNase inhibitor	1 µl
RNase-free water	to 50 µl
Incubation at 37°C for 5 min	
2 U/µl Poly(A) polymerase	1.5 µl
Incubation at 37°C for 1.5 h	

10 x C-tailing buffer

Tris/HCl pH 8.0	500 mM
NaCl	2 M
DTT	10 mM

The purified C-tailed RNAs were used as a template for first strand cDNA synthesis by reverse transcription with a 3' polyG anchor primer mix using the RT-PCR Access system (Promega).

Reverse transcription

C-tailed RNA	2.5 µl
3' polyG anchor primer mix (33 µM each)	0.5 µl
RT-mix 2	5 µl
RNase-free water	1.5 µl
Denaturing at 94°C for 3 min	
Cool down to 48°C	
AMV RT (Promega)	0.5 µl
48°C	45 min
94°C	10 min
8°C	pause

3' polyG anchor primer mix

5'-AGGAGCCATCGTATGTCGGGGGGGGGGGGGG**A**
5'-AGGAGCCATCGTATGTCGGGGGGGGGGGGGG**T**
5'-AGGAGCCATCGTATGTCGGGGGGGGGGGGGG**C**

RT-mix 2, 20 µl

AMV/Tf1 5 x buffer (Promega)	8 µl
10 mM dNTP	0.8 µl
25 mM $MgSO_4$	3.2 µl
RNase-free water	8 µl

Final amplification of cDNA and analysis, cloning and sequencing of PCR products was performed as in 3.8.1.

3.9 Affinity assay

Because association of P RNA and P protein as well as sustrate binding and product release are of fundamental importance for catalysis, assays for determining the affinity between these binding partners were performed. The measure of affinity is the equilibrium dissociation constant $\boldsymbol{K}_{\mathbf{d}}$, which is defined as the enzyme or protein concentration at which complex formation has reached half-maximum.

3.9.1 Spin column assay

Ternary complex formation between holoenzyme and substrate was analyzed by a spin column assay. As complex formation depended on P protein bound to P RNA at low salt concentrations, the assay was designed to indirectly evaluate P RNA-protein affinity.

In our assays, RNase P holoenzyme was reconstituted at high concentration (5 µM P RNA plus a five-fold molar excess of P protein). The holoenzyme was then diluted to different concentrations with prewarmed dilution buffer and was afterwards incubated with ^{32}P-labeled ptRNA (3.6.1) for complex formation. Calcium ions were utilized to help binding of substrate and enzyme while avoiding ptRNA processing during gel filtration experiments. Eventually, the whole mixture was loaded onto a 1 ml Sephadex^{TM} G-75 spin column (3.4.2.3) to separate bound and free ptRNA: Free ptRNAs are small enough to be retained in the pores of the column matrix, while bound ones pass through the column together with the holoenzyme.

Activity in the bound and flowthrough fraction was subsequently quantified with a scintillation counter.

5 x B3 buffer

NH_4OAc	1 M
Tris/CH_3COOH pH 7.1	250 mM

Dilution buffer, 1ml

		C_{end}
5 x B3 buffer	200 µl	1 x
100 mM $Ca(OAc)_2$	150 µl	15 mM
1 % Nonidet P40	50 µl	0.05 %
RNase-free water	600 µl	
Prewarmed at 37°C		

Reconstitution of the holoenzyme (5 µM), 10 µl

		C_{end}
50 µM P RNA	1 µl	5 µM
5 x B3 buffer	2 µl	1 x
100 mM $Ca(OAc)_2$	1.66 µl	15 mM
1 % Nonidet P40	0.5 µl	0.05 %
RNase-free water	(10 - a) µl	
Incubation at 37°C for 1 h		
E. coli C5 protein	a µl	25 µM
Incubation at 37°C for 15 min		

The enzyme was diluted with dilution buffer to different concentrations; diluted enzyme was then incubated at 37°C for 5 min.

ptRNA mix, 200 µl

		C_{end}
ptRNA (^{32}P-labeled)	80,000 cpm	4000 cpm/10 µl
5 x B3 buffer	40 µl	1 x
100 mM $Ca(OAc)_2$	30 µl	15 mM
1 % Nonidet P40	10 µl	0.05 %
RNase-free water	up to 200 µl	
Incubation at 37°C for 30 min		

To allow complex formation between holoenzyme and substrate, 10 µl of diluted enzyme were mixed with 10 µl of ptRNA mix, followed by incubation at 37°C for 5 min.
For controls, an assay with substrate only as well as an assay without protein were performed. For the former, 10 µl of 1 x B3 buffer supplemented with Nonidet P40 and $Ca(OAc)_2$ was incubated according to the protocol for holoenzyme preincubation and was then mixed with substrate. For the latter, P RNA was likewise mixed with B3 buffer, Nonidet P40 and $Ca(OAc)_2$ and water to a final volume of 10 µl without adding P protein.

3.9.2 Spin column assay data evaluation

The bound fraction of substrate ($BF_{substrate}$) can be calculated as follows:

$$BF_{substrate} = cpm_{bound\ substrate} / (cpm_{bound\ substrate} + cpm_{free\ substrate})$$

where $cpm_{free\ substrate}$ is the amount of radioactivity retained on the sephadex column and $cpm_{bound\ substrate}$ is the amount of radioactivity in the flowthrough. For further calculation, $BF_{substrate}$ of the control assay with substrate only was subtracted from $BF_{substrate}$ of the assays with enzyme, resulting in "true $BF_{substrate}$" values for each sample.
Because in our assays the concentration of enzyme far exceeded that of substrate, the total concentration of enzyme was considered equal to the concentration of free enzyme. The total concentration of enzyme ([enzyme]) and true $BF_{substrate}$ were fitted to the equation:

$$\text{true } BF_{substrate} = MBF_{substrate} \times [enzyme] / (K_d + [enzyme])$$

where $MBF_{substrate}$ is the maximal $BF_{substrate}$, the bound fraction of substrate at saturating enzyme concentration ([free enzyme] $\rightarrow \infty$). K_d and $MBF_{substrate}$ were computed by curve fitting (GraFit 3.0, Erithacus Software).

3.10 UV melting profiles

Besides native PAGE, measuring UV melting profiles of RNA is another method to assess RNA folding. When being heated, non-covalent interactions in RNA are disrupted, so that the RNA fold changes from an ordered, native state to a disordered, denatured state. For RNase P RNA, the fold goes from a collapsed native-like state to secondary structure, and then to an unfolded state, with the process being reversible. During melting of an RNA secondary structure, the UV absorbance gradually increases owing to unstacking of bases (hyperchromicity). Monitoring the course of UV absorbance thus generates a UV melting curve specific for an RNA species, where the curve reports the phase diagram for the transitions between different folding states.

$\mathbf{T_m}$ is defined as the temperature at the midpoint of the transition between the native and completely unfolded structure.

3.10.1 Running the measurement

In this study, a Cary 100 Bio UV-Visible spectrophotometer (VARIAN) was used. It has a heating block with drillings for 12 cuvettes; as temperature monitor, we used the one for the entire heating block.

To start the measurement, the machine was preheated for at least half an hour. The software "Thermol" (Cary Win UV software version 3.0) was initiated, and then the measuring program and parameters were set up in the module "Setup". "Wavelength" was set as 260 nm, "SBW" (required spectral bandwidth) as 1.0 nm and "Ave Time" as 2.000 s. The measuring program was as below.

Measuring program

Stage	Data Interval (°C)	Rate (°C/min)	End (°C)	Hold (min)
1	1.00	10.00	55.00	5.00
2	1.00	10.00	37.00	35.00
3	0.10	0.50	90.00	0.00
4	0.10	2.00	25.00	5.00

Stages 1 to 3 comprised a single round of measurement, where stage 1 and 2 were preincubation steps to help RNA folding. In stage 3 the UV melting curve was generated: the sample was heated at the rate of 0.5°C/min from 37°C to 90°C, and data were collected every 0.1°C. For more rounds of measurement, the sample was first cooled to 25°C (stage 4), and

then ran through stages 1 to 3 again. If the data are required in Excel format, one needs to select “Select for ASCII (CSV)” in the subdirectory of Setup/Reports/autoconvert.
For melting curve measurement of RNase P RNA, similar buffer conditions as for P RNA alone kinetics assays were adopted: 2 mM EDTA, 50 mM MES pH 6.0, 100 mM NH_4OAc, with the magnesium concentration reduced to 4.5 mM because high concentrations of divalent metal ions resulted in aberrant signals at high temperature.

Sample for melting curve measurement, 150 µl

	Sample	C_{end}	Control
5 x buffer	30 µl	1 x	30 µl
45 mM $Mg(OAc)_2$	15 µl	4.5 mM	15 µl
RNase-free water	90 µl		105 µl
2.5 µM P RNA	15 µl	250 nM	-

Samples (150 µl each) were pipetted into a standard cuvette (micro cell, 80 µl, 4 mm x 10 mm stoppered, VARIAN). The surface of the sample mix was covered using 200 µl of PCR grade mineral oil to prevent evaporation and condensation at high temperature. Then each cuvette was firmly sealed with its stopper. The cuvettes were placed into heating slots of the multicell holder, with a blank containing water or measuring buffer only placed in slot 1. The lid of the machine was closed. The button “Zero” within the “Thermol” menu was clicked for the blank. The measurement was initiated by clicking “Start”.

3.10.2 Data analysis

Data analysis was accomplished with the software “Thermol”. In the mode of “Maths”, after selecting a trace or a graph, one could choose one operation such as “Mean”, “Deriv” (the first derivative, d Abs/d T), “Normalize” or “Smooth” for the curves, “Apply” and then “=” had to be clicked. Usually, the mean curve was calculated from at least three measurements for an RNA species, normalized to 89 (°C) for the X axis and to 1.0 (normalized Abs) for the Y axis, and was then converted to the first derivative and finally smoothed. To combine several curves which had not been measured simultaneously, the curves were saved as Data [^{x}.DTM] files, then opened together by ticking “Overlay Data” and using the key “Strg” on the computer keyboard, and saved once more as a Batch [^{x}.BTM] file. Choosing curves and changing their colours was done in the mode “Trace preferences”. After normalization, each RNA species displayed a specific UV melting profile which could be reliably reproduced in

different rounds of experiments. The T_m was inferred manually by clicking the peak on the first derivative curve.

3.10.3 Cleaning of the cuvette

To clean the cuvettes after measurement, the sample solution and mineral oil were removed with a pipette. The cuvette was rinsed once with 70 % ethanol followed by three times with double-distilled water. Then 2 % cuvette wash solution (HELLMANEX®II, HELLMA) was filled into the cuvette, which was then left to incubate for a few minutes. Subsequently, the cuvette was washed another three times with double-distilled water. Finally, the remaining liquid was removed with a syringe and the cuvette was left to dry upside down on a piece of clean tissue paper.

3.11 Structure probing

Some metal ions and RNases can hydrolyze RNA at specific sites. They are utilized to study RNA structure under defined conditions using RNAs 3'- or 5'-endlabeled with ^{32}P (3.7.1, 3.11.1).

3.11.1 5'-^{32}P-endlabeling of RNA

With T4 PNK (IBM Fermentas), the labeling reaction was set up as below. The purification protocol is the same as for 5'-^{32}P-endlabeling of substrate (3.6.1).

5'-^{32}P-endlabeling of RNA

RNA	20 pmol
RNase-free water	up to 7.5 µl
10 x T4 PNK buffer A (forward)	0.75 µl
γ-^{32}P-ATP (3000 Ci/mmol, 10 µCi/µl)	1.5 µl
10 U/µl T4 PNK	2 µl
Incubation at 37°C for 1-2 h	

3.11.2 Ladder preparation

To identify the sites of hydrolysis within an RNA, size markers were required. For this purpose, ladders generated from the analyzed RNA itself were produced, either by I_2-induced hydrolysis (see 3.11.1.1), by partial alkaline hydrolysis (3.11.1.2), or by partial RNase T1 cleavage under denaturing conditions (G ladders, see 3.11.2.).

3.11.2.1 I_2-induced hydrolysis

Iodine can hydrolyze RNA carrying phosphorothioate modifications (one non-bridging phosphate oxygen replaced with sulphur), which can be incorporated during *in vitro* run-off T7 transcription (3.4.4). Depending on the type of the modified nucleotides used in transcription, iodine treatment generates A-, U-, G-, or C-specific sequence ladders visible on denaturing PAA gels.

I_2 solution, 50 µl

20 mg/ml I_2 (in ethanol)	2.5 µl
Ethanol abs.	7.5 µl
RNase-free water	40 µl

I_2 hydrolysis, 50 µl

3'- or 5'-^{32}P-endlabeled NMPα-S-modified RNA	0.5 µl (20,000 cpm)
100 mM HEPES pH 7.5	5 µl
10 µM cold NMPα-S-modified RNA	1 µl
RNase-free water	38.5 µl
Addition of 5 µl of I_2 solution	
Incubation at 37°C for 20 min	

The I_2 solution was freshly prepared just before use. The hydrolysis reaction was started by adding the I_2 solution and stopped by ethanol precipitation (mixing with 10 µl of 2 M NH_4OAc pH 7.0, 0.5 µl of 20 mg/ml glycogen as well as 125 µl of ethanol). After incubation at –20°C overnight, the precipitated RNA cleavage segments were collected by centrifugation, dissolved in 8 µl PPF buffer and subsequently resolved on a sequencing gel.

The sequencing gel (42 cm long, 0.5 mm thin, 8-12 % PAA, and 8 M urea) was run at 4-15 mA until xylene cyanol had migrated about 36 cm from the slot. For better resolution, the gel was kept cool and not run longer than 6 h. Heating samples at 90°C for 5 min before loading on the gel, and drying the gel with a slab gel dryer (3.7.2.1) prior to exposure of the image plate improved final image quality. The latter procedures were applied especially when H1 RNA variants were analyzed.

3.11.2.2 Partial alkaline hydrolysis

The phosphodiester bond between two ribonucleotides of an RNA can be broken by alkaline hydrolysis, which produces fragments with 5'-hydroxyl and 2', 3'-cyclic phosphate RNA termini. The cyclic phosphate quickly reacts to either a 2' or 3' monophosphate. The partial alkaline hydrolysis was carried out in 10 mM NaOH.

Partial alkaline hydrolysis, 10 µl

3'- or 5'-^{32}P-endlabeled RNA	0.5 µl (50,000 cpm)
10 mM NaOH	9.5 µl
Incubation at 90°C	

The incubation was done in a heating block with a metal block prewarmed to higher temperature on top to prevent condensation. Subsequently the reaction tube was placed on ice, the partially hydrolyzed RNA was precipitated with ethanol (3.1.5), dissolved in 8 µl PPF buffer and resolved on a sequencing gel (3.11.1.1).

For each RNA, conditions of alkaline hydrolysis (time of hydrolysis and alkaline concentration) needed to be optimized.

3.11.3 Partial RNase T1 hydrolysis

Ribonuclease T1 (RNase T1) is a fungal endoribonuclease that specifically cuts single-stranded RNA on the 3' side of guanosine residues, producing 3'-phosphate and 5'-hydroxyl RNA ends. The enzyme is active in a broad range of reaction buffers and does not require any metal ions.

3'- or 5'-^{32}P-endlabeled RNAs were incubated in denaturing or native buffers to generate linear or folded RNA, and then RNase T1 was added to start the hydrolysis.

3.11.3.1 RNase T1 hydrolysis under denaturing conditions

Partial RNase T1 hydrolysis under suitable denaturing conditions usually results in cleavage after every G residue. Such hydrolysis products were used as a control for native RNase T1 cleavage, as a G ladder, or both.

Prior to adding RNase T1, the reaction mix was incubated for 10 min at 37°C or 55°C. Then 1 µl of freshly diluted RNase T1 (0.8 U/µl) was added to initiate the hydrolysis reaction. The reaction was carried out at 37°C for 10 min, stopped by ethanol precipitation (3.1.5), and analyzed on a sequencing gel (3.11.1.1).

1.25 x T1 denaturing buffer (pH 5.0 in 1 x buffer)

Na-citrate	25 mM
Urea	8.75 M
EDTA	1.25 mM

RNase T1 hydrolysis, 50 µl

1.25 x T1 denaturing buffer	40 µl
3'- or 5'-^{32}P-endlabeled RNA	0.5 µl (20,000 cpm)
10 µM cold RNA	1 µl
RNase-free water	7.5 µl
Incubation at 37°C or 55°C for 10 min	
0.8 U/µl RNase T1	1µl
Incubation at 37°C for 10 min	

3.11.3.2 RNase T1 hydrolysis under native conditions

Under native conditions, RNA forms secondary and tertiary structures. In limited partial RNase T1 hydrolysis under native conditions, cleavage at a given site depends on its accessibility, so that the cleavage pattern provides information on the structure of the RNA.

In practice, the reaction mixture except for RNase T1 was first incubated for 10 min at 37°C or 55°C. Then hydrolysis was started by adding 1 µl of freshly diluted RNase T1 (0.8 U/µl), continued for 10 min at 37°C and stopped by ethanol precipitation (3.1.5); samples were resolved on a sequencing gel (3.11.1.1).

2 x T1 native buffer

Hepes-NaOH	100 mM
$Mg(OAc)_2$	9 mM
NH_4OAc	200 mM

pH 7.0 in 1 x buffer

RNase T1 hydrolysis in T1 native buffer, 50 µl

2 x T1 native buffer	25 µl
3'- or 5'-^{32}P-endlabeled RNA	0.5 µl (20,000 cpm)
10 µM cold RNA	1 µl
RNase-free water	22.5 µl
Incubation at 37°C or 55°C for 10 min	
0.8 U/µl RNase T1	1µl
Incubation at 37°C for 10 min	

For analysis of RNA HE (the chimaera of RNase P RNA from *H. sapiens* and *E. coli*), a modified protocol was used: RNase T1 cleavage of this RNA, with and without *E. coli* P protein, was analyzed in KN buffer (3.6.3) supplemented with 10 mM $Mg(OAc)_2$. The RNA mix was incubated at 55°C for 5 min, followed by 37°C for 30 min. After adding 1 µl *E. coli* P protein, incubation was continued at 37°C for another 5 min. Afterwards, hydrolysis was initiated by adding 1 µl of freshly diluted RNase T1 (0.003 U/µl). After 5 min at 37°C, the reaction was terminated by ethanol precipitation (3.1.5), and samples were resolved on a sequencing gel (3.11.1.1). In contrast to the reaction in T1 native buffer (see above), RNase T1 is more active in KN buffer and therefore used in smaller amounts.

RNase T1 hydrolysis in KN buffer, 10 µl

		control
3'- or 5'-^{32}P-endlabeled RNA	0.5 µl (20,000 cpm)	0.5 µl (20,000 cpm)
2 µM cold RNA	1 µl	1 µl
5 x KN buffer	2 µl	2 µl
50 mM $Mg(OAc)_2$	2 µl	2 µl
RNase-free water	2.5 µl	3.5 µl
Incubation at 55°C for 5 min and then at 37°C for 30 min		
10 µM *E. coli* P protein	1 µl	–
Incubation at 37°C for 5 min		
0.003 U/µl RNase T1	1 µl	1 µl
Incubation at 37°C for 5 min		

3.11.4 Lead-induced hydrolysis

A few metal ions are capable of inducing RNA hydrolysis at proper conditions, lead being one of them. For efficient RNA hydrolysis, Pb^{2+} is required to be positioned at an optimal distance from the 2' OH of the ribose. Lead ions cleave in single-stranded flexible regions and, even more prominently, near high affinity metal ion binding sites, thus allowing to extract structural information from Pb^{2+}-induced hydrolysis patterns.

In practice, the RNA to be investigated was labeled at the 3'- or 5'-end with ^{32}P and was then incubated in a buffer suitable for RNA folding. Cleavage was induced by addition of freshly prepared $Pb(OAc)_2$ (0.5-2 mM) and was terminated after 5-20 min by ethanol precipitation (3.1.5) or direct mixing with gel loading buffer (PPF, see section 3.1.2.2); cleavage products were analyzed on a sequencing gel (3.11.1.1).

In most assays performed in this study, reaction conditions were 50 mM Tris-HCl pH 7.5, 100 mM NH_4Cl, 2 mM $Mg(OAc)_2$, 0.5 mM $Pb(OAc)_2$, 0.25 µM cold RNA, and trace amounts of radioactive RNA (20,000 cpm). The setup of a hydrolysis reaction and its controls is described below.

5 x Pb^{2+} hydrolysis buffer

Tris-HCl	250 mM
NH_4Cl	500 mM

pH 7.5 in 1 x buffer

Lead-induced hydrolysis, 10 µl

	control	control	
3'- or 5'-^{32}P-endlabeled RNA (40,000 cpm/µl)	0.5 µl	0.5 µl	0.5 µl
2.5 µM cold RNA	1 µl	1 µl	1 µl
5 x Pb^{2+} hydrolysis buffer	2 µl	2 µl	2 µl
20 mM $Mg(OAc)_2$	1 µl	-	1 µl
RNase-free water	5.5 µl	5.5 µl	4.5 µl
Incubation at 55°C for 5 min and then at 37°C for 20 min			
5 mM $Pb(OAc)_2$	-	1 µl	1 µl
Incubation at 37°C for 10 min			

RNA HE (chimeric RNA composed of the C-domain of H1 RNA and the S-domain of *E. coli* P RNA) alone or with P protein was analyzed in KN buffer (3.6.3) supplemented with 10 mM $Mg(OAc)_2$ as depicted below.

Lead-induced hydrolysis in KN buffer, 10 µl

		control
3'- or 5'-^{32}P-endlabeled RNA	0.5 µl (20,000 cpm)	0.5 µl (20,000 cpm)
2 µM cold RNA	1 µl	1 µl
5 x KN buffer	2 µl	2 µl
50 mM $Mg(OAc)_2$	2 µl	2 µl
RNase-free water	2.5 µl	3.5 µl
Incubation at 55°C for 5 min and then at 37°C for 30 min		
10 µM *E. coli* P protein	1 µl	–
Incubation at 37°C for 5 min		
50 mM $Pb(OAc)_2$	1 µl	1 µl
Incubation at 37°C for 5 min		

3.12 References

Birnboim, H.C. 1983. A rapid alkaline extraction method for the isolation of plasmid DNA. *Method Enzymol.* **100:** 243-255.

Birnboim, H.C. and Doly, J. 1979. Rapid alkaline extraction procedure for screening recombinant plasmid DNA. *Nucleic Acids Res.* **7:** 1513-1523.

Cordier, A. and Schön, A. 1999. Cyanelle RNase P: RNA structure analysis and holoenzyme properties of an organellar ribonucleoprotein enzyme. *J. Mol. Biol.* **289:** 9-20.

Dubnau, D. and Davidoff.R. 1971. Fate of transforming DNA following uptake by competent *Bacillus subtilis*. *J. Mol. Biol.* **56:** 209-&.

Gössringer, M., Kretschmer-Kazemi Far, R., and Hartmann, R.K. 2006. Analysis of RNase P protein (*rnpA*) expression in *Bacillus subtilis* utilizing strains with suppressible rnpA expression. *J Bacteriol* **188:** 6816-6823.

Hansske, F. and Cramer, F. 1979. Modification of the 3' terminus of tRNA by periodate oxidation and subsequent reaction with hydrazides. *Method Enzymol.* **59:** 172-181.

Hardt, W.D. and Hartmann, R.K. 1996. Mutational analysis of the joining regions flanking helix P18 in *E. coli* RNase P RNA. *J. Mol. Biol.* **259:** 422-433.

Ishiwa, H. and Shibaharasone, H. 1986. New shuttle vectors for *Escherichia coli* and *Bacillus subtilis* IV. The Nucleotide sequence of pHY300PLK and some properties in relation to transformation. *Jpn. J. Genet.* **61:** 515-528.

Milligan, J.F. and Uhlenbeck, O.C. 1989. Synthesis of small RNAs using T7 RNA polymerase. *Method Enzymol.* **180:** 51-62.

Rivera-Leon, R., Green, C.J., and Vold, B.S. 1995. High-level expression of soluble recombinant RNase P protein from *Escherichia coli*. *J. Bacteriol* **177:** 2564-2566.

Saiki, R.K., Scharf, S., Faloona, F., Mullis, K.B., Horn, G.T., Erlich, H.A., and Arnheim, N. 1985. Enzymatic amplification of beta-globin genomic sequences and restriction site analysis for diagnosis of sickle cell anemia. *Science* **230:** 1350-1354.

Vonahsen, U. and Noller, H.F. 1995. Identification of bases in 16s-ribosomal RNA essential for transfer-RNA binding at the 30s ribosomal P site. *Science* **267:** 234-237.

Waugh, D.S. and Pace, N.R. 1990. Complementation of an RNase-P RNA (*rnpB*) gene deletion in *Escherichia coli* by homologous genes from distantly related eubacteria. *J. Bacteriol* **172:** 6316-6322.

Wegscheid, B., Condon, C., and Hartmann, R.K. 2006. Type A and B RNase P RNAs are interchangeable *in vivo* despite substantial biophysical differences. *EMBO Rep.* **7:** 411-417.

Wegscheid, B. and Hartmann, R.K. 2006. The precursor tRNA 3'-CCA interaction with Escherichia coli RNase P RNA is essential for catalysis by RNase P *in vivo*. *RNA* **12:** 2135-2148.

4 Results and Discussion

4.1 RNase P of the *Cyanophora paradoxa* cyanelle: A plastid ribozyme

Dan Li, Dagmar K. Willkomm, Astrid Schön, Roland K. Hartmann (2007)
Biochimie, **89**, 1528-1538.

Available online at www.sciencedirect.com
ScienceDirect
Biochimie 89 (2007) 1528–1538
BIOCHIMIE
www.elsevier.com/locate/biochi

Research paper

RNase P of the *Cyanophora paradoxa* cyanelle: A plastid ribozyme

Dan Li [a], Dagmar K. Willkomm [a,*], Astrid Schön [b], Roland K. Hartmann [a,*]

[a] *Institut für Pharmazeutische Chemie, Philipps-Universität Marburg, Marbacher Weg 6, D-35037 Marburg, Germany*
[b] *Universität Leipzig, Molekulare Zelltherapie, Biotechnologisch-Biomedizinisches Zentrum (BBZ), Deutscher Platz 5, D-04103 Leipzig, Germany*

Received 2 May 2007; accepted 4 August 2007
Available online 11 August 2007

Abstract

Ribonuclease P (RNase P) is a ribonucleoprotein enzyme that generates the mature 5′ ends of tRNAs. Ubiquitous across all three kingdoms of life, the composition and functional contributions of the RNA and protein components of RNase P differ between the kingdoms. RNA-alone catalytic activity has been reported throughout bacteria, but only for some archaea, and only as trace activity for eukarya. Available information for RNase P from photosynthetic organelles points to large differences to bacterial as well as to eukaryotic RNase P: for spinach chloroplasts, protein-alone activity has been discussed; for RNase P from the cyanelle of the glaucophyte *Cyanophora paradoxa*, a type of organelle sharing properties of both cyanobacteria and chloroplasts, the proportion of protein was found to be around 80% rather than the usual 10% in bacteria. Furthermore, the latter RNase P was previously found catalytically inactive in the absence of protein under a variety of conditions; however, the RNA could be activated by a cyanobacterial protein, but not by the bacterial RNase P protein from *Escherichia coli*. Here we demonstrate that, under very high enzyme concentrations, the RNase P RNA from the cyanelle of *C. paradoxa* displays RNA-alone activity well above the detection level. Moreover, the RNA can be complemented to a functional holoenzyme by the *E. coli* RNase P protein, further supporting its overall bacterial-like architecture. Mutational analysis and domain swaps revealed that this A,U-rich cyanelle RNase P RNA is globally optimized but conformationally unstable, since changes as little as a single point mutation or a base pair identity switch at positions that are not part of the universally conserved catalytic core led to a complete loss of RNA-alone activity. Likely related to this low robustness, extensive structural changes towards an *E. coli*-type P5–7/P15–17 subdomain as a canonical interaction site for tRNA 3′-CCA termini could not be coaxed into increased ribozyme activity.

Keywords: Cyanelle of *Cyanophora paradoxa*; RNase P; Ribozyme; Organellar RNase P; tRNA processing

1. Introduction

Throughout all three kingdoms of life, ribonuclease P (RNase P) plays an essential role in the maturation of precursor tRNAs (ptRNAs), where RNase P endonucleolytically cleaves off the 5′-flank to generate the mature 5′-ends [1]. The enzyme is a ribonucleoprotein, best characterized for bacteria: here the catalytic activity resides in the RNA subunit [2], within a conserved core as part of one of the two RNA's independent folding domains, the so-called catalytic (C-) domain [3]. The second domain of RNase P RNA (P RNA), the specificity (S-) domain, plays a crucial role in substrate binding, as it interacts with the T-stem-loop region of ptRNAs [4–6]. Finally, the single bacterial RNase P protein (P protein) subunit, binding to the P2/P3 region of the RNA, provides a cavity to accommodate the ptRNA 5′-flank, leads to favoured substrate over product binding and contributes to the affinity of catalytically relevant metal ions [7–9].

RNase P evolution has been a longstanding point of interest: The proportion of protein to RNA within the ribonucleoprotein enzyme increases from one small protein subunit in bacteria (10% of the overall mass of the enzyme) to mostly 4 proteins in archaea and at least 9 in eukarya. The archaeal P proteins have homologues among the eukaryal ones, but no homology is found between the bacterial and any of the archaeal or

* Corresponding authors. Tel.: +49 6421 282 5827; fax: +49 6421 282 5854.
E-mail addresses: willkomm@staff.uni-marburg.de (D.K. Willkomm), roland.hartmann@staff.uni-marburg.de (R.K. Hartmann).

0300-9084/$ - see front matter © 2007 Elsevier Masson SAS. All rights reserved.
doi:10.1016/j.biochi.2007.08.004

eukaryal P proteins [10]. Conversely, all RNA subunits stem from a common ancestor, as evident from sequence and structural conservation [11–13]. Yet, ribozyme activity of the RNA subunit in the absence of P proteins, to be observed *in vitro* at elevated metal ion concentrations, differs among P RNAs: the degree of ribozyme activity substantially decreases from bacterial to eukaryal ones [14], and has so far been observed only in some, but not all, archaea [15]. This overall scheme has been regarded as the natural course of evolution, leading from the pre-biotic RNA world towards today's protein-dominated one.

In this scenario, the position of organellar RNase P is not yet clear, as the few well-characterized enzymes are highly diversified: extremes range from endoribonucleoproteins with considerably reduced length of the RNA subunit and entire lack of some of the elements ubiquitously conserved among bacterial P RNAs, as reported for some mitochondrial RNase P enzymes [16,17], to preliminary evidence for a protein-alone RNase P enzyme in spinach chloroplasts [18]. One of the best-characterized RNase P enzymes from photosynthetic organelles is that of the cyanelles from the glaucophyte *Cyanophora paradoxa*. These organelles have retained a cell wall of their own and are considered to represent a primordial type of plastid very close to the endosymbiont stage, as confirmed by phylogenies that place these cyanelles close to the cyanobacterial root of the plastid phylogenetic tree [19]. The *C. paradoxa* cyanelle RNase P possesses an RNA subunit similar to the bacterial type A consensus. However, the RNA is unusually A,U-rich and displays several further idiosyncrasies [20]. Despite the likeness and in contrast to bacterial RNase P, no RNA-alone activity has been observed for the cyanellar P RNA in the absence of protein under a variety of conditions at subsaturating ribozyme concentrations [20,21]. Furthermore, biochemical analysis revealed a high protein content of ~80% for cyanelle RNase P [22], a trait characteristic of eukaryal but not bacterial RNase P. Yet, an active enzyme resulted from combining the RNA subunit with the single P protein from the cyanobacterium *Synechocystis* sp. PCC 6803, though not with the P protein from *Escherichia coli* [21].

With a view to increasing our knowledge on organellar RNase P extremists and with regard to ribozyme identity emerging as a ubiquitous trait of RNase P ribonucleoprotein enzymes after the recent discovery of ribozyme RNase P activity in eukaryotes [14], we have re-analyzed the cyanelle enzyme for RNA-alone activity. We indeed detected robust RNA-alone activity (10^{-3} min^{-1}) at very high P RNA concentrations (10 μM). Also, activity at low magnesium concentrations could be stimulated by the bacterial P protein from *E. coli*. We have further seeked to increase the rudimentary ribozyme activity by introducing structural changes towards the bacterial ribozyme consensus. One approach was to construct domain chimeras in which either the C- or S-domain of cyanelle P RNA was replaced with that from *E. coli*. In a less invasive approach, we introduced changes as small as single or double mutations into the cyanelle P RNA. We also stepwise exchanged the entire P5–7/P15–17 subdomain for that from *E. coli*, as this region deviates extensively from the bacterial type A consensus in the cyanelle RNA. Our mutational data revealed that tertiary folding of the cyanelle P RNA lacks the robustness of canonical bacterial counterparts, which is in line with the proteinaceous character of this RNase P enzyme variant.

2. Materials and methods

2.1. Construction of plasmids used as transcription templates

The construction of the wild-type (wt) cyanelle P RNA transcription clone pT7G3CyRPR has been described [22]. The mutations A22G, T57C, A213G and combinations thereof were introduced into this plasmid by a modification of the megaprimer mutagenesis technique [23]. For construction of the CyRPR mutant A22G, the mutagenesis PCR was performed with primers CyG22 and Cy3′ anti using pT7G3CyRPR as template. The product was amplified with primers EcoT7Cy5′-G3 and Cy3′-Fok, the resulting DNA digested with EcoRI and PstI and ligated into pUC19 to give pT7CyRPR-G22. For the mutant A213G, mutagenesis was performed with primers EcoT7Cy5′-G3 and CyG213, and amplification of the product with EcoT7Cy5′-G3 and Cy3′-Fok. The double mutant A22G/A213G was constructed accordingly, but using plasmid pT7CyRPR-G22 as template. The T57C mutation was then introduced into these plasmids (pT7CyRPR-G22-G213 and pT7CyRPR-G213) by using the primers EcoT7Cy5′-G3 and CyC57, and the product was amplified and cloned as described above. For generating plasmid pUC19-Cpa-mP6/P15–17, the mutagenized parts were introduced by PCR reactions amplifying essentially the entire plasmid with the changes located in the 5′-portions of the primers (''inside-out''-PCR): before each PCR reaction, both primers were phosphorylated by incubating 500 pmol of primer with 10 U of T4 polynucleotide kinase (PNK, MBI Fermentas) in 25 μl of 1 × T4 PNK buffer A (MBI Fermentas) and 1 mM ATP for 1 h at 37 °C; aliquots of the phosphorylated primers were added directly from the kinase reaction to the PCR reaction tube; to inactivate the kinase, PCR reactions were preceded by a denaturation step of 95 °C for 5 min. Gel-purified linear plasmid amplificates were then circularized by T4 DNA ligase according to standard procedures. In the first step towards pUC19-Cpa-mP6/P15–17, pT7G3CyRPR was thus mutated with primers 229 and 230; based on the new plasmid as template, pUC19-Cpa-mP6/P15–17 was obtained by the analogous procedure using primers 231 and 232. To construct pUC19-Ecat, an ''inside-out''-PCR with primers 145 and 146 was performed using plasmid pHY300-EE as template, which encodes *E. coli rnpB*; the *E. coli* catalytic domain of the *rnpB* gene in the resulting intermediate plasmid was then amplified with primers 136 and 149 and the PCR product was ligated into EcoRI-/BamHI-cleaved pUC19. Shorter stretches of mutations were introduced by site-directed DpnI mutagenesis as described for the QuikChange XL Site-Directed Mutagenesis Kit (Stratagene), with primers carrying internal mutations. Using this technique, we generated plasmid pUC19-Cpa-mP5–6/P15–17 by two mutagenesis rounds: the first step produced an intermediate plasmid by using primers 237 and 238 with pUC19-Cpa-mP6/P15–17 as the template; the second step

used the intermediate plasmid as the template and primers 235 and 236. Plasmid pUC19-Cpa-mP5−7/P15−17 was obtained with the same method by primers 239 and 240 and pUC19-Cpa-mP5−6/P15−17 as the template. pUC19-EC was created by first amplifying *C. paradoxa* cyanelle *rnpB* with primers 119 and 120, which contained terminal sequences of the *E. coli rnpB* catalytic domain at their 5′-ends. This PCR product was used instead of a primer pair in site-directed DpnI mutagenesis based on plasmid pHY300-EE containing *E. coli rnpB*. The resulting chimeric *rnpB* was amplified with primers 136 and 149, this PCR product was cut by EcoRI and BamHI and ligated into pUC19 cleaved with the same pair of enzymes. For pUC19-CE, first two PCR fragments were produced from *C. paradoxa* cyanelle *rnpB*, one (resulting from primers 113 and 114) containing the 5′-part of the *C. paradoxa* cyanelle C-domain, the other (obtained with primers 115 and 116) the 3′-part. The primers additionally introduced restriction enzyme cleavage sites, a T7 promoter and nucleotides matching the 5′- or 3′-termini of the *E. coli rnpB* specificity domain. After gel purification the two PCR products were used as primers for amplification of the *E. coli rnpB* specificity domain, followed by cloning of the final PCR product into pUC19 via BamHI and EcoRI restriction sites.

2.2. Oligonucleotides used for construction of plasmids

Mutations introduced by the primer sequences are underlined, with Δ where the primers bring about a deletion, EcoRI, BamHI and PstI restriction enzyme cleavage sites are highlighted by italics, T7 promoters in lower case letters.

CyG22: CGAATTTAATTAATGATTGCAGATTTATTC;
Cy3′anti: AAACGAACTTAATTTTAAGCCGGGTTTTG;
EcoT7Cy5′-G3: GC*GAATTC*taatacgactcactatagGGAAAC GAATTTAATTAATG;
Cy3′-Fok: CGC*CTGCAG*GATGTCCGGATCCAAACGAA CTTAATTTTAAG;
CyG213: CTTTGCTCCCGAACGGGGTTTAC;
CyC57: GCAATTCTAACCTTTAGGGAGCCCGGACTT TCC;
229 GCCGTACCTTATGAACCCCTATTTGGCCTTGC TCCTGAACGGGGTTTA;
230 CCGTACTGAACCCGGGTAGGCTGCTAGAAAAA TTGAGTAATTAATTTTGAAGACAG;
231 CCAAGGAGCCCGGACTTTCCTCAGATTG;
232 GCAGAATTGCTGGGTAATTCCCAGTACG;
145 GAAACACCCGGAGCAAGGCCA;
146 CACCCTGCCCTATGGAGCC;
136 GCG*GGATCC*taatacgactcactatagGAAGCTGACCA GACAGT;
149 CGC*GAATTC*AGGTGAAACTGACCGAT;
237 CTATACTTAGTAAACCCCGTTCΔGGAGCAAGG CCAAATAGGGGTTC;
238 GAACCCCTATTTGGCCTTGCTCCΔGAACGGGG TTTACTAAGTATAG;
235 GAAAGTCCGGGCTCCATAGGGCAGAATTGCTG;
236 CAGCAATTCTGCCCTATGGAGCCCGGACTTTC;
239 CGGGCTCCATAGGGCAGAACGCTGGGTAATT CCCAGTACG;
240 CGTACTGGGAATTACCCAGCGTTCTGCCCTA TGGAGCCCG;
119 GTCCGGGCTCCATAGGGCAGAATTGCTGGGT AATTCCCAG;
120 CCTATTTGGCCTTGCTCCGAACGGGGTTTAC TAAGTAT;
136 GCG*GGATCC*taatacgactcactatagGAAGCTGACCA GACAGT;
113 GCG*GGATCC*taatacgactcactatagCGAATTTAATTAA TGATTACAG;
114 CAGGCGTTACCTGGCACCCTAACCTTATAG GAGCC;
115 GTGGCACGGTAAACTCCACCCAGGAGCAAAG TTTAGCG;
116 GCG*GAATTC*AAAACGAACTTAATTTTAAGCC.

2.3. In vitro transcription and 5′-end labeling of P RNAs and substrate ptRNA

Run-off transcription with bacteriophage T7 RNA polymerase as well as 5′- and 3′-endlabeling were performed essentially as described [24,25]. The *Thermus thermophilus* ptRNA^{Gly} substrate was transcribed from plasmid pSBpt3'HH linearized with BamHI [25]. *In vitro* transcription for *E. coli* P RNA used plasmid pDW98 linearized with BsaAI [24]. *C. paradoxa* cyanelle wt P RNA was transcribed from plasmid pT7G3CyRPR [22] and mutant cyanelle P RNAs from the constructs described above; all cyanelle templates were linearized with FokI and the templates for EC and CE chimeras with EcoRI.

2.4. Expression and purification of recombinant E. coli RNase P protein

E. coli RNase P protein (equipped with an N-terminal hexahistidyl-tagged peptide leader MRGSHHHHHHGS, encoded in plasmid pQE-30) was expressed in *E. coli* JM109 and purified by Ni-NTA affinity chromatography precisely as described in ref. [26].

2.5. RNase P activity assays

For all processing assays, RNAs were preincubated separately in the assay buffer (ptRNA^{Gly} substrate for 5 min at 55° and 20 min at 37°, P RNAs for 5 min at 55° and 35 min at 37°). For holoenzyme reactions, P protein was added to the P RNA 5 min before combining enzyme and substrate. Conditions of RNA-alone assays were trace amounts (<1 nM) of substrate, P RNA concentrations as indicated, 100 mM $Mg(OAc)_2$, 100 mM NH_4OAc, 50 mM MES and 2 mM EDTA, pH 6.0 and 37 °C. Holoenzyme reactions were performed under two different sets of conditions: (a) with 10 nM P RNA, 50 nM *E. coli* RNase P protein and 100 nM substrate at 37 °C in buffer KN4.5, designed to closely resemble physiological conditions (20 mM Hepes-KOH pH 7.4, 4.5 mM $Mg(OAc)_2$, 150 mM NH_4OAc, 2 mM spermidine, 0.05 mM spermine and 4 mM

β-mercaptoethanol [26]). (b) Alternatively, conditions deviated from (a) by 10 mM $Mg(OAc)_2$ (instead of 4.5 mM), 200 nM P RNA, 1 μM *E. coli* P protein, and trace amounts (<1 nM) of substrate. Analysis of cleavage reactions and data evaluation were carried out as described [25], all quantifications are based on at least three independent experiments.

2.6. Folding analysis by native PAGE

P RNAs to be analyzed were 3′-endlabeled with ^{32}P and preincubated at a concentration of 10 nM in buffer KN4.5 (see above) for 5 min at 55 °C and then 50 min at 37 °C. At room temperature, 1 volume of gel loading buffer (10% [v/v] glycerol, 2 mM $MgCl_2$, xylene cyanol and bromophenol blue) was added and the samples were immediately loaded onto nondenaturing polyacrylamide gels containing 11.25% (v/v) polyacrylamide, 66 mM HEPES, 33 mM Tris (pH 7.4), 0.1 mM EDTA, 100 mM NH_4OAc and 4.5 mM $MgCl_2$. Running of the gels and visualization of the RNAs were as described [26].

2.7. Complementation studies in the Bacillus subtilis conditional RNase P mutant strain SSB318

Complementation analyses were conducted exactly as described using the *B. subtilis* RNase P RNA (*rnpB*) mutant strain SSB318 [27,28]. In this strain, the chromosomal *rnpB* gene is under the control of an IPTG-inducible P_{spac} promoter. In the absence of IPTG, cell growth depends on the presence of a functional *rnpB* gene provided on a plasmid (pHY300 derivatives in our study; pHY300 is an *E. coli* − *B. subtilis* shuttle vector obtained from Takara Shuzo Co., Kyoto, Japan).

3. Results

3.1. Detection of cyanelle RNase P RNA-alone activity

Initially, based on previous data we assumed that the *C. paradoxa* cyanelle P RNA (Fig. 1, termed CC RNA) is catalytically inactive in the absence of protein components [20]. Since S- and C-domains were shown to be independent folding domains [3], we created chimeras of cyanelle and *E. coli* P RNAs as a first step to localize the global cause of the low activity of cyanelle P RNA − deficits in the S-domain, the C-domain, or both. The S-domain of the cyanelle RNA was replaced with the corresponding domain of *E. coli* P RNA in the chimera CE, whereas the reciprocal combination was present in variant EC (Fig. 2). In the first set of activity assays we employed single turnover conditions at 300 nM P RNA, conditions which were at the limit for manual execution of kinetic experiments with respect to *E. coli* P RNA (termed EE RNA)

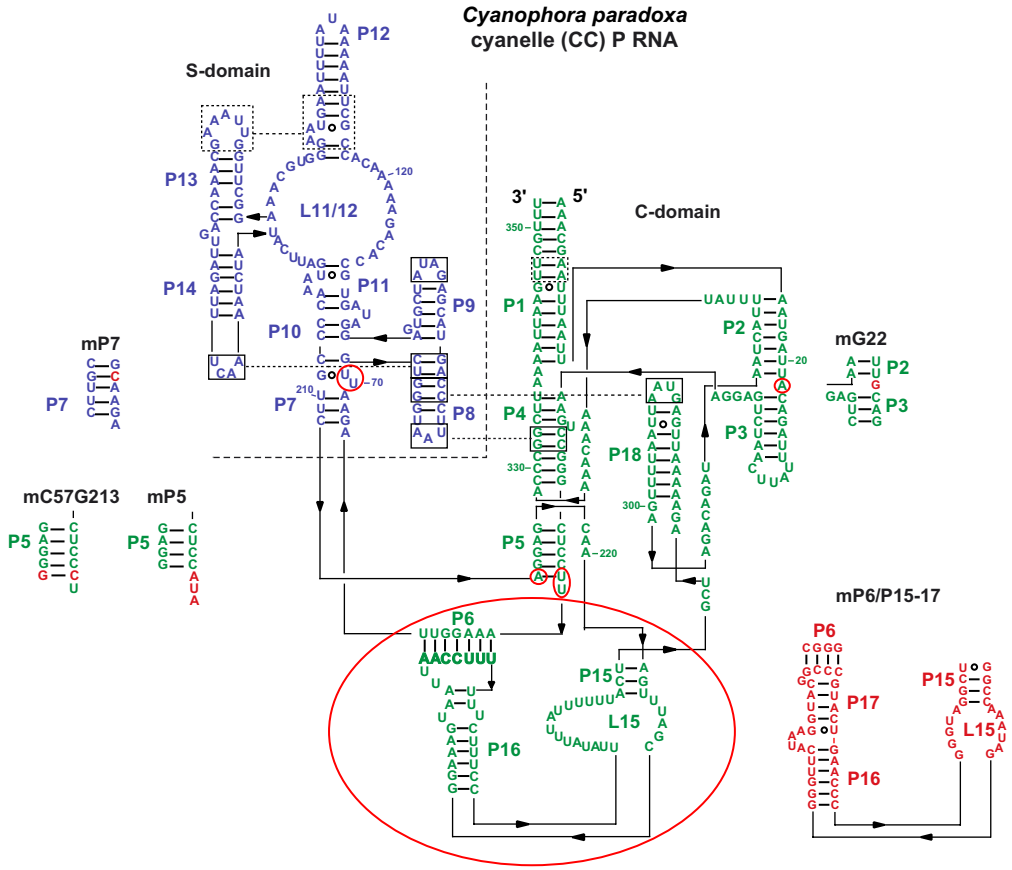

Fig. 1. *C. paradoxa* cyanelle P RNA in the 2D structure presentation according to ref. [37]. The C-domain is depicted in green and the S-domain in blue. Sites mutated within this work are circled in red, and the corresponding sequence of the respective mutant is given alongside with the altered nucleotides highlighted in red. Throughout the paper, the combination of mP6/P15−17 plus mP5 was named mP5−6/P15−17, that of mP6/P15−17 plus mP5 plus mP7 was named mP5−7/P15−17.

used as the positive control (Table 1, first line). Under these conditions, only the EC chimera (*E. coli* C-domain, cyanelle S-domain; Fig. 2) showed low but reproducible activity within up to 4 h of incubation at 37 °C. To fathom out if CC RNA is indeed catalytically active in the absence of protein cofactors, we increased the P RNA concentration to 10 μM in single turnover assays, with incubation periods of up to 20 h. Under these conditions CC and CE RNA turned out to be unequivocally active at rates of about 10^{-3} min^{-1} (Table 1 and Fig. 3A), thus considerably above the limit of detection (ca.

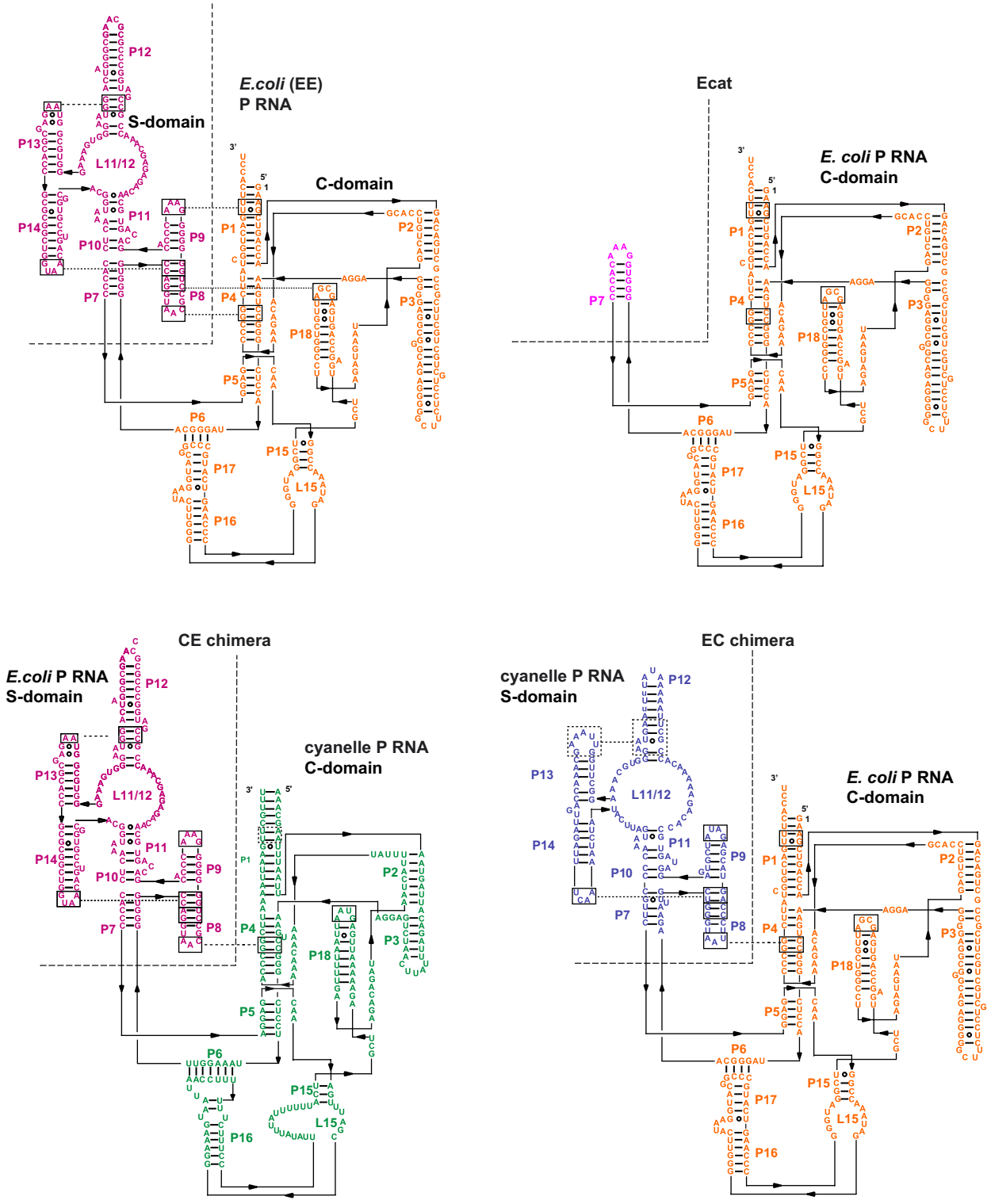

Fig. 2. 2D structure presentation according to ref. [37] of *E. coli* P RNA (EE), the EC and CE chimeras and the Ecat variant (C-domain of *E. coli* only). C- and S-domains derived from *E. coli* P RNA are depicted in orange and magenta, respectively; C- and S-domains derived from CC RNA (Fig. 1) are shown in green and blue, respectively.

Table 1
Kinetic data of P RNA-alone reaction

RNase P RNA	Concentration [μM]	k_{obs} [$min^{-1} \times 10^{-4}$]
EE	0.3	$5.1 \times 10^4 \pm 0.4 \times 10^4$
EC	0.3	2 ± 1
EC	10	37 ± 4.0
CE	10	7.5 ± 0.5
CC	10	10.0 ± 3.0
Ecat	10	Not detectable
CC-mG22	10	Not detectable
CC-mC57G213	10	Not detectable
CC-mG22/C57G213	10	Not detectable
CC-mP6/P15−17	10	Not detectable
CC-mP5−6/P15−17	10	Not detectable
CC-mP5−7/P15−17	10	Not detectable

Kinetic data of RNA-alone reaction. Reaction conditions and abbreviations are as in Fig. 3A (100 mM $Mg(OAc)_2$, 100 mM NH_4OAc, 50 mM MES pH 6.0, 2 mM EDTA and <1 nM substrate at 37 °C) with amounts of P RNAs as indicated.

$5 \times 10^{-6}\ min^{-1}$) [14]. With 10 μM CC RNA, about 80% of ptRNA was converted to mature tRNA after 20 h of incubation (data not shown). The question if CC RNA had cleaved the bacterial $ptRNA^{Gly}$ substrate (14-nt 5′-flank) at the canonical cleavage site was scrutinized by performing a reference reaction documented to result in canonical cleavage (between nt −1 and +1) as well as miscleavage at the next phosphodiester in the 5′-direction (between nt −2 and −1) [26]: a $ptRNA^{Gly}$ variant with a point mutation in the 3′-CCA end (C74G) but with the same 5′-flank was incubated with the *E. coli* holoenzyme, and cleavage products were analyzed next to those generated by EE and CC RNA acting on wt $ptRNA^{Gly}$ (Fig. 3B, lanes 1−3). This experiment clearly demonstrated that the organellar P RNA selects the canonical RNase P cleavage site. In conclusion, cyanelle P RNA has retained the basic capacity for genuine RNase P RNA-alone catalysis, despite the highly proteinaceous nature of this ribonucleoprotein [22].

3.2. Relative RNA-alone activities of chimeric P RNAs

To examine if there is cooperation between the heterologous C- and S-domains in the EC chimera, we included a truncated *E. coli* P RNA for comparison (Ecat, Fig. 2), consisting of the catalytic domain only. The catalytic domain of *E. coli* P RNA was shown to retain residual activity, but only in the presence of the protein cofactor [29]. In the RNA-alone reaction at 10 μM enzyme (Table 1), activity of the CE chimera roughly equaled that of the CC wt RNA. The EC variant was about 4-fold more active, whereas the truncated Ecat RNA was inactive as expected. Based on the inactivity of Ecat, our data document that the cyanelle S-domain is able to functionally support the *E. coli* C-domain (variant EC). Likewise, the *E. coli* S-domain cooperates with the cyanelle C-domain (variant CE), assuming that the cyanelle C-domain alone, although not analyzed here, is completely inactive based on the inactivity of Ecat.

From another perspective, the activity of the CE variant was roughly identical to that of the wild-type CC RNA, indicating that the surmised better substrate binding and ribozyme stabilizing capabilities of the *E. coli* S-domain could not be coaxed into substantially higher processing rates of the chimera. Similarly, the high catalytic potential of the *E. coli* C-domain was only marginally realized in the EC variant.

3.3. Activation by the E. coli RNase P protein

We further tested the different P RNA variants (EE, CC, CE, EC and Ecat) in the holoenzyme reaction utilizing the P protein of *E. coli*. Under our standard holoenzyme conditions (buffer KN4.5 including 4.5 mM Mg^{2+}, 10 nM RNase P and 100 nM ptRNA), roughly equal cleavage rates were observed with EC and Ecat, yet about 1000- to 2000-fold lower than for EE RNA (Table 2, lower part). For the other variants, activities were at the limit of detection. However, at higher enzyme concentrations (200 nM P RNA, 1 μM P protein), 10 mM Mg^{2+} and <1 nM ptRNA substrate, all variants showed robust processing activities (Fig. 3C and Table 2, top). This finding demonstrated that the wt cyanelle RNase P RNA is able to form a functional holoenzyme with a γ-proteobacterial RNase P protein. There was one major difference in the hierarchy of activities for EC, CE and CC in the holoenzyme assays compared with the RNA-alone reaction: CE RNA was roughly 4-fold more active than CC RNA in the presence of the *E. coli* P protein. The cyanelle catalytic domain was thus activated to some extent by the *E. coli* S-domain in the presence of the *E. coli* P protein. Moreover, the EC chimera, though more active than the cyanelle wild-type, displayed about one third of the activity of the *E. coli* catalytic domain alone (Table 2). Thus, the presence of the cyanelle S-domain failed to improve catalytic performance of the *E. coli* C-domain in the holoenzyme reaction. The differential performance of the chimeras in the RNA-alone versus holoenzyme reaction may have many reasons, including effects of the protein on P RNA folding, substrate binding and metal ion affinity, or distinct contribution of rate-limiting steps to the observed rates in RNA-alone versus holoenzyme reaction. Altogether, these results document that the cyanelle and *E. coli* C- and S-domains can be combined to functional P RNAs. However, activity of such chimeras remained low in both directions (CE and EC), suggesting that there is no major asymmetry in the contribution of cyanelle C- and S-domain to the structural deficits of the chimeras. Also, interaction of the heterologous domains and/or overall P RNA folding may be suboptimal in the CE and EC chimeras.

3.4. Cyanelle (CC) P RNA with specific structural alterations

Since the approach of domain swaps did not yield information on specific catalytic deficits of the cyanelle RNA, we took to introducing more subtle changes into the molecule towards restoring the bacterial consensus at positions where the cyanelle P RNA sequence deviates [20,30]. First, we tested mutants generated during our previous work (Cordier, Heubeck and Schön, unpublished). One is nucleotide 22 (*C. paradoxa*

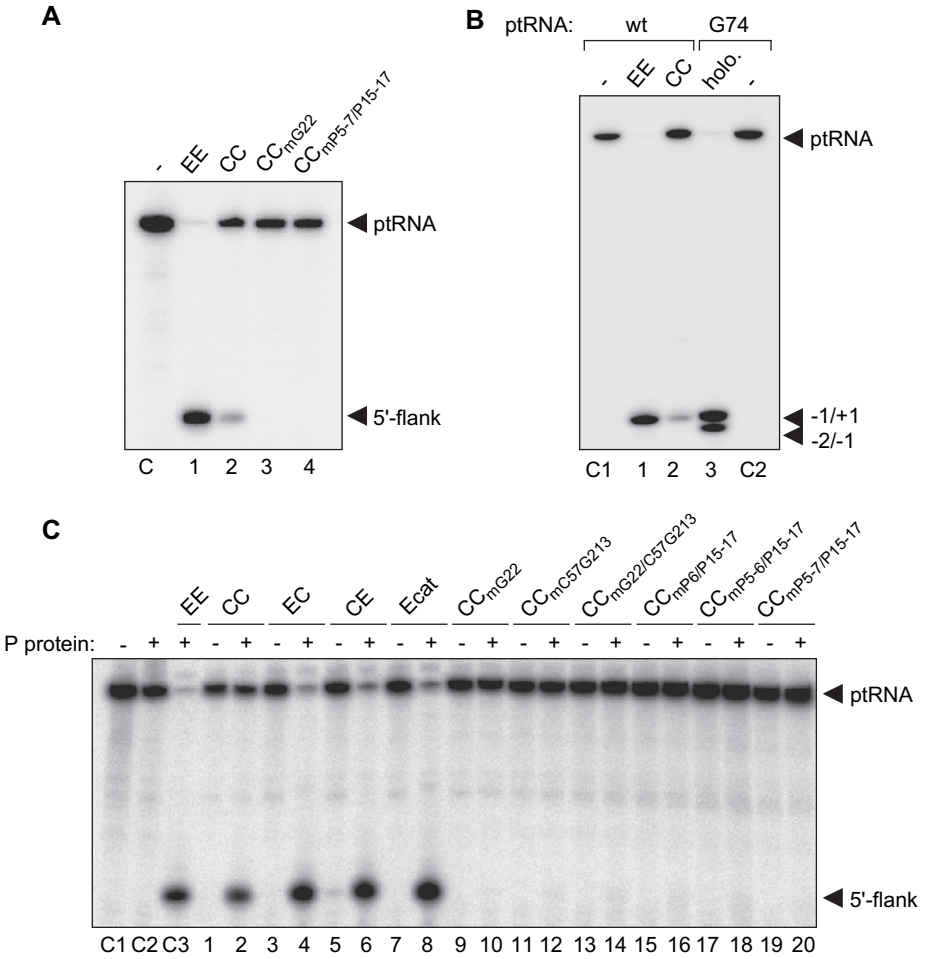

Fig. 3. Processing assays of *C. paradoxa* cyanelle P RNA (CC) and mutants thereof. (**A**) RNA-alone reactions. Assays were performed at 10 μM P RNA, 100 mM $Mg(OAc)_2$, 100 mM NH_4OAc, 50 mM MES pH 6.0 and 2 mM EDTA with trace amounts (<1 nM) of substrate (wt $ptRNA^{Gly}$); processing reactions were incubated for 4 h at 37 °C. Lane C, substrate incubated under identical conditions in the absence of P RNA; lane 1, *E. coli* P RNA (EE, 300 nM) incubated with substrate for 15 min. (**B**) Cleavage site analysis. Lanes 1 and 2: *E. coli* P RNA (300 nM, lane 1) incubated with substrate (wt $ptRNA^{Gly}$) for 30 min and CC RNA (10 μM, lane 2) for 2 h at 37 °C in the same buffer as specified in panel A; lane C1, substrate incubated as in lane 2 but in the absence of P RNA; lane 3: reference reaction with *E. coli* P RNA and protein (holo. = holoenzyme) performed as in lane C3 of panel C, but with a $ptRNA^{Gly}$ substrate that carries a C74G mutation previously reported to induce miscleavage at position −1/−2 [26]; lane C2, $ptRNA^{Gly}$G74 incubated as in lane 3 but in the absence of P RNA and protein. The 5′-cleavage products (5′-flank) are assigned on the right; −2/−1, miscleavage between nt −2 and −1; −1/+1, cleavage at the canonical site. (**C**) Holoenzyme reactions with *E. coli* P protein. Reaction conditions were 200 nM P RNA, buffer KN (see Section 2) with 10 mM Mg^{2+}, trace amounts (<1 nM) of substrate and 4 h incubation in the presence (+) or absence (−) of 1 μM *E. coli* P protein. C1 and C2, substrate incubated under identical conditions in the absence of P RNA without (C1) and with (C2) P protein; in C2, also a truncated tRNA lacking the first 18 nucleotides of its mature sequence [44] was added to the same total amount of RNA as in samples with P RNA (∼1.2 ng/μl); C3, reference with *E. coli* RNase P holoenzyme (10 nM P RNA, 50 nM P protein) incubated in buffer KN4.5 for 30 min. In RNA-alone as well as the holoenzyme reactions, P RNA species are indicated above the gel; CC and EE denote wild-type P RNA of the *C. paradoxa* cyanelle and of *E. coli*, respectively. For mutants of CC RNA, see Fig. 1; for CE, EC and Ecat RNA, see Fig. 2.

cyanelle numbering), located at the P2/P3 junction, which we changed from A in the cyanelle towards the consensus G (Fig. 1). Surprisingly, this mutation completely abrogated P RNA-alone activity (Table 1 and Fig. 3A), and reduced cleavage in the holoenzyme reaction to rates of $\leq 2 \times 10^{-5}$ min^{-1} (Table 2). A second position highly conserved in bacteria, but deviating in the cyanelle, is a C57-G213 base-pair at the distal end of P5, A-U in the cyanelle RNA (Fig. 1). The respective mutation towards the consensus again had the effect of reducing activity to non-detectable (Table 1) or to activities at the detection limit (Table 2 and Fig. 3C), as was the case for a triple mutant of these three, CC-mG22/C57G213.

The most prominent deviation of the cyanelle P RNA from the type A bacterial consensus regards the entire region of P5–P6 and P15–P17 harboring the CCA binding site in many bacterial P RNAs (Fig. 1). We stepwise converted this region and the adjacent helix P7 towards the bacterial consensus. In the first construct, CC-mP6/P15–17, the complete P15–17 module and the tertiary helix P6 of CC RNA were replaced with the corresponding elements from *E. coli* (Fig. 1). Since P5 is only 4 bp in the type A consensus with the sequence AYA (J5/6) separating P5 and P6 [31,32], we further adapted this alteration, resulting in variant CC-mP5–6/P15–17. Finally, we additionally converted helix P7 to the

Table 2
Kinetic data of RNase P holoenzyme reaction with *E. coli* P protein

Assay conditions	RNase P RNA	k_{obs} [$min^{-1} \times 10^{-3}$]
Single turnover:	EC	53 ± 15
10 mM Mg^{2+}	CE	14 ± 1
200 nM P RNA	Ecat	150 ± 40
<1 nM substrate	CC	3.6 ± 0.2
	CC-mG22	≤0.02
	CC-mC57G213	≤0.02
	CC-mG22/C57G213	≤0.02
	CC-mP6/P15–17	≤0.02
	CC-mP5–6/P15–17	≤0.02
	CC-mP5–7/P15–17	≤0.02
Multiple turnover:		*v* [$min^{-1} \times 10^{-3}$]
4.5 mM Mg^{2+}	EE	8200 ± 200
10 nM P RNA	EC	3.7 ± 1.0
100 nM substrate	Ecat	7.7 ± 0.6

Kinetic data of the RNase P holoenzyme reaction with *E. coli* P protein. Reactions were performed at 37 °C as described in Section 2 with concentrations of Mg^{2+}, P RNA and substrate as indicated. For both types of conditions, concentrations of the *E. coli* P protein were five times that of the P RNAs; k_{obs} is the pseudo-first-order rate constant of cleavage under single turnover conditions; for multiple turnover, *v* defines nmoles substrate converted per nmole of P RNA per min.

consensus regular 5-bp helix (variant CC-mP5–7/P15–17). All three variants were inactive in the RNA-alone reaction (Fig. 3A, Table 1) or resulted in cleavage rates of $\leq 2 \times 10^{-5}$ min^{-1} in the holoenzyme assay employing the *E. coli* RNase P protein as cofactor (Table 2, Fig. 3C).

3.5. Structure analysis by native PAGE

The distinct activities of variants EE, CC, CE, EC and the CC mutant RNAs prompted us to analyze overall folding by native polyacrylamide gel electrophoresis (Fig. 4), which has previously been reported as a system in which catalytically active RNase P RNA species adopt a compacted structure relative to less active conformers [9,26,33]. However, no such compaction of structure upon preincubation at 55 °C/37 °C could be observed for CC RNA, the inactive mutant CCmG22 or the domain swap chimeras EC and CE, in line with their low activity. In contrast, the CC mP5–7/P15–17 variant showed a migration pattern of a double band similar to that observed for *E. coli*, with the faster migrating band even accumulating upon preincubation. For *E. coli* P RNA, the faster migrating band has been assigned to the native fold and the upper band to a folding intermediate [26]. Such interpretation cannot be adopted to the CC mP5–7/P15–17 variant, because it was catalytically inactive. Possibly, CC mP5–7/P15–17 P RNA folds into a native-like compacted overall conformation, but some elements may still be oriented or folded inappropriately.

3.6. Complementation analysis in the B. subtilis conditional RNase P mutant strain SSB318

Although *B. subtilis* encodes a type B RNase P RNA, we recently demonstrated that even the P RNA gene (*rnpB*)

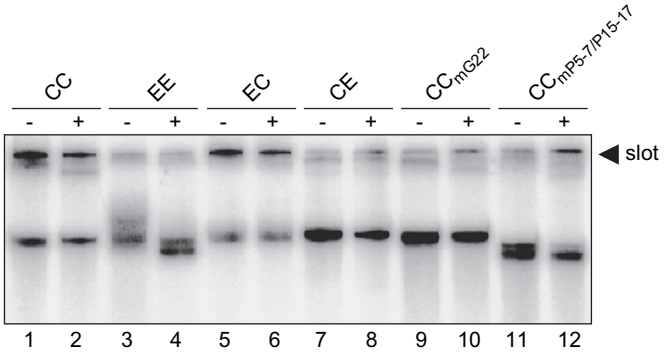

Fig. 4. Native 11.25% PAGE analysis of P RNAs from *E. coli* (EE), the *C. paradoxa* cyanelle (CC), and variants thereof. Samples were loaded onto the gel either after storage for 55 min on ice (−) or after preincubation for 5 min at 55 °C and 50 min at 37 °C (+). For details, see Section 2.

from *E. coli*, transcribed from a single chromosomal copy, is able to functionally replace the *B. subtilis* P RNA *in vivo* [27]. The *rnpB* genes (under control of the native *E. coli* *rnpB* promoter) encoding CC (or the double and triple mutants thereof), EC, CE and Ecat RNA were all unable to rescue the mutant phenotype (Table 3); only *E. coli* wild-type (EE) *rnpB* was functional in strain SSB318. These *in vivo* phenotypes are in line with the low *in vitro* activities of all cyanelle P RNA variants including the chimeras EC and CE (Tables 1 and 2).

4. Discussion

In this work we have for the first time demonstrated RNA-alone activity for *C. paradoxa* cyanelle RNase P RNA. This was observed in single turnover reactions at high ribozyme concentrations and thus parallels the recent finding of RNA-alone activity in eukaryal P RNA which until now had also been regarded as catalytically inactive [14]. The high ribozyme concentrations needed to demonstrate RNA-alone activity (Fig. 3A) are explained by low affinity of naked cyanelle P RNA for ptRNA substrates [34]. We were also able to reconstitute a functional holoenzyme from *C. paradoxa* cyanelle P RNA with the bacterial P protein from *E. coli*. Again, this is

Table 3
Complementation of *rnpB* genes in the *B. subtilis* P RNA mutant strain SSB318

rnpB gene	+IPTG		−IPTG	
	24 h	48 h	24 h	48 h
EE	+	+	+	+
−	+	+	−	−
CC	+	+	−	−
CC-mC57G213	+	+	−	−
CC-mG22/C57G213	+	+	−	−
EC	+	+	−	−
CE	+	+	−	−
Ecat	+	+	−	−

Growth of SSB318 bacteria transformed with the different derivatives of plasmid pHY300 were analyzed for growth on LB plates (+, normal growth; −, no colonies).

in contrast to work reported earlier, where a functional hybrid holoenzyme could be formed with a cyanobacterial P protein, but not with that of the γ-proteobacterium *E. coli* [21]. The conflicting data may be attributed to different ptRNA substrates used here and in the previous study or to differences in the protein purification procedure, as we saw this activity (data not shown) also under the conditions used in the study just mentioned (200 nM P RNA, 1 μM P protein, 50 mM Tris–HCl, pH 7.5, 50 mM $MgCl_2$). Our findings demonstrate that this organellar P RNA has preserved the basic capacity for RNA catalysis in the absence of protein cofactor(s) and has retained the potential to cooperate not only with P proteins from cyanobacteria, to the P RNA of which the cyanelle RNA shows the strongest structural similarity, but also with protein cofactors from phylogenetically more distant bacteria such as *E. coli*.

Our approach of constructing C-domain/S-domain chimeras of the cyanelle P RNA and that of *E. coli* in all cases resulted in hybrid ribozymes with activities roughly equal to that of the cyanelle wt P RNA or at best 4–15-fold higher (EC variant, Tables 1 and 2). Thus, the full functional potential of *E. coli* C- and S-domains could not be coaxed into largely increased ribozyme activity of the chimeras. Based on the finding that C- and S-domains fold independently [3], our results suggest that the low ribozyme activity of the cyanelle P RNA results from deficits in both domains rather than being a prominent feature of one domain only. A similar domain swap approach has recently been pursued for mitochondrial P RNAs, although the chimeras differed such that the P5–7 and P15–17 regions were swapped as part of the respective S-domain [16]. Chimeras of mitochondrial P RNAs with the C- or S-domain from *E. coli* gained ribozyme activity, whereas the original RNAs were reported to be inactive under the conditions tested [16]. However, activity of these mitochondrial/*E. coli* chimeras also remained very low compared with *E. coli* RNase P (RNA). A more specific comparison with our results though is impossible, because the boundaries between heterologous C- and S-domains in the chimeras as well as cleavage assay conditions differed, and cleavage rates were not determined in the previous study [16].

In the search for reasons why the chimeras performed poorly, one has to consider the possibility that the principle of independent C- and S-domain folding may become invalid; combining the A,U-rich and structurally less robust cyanelle domains (36% G/C content) with the more G,C-rich *E. coli* elements might lead to misfolding of the organellar domains. The same pertains to the mitochondrial domain swaps mentioned above, as those P RNAs were A,U-rich to a similar extent (e.g. 26% G/C content for *Reclinomonas americana* mitochondrial P RNA; [16]).

Also, despite the fact that the two P RNA domains fold independently, they nevertheless form a series of interdomain contacts, as confirmed by the recent crystal structures [35,36]. Here, the *E. coli* and *C. paradoxa* cyanelle P RNA domains may simply not interact in a manner as would be required for largely improved catalytic performance. In wt CC RNA, two of the three interdomain interactions within type A P RNAs, P8–L18 and L8–P4, follow the consensus: loop L8 abides by the consensus 5′-UAAYD and interacts with two conserved G-C pairs in P4, and the L18–P8 contact is sequence-identical to that of *Thermotoga maritima* P RNA, for which the crystal structure revealed formation of an A minor type II and a distorted A minor type I interaction involving the two A residues in L18 [35]. L9 of CC RNA (GAUA) deviates from the GNRA consensus and its potential receptor site would consist of two consecutive A-U base pairs, which is not observed among bacterial sequences [37]. This leaves open whether this contact forms at all in the cyanelle P RNA. In the EC and CE chimera, the L18–P8 contact will be disturbed, as the nucleoside triples A:C-G (for the GYAA tetraloop) or alternatively G:U-A (for the GYGA tetraloop) cannot form in the chimeras [31,35,38]. Taking into account that CC RNA activity was very sensitive even to a single mutation (variant CC-mG22, see below), weakening of the L18–P8 interdomain strut may have contributed to the low overall activity of CE and EC RNA.

The major difference between the cyanelle P RNA and the bacterial type A P RNA consensus is the deviation of the P15 module in the cyanelles. Type A bacterial P RNAs harbour a conserved GGU sequence in loop L15, of which the two guanosines form Watson-Crick base pairs to the 3′ CCA end of ptRNAs [26,39,40]. Here the cyanelle P RNA follows the concept of cyanobacterial P RNAs where the loop is highly asymmetric and generally lacks this nucleotide conservation [32,41]. CC RNA also has the special feature of a J16/15 segment solely consisting of A and U residues (Fig. 1). It should be mentioned here that the cyanelle P RNA follows an alternative structural concept for the P5–6/P15–17 region shared with cyanobacterial P RNAs [32]: the P6 pseudoknot, as opposed to the conserved 4 base pairs in the majority of type A bacterial P RNAs, consists of 7 base pairs in the cyanelle and is linked to P5 by only one nucleotide rather than the three nucleotides (AYA) in the majority of type A P RNAs; in addition, P15 is only 3 base pairs in length and P17 is shortened as well (compare Fig. 1 and *E. coli* P RNA in Fig. 2). P6 and P17 are assumed to stack, explaining why the lengths of these helices are inversely correlated in *E. coli*-like versus cyanobacteria-like P RNAs and consistent with the observation that the sum of the lengths of these helices is more conserved than the lengths of each helix individually [32].

To restore the CCA binding region in cyanelle P RNA and taking into account the different structural concept of this region in cyanobacteria-like P RNAs, we eventually introduced the entire P5–7/P15–17 subdomain from *E. coli* into the cyanelle P RNA. The observed inactivity of such a chimera (Tables 1 and 2) was unexpected, but might be attributed to the fact that our approach of module exchange was rather crude and more fine-tuning when embedding the module into the overall architecture of the molecule would have been required. Nevertheless the importance of this module for folding is corroborated by our native PAGE analysis: the *E. coli* P RNA-like pattern we observed for the respective cyanelle P RNA mutant reflects that incorporating the respective P5–7/P15–17 module from an *E. coli*-like type A P RNA into the cyanelle homologue leads to a largely different conformation of the entire P

RNA molecule, indicating that this module is one of the major driving forces for overall folding of P RNAs. However, this example also shows that structural compaction is not necessarily associated with robust ribozyme activity.

The deleterious effect of the G22 mutations was surprising as well. This nucleotide, connecting helix P2 and P3, is located at the binding interface for the bacterial protein cofactor [42]. Although conserved in bacterial P RNAs of type A [31,32] this position is not generally conserved among all bacterial P RNAs. While not resolved in the crystal structure of the *T. maritima* P RNA (type A [35]), in the *Bacillus stearothermophilus* structure (type B [36]) the respective residue may form a single weak hydrogen bond from its exocylic amino group to the N9 of nucleotide 338, involved in the terminal base pair of P2 in this P RNA. Such interaction would hardly be thought likely to have such major effect on activity. Similarly, the nt 57/213 base pair at the end of P5 is widely but not universally conserved [13], yet also here changing a Watson-Crick U-A bp to C-G abrogated activity. Possibly, although not conserved in bacteria, the positions we mutated here were among those crucial to the cyanelles' RNase P function. More likely, the strong effects we observed reflect that the structure and function of cyanelle P RNA is generally fragile in the absence as well as the presence of the bacterial protein and accordingly very susceptible to any mutation even at positions not functionally crucial per se. Support for this notion also comes from work by Vioque and coworkers. They converted loop L14 (5′-UCAA) of cyanelle P RNA to the bacterial GNRA consensus (5′-GCGA) by two point mutations in order to restore the L14-P8 tertiary interaction, but this surprisingly abolished holoenzyme activity with the *Synechocystis* P protein [21]. The same group further demonstrated that the cyanelle and two other plastid P RNAs have an increased sensitivity towards hydrolysis by Pb^{2+}-ions compared with cyanobacterial P RNA from *Synechocystis* [34]. Also, a prominent Pb^{2+}-hydrolysis site (Ia) in the S-domain, a hallmark of bacterial P RNAs, was not observed in cyanelle P RNA [34]. All these findings are consistent with low rigidity and robustness of the plastid P RNA and, combined with the generally low activity observed in the RNA-alone and reconstituted holoenzyme reaction, fit well with a larger role played by the cyanelle RNase P protein moiety – in line with the increased ratio of protein to RNA observed for this RNase P.

5. Conclusion

Our findings indicate that, in contrast to previous reports, RNase P from the cyanelle of *C. paradoxa* displays RNA-alone activity and is activated towards a functional holoenzyme by bacterial P proteins not only of cyanobacterial [21] but also of proteobacterial (this study) origin. Analysis of C- and S-domain swaps between cyanelle and *E. coli* P RNA revealed that the organellar and bacterial domains still have the capacity to cooperate, because the hybrid RNAs were functional. However, activities of the chimeras lagged behind the catalytic performance of the bacterial P RNA, suggesting that both the C- and S-domain of the cyanelle P RNA are weakly functional, thus limiting the activity of each type of chimera (EC or CE). In addition or alternatively, domain interaction and overall folding may be suboptimal in the chimeras, as it likely is in the wild-type cyanelle P RNA. Furthermore, the organellar ribozyme is unusual compared to the consensus of bacterial P RNAs: RNA-alone activity is low and structural alterations as small as point mutations or a switch in Watson-Crick base pair identity at positions that are not part of the universally conserved catalytic core abrogate activity as does incorporating the *E. coli* L15–16 loop and adjacent regions. In contrast, bacterial P RNA-alone activity is so robust that an RNA variant (Micro P RNA) lacking all evolutionary variable structures and thus reduced in size to almost half of that of *E. coli* P RNA still retained substantial ribozyme activity [43]. Together with the protein content of ~80% the findings reflect that indeed the cyanelle RNase P is not simply a slightly degenerate form of bacterial RNase P, but it seems to represent an RNase P type of its own. In this context the *E. coli* P protein nevertheless emerged as a universal player in P RNA activation, and it will be all the more interesting to see if bacterial P proteins are related to any of the P protein components specific to the *C. paradoxa* cyanelle that yet await identification.

Acknowledgments

This work was supported by the Deutsche Forschungsgemeinschaft (HA 1672/14-1 and GK 1384) and the Fonds der Chemischen Industrie.

References

[1] S.C. Walker, D.R. Engelke, Ribonuclease P: the evolution of an ancient RNA enzyme, Crit. Rev. Biochem. Mol. Biol. 41 (2006) 77–102.
[2] C. Guerrier-Takada, K. Gardiner, T. Marsh, N. Pace, S. Altman, The RNA moiety of ribonuclease P is the catalytic subunit of the enzyme, Cell 35 (1983) 849–857.
[3] A. Loria, T. Pan, Domain structure of the ribozyme from eubacterial ribonuclease P, RNA 2 (1996) 551–563.
[4] A. Loria, T. Pan, Recognition of the T stem-loop of a pre-tRNA substrate by the ribozyme from *Bacillus subtilis* ribonuclease P, Biochemistry 36 (1997) 6317–6325.
[5] M.E. Harris, E.L. Christian, Recent insights into the structure and function of the ribonucleoprotein enzyme ribonuclease P, Curr. Opin. Struct. Biol. 13 (2003) 325–333.
[6] A.V. Kazantsev, N.R. Pace, Bacterial RNase P: a new view of an ancient enzyme, Nat. Rev. Microbiol. 4 (2006) 729–740.
[7] J.C. Kurz, S. Niranjanakumari, C.A. Fierke, Protein component of *Bacillus subtilis* RNase P specifically enhances the affinity for precursor-$tRNA^{Asp}$, Biochemistry 37 (1998) 2393–2400.
[8] J.C. Kurz, C.A. Fierke, The affinity of magnesium binding sites in the *Bacillus subtilis* RNase P • pre-tRNA complex is enhanced by the protein subunit, Biochemistry 41 (2002) 9545–9558.
[9] A.H. Buck, A.B. Dalby, A.W. Poole, A.V. Kazantsev, N.R. Pace, Protein activation of a ribozyme: the role of bacterial RNase P protein, EMBO J. 24 (2005) 3360–3368.
[10] E. Hartmann, R.K. Hartmann, The enigma of ribonuclease P evolution, Trends Genet. 19 (2003) 561–569.
[11] A.C. Forster, S. Altman, Similar cage-shaped structures for the RNA components of all ribonuclease P and ribonuclease MRP enzymes, Cell 62 (1990) 407–409.
[12] J.L. Chen, N.R. Pace, Identification of the universally conserved core of ribonuclease P RNA, RNA 3 (1997) 557–560.

[13] S.M. Marquez, J.K. Harris, S.T. Kelley, J.W. Brown, S.C. Dawson, E.C. Roberts, N.R. Pace, Structural implications of novel diversity in eucaryal RNase P RNA, RNA 11 (2005) 739–751.
[14] E. Kikovska, S.G. Svärd, L.A. Kirsebom, Eukaryotic RNase P RNA mediates cleavage in the absence of protein, Proc. Natl. Acad. Sci. U.S.A. 104 (2007) 2062–2067.
[15] J.A. Pannucci, E.S. Haas, T.A. Hall, J.K. Harris, J.W. Brown, RNase P RNAs from some Archaea are catalytically active, Proc. Natl. Acad. Sci. USA 96 (1999) 7803–7808.
[16] E. Seif, A. Cadieux, B.F. Lang, Hybrid *E. coli*-Mitochondrial ribonuclease P RNAs are catalytically active, RNA 12 (2006) 1661–1670.
[17] C.A. Wise, N.C. Martin, Dramatic size variation of yeast mitochondrial RNAs suggests that RNase P RNAs can be quite small, J. Biol. Chem. 266 (1991) 19154–19157.
[18] M.J. Wang, N.W. Davis, P. Gegenheimer, Novel mechanisms for maturation of chloroplast transfer RNA precursors, EMBO J. 7 (1988) 1567–1574.
[19] W. Martin, B. Stoebe, V. Goremykin, S. Hapsmann, M. Hasegawa, K.V. Kowallik, Gene transfer to the nucleus and the evolution of chloroplasts, Nature 393 (1998) 162–165.
[20] M. Baum, A. Cordier, A. Schön, RNase P from a photosynthetic organelle contains an RNA homologous to the cyanobacterial counterpart, J. Mol. Biol. 257 (1996) 43–52.
[21] A. Pascual, A. Vioque, Functional reconstitution of RNase P activity from a plastid RNA subunit and a cyanobacterial protein subunit, FEBS Lett. 442 (1999) 7–10.
[22] A. Cordier, A. Schön, Cyanelle RNase P: RNA structure analysis and holoenzyme properties of an organellar ribonucleoprotein enzyme, J. Mol. Biol. 289 (1999) 9–20.
[23] V. Picard, E. Ersdal-Badju, A. Lu, S.C. Bock, A rapid and efficient one-tube PCR-based mutagenesis technique using Pfu DNA polymerase, Nucleic Acids Res. 22 (1994) 2587–2591.
[24] C. Heide, T. Pfeiffer, J.M. Nolan, R.K. Hartmann, Guanosine 2-NH_2 groups of *Escherichia coli* RNase P RNA involved in intramolecular tertiary contacts and direct interactions with tRNA, RNA 5 (1999) 102–116.
[25] S. Busch, L.A. Kirsebom, H. Notbohm, R.K. Hartmann, Differential role of the intermolecular base-pairs G292-C_{75} and G293-C_{74} in the reaction catalyzed by *Escherichia coli* RNase P RNA, J. Mol. Biol. 299 (2000) 941–951.
[26] B. Wegscheid, R.K. Hartmann, The precursor tRNA 3′-CCA interaction with *Escherichia coli* RNase P RNA is essential for catalysis by RNase P *in vivo*, RNA 12 (2006) 2135–2148.
[27] B. Wegscheid, C. Condon, R.K. Hartmann, Type A and B RNase P RNAs are interchangeable *in vivo* despite substantial biophysical differences, EMBO Rep. 7 (2006) 411–417.
[28] B. Wegscheid, R.K. Hartmann, *In vivo* and *in vitro* investigation of bacterial type B RNase P interaction with tRNA 3′-CCA, Nucleic Acids Res. 35 (2007) 2060–2073.
[29] C.J. Green, R. Rivera-Leon, B.S. Vold, The catalytic core of RNase P, Nucleic Acids Res. 24 (1996) 1497–1503.
[30] E.S. Haas, J.W. Brown, C. Pitulle, N.R. Pace, Further perspectives on the catalytic core and secondary structure of ribonuclease P RNA, Proc. Natl. Acad. Sci. USA 91 (1994) 2527–2531.
[31] Massire, C., Développement de logiciels d'aide à la modélisation d'ARN. Application à la composante ribonucléique de la ribonucléase P bactérienne, Ph.D. thesis, Université Louis Pasteur, Strasbourg, 1998.
[32] E.S. Haas, J.W. Brown, Evolutionary variation in bacterial RNase P RNAs, Nucleic Acids Res. 26 (1998) 4093–4099.
[33] S.M. Marquez, J.L. Chen, D. Evans, N.R. Pace, Structure and function of eukaryotic ribonuclease P RNA, Mol. Cell 24 (2006) 445–456.
[34] J. de la Cruz, A. Vioque, A structural and functional study of plastid RNAs homologous to catalytic bacterial RNase P RNA, Gene 321 (2003) 47–56.
[35] A. Torres-Larios, K.K. Swinger, A.S. Krasilnikov, T. Pan, A. Mondragon, Crystal structure of the RNA component of bacterial ribonuclease P, Nature 437 (2005) 584–587.
[36] A.V. Kazantsev, A.A. Krivenko, D.J. Harrington, S.R. Holbrook, P.D. Adams, N.R. Pace, Crystal structure of a bacterial ribonuclease P RNA, Proc. Natl. Acad. Sci. USA 102 (2005) 13392–13397.
[37] C. Massire, L. Jaeger, E. Westhof, Derivation of the three-dimensional architecture of bacterial ribonuclease P RNAs from comparative sequence analysis, J. Mol. Biol. 279 (1998) 773–793.
[38] J.W. Brown, J.M. Nolan, E.S. Haas, M.A.T. Rubio, F. Major, N.R. Pace, Comparative analysis of ribonuclease P RNA using gene sequences from natural microbial populations reveals tertiary structural elements, Proc. Natl. Acad. Sci. USA 93 (1996) 3001–3006.
[39] L.A. Kirsebom, S.G. Svärd, Base pairing between *Escherichia coli* RNase P RNA and its substrate, EMBO J 13 (1994) 4870–4876.
[40] S.G. Svärd, U. Kagardt, L.A. Kirsebom, Phylogenetic comparative mutational analysis of the base-pairing between RNase P RNA and its substrate, RNA 2 (1996) 463–472.
[41] A. Schön, C. Fingerhut, W.R. Hess, Conserved and variable domains within divergent RNase P RNA gene sequences of *Prochlorococcus* strains, Int. J. Syst. Evol. Microbiol. 52 (2002) 1383–1389.
[42] A.H. Buck, A.V. Kazantsev, A.B. Dalby, N.R. Pace, Structural perspective on the activation of RNAse P RNA by protein, Nat. Struct. Mol. Biol. 11 (2005) 958–964.
[43] R.W. Siegel, A.B. Banta, E.S. Haas, J.W. Brown, N.R. Pace, *Mycoplasma fermentans* simplifies our view of the catalytic core of ribonuclease P RNA, RNA 2 (1996) 452–462.
[44] T. Persson, S. Cuzic, R.K. Hartmann, Catalysis by RNase P RNA: unique features and unprecedented active site plasticity, J. Biol. Chem. 278 (2003) 43394–43401.

4.2 Minor changes largely restore catalytic activity of archaeal RNase P RNA from *Methanothermobacter thermoautotrophicus*

Dan Li, Dagmar K. Willkomm, Roland K. Hartmann (2009)
Nucleic Acids Research, **37** (1), 231-242.

Published online 26 November 2008

Nucleic Acids Research, 2009, Vol. 37, No. 1 ***231–242***
doi:10.1093/nar/gkn915

Minor changes largely restore catalytic activity of archaeal RNase P RNA from *Methanothermobacter thermoautotrophicus*

Dan Li, Dagmar K. Willkomm and Roland K. Hartmann*

Institut für Pharmazeutische Chemie, Philipps-Universität Marburg, D-35037 Marburg, Germany

Received April 30, 2008; Revised October 27, 2008; Accepted October 30, 2008

ABSTRACT

The increased protein proportion of archaeal and eukaryal ribonuclease (RNase) P holoenzymes parallels a vast decrease in the catalytic activity of their RNA subunits (P RNAs) alone. We show that a few mutations toward the bacterial P RNA consensus substantially activate the catalytic (C-) domain of archaeal P RNA from *Methanothermobacter*, in the absence and presence of the bacterial RNase P protein. Large increases in ribozyme activity required the cooperative effect of at least two structural alterations. The P1 helix of P RNA from *Methanothermobacter* was found to be extended, which increases ribozyme activity (ca 200-fold) and stabilizes the tertiary structure. Activity increases of mutated archaeal C-domain variants were more pronounced in the context of chimeric P RNAs carrying the bacterial specificity (S-) domain of *Escherichia coli* instead of the archaeal S-domain. This could be explained by the loss of the archaeal S-domain's capacity to support tight and productive substrate binding in the absence of protein cofactors. Our results demonstrate that the catalytic capacity of archaeal P RNAs is close to that of their bacterial counterparts, but is masked by minor changes in the C-domain and, particularly, by poor function of the archaeal S-domain in the absence of archaeal protein cofactors.

INTRODUCTION

The ribonucleoprotein enzyme ribonuclease P (RNase P) throughout phylogeny removes 5′ leader sequences of precursor tRNAs (ptRNAs) to generate mature tRNA 5′ ends. The enzyme harbors a single RNA subunit (P RNA) of common ancestry, but only bacterial P RNAs are efficient catalysts *in vitro* in the absence of the single bacterial protein cofactor (1,2). Very low RNA-alone activity of archaeal, eukaryal and organellar P RNAs (3–5) correlates with the presence of multiple protein subunits (usually 4 in Archaea and 9–10 in Eukarya).

Bacterial P RNAs are composed of two independent folding domains, the catalytic (C-) domain and the specificity (S-) domain (6,7; Figure 1), the latter playing a crucial role in substrate binding via its interaction with the T stem-loop region of ptRNAs (for review, see 8). The single bacterial RNase P protein (P protein), dispensable *in vitro* but essential *in vivo* (9,10), binds to the P2–J2/3–J3/4–P4–J18/2 region in the C-domain of P RNA (11–14). The protein increases substrate affinity through interaction with the 5′-leader (14,15), which entails tighter binding of key metal ions involved in substrate positioning and catalysis (16).

Activity of archaeal P RNA in the absence of the archaeal RNase P protein cofactors Pop5, Rpp21, Rpp29 and Rpp30 was observed solely for one of the two types of archaeal P RNAs, type A, but not type M (3). Archaeal type A RNAs are structurally related to bacterial P RNAs, but lack the P13/14 stem and helix-P18 among several other deviations from the bacterial consensus (17; Figure 1). Type A archaeal P RNA-alone activity was observed to be low and limited to conditions of very high ionic strength for optimal activity, such as 3 M NH_4^+ and 0.3 M Mg^{2+} in the case of P RNA from the euryarchaeon *Methanothermobacter thermoautotrophicus* (3). Addition of the P protein from *Bacillus subtilis* activated the archaeal P RNA to some extent at lower ionic strength (3).

For bacterial type A RNA, three loop-helix interdomain contacts (L8–P4, L9–P1 and L18–P8) have been identified (18–21) and are thought to orient the C- and S-domains toward each other (Figure 1). Only one of these contacts, L8–P4, can form in the *M. thermoautotrophicus* P RNA structure, since the P18 element is missing and the reported 5′- and 3′-ends of the RNA (3) only permit formation of a P1 helix too short to serve as a receptor site for L9 (Figure 1).

*To whom correspondence should be addressed. Tel: +49 6421 2825827; Fax: +49 6421 2825854; Email: roland.hartmann@staff.uni-marburg.de

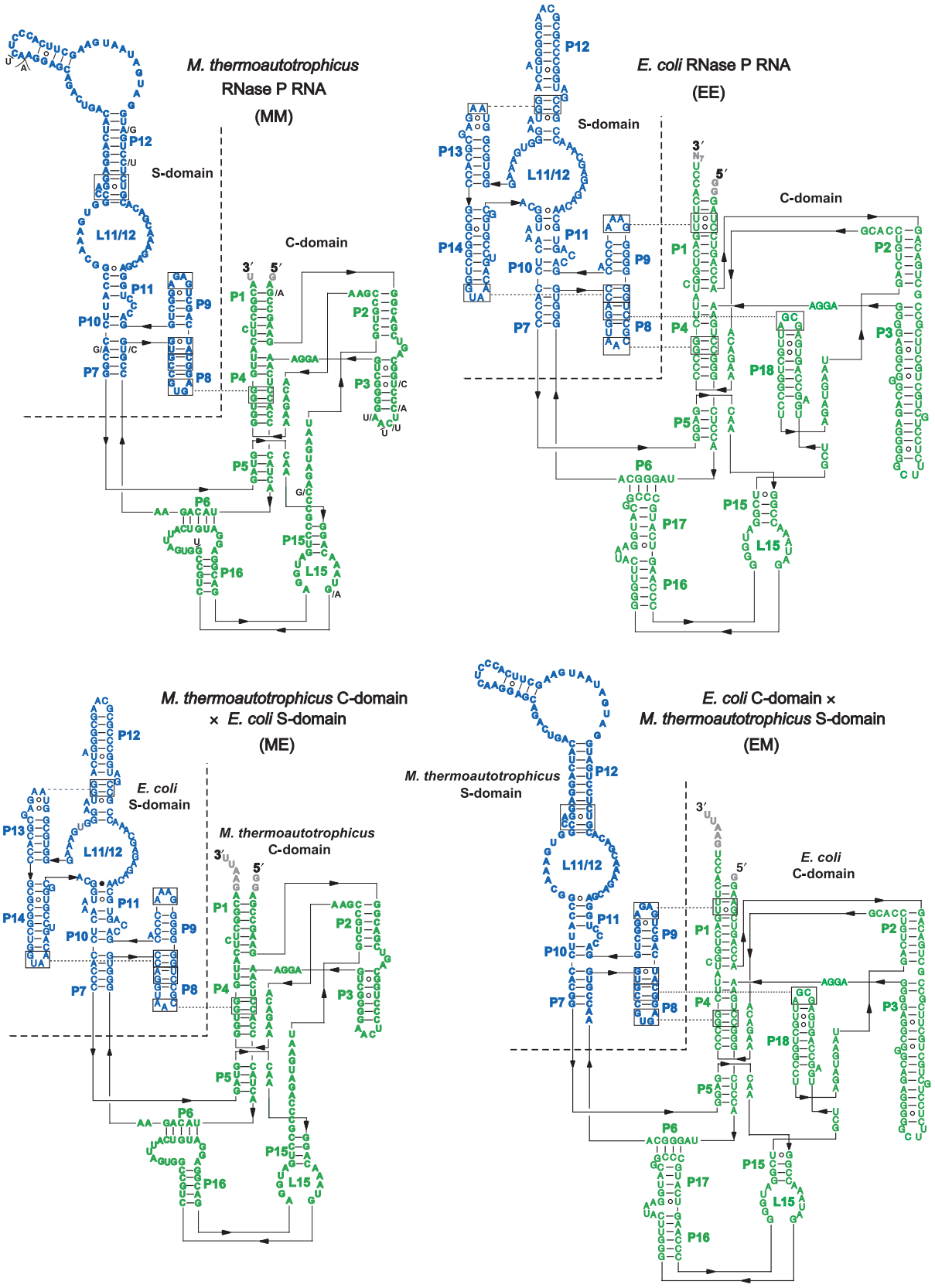

Figure 1. Secondary structure presentation according to Massire *et al.* (20) of *M. thermoautotrophicus* ΔH RNase P RNA (MM), *E. coli* P RNA (EE), and chimeras with the C-domain from *M. thermoautotrophicus* and the S-domain from *E. coli* (ME) and vice versa (EM). The 13 nucleotide exchanges and the single 1-nt insertion in P RNA of strain *M. thermoautotrophicus* strain Marburg (MM-Marburg in the tables) relative to *M. thermoautotrophicus* ΔH are indicated along the sequence in the secondary structure of MM RNA. The C-domain is depicted in green and the S-domain is depicted in blue. Grey nucleotides at the 5′- and 3′-ends indicate non-natural additions present in the T7 *in vitro* transcripts.

Previous attempts to increase the RNA-alone activity of archaeal or organellar P RNAs by insertion of structural elements or by *in vitro* selection have failed to identify variants with improved RNA-alone activity relative to the corresponding wild-type RNA (5,17,22). We have reinvestigated this issue in a more systematic manner by constructing a series of archaeal C-domain variants with confined alterations towards the bacterial P RNA consensus. The aim of this approach was to identify specific deficits of archaeal P RNAs that limit their RNA-alone activity and make them depend so much more on protein cofactors than their bacterial homologs. Combining the archaeal C-domain from *M. thermoautotrophicus* P RNA with the S-domain of *Escherichia coli* P RNA we were able to increase activity—up to three orders of magnitude—by simultaneously introducing a few minor alterations into the archaeal C-domain. All variants were screened at two Mg^{2+} concentrations, 100 mM in the RNA-alone reaction and 4.5 mM in the holoenzyme reaction. Observed activity gains may well include contributions from improved Mg^{2+} binding, which in turn could have affected folding, substrate binding, catalysis or binding of the RNase P protein. Thus, activity differences between tested P RNA variants might be mitigated to some extent at Mg^{2+} concentrations higher than those applied here (see Discussion section). We further provide evidence that the genuine 5′-and 3′-ends of P RNA from *Methanothermobacter* are longer than previously determined (3). This longer P1, which resulted in 100–200-fold higher RNA-alone activity, may exert its effect primarily through formation of the L9–P1 contact. Finally, analysis of ternary complex formation (P RNA, P protein, ptRNA) revealed that the archaeal S-domain has lost the capacity of bacterial S-domains to confer affine and productive interaction with the substrate, thereby masking the catalytic capacity of archaeal C-domains.

MATERIAL AND METHODS

Construction of plasmids for complementation and *in vitro* transcription

Plasmids were constructed by standard cloning and PCR methods as described in (5). For specific details of plasmid construction and the oligonucleotides used, see Supplementary Information.

In vitro transcription and 5′ endlabelling of P RNAs and substrate ptRNA

Run-off transcription with bacteriophage T7 RNA polymerase and 5′ and 3′ endlabelling with T4 polynucleotide kinase and T4 RNA ligase were performed essentially as described (23,24). Templates used were pSBpt3′HH linearized with BamHI for the *Thermus thermophilus* $ptRNA^{Gly}$ substrate (23), pDW98 linearized with BsaAI for *E. coli* P RNA (24) and pUC119_T7_M.th._rnpB linearized with BsaI for *M. thermoautotrophicus* wild-type P RNA (3). Mutants of the latter were transcribed from the pUC19 constructs described in Supplementary Information; all pUC19 derivatives were linearized with EcoRI.

Expression and purification of recombinant *E. coli* RNase P protein

E. coli RNase P protein (tagged with an N-terminal hexahistidyl peptide leader MRGSHHHHHHGS, encoded in plasmid pQE-30) was recombinantly expressed in *E. coli* JM109 and purifed by Ni-NTA affinity chromatography as described (25).

RNase P processing assays

The $ptRNA^{Gly}$ substrate (23) was preincubated in assay buffer for 5 min at 55°C and 25 min at 37°C, P RNAs (separately) for 5 min at 55°C and 35 min at 37°C. For holoenzyme reactions, *E. coli* P protein was added to the P RNA 5 min before combining enzyme and substrate. Conditions of RNA-alone reactions were single turnover with trace amounts (<1 nM) of 5′-^{32}P-labelled substrate, 300 nM or 10 μM P RNA, 100 mM $Mg(OAc)_2$, 100 mM NH_4OAc, 50 mM MES and 2 mM EDTA, pH 6.0 and 37°C. Holoenzyme reactions were performed as multiple turnover reactions at concentrations of 10 nM P RNA, 50 nM P protein, 100 nM $ptRNA^{Gly}$, and buffer KN (20 mM HEPES-KOH pH 7.4, 4.5 mM $Mg[OAc]_2$, 150 mM NH_4OAc, 2 mM spermidine, 0.05 mM spermine and 4 mM β-mercaptoethanol) at 37°C. Analysis of reactions by denaturing PAGE and evaluation of data was done as described (23); all quantifications were based on at least three independent experiments.

Folding analysis by native PAGE

3′-End-labelled P RNAs were preincubated at a concentration of 10 nM in buffer KN for 5 min at 55°C and then 50 min at 37°C. After addition of 1 volume of gel loading buffer (10% [v/v] glycerol, 4.5 mM $MgCl_2$, xylene cyanol and bromophenol blue) at room temperature, the samples were immediately loaded onto non-denaturing polyacrylamide gels (11.25% [v/v] polyacrylamide, 66 mM HEPES, 33 mM Tris [pH 7.4], 0.1 mM EDTA, 100 mM NH_4OAc and 4.5 mM $MgCl_2$). Gels were run and the RNAs visualized as described (25).

UV melting profiles

UV melting profiles were recorded at 260 nm on a CARY 100 Bio UV-Visible spectrophotometer, using the Cary Win UV software version 3.00.

Bacterial strains

Total RNAs for RACE experiments were prepared from cells of *M. thermoautotrophicus* strain Marburg (DSM 2133, syn. *M. marburgensis*), whereas the *Methanothermobacter* RNase P RNA used throughout this study is that of *M. thermoautotrophicus* strain ΔH (DSM 1053).

Determination of equilibrium dissociation constants

Equilibrium dissociation constants (K_d) of complex formation between RNase P holoenzymes and ptRNA substrate were determined by spin column assays essentially as described (26,27) in a binding buffer containing 50 mM Tris-acetate, pH 7.1, 200 mM NH_4OAc, 0.05% Nonidet P-40, and 15 mM $Ca(OAc)_2$. Ca^{2+} was used instead of

Mg^{2+} to prevent substrate cleavage during binding and the concentration of 15 mM was chosen to increase sensitivity of the assay, because the K_d's measured at this Ca^{2+} concentration are substantially lower than those obtained at lower concentrations (e.g. 5 mM Ca^{2+}). Before the assay, holoenzymes were reconstituted from P RNA variants and *E. coli* P protein by incubating 1 μM P RNA in binding buffer for 1 h at 37°C and then adding *E. coli* P protein to 5 μM, followed by another 15 min at 37°C. Holoenzymes were then diluted in binding buffer to desired concentrations, incubated for 5 min at 37°C, mixed with trace amounts (<1 nM) of 5′-^{32}P-labelled substrate (preincubated for 30 min at 37°C in binding buffer) and incubated at 37°C for 5 min.

RESULTS

Analysis of *E. coli* and *M. themoautotrophicus* wild-type and chimeric P RNAs

Starting from *M. thermoautotrophicus* wild-type P RNA (henceforth called MM RNA) and *E. coli* wild-type P RNA (termed EE RNA; Figure 1), we constructed P RNA chimeras by combining the S-domain of *E. coli* P RNA with the C-domain of *M. thermoautotrophicus* (termed ME RNA) or the *E. coli* C-domain with the *M. thermoautotrophicus* S-domain (termed EM RNA; Figure 1). The chimeric P RNAs allowed us to address if the heterologous domains are able to cooperate and if there is a major asymmetry in the contribution of the archaeal C- and S-domains to the low RNA-alone activity of the archaeal P RNA.

RNA-alone single turnover reactions (E>>S) at pH 6.0 in the presence of 300 nM P RNA, trace amounts (<1 nM) $ptRNA^{Gly}$ and 0.1 M each Mg^{2+} and NH_4^+ revealed only very weak cleavage by EM RNA (2×10^{-4} min^{-1}) and no activity at all with ME and MM P RNA (Table 1). The activity of EM RNA increased linearly with concentration (tested from 300 nM to 10 μM, data not shown), indicating low substrate affinity. At 10 μM P RNA concentration, activities were detectable for all P RNA variants, with the chimeras EM and ME being 34–44-fold more active than the archaeal MM RNA (Table 1). The finding of activity at 10 μM but not at 0.3 μM for the MM and ME variants suggested that weak substrate affinity is also a major cause for the poor performance of these two P RNAs. The lower RNA-alone activity of MM versus EM and ME RNA (Table 1) showed that deficits of MM RNA are located in its S- as well as its C-domain.

As in the RNA-alone reactions, RNase P holoenzymes reconstituted with the *E. coli* P protein and tested for multiple turnover under near-physiological salt conditions (buffer KN, 4.5 mM Mg^{2+}, 10 nM P RNA, 50 nM P protein, 100 nM $ptRNA^{Gly}$) yielded very low cleavage rates for MM RNA and the ME chimera (Table 1). The EM variant was 35-fold more active than MM and ME, though still a factor of >1000 slower than EE RNA. Higher activity of EM RNA, harbouring the *E. coli* C-domain, was anticipated because the primary binding site of the bacterial P protein is in the C-domain (11–14). The fact that EM RNA activity equaled that of the isolated C-domain of *E. coli* P RNA (Ecat; Table 1) indicates that the archaeal S-domain made no functional contribution under the applied conditions of the holoenzyme assay. Not unexpected, alleles encoding MM, EM and ME RNAs were unable to rescue the mutant phenotype of a bacterial RNase P mutant strain (Table S3).

Table 1. ptRNA processing activity of *E. coli*/*M. thermoautotrophicus* P RNA domain swop chimeras in RNA-alone and holoenzyme assays

P RNA alone		Holoenzyme	
P RNA	k_{obs} [$min^{-1} \times 10^{-4}$]	P RNA	k_{obs} [$min^{-1} \times 10^{-4}$]
EE (0.3 μM)	51 000 ± 4000	EE (10 nM)	82 000 ± 2000
EM (0.3 μM)	2 ± 1	EM	Not analyzed
ME (0.3 μM)	Not detectable	ME	Not analyzed
MM (0.3 μM)	Not detectable	MM	Not analyzed
EM (10 μM)	88 ± 19	EM (10 nM)	70 ± 10
ME (10 μM)	67 ± 17	ME (10 nM)	2 ± 1
MM (10 μM)	2 ± 0.1	MM (10 nM)	2 ± 1
Ecat (10 μM)	Not detectable	Ecat (10 nM)	77 ± 6

Assay conditions for the RNA-alone reaction were 50 mM MES pH 6.0 at 37°C, 2 mM EDTA, 100 mM NH_4OAc, 100 mM $Mg(OAc)_2$, trace amounts of ptRNA and 10 μM P RNA unless otherwise indicated. Holoenzyme activity assays were performed at 20 mM HEPES pH 7.4 at 37°C, 2 mM spermidine, 0.05 mM spermine, 4 mM β-mercaptoethanol, 150 mM NH_4OAc, 4.5 mM $Mg(OAc)_2$, 100 nM ptRNA, 10 nM P RNA and 50 nM recombinant *E. coli* P protein with N-terminal His tag. Errors are standard deviations; all values are based on at least three independent experiments. For further experimental details see Materials and methods section. Values for EE and Ecat RNA are taken from ref. (5).

ME RNA variants with specific structural alterations in the archaeal C-domain

With its substantial increase in RNA-alone activity compared to MM RNA (Table 1), we assumed ME RNA to be more sensitive toward activating changes in the archaeal C-domain. We thus generated an initial set of ME derivatives that were mutated towards the bacterial type A RNase P RNA consensus (28) by mutations ranging from single nucleotide exchanges to exchange of defined modules (Figure 2). RNA-alone and holoenzyme assays were conducted as specified in Table 1, and activities of the ME variants illustrated in Figure 2 are summarized in Table 2.

RNA-alone activity

Among the initial set of eight variants, only a single variant, with a point mutation in the region that joins P15 and P18 in bacterial P RNA, had increased RNA-alone activity relative to ME RNA (ME-mJ15/18, 4-fold increase; Table 2). The other variants displayed RNA-alone cleavage rates decreased from 2-fold to below the level of detection in the case of ME-mP17. The latter alteration introduced the P6/16/17 elements of *E. coli* P RNA, based on the idea that this may help to position the L15 loop for interaction with the tRNA 3′-CCA end. The next most prominent impairments were seen for ME-mP1 (176-fold), which introduced the *E. coli* P1 helix intended to restore the L9–P1 interdomain contact, and for

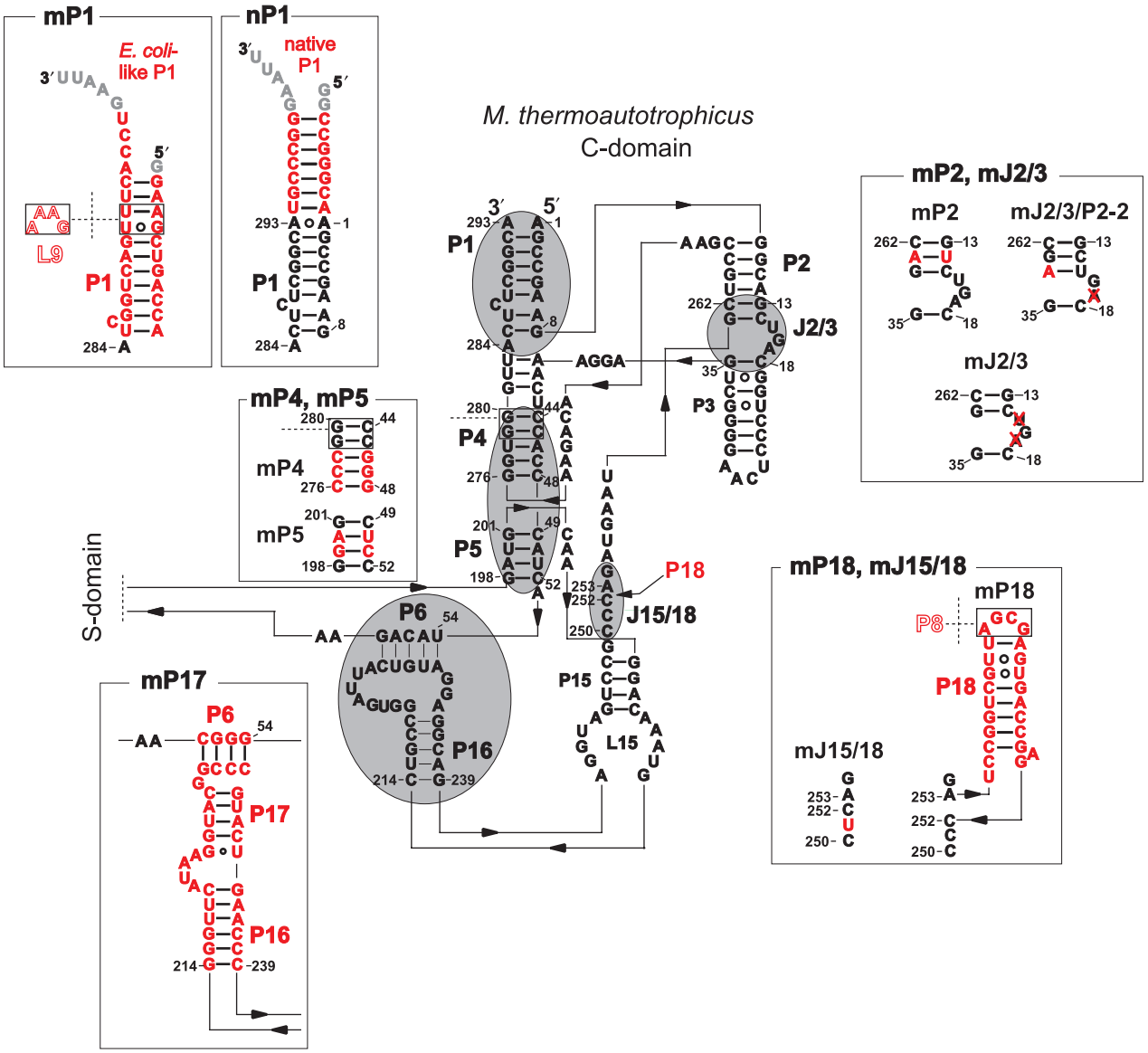

Figure 2. Secondary structure presentation of the C-domain from *M. thermoautotrophicus* according to Massire *et al.* (20) with mutations introduced during this work. Regions subjected to mutation are circled and highlighted in grey; sequences of the respective mutants (indicated by the prefix 'm', e.g. mP1) are given in the adjacent boxes with the altered nucleotides coloured in red. Throughout the paper, combinations of mutations are indicated by a slash inbetween, e.g. ME-mJ2/3/P2 refers to mutation mJ2/3 as well as mutation mP2 within one construct, with the ME in front indicating that the construct possesses an *M. thermoautotrophicus* C-domain and an *E. coli* S-domain. Grey nucleotides at the 5′- and 3′-ends indicate non-natural additions present in the T7 *in vitro* transcripts. Nucleotide numbering is that of *M. thermoautotrophicus* ΔH P RNA.

ME-mP4 (24-fold) with three Watson-Crick base pair identities in P4 changed towards the bacterial consensus (Figure 2, Table 2). Likewise, insertion of *E. coli* P18 (ME-mP18) to restore the L18–P8 interdomain contact failed to improve activity, in line with a previous study (17).

In a second round, the variant with increased activity, ME-mJ15/18, was combined with each of the other structural alterations. RNA-alone activities of the double mutants either equalled that of ME RNA (within a factor of two) or remained substantially lower (ME-mJ15/18/P1, ME-mJ15/18/P17), with one notable exception: incorporation of *E. coli* P18 (ME-mJ15/18/P18) significantly increased activity compared to ME and also ME-mJ15/18 (Table 2). If the individual changes (mJ15/18 and mP18) were independent and additive, one would have expected a roughly 2-fold increase in activity. However, the 49-fold increase for ME-mJ15/18/P18 versus ME indicates positive cooperativity between the two structural alterations.

Activity with the bacterial P protein as cofactor

When we assayed P RNA mutants for holoenzyme activity using the *E. coli* P protein as cofactor (Table 2, right columns), again only a single variant showed a marked

Table 2. Activity of ME variants in RNA-alone and holoenzyme assays

RNase P RNA	RNA-alone		Holoenzyme	
	k_{obs} [$min^{-1} \times 10^{-4}$]	Change	k_{obs} [$min^{-1} \times 10^{-4}$]	Change
ME	67 ± 17	1	2.0 ± 1.0	1
ME-mP1	0.4 ± 0.1	↓ 176×	1.1 ± 0.1	↓ 2×
ME-mP2	9.7 ± 1.2	↓ 7×	1.1 ± 0.2	↓ 2×
ME-mP4	2.8 ± 1.8	↓ 24×	1.2 ± 0.1	↓ 2×
ME-mP5	41 ± 5	↓ 2×	1.2 ± 0.1	↓ 2×
ME-mP17	Not detectable		1.1 ± 0.1	↓ 2×
ME-mP18	39 ± 6	↓ 2×	4.0 ± 0.3	↑ 2×
ME-mJ15/18	250 ± 45	↑ 4×	6.5 ± 0.3	↑ 3×
ME-mJ2/3	7.7 ± 1.2	↓ 9×	52 ± 6	↑ 26×
ME-mJ15/18/P1	0.5 ± 0.1	↓ 143×	1.3 ± 0.2	↓ 2×
ME-mJ15/18/P2	29 ± 7.2	↓ 2×	3.6 ± 0.3	↑ 2×
ME-mJ15/18/P4	160 ± 15	↑ 2×	3.2 ± 0.3	↑ 2×
ME-mJ15/18/P5	100 ± 25	1×	3.2 ± 0.4	↑ 2×
ME-mJ15/18/P17	1.6 ± 1.2	↓ 42×	1.3 ± 0.1	↓ 2×
ME-mJ15/18/P18	3250 ± 400	↑ 49×	12 ± 0.2	↑ 6×
ME-mJ15/18/2/3	33 ± 3.5	↓ 2×	320 ± 30	↑ 160×
ME-mJ2/3/P2	1350 ± 240	↑ 20×	900 ± 200	↑ 450×
ME-mJ2/3/P2-2	480 ± 120	↑ 7×	480 ± 50	↑ 240×
ME-mJ15/18/2/3/P2	5400 ± 910	↑ 81×	930 ± 20	↑ 465×
ME-mJ15/18/2/3/P2/nP1	9880 ± 2520	↑ 147×	3000 ± 500	↑1500×

For assay conditions and experimental details, see legend to Table 1 and Materials and methods section.

increase in activity (26-fold) over ME RNA (ME-mJ2/3, with J2/3 reduced from 3 to 1 nt; Figure 2). The fact that this small alteration caused a 9-fold activity decrease in the RNA-alone reaction, but 26-fold increase in the holoenzyme reaction suggested an effect on P protein binding, which is consistent with current knowledge about the P RNA binding interface of the bacterial P protein (Figure S1). All other individual changes had little effect (within 3-fold) on the holoenzyme reaction.

Combination of the J15/18 mutation with one of the other structural alterations in the second round revealed two variants with substantially improved activity in the holoenzyme reaction: ME-mJ15/18/P18 (6-fold) and ME-mJ15/18/J2/3 (160-fold; Table 2).

Changes in P2–P3 and the triple mutant ME-J15/18/2/3/P2

The activity increase in the holoenzyme reaction owing to deletion of two nucleotides in J2/3 prompted us to combine changes towards the bacterial consensus in J2/3 and P2, aiming at a further improvement of *E. coli* P protein binding to the ME chimera. Helix-P2, which is part of the bacterial P protein binding site (see Introduction section and Figure S1), consists of 6 bp in MM RNA compared with 7 bp in bacterial P RNAs. We thus constructed P RNA variants that combine the J2/3 mutation with a P2 helix extended by 1 bp. In the first mutant an U–A bp was inserted between the fifth and the sixth base pair (counted from the 5′-end; Figure 2) of the archaeal P2 helix. This increased RNA-alone activity 20-fold (ME-mJ2/3/P2), whereas these alterations individually impaired activity 9-fold (mJ2/3) and 7-fold (mP2; Table 2). In the holoenzyme reaction, the activity gain for variant ME-mJ2/3/P2 was 450-fold over ME RNA, compared with a 26-fold rate increase for variant ME-mJ2/3 and a 2-fold drop for variant ME-mP2. Thus, we observed positive cooperativity effects for the combined mJ2/3/P2 changes in the RNA-alone and holoenzyme assays, indicating that the P2–J2/3–P3 region not only contributes to bacterial P protein binding, but also to folding of the catalytic core.

We further constructed variant ME-mJ2/3/P2-2 with the goal to restore the bacterial consensus with minimal structural alteration, solely deleting 1 nt in J2/3 and introducing a point mutation that creates an additional U–A bp at the end of P2. This variant improved RNA-alone activity of ME RNA 7-fold and raised substrate turnover 240-fold in the holoenzyme reaction (Table 2). The 2–3-fold weaker performance of variant ME-mJ2/3/P2-2 relative to ME-mJ2/3/P2 suggests that a terminal U–A bp at the P2/P3 junction has a slightly destabilizing effect compared with a closing C–G bp.

We then combined the mJ15/18 point mutation with the mJ2/3/P2 alteration to generate variant ME-J15/18/2/3/P2. This further increased activity roughly 4-fold relative to ME-mJ2/3/P2 in the RNA-alone reaction, but showed little additional effect in the holoenzyme reaction (Table 2), for unknown reasons.

Length of P1 and the L9–P1 interdomain contact

In some bacterial P RNAs, a long-range tertiary interaction between loop L9 docking onto helix P1 serves as an interdomain strut of major importance for the global RNA fold (20,29). The mature 5′- and 3′-ends of MM RNA, mapped in a previous study (3), would be too short to allow formation of such an L9–P1 contact. However, some archaeal P RNAs seem to have an extended P1 helix compatible with formation of the L9–P1 contact, and even the MM RNA gene sequence encodes the potential for an extended P1 helix that, if part of the P RNA transcript, may enable formation of the P1–L9 interaction. (17). We thus constructed an MM RNA variant with P1 extended by 7 bp based on the sequence of the P RNA (*rnpB*) gene of *M. thermautotrophicus* strain ΔH. This increased the RNA-alone activity of MM RNA 200-fold (Table 3). Introduction of this P1 extension into variant ME-mJ15/18/2/3/P2 to generate ME-mJ15/18/2/3/P2/nP1 further increased activity to 147-fold (RNA-alone) and 1500-fold (holoenzyme) over ME RNA (Table 2).

The stimulating effect of extension nP1 on MM RNA-alone activity prompted us to reinvestigate the 5′- and 3′-boundaries of MM RNA by RACE. This was done with the closely related *M. thermoautotrophicus* strain Marburg instead of the original source strain *M. thermautotrophicus* ΔH, because we had access to freshly grown cells of the former only. Owing to the switch of strains we performed several control experiments before conducting the RACE experiment: (i) sequencing of the gene encoding the MM-Marburg RNA revealed a few nucleotide changes relative to MM RNA of strain ΔH (Figure 1), but *in vitro* transcribed MM-Marburg RNA with the short P1 helix as in MM RNA (Figure 1) showed RNA-alone activity

Table 3. Activity of MM variants in RNA-alone and holoenzyme assays

RNase P RNA	RNA-alone		Holoenzyme	
	k_{obs} [$min^{-1} \times 10^{-4}$]	Change	k_{obs} [$min^{-1} \times 10^{-4}$]	Change
MM	1.7 ± 0.1	1	2 ± 1	1
MM-nP1	340 ± 60	↑ 200×	1.3 ± 0.1	↓ 2×
MM-mJ15/18/P18	2 ± 1	1	1.2 ± 0.1	↓ 2×
MM-mJ2/3/P2	230 ± 50	↑ 135×	7 ± 1	↑ 4×
MM-mJ2/3/P2-2	100 ± 20	↑ 59×	6.7 ± 0.8	↑ 4×
MM-mJ15/18/2/3/P2	270 ± 60	↑ 159×	80 ± 10	↑ 40×
MM-mJ15/18/2/3/P2/nP1	740 ± 60	↑ 435×	75 ± 4	↑ 38×
MM-Marburg	3.3 ± 0.6		Not detectable	
MM-Marburg-nP1	310 ± 20		2.1 ± 0.9	
MM-Marburg-mapped ends	240 ± 20		1.0 ± 0.2	

For assay conditions and experimental details, see legend to Table 1 and Materials and methods section. For structural details on P1 elements in RNAs MM-Marburg, MM-Marburg-nP1 and MM-Marburg-mapped ends, see Figure S2B.

Table 4. Affinity of reconstituted RNase P holoenzymes for the $ptRNA^{Gly}$ substrate

RNase P RNA	K_d (nM)	K_d change	k_{obs} change (holoenzymes)
MM	n.d.		1
MM-mJ2/3/P2	n.d.		↑ 4×
MM-mJ15/18/2/3/P2	n.d.		↑ 40×
MM-mJ15/18/2/3/P2/nP1	n.d.		↑ 38×
ME	n.d.		1
ME-mJ2/3	448 ± 30	↑ 895×	↑ 2×
ME-mJ2/3/P2	47 ± 11	↑ 94×	↑ 450×
ME-mJ15/18/2/3	48 ± 4	↑ 96×	↑ 160×
ME-mJ15/18/2/3/P2	4.2 ± 1.2	↑ 8×	↑ 465×
ME-mJ15/18/2/3/P2/nP1	5.0 ± 1.0	↑ 10×	↑ 1500×
EE	0.5 ± 0.1	1	↑ 41 000×

Errors for K_d are standard errors of the curve fit; n.d., non-determinable because of affinities too low for K_d determination by this assay. K_d changes are given as *n*-fold increase in K_d relative to the *E. coli* holoenzyme (EE). Note that in our assay for all variants ptRNA binding to P RNA in the absence of protein did not exceed background values (ptRNA alone). Thus, the binding data for the ternary complex indirectly permit to assess P protein binding to P RNA; k_{obs} changes listed for comparison are taken from Tables 2 and 3.

very similar to that of MM RNA (Table 3); (ii) introducing the same 7-bp extension as present in MM-nP1 into the MM-Marburg RNA, resulting in variant MM-Marburg-nP1 (Figure S2B), indeed revealed a similar activity increase (ca. 100-fold) as seen for MM-nP1 RNA (Table 3). Having confirmed that MM-Marburg RNA is an appropriate mimic of MM RNA, we carried out 5′- and 3′-RACE (Figure S2A), which unveiled that *in vivo* transcripts of MM-Marburg RNA, and by inference of MM RNA, carry 5′- and 3′-ends that permit formation of an extended P1 helix (Figure S2B) to provide a receptor site for loop L9.

Construction and analysis of MM variants

Next we addressed the question if the activating structural changes nP1, mJ2/3, mP2 and mJ15/18, initially explored in the context of variant ME, would be beneficial in the natural context of MM RNA as well. Indeed, RNA-alone activity of MM RNA increased 435-fold by introducing these four minor changes (Table 3), while the activity gain was only 38-fold in the holoenzyme reaction (Table 3, columns on the right). Noteworthy, based on the comparison of cleavage rates (k_{obs}) for P RNA MM-mJ15/18/2/3/P2/nP1 (Table 3) and its counterpart ME-mJ15/18/2/3/P2/nP1 (Table 2), the presence of the archaeal S-domain in the MM variant reduced activity 13- and 40-fold in the RNA-alone and holoenzyme reactions, respectively.

Measurement of holoenzyme-substrate affinity

The relatively low catalytic performance of variant MM-mJ15/18/2/3/P2/nP1, particularly in the holoenzyme reaction, led us to analyze substrate affinities of P RNA variants reconstituted with the *E. coli* P protein. We initially tried direct measurements of affinity between P RNA and protein, but different approaches were unsuccessful in our hands. We thus switched to measuring ternary complex formation between holoenzyme and substrate (Table 4). As complex formation depended on P protein binding to P RNA under the applied low salt concentrations, the assay indirectly measured P RNA–protein affinities.

For the original ME chimera as well as MM RNA and all variants thereof ptRNA affinity was too low for K_d determination (Table 4). This changed with variant ME-mJ2/3, for which a K_d of 450 nM could be determined. Additional introduction of the J15/18 mutation increased affinity roughly tenfold. Similarly, the P2 mutation introduced into either the single mutant ME-mJ2/3 or the double mutant ME-mJ15/18/2/3 in either case led to a tenfold increase in affinity. The lowest K_d (4.2 nM) was obtained for the ME-mJ15/18/2/3/P2 RNA; additional incorporation of the nP1 extension did not further reduce K_d (5 nM). Thus, ptRNA affinities obtained with the best ME variants were 10-fold lower than that of the *E. coli* holoenzyme (EE RNA, K_d = 0.5 nM; Table 4).

For the ME variants, increases in affinity (reductions in K_d) nicely correlated with increases in bacterial holoenzyme activity, with the exception of the nP1 extension which enhanced activity ca. 3-fold when added to variant ME-mJ15/18/2/3/P2, but left substrate affinity essentially unaffected (Table 4). Low substrate affinity of the MM variants explains why activity gains in the bacterial holoenzyme assay were moderate (4–40-fold): since the archaeal S-domain is defective in substrate binding based on our K_d measurements and thus limits the rate of the cleavage reaction, beneficial effects of alterations mJ2/3, mJ15/18 and mP2 in the archaeal C-domain could not be coaxed into activities as high as in the presence of the *E. coli* S-domain.

Folding analysis of P RNA variants by native PAGE

Previous studies have shown that increased activity of P RNAs often goes along with compacted conformers

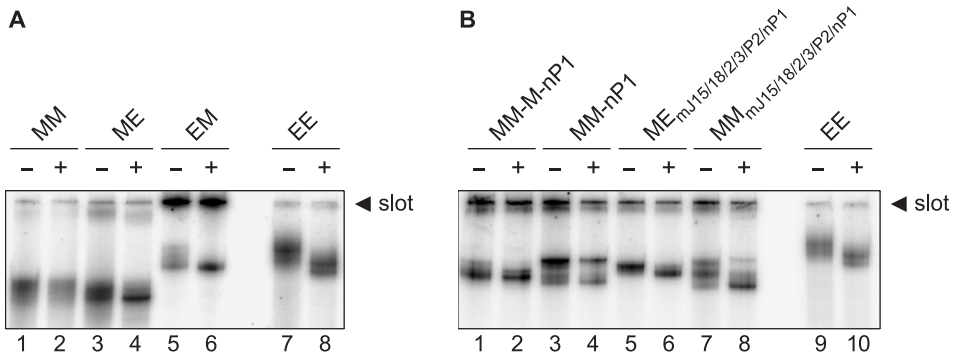

Figure 3. Native 11.25% PAGE analyses to compare the conformations of P RNA variants. (**A**) P RNAs from *M. thermoautotrophicus* (MM), *E. coli* (EE) and *E. coli*/*M. thermoautotrophicus* chimeras (EM and ME); (**B**) MM and MM-Marburg P RNA variants with P1 extension (MM-nP1, MM-M-nP1), as well as corresponding C-domain mutants of ME and MM RNA. Assay conditions were the same as in the holoenzyme activity assay (see legend to Table 1 and Material and methods section). Samples were loaded onto the gel either after storage for 55 min on ice (–) or after preincubation for 5 min at 55°C and 50 min at 37°C (+). For further details, see Materials and methods section.

becoming more prominent in native PAA gels (5,25,29,30). Consistent with this observation, MM RNA showed the most diffuse migrational behaviour in native gels, pointing to a multitude of coexisting conformations (Figure 3A). All other P RNAs analyzed, with a gain in activity compared to that of MM, displayed more distinct bands and some additional compaction, at least after the preincubation step to that allows RNA folding. Replacement of either domain of MM with the counterpart of EE RNA (variants ME and EM) resulted in stabilization of distinct folds, although EM RNA suffered from substantial aggregation as inferred from RNA retained in the gel pocket (Figure 3A). Extension of the P1 helix (MM-nP1) obviously supports tertiary folding (Figure 3B), as distinct conformers appeared relative to MM RNA. Interestingly, RNAs MM-nP1 and MM-M-nP1 differ in that one major conformer appears for the latter compared with two conformers in the case of RNA MM-nP1 (Figure 3B). This finding shows that even minor changes between two related RNAs may have profound effects on conformational equilibria. Gel mobility of variants ME-mJ15/18/2/3/P2/nP1 and MM-mJ15/18/2/3/P2/nP1 differed substantially, with the former resembling ME RNA in showing a single major band and the latter displaying at least two major conformers, similar to MM-nP1 RNA. However, the additional changes mJ15/18, mJ2/3 and mP2 further affected conformation relative to RNA MM-nP1, as inferred from weaker relative intensity of the upper conformer and faster migration of the lower conformer in the case of RNA MM-mJ15/18/2/3/P2/nP1.

UV melting profiles of selected P RNA variants

UV melting profiles were analyzed for P RNA variants ME, MM and MM-nP1, as well as the mJ15/18/2/3/P2/nP1 variants of ME and MM RNA. Conditions were 4.5 mM Mg^{2+} and 100 mM NH_4^+ (Figure 4), resembling those of our kinetic holoenzyme assay. Variant MM (red curve) had the lowest T_m value (73.1°C), which increased to 74.4°C when helix P1 was extended to its natural length (MM-nP1, black curve). Thus, helix P1 has an overall stabilizing effect, in line with large activity losses of bacterial P RNA variants with disrupted P1 elements (31). In addition, there is only one major unfolding transition for MM-nP1, based on the first derivative of the melting profile (dA_{260}/dT), whereas more unfolding of substructures occurred in MM RNA (shoulders between 60°C and 65°C and at approx. 77°C) aside from the major transition at 73.1°C. Variant ME (blue curve) showed a major unfolding transition around 76°C, but also substantial unfolding of substructures between 50°C and 70°C. In contrast, much less unfolding of substructures at lower temperatures was seen for variant ME-mJ15/18/2/3/P2/nP1 (gray curve), for which the P1 extension might be the major cause, in analogy to the profiles of MM versus MM-nP1 RNA.

It is further instructive to compare variant MM-mJ15/18/2/3/P2/nP1 with MM-nP1. The former (green curve) has a similar T_m and derivative melting profile as RNA MM-nP1, but shows more unfolding of local structures below 65°C than MM-nP1. Thus, introducing the set of minor changes (mJ15/18/2/3/P2) towards the bacterial consensus into the concertedly folding MM-nP1 RNA uncoupled unfolding of some local structures from unstacking of the bulk of RNA structure. Notably, the derivative melting profiles of variants MM-mJ15/18/2/3/P2/nP1 and ME-mJ15/18/2/3/P2/nP1 were identical up to 65°C, but the major unfolding transition for the latter was broader and shifted to higher temperatures (T_m = 76.3°C versus 75.0°C). Therefore, replacement of the archaeal S-domain with the *E. coli* counterpart increased overall folding stability but reduced the extent of coordinate unstacking.

Kinetic parameters of ME-mJ15/18/2/3/P2/nP1 and its MM counterpart

We determined the RNA-alone single turnover kinetic parameters for the best-performing variant ME-mJ15/18/2/3/P2/nP1 to further explore the catalytic capacity of the engineered archaeal C-domain. This analysis revealed a maximum rate (k_{react}) of approx. 1.4 min^{-1} and a $K_{m(sto)}$ of about 4 μM for the P RNA ME-mJ15/18/2/3/P2/nP1

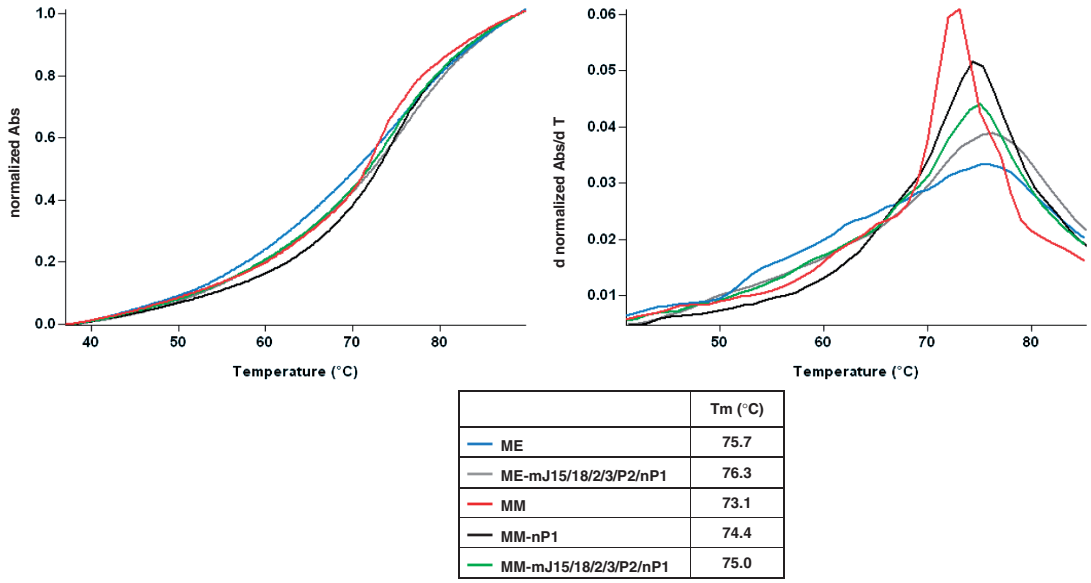

Figure 4. UV melting profiles of selected P RNA variants. The shown curves represent the mean of at least three measurements; assay conditions: 250 nM P RNA, 50 mM MES pH 6.0, 2 mM EDTA, 100 mM NH_4OAc, 4.5 mM $Mg(OAc)_2$; for UV absorbance (260 nm) melting profiles (left), the *y*-axis of every species was normalized to 0.0 – 1.0 (normalized Abs); normalized melting curve shapes were not affected by variation of P RNA concentration, indicating that intramolecular unfolding was measured; 'd normalized Abs/dT' (right panel): first derivatives of the melting curves on the left; the measuring program consisted of three steps: step 1 (preincubation): heating of the sample to 55°C at a rate of 10°C/min, incubation for 5 min at 55°C, cooling of the sample to 37°C at a rate of 10°C/min, incubation at 37°C for 35 min; step 2 (measuring of melting profile): heating of the sample from 37 to 90°C at a rate of 0.5°C/min with data recording every 0.1°C; stage 3: immediately after reaching 90°C in step 2, the sample was cooled to 25°C at a rate of 2°C/min and kept at 25°C for 5 min; the next round of measurement was again started with step 1.

(Figure 5A). For comparison, k_{react} and $K_{m(sto)}$ were determined as 10 min^{-1} and 0.24 μM, respectively, for *E. coli* wild-type P RNA under the same conditions (32). Thus, P RNA ME-mJ15/18/2/3/P2/nP1 differs from *E. coli* P RNA by only a 7-fold lower maximum cleavage rate and a 17-fold higher $K_{m(sto)}$. In contrast, the rate of cleavage by variant MM-mJ15/18/2/3/P2/nP1 showed a linear dependence on P RNA concentration up to 10 μM (Figure 5B), indicative of enzyme concentration being subsaturating and consistent with low substrate affinity in the presence of the archaeal S-domain.

We further tested P RNA ME-mJ15/18/2/3/P2/nP1 for function in *B. subtilis* and *E. coli rnpB* mutant strains, also under conditions of simultaneous overexpression of bacterial P proteins to compensate for reduced P RNA-P protein affinity. However, P RNA ME-mJ15/18/2/3/P2/nP1 was unable to rescue the mutant phenotypes (Table S3).

DISCUSSION

We have shown here that a few mutations toward the bacterial P RNA consensus substantially activate the C-domain of archaeal P RNA from *Methanothermobacter*, in the absence and presence of the bacterial RNase P protein. All variants were screened at two Mg^{2+} concentrations, 100 mM in the RNA-alone reaction and 4.5 mM in the holoenzyme reaction. Activity measurements at the two Mg^{2+} concentrations provide snapshots, as the individual variants may have different Mg^{2+} optima. Such potential differences in Mg^{2+} requirements imply that the structural changes introduced into the archaeal C-domain may exert their effects on folding, substrate binding, catalysis or binding of the RNase P protein at least partly through changes in binding of crucial Mg^{2+} ions, which has to be considered when interpreting the data. In a recent study on the RNA-alone reaction catalyzed by *E. coli* RNase P RNA, Kirsebom and coworkers demonstrated that the Mg^{2+} requirements with respect to cleavage increased when substrate contacts to the C-domain (involving substrate functional groups near the cleavage site) as well as contacts to the S-domain (involving the T-stem/loop region of the substrate) are weakened (33). The improvement in substrate positioning seen for variant ME-mJ15/18/2/3/P2 in our probing experiments (see below) may thus well include contributions from improved Mg^{2+} binding to P RNA regions that mediate contacts to the substrate. Along these lines, we showed previously for *E. coli* and *B. subtilis* P RNAs with mutations in the substrate 3′-CCA binding region that *in vitro* processing defects in the holoenzyme reaction were exacerbated when Mg^{2+} concentrations were lowered from e.g. 4.5 mM to 2 mM (34,35). Likewise, P RNAs with structural deletions (36) or substrates with ribose 2′-substitutions at strategic positions were reported to cause an increase in the Mg^{2+} requirement of P RNA-alone reactions (37,38). On the basis of these findings it is reasonable to predict that low activity P RNA variants in the study presented here will tend to perform relatively better at higher Mg^{2+} concentrations compared to the variants with improved catalytic performance.

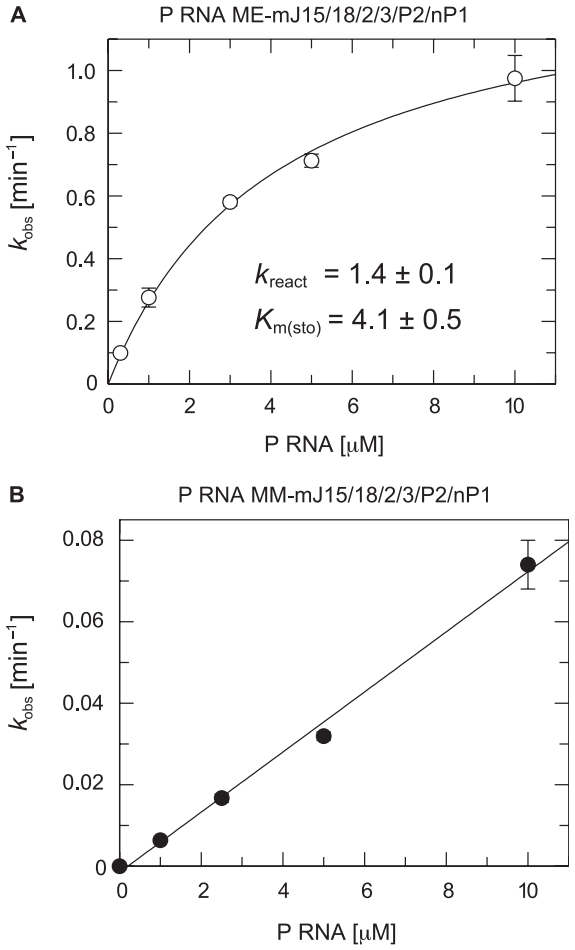

Figure 5. RNA-alone single turnover kinetics of P RNAs (**A**) ME-mJ15/18/2/3/P2/nP1 and (**B**) MM-mJ15/18/2/3/P2/nP1 as a function of the P RNA concentration. Processing assays were performed in the presence of <1 nM 5′-endlabelled ptRNA, 100 mM $Mg(OAc)_2$, 100 mM NH_4OAc, 50 mM MES and 2 mM EDTA, at pH 6.0 and 37°C. The k_{obs} values are mean values from at least three independent experiments, with error bars indicating the standard error of the mean. For P RNA ME-m J15/18/2/3/P2/nP1, the single turnover kinetic parameters could be derived. $K_{m(sto)}$ is the single turnover K_m (describes the enzyme concentration at which the half maximum rate under conditions of [E] >> [S] is achieved), and k_{react} is the single turnover V_{max}. For further details, see Materials and methods section.

A central finding of our study was that ribozyme activity of *M. thermoautotrophicus* P RNA is much higher (100 to 200-fold) than previously assumed owing to the presence of an extended P1 helix (Table 3, Figure 2). This P1 extension also stabilizes the global fold as inferred from native PAGE analysis (Figure 3) and UV melting profiles (Figure 4). A likely explanation is that the extension creates a receptor site for loop L9. Since the L18–P8 interdomain contact is lacking, the archaeal RNA may strongly depend on the L9–P1 contact for interdomain orientation of its type A architecture. The presence of an extended P1 helix is also likely for other archaeal P RNAs (Figure S3). Interestingly, a common motif of archaeal P1 elements is an A:A or C:A mismatch at identical position in type A and type M archaeal P RNAs proposed to interact with the third G residue of a conserved 5′-GAGA L9 tetraloop (17). We have recently demonstrated that a special L9–P1 interaction, occurring in some bacterial P RNAs from thermophiles, represents a major determinant for thermostability of the P RNAs, for RNase P holoenzyme activity at physiological Mg^{2+}-concentrations and for conformational compaction (29). Of note, some bacterial P RNAs harbouring this thermostable P1–P9 module also lack the L18–P8 interaction and have apparently compensated for its absence by strengthening the L9–P1 interdomain contact (29,32). We recently reported that the P1–L9 interaction is degenerate in *E. coli*-like mesophilic type A RNase P RNAs, and thus unlikely forms at all, because mutations intended to disrupt this contact remained without effect on *E. coli* P RNA function *in vitro* as well as *in vivo* (29). This finding explains why variant ME-mP1, designed to restore the *E. coli*-like L9–P1 contact when its degeneracy was still unknown, failed to improve RNA-alone activity (Table 2). However, it remains unclear why the impairment of activity was this severe (176-fold).

A pattern emerging from our reactivation study is that mutations within a single structural element were usually insufficient to improve RNA-alone activity. With the exception of the P1 extension, it took the cooperative effect of at least two alterations to be substantially beneficial for ribozyme activity, such as mP18 plus mJ15/18, mP2 plus mJ2/3 or mP2 plus mJ2/3 plus mJ15/18 (Table 2). Successful double mutants combined introduction (mP18) or alteration (mP2) of a helix and fine adjustments within adjacent joining regions likely involved in proper positioning of these structural elements. The stimulatory effects of combined changes mJ2/3/P2 on RNA-alone activity were, however, unexpected. Yet, since P2 and P3 are part of the catalytic core, length changes in J2/3 may affect coaxial stacking of P2 and P3 and thereby, combined with the P2 extension, induce subtle changes in folding of the entire core comprising the P1/P4/P5 and P2/P3 stacks as well as the respective joining segments.

Surprisingly, in several cases activity increases in the RNA-alone and holoenzyme assays differed substantially. The combined changes in J2/3 and P2 activated RNA-alone activity of variant ME-mJ2/3/P2 20-fold (relative to ME RNA; Table 2) and that of variant MM-mJ2/3/P2 135-fold (relative to MM RNA; Table 3); however, in the holoenzyme reaction activity stimulation was 450-fold for variant ME-mJ2/3/P2, but only 4-fold for P RNA MM-mJ2/3/P2 (Table 2 and 3). A similar situation was seen for the mJ15/18/2/3/P2/nP1 mutation (RNA-alone reaction: 147-fold in the ME, 435-fold in the MM context; holoenzyme reaction: 1500-fold in the ME, 38-fold in the MM context). Such relatively low stimulatory effect on MM variants in the holoenzyme reaction could be attributed to the failure of the archaeal S-domain to confer ternary complex formation at the low metal ion and enzyme concentrations present in the holoenzyme reactions. Indeed, throughout low activities for variants carrying the archaeal instead of the *E. coli* S-domain (Tables 2 and 3, Figure 5) were generally paralleled by very little formation of holoenzyme-substrate complexes (Table 4). The less severe phenotype of variants

harboring the archaeal S-domain in the RNA-alone relative to the holoenzyme reaction can be attributed to the fact that RNA-alone assays were performed at very high P RNA concentrations (10 μM) and high Mg^{2+} (100 mM), which apparently mitigated the effect of low substrate affinity.

These findings pinpoint the S-domain as the limiting part of the archaeal P RNA. In contrast, the archaeal C-domain with a few mutations not only displayed substantial catalytic proficiency, but also highly productive interaction with the bacterial P protein. It remains to be shown whether minor mutations will be able to partially cure the S-domain's defect, or if larger architectural alterations, for example, the incorporation of additional structural elements such as P13/P14, will be required to restore S-domain function in the absence of archaeal protein cofactors.

The more pronounced activity gain of the mJ15/18/2/3/P2/nP1 mutation in the ME versus MM context (1500-fold versus 38-fold; Table 2 and 3) is of further interest in view of the fact that RNAs MM and ME had equal activities in the holoenzyme reaction ($2 \times 10^{-4}\,min^{-1}$; Table 2 and 3). This discrepancy can be explained by interdomain cooperativity between the *E. coli* S-domain and the engineered archaeal C-domain carrying the mJ15/18/2/3/P2/nP1 mutations. Indeed, our structure probing data indicate changes in the *E. coli* S-domain between variants ME and ME-mJ15/18/2/3/P2 (see below).

The C to U exchange in J15/18 was the only single change that had a beneficial effect on the RNA-alone reaction by itself (Table 2). The molecular basis of this effect is not immediately clear, since the corresponding nucleotide in the crystal structure of the type A RNase P RNA from *Thermotoga maritima* is not resolved (21) and type B RNase P RNAs have a purine at this position (28,39). In *E. coli* P RNA, a 2′-deoxy modification at this U residue and Rp-phosphorothioate as well as inosine modification at the conserved 5′-terminal G of J15/18, two nucleotides upstream of the U residue (Figure 2), interfered with tRNA binding (24,40). This G residue forms a *trans* Hoogsteen/sugar edge base pair with the 3′-terminal A residue in J5/15 in the crystal structure of type B RNase P RNA from *B. stearothermophilus* (39). These findings suggest the J15/18 region to be involved in a structurally and functionally important network of interactions.

Comparative probing of P RNAs ME and ME-mJ15/18/2/3/P2 with RNase T1 and Pb^{2+} ions under native conditions unveiled distinct structural differences between the two RNA variants, surprisingly spanning the entire subregion P6, J6/16, P16, J16/15, P15, J15/18 and J5/15 (Supplementary Figure S4). J16/15 is the site of interaction with the tRNA 3′-CCA end. With respect to J15/18 itself, the 5′-terminal G residue was observed to be more accessible to RNase T1 cleavage in ME versus ME-mJ15/18/2/3/P2 RNA, whereas the site of mutation and the following C residue were more accessible to Pb^{2+}-induced hydrolysis in ME-mJ15/18/2/3/P2 relative to ME RNA (Figure S4). Surprisingly, differences in accessibility were also seen in L11/12 and P11, although these regions are identical in both P RNA variants. This indicates that changes mJ15/18/2/3/P2 in the C-domain have long-range effects on S-domain structure. L11/12 and P11 are close to the T-loop region in the P RNA-tRNA complex model based on the *T. maritima* P RNA X-ray structure (21). In conclusion, changes mJ15/18/2/3/P2 seem to affect regions that interact with the substrate (J15/16) or which are close to the substrate binding interface (L11/12 and P11). The beneficial effects of these changes on P RNA activity thus seem to stem from improvements in substrate positioning. The structural probing data raise the question if the mutations introduced in P RNA ME-mJ15/18/2/3/P2 will have similar structural and functional consequences when placed into other archaeal C-domains.

With respect to evolutionary implications of our approach, several findings are remarkable. First, only three minor changes, in J2/3, J15/18 and P2, were required to stimulate RNA-alone activity 80-fold in the ME and 160-fold in the MM context (465- and 40-fold, respectively, in the holoenzyme assay). Second, combining the changes in J2/3 and P2 improved activity in the absence as well as presence of the bacterial P protein. Thus, the latter exerts its function by making use of a structural element crucially important for RNA-alone activity. This may suggest an evolutionary scenario according to which the bacterial P protein was recruited to the catalytic RNA and adapted to it without eliciting significant co-evolution of the RNA subunit. In contrast, the strong dependence of archaeal/eukaryal P RNAs on their protein subunits for enzyme function indicates RNA/protein co-evolution, during which the archaeal P RNA subunit adapted to the protein components concomitant with substantial losses of RNA-alone activity. From a mirror-image perspective, it will be intriguing to explore if, for example, P RNA ME-mJ2/3/P2 may be impaired in its capacity to cooperate with the archaeal C-domain binding proteins Pop5 and Rpp30 (41). Along these lines, the substantial activation of the archaeal C-domain by surprisingly little changes suggests only minor differences in RNA conformation between bacterial and archaeal C-domains, in line with the structure probing results (see above). This may imply that the main function of the archaeal C-domain binding proteins Pop5 and Rpp30 for the C-domain itself is to merely fine-tune the conformation of the catalytic core.

Finally, the maximum single turnover cleavage rate of variant ME-mJ15/18/2/3/P2/nP1 was only 7-fold lower and the $K_{m(sto)}$ only 17-fold higher than the corresponding values measured for *E. coli* P RNA. It will be interesting to see if restoring the L9–P1 and/or L18–P8 interdomain struts in this ME chimera will further reduce these differences. In conclusion, the profound activation of the archaeal C-domain by minor changes demonstrates the evolutionary closeness of the archaeal and bacterial P RNAs, at least in terms of C-domain structure and function.

SUPPLEMENTARY DATA

Supplementary Data are available at NAR Online.

ACKNOWLEDGEMENTS

The gifts of pUC119_T7_M.th._rnpB (James W. Brown, North Carolina State University) and cells of *M. thermoautotrophicus* strain Marburg (Rolf Thauer, Max Planck Institute for Terrestrial Microbiology, Marburg) are gratefully acknowledged.

FUNDING

This work was supported by the Deutsche Forschungsgemeinschaft (HA 1672/14-1 and GK 1384). Funding for open access charge: DFG/GK 1384.

Conflict of interest statement. None declared.

REFERENCES

1. Guerrier-Takada,C., Gardiner,K., Marsh,T., Pace,N. and Altman,S. (1983) The RNA moiety of ribonuclease P is the catalytic subunit of the enzyme. *Cell*, **35**, 849–857.
2. Evans,D., Marquez,S.M. and Pace,N.R. (2006) RNase P: interface of the RNA and protein worlds. *Trends Biochem. Sci.*, **31**, 333–341.
3. Pannucci,J.A., Haas,E.S., Hall,T.A., Harris,J.K. and Brown,J.W. (1999) RNase P RNAs from some Archaea are catalytically active. *Proc. Natl Acad. Sci. USA*, **96**, 7803–7808.
4. Kikovska,E., Svärd,S.G. and Kirsebom,L.A. (2007) Eukaryotic RNase P RNA mediates cleavage in the absence of protein. *Proc. Natl Acad. Sci. USA*, **104**, 2062–2067.
5. Li,D., Willkomm,D.K., Schön,A. and Hartmann,R.K. (2007) RNase P of the *Cyanophora paradoxa* cyanelle: A plastid ribozyme. *Biochimie*, **89**, 1528–1538.
6. Loria,A. and Pan,T. (1996) Domain structure of the ribozyme from eubacterial ribonuclease P. *RNA*, **2**, 551–563.
7. Loria,A. and Pan,T. (1997) Recognition of the T stem-loop of a pre-tRNA substrate by the ribozyme from *Bacillus subtilis* ribonuclease P. *Biochemistry*, **36**, 6317–6325.
8. Kirsebom,L.A. (2007) RNase P RNA mediated cleavage: substrate recognition and catalysis. *Biochimie*, **89**, 1183–1194.
9. Schedl,P., Primakoff,P. and Roberts,J. (1974) Processing of *E. coli* tRNA precursors. *Brookhaven Symp. Biol.*, **26**, 53–76.
10. Gößringer,M., Kretschmer-Kazemi Far,R. and Hartmann,R.K. (2006) Analysis of RNase P protein (*rnpA*) expression in *Bacillus subtilis* utilizing strains with suppressable *rnpA* expression. *J. Bacteriol.*, **188**, 6816–6823.
11. Biswas,R., Ledman,D.W., Fox,R.O., Altman,S. and Gopalan,V. (2000) Mapping RNA-protein interactions in ribonuclease P from *Escherichia coli* using disulfide-linked EDTA-Fe. *J. Mol. Biol.*, **296**, 19–31.
12. Tsai,H.Y., Masquida,B., Biswas,R., Westhof,E. and Gopalan,V. (2003) Molecular modeling of the three-dimensional structure of the bacterial RNase P holoenzyme. *J. Mol. Biol.*, **325**, 661–675.
13. Rox,C., Feltens,R., Pfeiffer,T. and Hartmann,R.K. (2002) Potential contact sites between the protein and RNA subunit in the *Bacillus subtilis* RNase P holoenzyme. *J. Mol. Biol.*, **315**, 551–560.
14. Buck,A.H., Kazantsev,A.V., Dalby,A.B. and Pace,N.R. (2005) Structural perspective on the activation of RNAse P RNA by protein. *Nat. Struct. Mol. Biol.*, **12**, 958–964.
15. Kurz,J.C., Niranjanakumari,S. and Fierke,C.A. (1998) Protein component of *Bacillus subtilis* RNase P specifically enhances the affinity for precursor-tRNA^{Asp}. *Biochemistry*, **37**, 2393–2400.
16. Kurz,J.C. and Fierke,C.A. (2002) The affinity of magnesium binding sites in the *Bacillus subtilis* RNase P x pre-tRNA complex is enhanced by the protein subunit. *Biochemistry*, **41**, 9545–9558.
17. Harris,J.K., Haas,E.S., Williams,D., Frank,D.N. and Brown,J.W. (2001) New insight into RNase P RNA structure from comparative analysis of the archaeal RNA. *RNA*, **7**, 2.
18. Brown,J.W., Nolan,J.M., Haas,E.S., Rubio,M.A., Major,F. and Pace,N.R. (1996) Comparative analysis of ribonuclease P RNA using gene sequences from natural microbial populations reveals tertiary structural elements. *Proc. Natl Acad. Sci. USA.*, **93**, 3001–3006.
19. Massire,C., Jaeger,L. and Westhof,E. (1997) Phylogenetic evidence for a new tertiary interaction in bacterial RNase P RNAs. *RNA*, **3**, 553–556.
20. Massire,C., Jaeger,L. and Westhof,E. (1998) Derivation of the three-dimensional architecture of bacterial ribonuclease P RNAs from comparative sequence analysis. *J. Mol. Biol.*, **279**, 773–793.
21. Torres-Larios,A., Swinger,K.K., Krasilnikov,A.S., Pan,T. and Mondragon,A. (2005) Crystal structure of the RNA component of bacterial ribonuclease P. *Nature*, **437**, 584–587.
22. Williams,D. and Brown,J.W. (2004) *In vitro* selection of an archaeal RNase P RNA mimics natural variation. *Archaea*, **1**, 241–245.
23. Busch,S., Kirsebom,L.A., Notbohm,H. and Hartmann,R.K. (2000) Differential role of the intermolecular base-pairs G292-C_{75} and G293-C_{74} in the reaction catalyzed by *Escherichia coli* RNase P RNA. *J. Mol. Biol.*, **299**, 941–951.
24. Heide,C., Pfeiffer,T., Nolan,J.M. and Hartmann,R.K. (1999) Guanosine 2-NH_2 groups of *Escherichia coli* RNase P RNA involved in intramolecular tertiary contacts and direct interactions with tRNA. *RNA*, **5**, 102–116.
25. Wegscheid,B. and Hartmann,R.K. (2006) The precursor tRNA 3′-CCA interaction with *Escherichia coli* RNase P RNA is essential for catalysis by RNase P *in vivo*. *RNA*, **12**, 2135–2148.
26. Beebe,J.A. and Fierke,C.A. (1994) A kinetic mechanism for cleavage of precursor tRNA(Asp) catalyzed by the RNA component of *Bacillus subtilis* ribonuclease P. *Biochemistry*, **33**, 10294–10304.
27. Warnecke,J.M., Held,R., Busch,S. and Hartmann,R.K. (1999) Role of metal ions in the hydrolysis reaction catalyzed by RNase P RNA from *Bacillus subtilis*. *J. Mol. Biol.*, **290**, 433–445.
28. Massire,C. (1999) Développement de logiciels d'aide à la modélisation d'ARN. Application à la composante ribonucléique de la ribonucléase P bactérienne, Ph.D. thesis, Université Louis Pasteur Strasbourg.
29. Marszalkowski,M., Willkomm,D.K. and Hartmann,R.K. (2008) Structural basis of a ribozyme's thermostability: P1-L9 interdomain interaction in RNase P RNA. *RNA*, **14**, 1–7.
30. Buck,A.H., Dalby,A.B., Poole,A.W., Kazantsev,A.V. and Pace,N.R. (2005) Protein activation of a ribozyme: the role of bacterial RNase P protein. *EMBO J.*, **24**, 3360–3368.
31. Schlegl,J., Hardt,W.-D., Erdmann,V.A. and Hartmann,R.K. (1994) Contribution of structural elements to *Thermus thermophilus* ribonuclease P RNA function. *EMBO J.*, **13**, 4863–4869.
32. Marszalkowski,M., Teune,J.H., Steger,G., Hartmann,R.K. and Willkomm,D.K. (2006) Thermostable RNase P RNAs lacking P18 identified in the *Aquificales*. *RNA*, **12**, 1915–1921.
33. Brännvall,M., Kikovska,E., Wu,S. and Kirsebom,L.A. (2007) Evidence for induced fit in bacterial RNase P RNA-mediated cleavage. *J. Mol. Biol.*, **372**, 1149–1164.
34. Wegscheid,B. and Hartmann,R.K. (2006) The precursor tRNA 3′-CCA interaction with *Escherichia coli* RNase P RNA is essential for catalysis by RNase P *in vivo*. *RNA*, **12**, 2135–2148.
35. Wegscheid,B. and Hartmann,R.K. (2007) *In vivo* and *in vitro* investigation of bacterial type B RNase P interaction with tRNA 3′-CCA. *Nucleic Acids Res.*, **35**, 2060–2073.
36. Siegel,R.W., Banta,A.B., Haas,E.S., Brown,J.W. and Pace,N.R. (1996) *Mycoplasma fermentans* simplifies our view of the catalytic core of ribonuclease P RNA. *RNA*, **2**, 452–462.
37. Perreault,J.P. and Altman,S. (1992) Important 2′-hydroxyl groups in model substrates for M1 RNA, the catalytic RNA subunit of RNase P from *Escherichia coli*. *J. Mol. Biol.*, **226**, 399–409.
38. Cuzic,S. and Hartmann,R.K. (2007) A 2′-methyl or 2′-methylene group at G+1 in precursor tRNA interferes with Mg^{2+} binding at the enzyme-substrate interface in E-S complexes of *E. coli* RNase P. *Biol. Chem.*, **388**, 717–726.
39. Kazantsev,A.V., Krivenko,A.A., Harrington,D.J., Holbrook,S.R., Adams,P.D. and Pace,N.R. (2005) Crystal structure of a bacterial ribonuclease P RNA. *Proc. Natl Acad. Sci. USA.*, **102**, 13392–13397.
40. Hardt,W.-D., Erdmann,V.A. and Hartmann,R.K. (1996) Rp-deoxy-phosphorothioate modification interference experiments identify 2′-OH groups in RNase P RNA that are crucial to tRNA binding. *RNA*, **2**, 1189–1198.
41. Tsai,H.Y., Pulukkunat,D.K., Woznick,W.K. and Gopalan,V. (2006) Functional reconstitution and characterization of *Pyrococcus furiosus* RNase P. *Proc. Natl Acad. Sci. USA*, **103**, 16147–16152.

4.3 Improvements of human RNase P RNA (H1 RNA) activity are limited by the RNA's global instability

Dan Li, Dagmar K. Willkomm, Leif A. Kirsebom, Roland K. Hartmann* (in preparation)

INTRODUCTION

RNase P RNAs (P RNAs) from human and the lower eukaryote *Giardia lamblia* were recently found to have residual catalytic activity when analysed at pH 6.0 to reduce metal ion-induced RNA fragmentation and acting on a substrate ^{32}P-labelled with very high specific radioactivity (≥ 5 Ci/mmol) *in vitro* (Kikovska *et al.* 2007). Nevertheless, the highest activities measured for these eukaryotic P RNAs are more than five orders of magnitude lower than those obtained with bacterial RNAs, being just above the detection level under the optimised conditions mentioned above.

Compared with bacterial RNase P, eukaryal RNase P has a shorter and simpler RNA moiety, but is more complex in terms of its protein composition. The eukaryal RNA moiety is typically two-thirds the length of a bacterial one, and 9-10 protein subunits associate with eukaryotic P RNA (Jarrous 2002; Xiao *et al.* 2002), thus contributing at least 70% to the molecular mass of the enzyme in contrast to 10% in bacteria. Apparently, the weak activity of the RNA moiety alone is compensated for by the involvement of more protein components.
Phylogenetic comparative analysis of eukaryal P RNAs reveals five conserved regions CRI-V (Fig. 1.2.3 a) found also in bacterial and archaeal P RNAs (Frank *et al.* 2000). In contrast to bacterial P RNAs (Fig. 1.2.3 b), the eukaryal homologues in general have larger P3 elements and, similar to archaeal P RNAs, extended P12 regions. Furthermore, they lack a few structural elements, P5, P6, and P15-18, thought to be critical for both substrate binding and catalysis. Crosslinking experiments indicate that eukaryal P RNAs nevertheless fold into functional structures that specifically bind tRNA even in the absence of protein subunits (Marquez *et al.* 2006). A tertiary structure model of eukaryal P RNA was built on the basis of crosslinking results and crystal structures of bacterial P RNAs (Marquez et al. 2006). It suggests that the eukaryal P RNA contains a core structure similar to the bacterial P RNA, but lacks some structural elements that contribute to catalysis and global stability of tertiary structure.

Following the approach by which we largely restored catalytic activity of archaeal P RNA from *Methanothermobacter thermoautotrophicus* (Li *et al.* 2009), we constructed a series of mutants of the human RNase P RNA termed H1 RNA. The H1 RNA variants were analysed by kinetics assays, and select variants were further characterised.

RESULTS AND DISCUSSION

Construction and functional analysis of H1 RNA variants

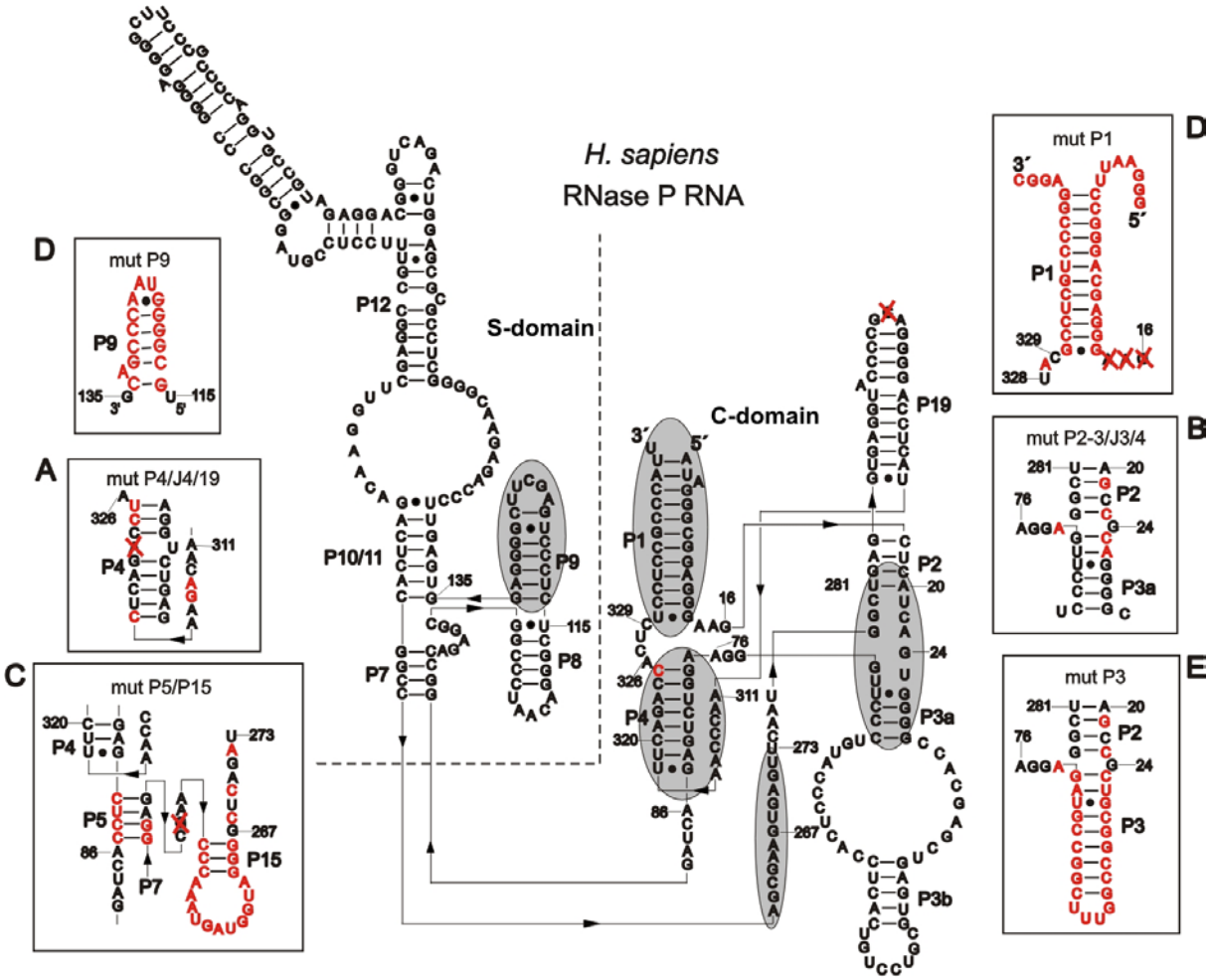

H1 RNA variants		HE variants
H1 RNA 1	mΔ298C325	HE
H1 RNA 2	mΔ298C325-P2-3/3/4 **(B)**	
H1 RNA 3	mΔ298C325-P2-4/J4/19 **(A+B)**	HE RNA 3 (HE 2)
H1 RNA 4	mΔ298C325-P5/P15r **(C)**	
H1 RNA 5	mΔ298C325-P4/J4/19 **(A)**	HE RNA 5 (HE 1)
H1 RNA 6	mΔ298C325-P2-5/P15/J4/19 **(A+B+C)**	HE RNA 6 (HE 3)
H1 RNA 7	mΔ298C325-P1/P9 (*T. th* P1, P9) **(D)**	
H1 RNA 8	mΔ298C325-P3 (*B. st* P3) **(E)**	

Fig. 4.3.1: Secondary structure of H1 RNA variants. Black nucleotides represent the original H1 RNA sequence. Middle: H1 RNA 1 secondary structure, with the nucleotide identities where H1RNA 1 differs from the wild type (Δ298 and C325) shown in red. Regions subjected to further mutation are highlighted by grey ovals. Sequences of the respective mutants (indicated by prefix "mut", e.g. mut P1) are given in the adjacent boxes with the altered nucleotides colored in red. Nucleotide numbering is that of H1 RNA. HE stands for chimera P RNA composed of H1 RNA 1 C domain and M1 RNA S domain.

In the previous study (Kikovska et al. 2007), H1 RNA variant Δ298C325 was shown to have higher catalytic activity than variants Δ298U325, C298U325 as well as C298C325; the latter two have been reported in the literature as natural variants of H1 RNA (Kikovska et al. 2007). H1 RNA variant Δ298C325, named H1 RNA 1, was used as the parental RNA in our study, into which we introduced several changes towards the bacterial consensus (see Fig. 4.3.1).

Mutations **A** (mut P4/J4/19) were introduced to construct a bacterial-like helix P4 and junction J4/19. Exactly as in bacterial RNase P RNAs, the new P4 was designed to form 8 base pairs with a U bulge in the middle. The mutated nucleotides in J4/19 followed the bacterial consensus. X-ray structures of bacterial RNase P RNAs (Kazantsev *et al.* 2005; Torres-Larios *et al.* 2005) suggested that the universally conserved P4 helix and its adjoining single-stranded regions in the core are crucial in stabilizing the functional conformation of the RNA. This is in line with previous biochemical studies indicating a key role of P4 in many aspects of RNase P function, such as positioning of divalent metal ions (Frank and Pace 1998; Christian *et al.* 2000), substrate binding and catalysis (Hardt *et al.* 1995; Harris and Pace 1995; Hardt *et al.* 1996; Kazantsev and Pace 1998; Heide *et al.* 1999; Siew *et al.* 1999). Mutations **B** (mut P2-3/3/4) were designed to restore a bacterial-like P2-P3 subdomain, which included a shortening of junction J2/3 to a single G residue. P2 and the bottom part of P3 were extended to 7 and 6 bp, respectively. An A residue was inserted in J3/4 in line with the bacterial consensus. The P2/P3 region, in addition to being important for the function of the catalytic RNA, is at the bacterial P protein binding interface (Buck *et al.* 2005; Niranjanakumari *et al.* 2007; Li et al. 2009). Mutations B were introduced into H1 RNA to analyze if this improves RNA-alone function and possibly interaction with the bacterial P protein Mutations **C** (mut P5/P15) installed P5 and P15 with bacterial-like flanking sequences. Helix P5 and junction J5/15 were the same as in bacterial type A RNAs. Helix P15 and loop L15 were those of *Bacillus stearothermophilus* (type B). The lack of P5 and P15 is one of the most obvious distinctions between H1 RNA and bacterial RNase P RNA. In bacterial RNAs, the two modules positioned in the core structure are important for overall conformation and substrate binding. The absence of P5 and P15 is expected to render the core structure floppy, likely being a major cause for defective enzyme function. We further constructed H1 RNA 3 (mutations **A** + **B**) and H1 RNA 6 (mutations **A** + **B** + **C**) to monitor the effect of combined changes.

L9-P1 is one of the loop-helix interdomain contacts in bacterial RNase P RNAs. In our study of the archaeal type A RNase P RNA from *Methanothermobacter thermoautotrophicus*, the presence of the natural (extended) P1 resulted in a 200-fold increased RNA-alone activity

compared with an RNA variant carrying a shortened P1 helix (Li et al. 2009), which we interpreted as evidence for the formation of the L9-P1 contact in this archaeal RNA. Also, when we swapped the P1 and P9 modules form a thermostable RNase P RNA (from *Thermus thermophilus*) into that of *E. coli*, we were able to converted the latter to a thermostable ribozyme (Marszalkowski *et al.* 2008), emphasizing the important functional role of this tertiary interaction. We therefore introduced the P1 and P9 modules of *T. thermophilus* RNase P RNA into H1 RNA 1 (mutations **D**) to reinforce this interdomain contact (variant H1 RNA 7, mut P1/P9).

One of the prominent structural features of eukaryal P RNA is their P3 element harbouring a large internal loop. A main site of crosslinking between tRNA 3‘-ends and *Schizosaccharomyces pombe* P RNA is the P3 internal loop (Marquez et al. 2006). The P3 element of bacterial RNase P RNA lies beside P15 in the crystal structures. In 3D models of eukaryal P RNA, P3 was oriented in the region where P15 is in bacterial P RNA (Marquez et al. 2006), pointing to the possibility that the P3 internal loop of eukaryal P RNAs may occupy the space that is filled by the P15 module in bacterial RNAs. Here we replaced the eukaryal P3 with that of *B. stearothermophilus* (mutations **E**), including mutations in adjacent single stranded segments (variant H1 RNA 8, mutP3). This resulted indeed in an entirely bacterial version of the P2/P3 region.

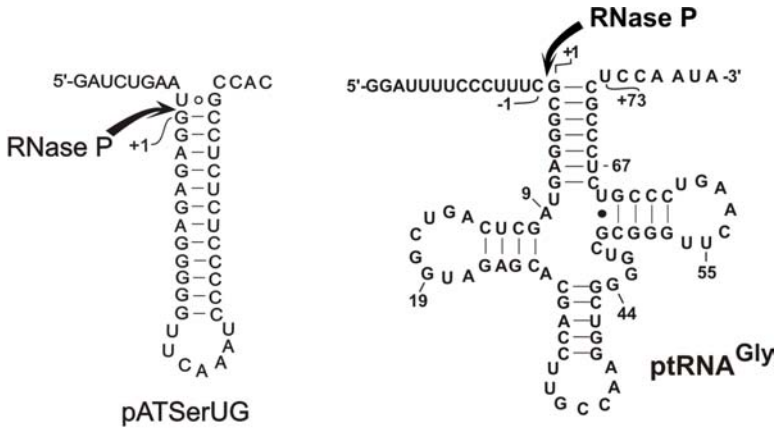

Fig. 4.3.2: Secondary structures of substrates ptRNA^{Gly} and pATSerUG. The RNase P cleavage sites are marked with arrows.

The H1 RNA variants described above were tested for RNA-alone activity with two substrates, ptRNA^{Gly} and a hairpin substrate (Fig. 4.3.2), pATSerUG, also used in the previous study (Kikovska et al. 2007). H1 RNA 1 showed very low but detectable RNA-alone activity compared to the reaction without enzyme (Fig. 4.3.3 and Table 4.3.1), in line with

Kikovska *et al.* (2007). This activity was clearly increased for H1 RNAs 3, 5 and 6 with both substrates, pATSerUG and ptRNA^{Gly}.

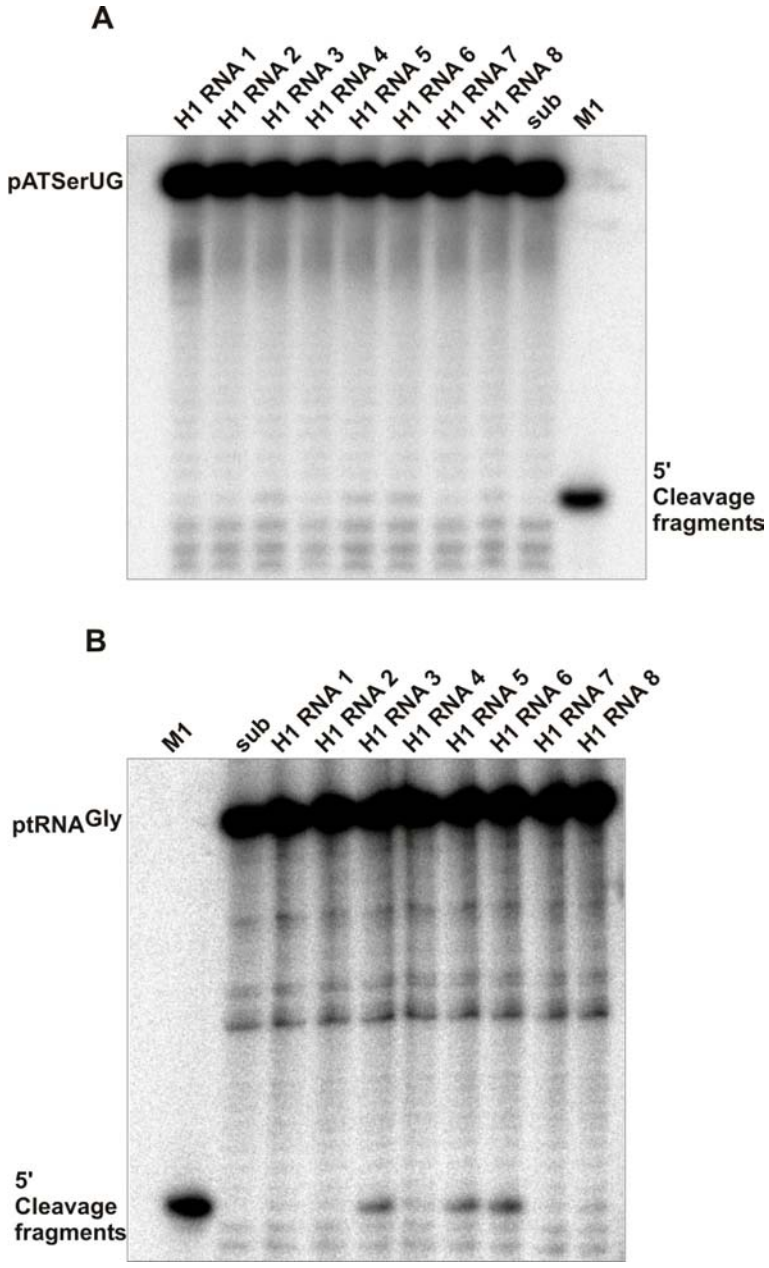

Fig. 4.3.3: Cleavage of pATSerUG and ptRNA^{Gly} by H1 RNA variants 1 to 8. (**A**) Analysis with pATSer UG. (**B**) Analysis with ptRNA^{Gly}. Lane sub: no enzyme present; lane M1: assay with *E. coli* P RNA. 5'-[^{32}P]-labeled substrates (approx. 10 nM, 40,000-50,000 Cerenkov cpm per reaction and gel lane) were preincubated in assay buffer for 5 min at 55°C and 25 min at 37°C, and P RNAs for 5 min at 55°C and 35 min at 37°C. H1 RNA variants were assayed at a concentration of 6 µM, *E. coli* P RNA (M1 RNA) at 370 nM, in buffer A (50 mM MES pH 6.0 [37°C], 800 mM NH_4OAc, 160 mM $Mg[OAc]_2$). Reactions with H1 RNA variants were incubated at 37°C for 22 h, with M1 RNA at 37°C for 30 min. Reactions were analyzed by 22% denaturing PAGE (7 M urea).

	k_{obs} (min^{-1})	
	pATSerUG	$ptRNA^{Gly}$
H1 RNA 1	$< 10^{-7}$	$< 10^{-7}$
H1 RNA 2	$< 10^{-7}$	$< 10^{-7}$
H1 RNA 3	$3.1 \times 10^{-7} \pm 7.9 \times 10^{-8}$	$3.1 \times 10^{-6} \pm 1.1 \times 10^{-6}$
H1 RNA 4	$< 10^{-7}$	$< 10^{-7}$
H1 RNA 5	$3.0 \times 10^{-7} \pm 9.5 \times 10^{-8}$	$2.7 \times 10^{-6} \pm 1.2 \times 10^{-6}$
H1 RNA 6	$4.4 \times 10^{-7} \pm 1.1 \times 10^{-7}$	$4.2 \times 10^{-6} \pm 9.0 \times 10^{-7}$
H1 RNA 7	$< 10^{-7}$	$< 10^{-7}$
H1 RNA 8	$< 10^{-7}$	$< 10^{-7}$
HE	n.d.	n.d.
HE 1	n.d.	n.d.
HE 2	n.d.	n.d.
HE 3	n.d.	n.d.

Table 4.3.1: Processing rates with H1 RNA 1 to 8 and chimeric HE variants in P RNA-alone reactions; n.d.: not detectable.

The other variants displayed catalytic activities similar to that of H1 RNA 1 or lower. Mutations **B** (H1 RNA 2) were neutral to activity, and processing rates of H1 RNA 3 and 5 were comparable, indicating that. mutations **B** provided no additional advantage over mutations **A** being present alone. The activity of H1 RNA 4 did not exceed that of H1 RNA 1, indicating that mutations **C** alone were neutral to catalytic performance. However, H1 RNA 6, comprising mutations **A** + **C** + **B**, slightly increased k_{obs} for both substrates, thus being detectably more active than H1 RNA 3 (only mutations **A** + **B**). Apparently, the restored P5 and inserted P15 elements improved function when combined with mutations **A** and **B**. The inserted module might exert its beneficial effect through cooperative interactions with P4, as it is located next to P4 in the bacterial crystal structure (Kazantsev et al. 2005). The increased activity of H1 RNA 6 might reflect some adjustment of the catalytic core structure, leading to improved Mg^{2+} binding properties and/or improvements in substrate affinity and positioning. Nevertheless, the poor overall activities of all variants preclude more detailed analyses of the molecular basis of these improvements. An interesting point is that the most active variants, H1 RNA 3, 5 and 6, all contain mutations **A**. H1 RNA 5 (mutations **A** only) is the sole variant with locally confined mutations that showed increased activity. Apparently, the bacterial-type

P4 helix improved the catalytic activity of H1 RNA 1. A likely interpretation is that H1 RNA has a degenerated P4 and core structure which has become dependent on association with its natural protein cofactors in order to adopt an active conformation. Introduction of *T. thermophilus* P RNA elements P1/P9, intended to reinforce interdomain interactions, (mutations **D**) exhibited at best a neutral effect on the catalytic capacity of H1 RNA. In this case, the domain interaction may either not be established owing to improper folding, or the contact forms but remains without effect in the context of H1 RNA.

H1 RNA variants 1 to 8 were also analysed for catalytic activity in the presence of the *E. coli* P protein. None of these RNAs could be stimulated by the bacterial P protein. This is in consistent with the notion that archaeal/eukaryal RNase P proteins are evolutionary unrelated to the bacterial P protein (Hartmann and Hartmann 2003). H1 RNAs 2, 3, 6 and 8, although having a bacterial-like version of P2/P3, failed to show detectable holoenzyme activity with the *E. coli* P protein. An explanation might be that either the P protein binding surface does not form in the context of H1 RNA. Alternatively, the *E. coli* P protein might bind to the P2/P3 region, but is unable to support catalysis owing to defects in other parts of the H1 RNA C-domain.

Human-bacterial RNase P RNA chimeras

Chimeras consisting of the *E. coli* RNase P RNA S-domain and the C-domain of H1 RNA 1 (HE chimeras) were constructed (Fig. 4.3.4) to improve substrate affinity and positioning. This might in turn provide a basis for increased human C domain activity, similar to what we observed for archaeal RNase P RNA (Li et al., 2009). Then mutations **A**, **A + B** and **A + B + C,** which improved activity of H1 RNA 1 (Table 4.3.1) were introduced into HE RNA 1, giving rise to variants HE RNA 3, 5 and 6 (variants HE 2, 1, and 3). Surprisingly, all chimeric HE RNA variants failed to catalyze detectable cleavage of substrates pATSerUG or ptRNAGly, neither in the RNase P RNA-alone nor in the holoenzyme reaction in the presence of the *E. coli* RNase P protein Unlike archaeal RNase P RNAs (Pulukkunat and Gopalan 2008; Li et al. 2009), the H1 RNA C-domain is unable to productively cooperate with a bacterial S-domain. Even worse, the S-domain swap eliminated the residual activity of the H1 RNA C-domain in the presence of its native S-domain.

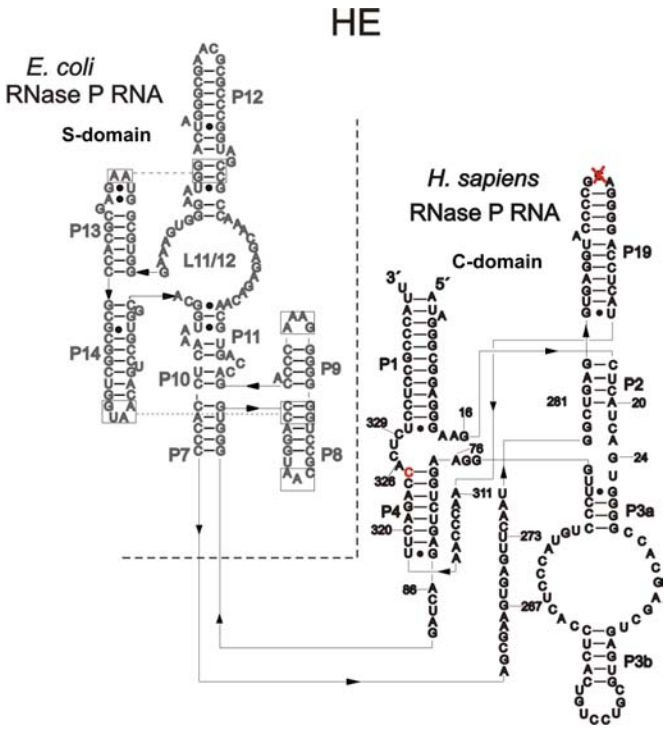

Fig. 4.3.4: Secondary structure of HE chimera. The S-domain from *E. coli* is shown in grey. The C-domain of H1 RNA 1 is depicted as in Fig 4.3.1.

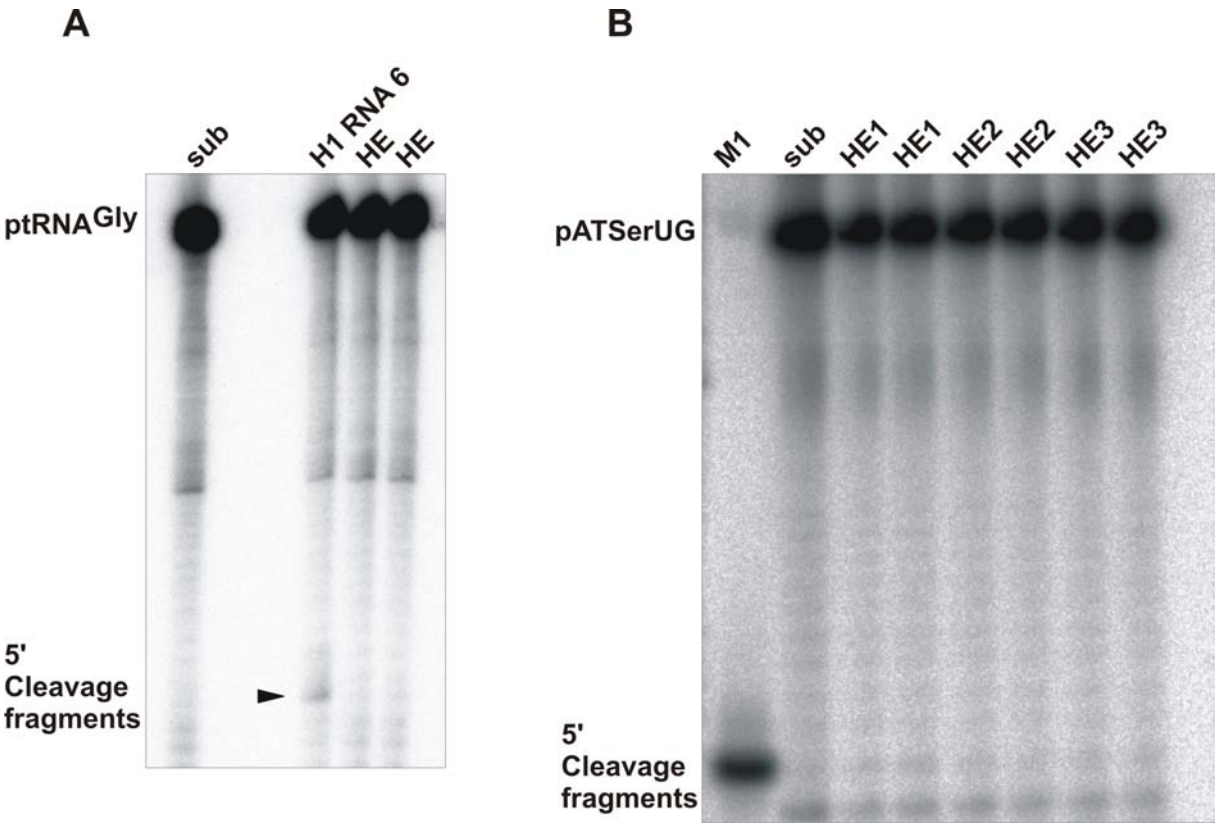

Fig. 4.3.5: Cleavage assays with the HE chimera and its derivatives. Lane sub: no enzyme present; lane M1: assay with *E. coli* P RNA. The assays were done as for H1 RNA variants (see Fig. 4.3.3).

Tethered H1 RNA-substrate constructs

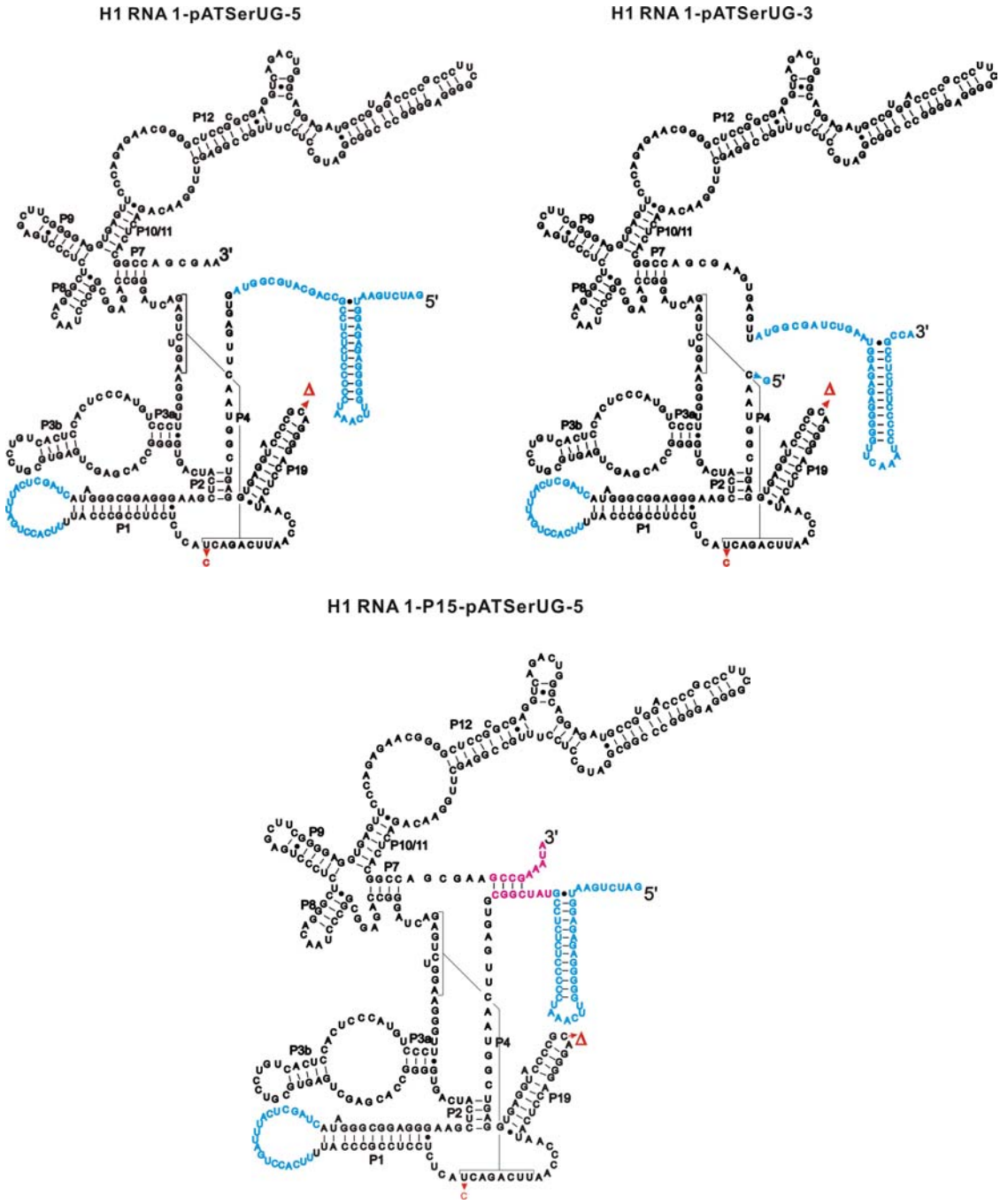

Fig. 4.3.6: The secondary structures of circularly permuted substrate-H1 RNA conjugates. Red marks indicate the specific sequence identities of H1 RNA 1 (Δ298C325). Inserted nucleotides including the substrate pATSerUG are in blue. The reconstructed P15 module is shown in magenta.

Recently, the archaeal type M RNase P RNA from *Methanococcus jannaschii* was found to be catalytically inactive in the normal *trans*-cleavage reaction in the absence of its protein cofactors: However, a ptRNA or smaller hairpin substrate covalently tethered to this P RNA was efficiently cleaved *in cis* (Pulukkunat and Gopalan 2008). We followed this strategy and

designed corresponding H1 RNA-substrate conjugates, H1 RNA 1-pATSerUG-5 and H1 RNA 1-pATSerUG-3 (Fig. 4.3.6). Since loop L15 is part of the substrate binding interface in bacterial P RNA, H1 RNA contacts to the substrate were expected to be at the same location. For this reason, the single-stranded nucleotides between P3 and P7 (where P15 is in bacteria) were opened, and the artificial hairpin substrate pATSerUG was linked either to the 3‘- or 5‘-end at this breakage point in H1 RNA 1. A few nucleotides were inserted at the linkage site to ensure flexibility of substrate positioning. Finally, the natural H1 RNA 5‘- and 3‘-ends were connected via a large loop in these circularly permuted constructs (Fig. 4.3.6). Considering that the overall structure might be rather floppy in constructs H1 RNA 1-pATSerUG-5 and -3, we designed a third conjugate, H1 RNA 1-P15-pATSerUG-5. Here, a 4-bp long P15 helix was built in to rigidify the attachment site of pATSerUG in H1 RNA 1 (Fig. 4.3.6).

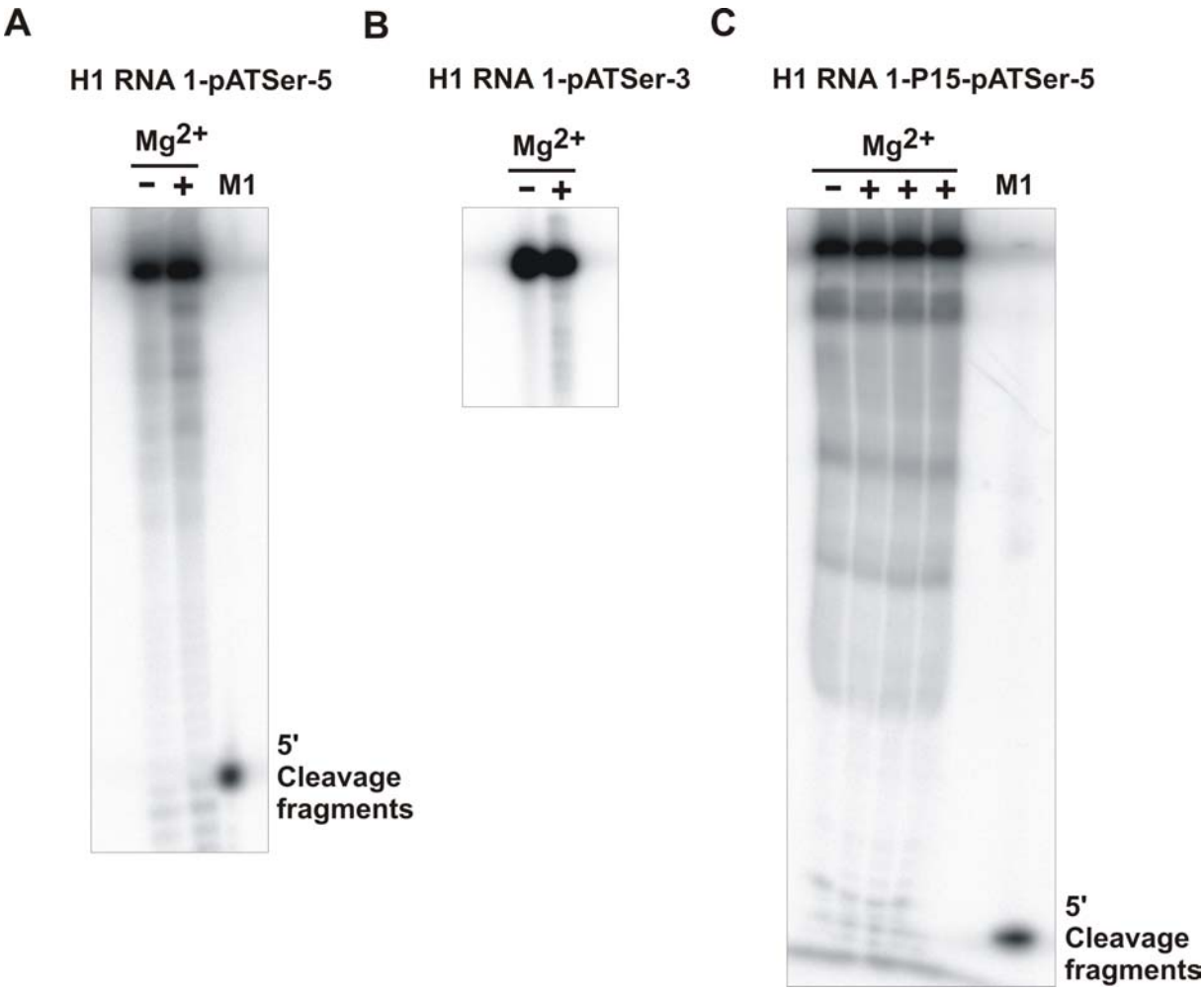

Fig. 4.3.7: *Cis*-cleavage assays of substrate-H1 RNA 1 conjugates. Lane M1: assay with *E. coli* P RNA. The substrate-H1 RNA conjugates were analyzed in buffer C: 50 mM MES pH 6.0 (37°C), 800 mM NH_4OAc) with or without 160 mM $Mg(OAc)_2$. The reaction solution, containing approx. 10 nM (40,000-50,000 Cerenkov cpm)

of 5'-endlabeld RNA, was heated at 55°C for 5 min, followed by incubation at 37°C for 22 h. Reactions were analyzed by 22% denaturing PAGE (7 M urea).

None of the enzyme-substrate conjugates underwent detectable *cis*-cleavage under the tested high salt conditions (0.8 M NH_4OAc, 0.16 M $Mg[OAc]_2$) (Fig. 4.3.7). This finding, together with the inactivity of the HE chimeras reveal that the catalytic defect of H1 RNA is not simply a problem of low substrate affinity, but rather seems to reflect a severe folding problem of the eukaryal C-domain.

Structure probing of selected H1 RNA variants

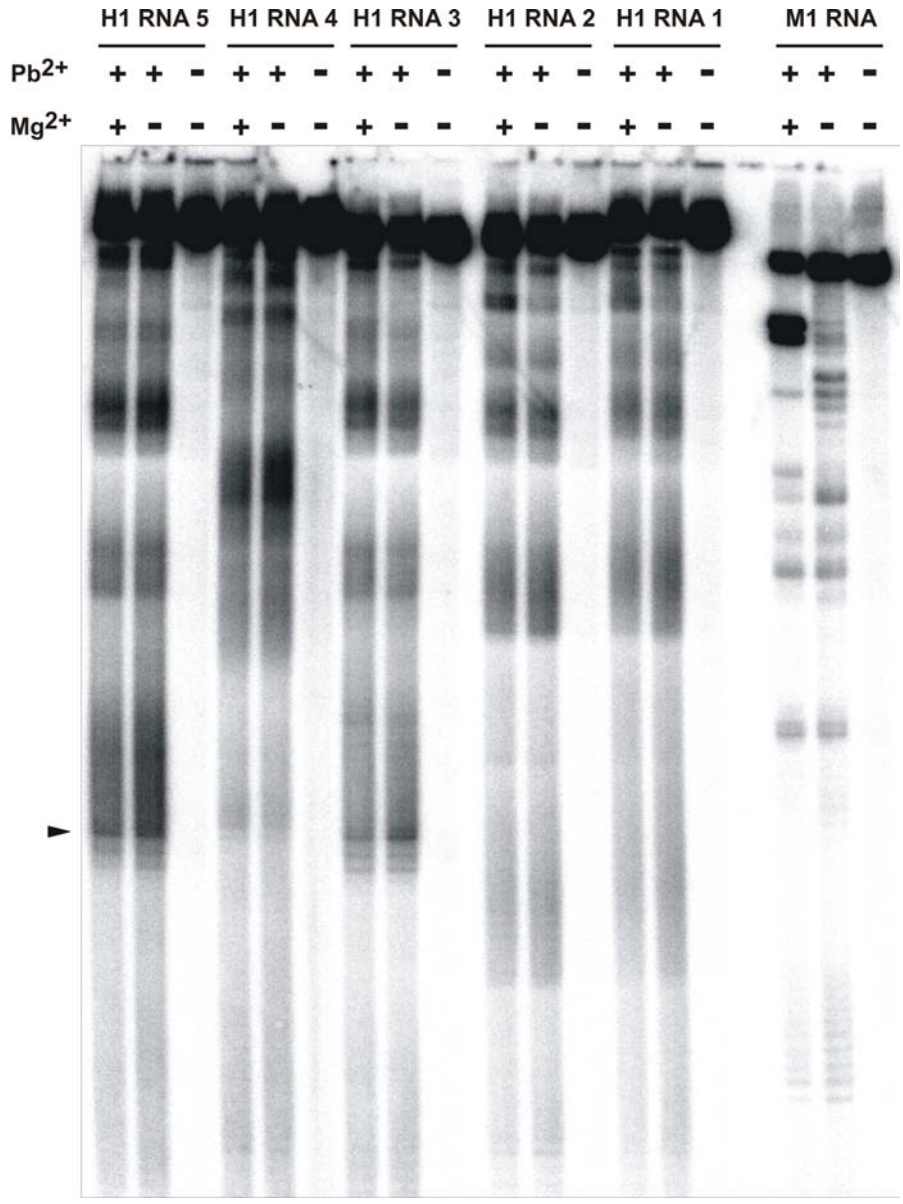

Fig. 4.3.8: Lead-induced hydrolysis of H1 RNAs 1 to 5 (3'-^{32}P-endlabeled). The RNase P RNAs to be investigated (0.25 μM unlabeled RNA plus 20,000 cpm [≤ 50 nM] of 3'-endlabeled RNA) were preincubated in

50 mM Tris-HCl pH 7.5, 100 mM NH_4Cl, 2 mM $Mg(OAc)_2$ for 2 min at 70°C and then for 10 min at 37°C. The hydrolysis was initiated by adding freshly diluted $Pb(OAc)_2$ to a final concentration of 0.5 mM. The reactions were performed at 37°C for 6 min, terminated by mixing with loading buffer (10 M urea, 10 mM EDTA, 2 % BPB), and analyzed on a 8% PAA (7 M urea) sequencing gel. Two controls were prepared in parallel. One was without $Mg(OAc)_2$, the other was without $Mg(OAc)_2$ and $Pb(OAc)_2$.

H1 RNAs 1 to 5 were analysed by lead-induced hydrolysis. In contrast to the distinct Pb^{2+} hydrolysis pattern of *E. coli* P RNA (M1 RNA), hydrolysis products of the H1 RNA variants exhibited smeary migration behaviour. In principle, M1 RNA (377 nt) is larger than the H1 RNA variants (~ 350 nt), but migrated faster than all H1 RNA variants in denaturing PAA gels (Fig. 4.3.8). An explanation is that H1 RNA variants, compared with M1 RNA, have less stable secondary structure elements that persist under denaturing PAGE and cause some compaction of M1 RNA during electrophoresis. Alternatively, the extended P12 element of H1 RNAs may still be able to form during electrophoresis, providing a protuberance that retards gel mobility. A problem arising from the smeary gel migration of H1 RNA fragments is that we could not accurately verify the size of cleavage fragments to assign the cleavage sites.

There are also clear differences between the individual H1 RNA variants. Full-length H1 RNA variants 2 and 3 migrated faster than variants 1, 4 and 5. The common feature of variants RNA 2 and 3 is a bacterial version of P2/P3. The reinforced P2/P3 elements may resist denaturation during electrophoresis, resulting in a more compacted structure and faster migration. H1 RNAs 3 and 5 displayed similar Pb^{2+} hydrolysis patterns which differed from H1 RNA 1. They both contain mutations **A** (mut P4/J4/19). These mutations in the P4 region resulted in increased susceptibility to Pb^{2+} hydrolysis in the region marked with an black arrow in Fig. 4.3.6. This correlates with the increased catalytic activity of variants 3 and 5 (Table 4.3.1). The presence of P5/P15 in H1 RNA variant 4 also caused idiosyncratic changes in the Pb^{2+} hydrolysis pattern. We recently showed in the context of the plastid RNase P RNA from the cyanelle of *Cyanophora paradoxa* (Li *et al.* 2007) that this part of the RNA is a major determinant in overall folding of P RNAs.

From the smeary Pb^{2+} hydrolysis fragment patterns observed for H1 RNA variants compared with M1 RNA we conclude that the low catalytic proficiency of the H1 RNA C-domain originates to a substantial extent from folding instability.

References

Buck, A.H., Kazantsev, A.V., Dalby, A.B., and Pace, N.R. 2005. Structural perspective on the activation of RNAse P RNA by protein. *Nat. Struct. Mol. Biol.* **12:** 958-964.

Christian, E.L., Kaye, N.M., and Harris, M.E. 2000. Helix P4 is a divalent metal ion binding site in the conserved core of the ribonuclease P ribozyme. *RNA* **6:** 511-519.

Frank, D.N., Adamidi, C., Ehringer, M.A., Pitulle, C., and Pace, N.R. 2000. Phylogenetic-comparative analysis of the eukaryal ribonuclease P RNA. *RNA* **6:** 1895-1904.

Frank, D.N. and Pace, N.R. 1998. Ribonuclease P: unity and diversity in a tRNA processing ribozyme. *Annu Rev Biochem* **67:** 153-180.

Hardt, W.D., Erdmann, V.A., and Hartmann, R.K. 1996. Rp-deoxy-phosphorothioate modification interference experiments identify 2'-OH groups in RNase P RNA that are crucial to tRNA binding. *RNA* **2:** 1189-1198.

Hardt, W.D., Warnecke, J.M., Erdmann, V.A., and Hartmann, R.K. 1995. Rp-phosphorothioate modifications in RNase P RNA that interfere with tRNA binding. *EMBO J* **14:** 2935-2944.

Harris, M.E. and Pace, N.R. 1995. Analysis of the tertiary structure of bacterial RNase P RNA. *Mol Biol Rep* **22:** 115-123.

Hartmann, E. and Hartmann, R.K. 2003. The enigma of ribonuclease P evolution. *Trends Genet.* **19:** 561-569.

Heide, C., Pfeiffer, T., Nolan, J.M., and Hartmann, R.K. 1999. Guanosine 2-NH_2 groups of Escherichia coli RNase P RNA involved in intramolecular tertiary contacts and direct interactions with tRNA. *RNA* **5:** 102-116.

Jarrous, N. 2002. Human ribonuclease P: Subunits, function, and intranuclear localization. *RNA* **8:** 1-7.

Kazantsev, A.V., Krivenko, A.A., Harrington, D.J., Holbrook, S.R., Adams, P.D., and Pace, N.R. 2005. Crystal structure of a bacterial ribonuclease P RNA. *Proc. Nat. Acad. Sci. U.S.A.* **102:** 13392-13397.

Kazantsev, A.V. and Pace, N.R. 1998. Identification by modification-interference of purine N-7 and ribose 2 '-OH groups critical for catalysis by bacterial ribonuclease P. *RNA* **4:** 937-947.

Kikovska, E., Svard, S.G., and Kirsebom, L.A. 2007. Eukaryotic RNase P RNA mediates cleavage in the absence of protein. *Proc. Nat. Acad. Sci. U.S.A.* **104:** 2062-2067.

Li, D., Willkomm, D.K., and Hartmann, R.K. 2009. Minor changes largely restore catalytic activity of archaeal RNase P RNA from Methanothermobacter thermoautotrophicus. *Nucleic Acids Res.* **37:** 231-242.

Li, D., Willkomm, D.K., Schon, A., and Hartmann, R.K. 2007. RNase P of the Cyanophora paradoxa cyanelle: a plastid ribozyme. *Biochimie* **89:** 1528-1538.

Marquez, S.M., Chen, J.L., Evans, D., and Pace, N.R. 2006. Structure and function of eukaryotic Ribonuclease P RNA. *Mol. Cell* **24:** 445-456.

Marszalkowski, M., Willkomm, D.K., and Hartmann, R.K. 2008. Structural basis of a ribozyme's thermostability: P1-L9 interdomain interaction in RNase P RNA. *RNA* **14:** 127-133.

Niranjanakumari, S., Day-Storms, J.J., Ahmed, M., Hsieh, J., Zahler, N.H., Venters, R.A., and Fierke, C.A. 2007. Probing the architecture of the B. subtilis RNase P holoenzyme active site by cross-linking and affinity cleavage. *RNA* **13:** 521-535.

Pulukkunat, D.K. and Gopalan, V. 2008. Studies on *Methanocaldococcus jannaschii* RNase P reveal insights into the roles of RNA and protein cofactors in RNase P catalysis. *Nucleic Acids Res.* **36:** 4172-4180.

Siew, D., Zahler, N.H., Cassano, A.G., Strobel, S.A., and Harris, M.E. 1999. Identification of adenosine functional groups involved in substrate binding by the ribonuclease P ribozyme. *Biochemistry-US* **38:** 1873-1883.

Torres-Larios, A., Swinger, K.K., Krasilnikov, A.S., Pan, T., and Mondragon, A. 2005. Crystal structure of the RNA component of bacterial ribonuclease P. *Nature* **437:** 584-587.

Xiao, S.H., Scott, F., Fierke, C.A., and Engelke, D.R. 2002. Eukaryotic ribonuclease P: A plurality of ribonucleoprotein enzymes. *Annu. Rev. Biochem.* **71:** 165-189.

5 Summary

RNase P catalyzes tRNA 5'-end maturation in all organisms and organelles. The enzyme is composed of a single RNA subunit plus a number of proteins that increases from bacteria (one protein) over archaea (at least four proteins) to eukarya (nine to ten proteins). Conserved base identities indicate that the RNase P RNA subunits (P RNAs) from all three kingsdoms of life stem from a common ancestor. Yet, only in bacteria the P RNA alone is substantially active *in vitro* without the protein, whereas archaeal and eukaryal P RNAs are more dependent on the contribution of their protein moieties and display only residual activity when these are absent. RNase P thus represents a natural model system for the switch from ribozyme to ribonucleoprotein enzyme, generally accepted to have occurred during natural evolution of the RNA world to the protein world.

RNase P of the *Cyanophora paradoxa* cyanelle: A plastid ribozyme

The RNA subunit of cyanelle RNase P from *Cyanophora paradoxa* contains essentially all structural elements of bacterial P RNAs, but has been reported to be catalytically inactive. In contrast to these previous observations, we were able to detect activity of this P RNA in the absence of protein cofactors. Furthermore, the *C. paradoxa* P RNA forms a functional holoenzyme with proteobacterial P proteins. Analysis of C- and S-domain swaps between cyanelle and *Escherichia coli* P RNA revealed that their domains have the capacity to cooperate, because the hybrid RNAs were functional. However, activities of the chimeras lagged behind the catalytic performance of the bacterial P RNA, suggesting that both the C- and S-domain of the cyanelle P RNA are weakly functional, thus limiting the activity of each type of chimera (EC or CE). In addition or alternatively, domain interaction and overall folding may be suboptimal in the chimeras, as it likely is in the wild-type cyanelle P RNA. Furthermore, the organellar ribozyme is unusual compared to the consensus of bacterial P RNAs: RNA-alone activity is low and structural alterations as small as point mutations or switches in Watson-Crick base pair identity at positions that are not part of the universally conserved catalytic core abrogate activity as does incorporating the *E. coli* L15-16 loop and adjacent regions. These findings indicate that the A,U-rich cyanelle RNase P RNA is globally optimized but conformationally unstable, thus representing an RNase P type of its own rather than simply being a slightly degenerate form of bacterial RNase P. In this context the *E. coli* P protein nevertheless emerged as a universal player in P RNA activation, and it will be all the more interesting to see if bacterial P proteins are related to any of the P protein components specific to the *C. paradoxa* cyanelle that yet await identification.

Minor changes largely restore catalytic activity of archaeal RNase P RNA from *Methanothermobacter thermoautotrophicus*

The increased protein proportion of archaeal and eukaryal RNase P holoenzymes parallels a vast decrease in the catalytic activity of their RNA subunits (P RNAs) alone. We show that a few mutations toward the bacterial P RNA consensus substantially activate the C-domain of archaeal P RNA from *M. thermoautotrophicus*, in the absence and presence of the bacterial RNase P protein. Large increases in ribozyme activity required the cooperative effect of at least two structural alterations. The P1 helix of P RNA from *M. thermoautotrophicus* was found to be extended, which increases ribozyme activity (ca 200-fold) and stabilizes the tertiary structure. Activity increases of mutated archaeal C-domain variants were more pronounced in the context of chimeric P RNAs carrying the bacterial S-domain of *Escherichia coli* instead of the archaeal S-domain. This could be explained by the loss of the archaeal S-domain's capacity to support tight and productive substrate binding in the absence of protein cofactors. Our results demonstrate that the catalytic capacity of archaeal P RNAs is close to that of their bacterial counterparts, but is masked by minor changes in the C-domain and, particularly, by poor function of the archaeal S-domain in the absence of archaeal protein cofactors.

Improvements of human RNase P RNA (H1 RNA) activity are limited by the RNA's global instability

The eukaryal RNase P RNAs from human (H1 RNA) and the lower eukarya *Giardia lamblia* were recently found to have residual catalytic activity. Nevertheless, the highest activities measured for these eukaryotic P RNAs are more than five orders of magnitude lower than those obtained with bacterial P RNAs. To investigate the structure and function of H1 RNA, we analyzed if the RNA-lone activity of H1 RNA could be improved by approaches that have proven successful in the activation of *M. thermoautotrophicus* archaeal RNase P RNA. A few H1 RNA variants, HE chimeras and H1 RNA-substrate conjugates were constructed and analyzed. H1 RNA 5, only containing mutations P4/J4/19, is the sole variant with locally confined mutations that showed increased activity. The mutations P4/J4/19 were introduced to restore a bacterial-like P4 known to be a crucial for catalytic activity. The additionally introduced back-to-bacteria mutations P5/P15 further improved catalytic activity slightly, possibly by rigidifying the core structure and/or improving substrate binding. Furthermore, the S-domain of *E. coli* is unable to productively cooperate with the H1 RNA C-domain, as the chimeric P RNA HE was found to be inactive. Tethering the substrate to H1 RNA,

designed to mitigate weak substrate affinity, even reduced H1 RNA activity to non-detectable levels. The kinetic data together with our structural probing and UV melting (not shown) data suggest that H1 RNA has an extremely degenerated, globally unstable structure that is strictly dependent on its natural protein cofactors.

6 Appendix

6.1 Chemicals

Acrylamide M-Bis (50 % stock solution 24:1)	Gerbu
Agar	Serva
Agarose	Roth
Ampicillin	Gerbu
Ammonium acetate	Fluka
Boric acid	Roth
Bovine serum albumin (BSA)	Sigma
Bromophenol blue (BPB)	Merck
Chloramphenicol	Sigma
Chloroform	Merck
Crystal violet	Fluka
Deoxynucleosidtriphosphates (dNTPs)	Boehringer
Disodiumhydrogenphosphate	Merck
Dithiothreitol (DTT)	Gerbu
Ethanol p.a. 99.8 %	Roth
Ethidiumbromide	Roth
Glycerol	Gerbu
Glycogen	Roche
Iodine (I_2)	Merc
Isopropanol	Roth
Lead acetate	Roth
β-Mercaptoethanol	Serva
Nucleosidtriphosphates (NTPs)	Roche
Nucleosidtriphosphates phosphorothioates (ITPαS)	Boehringer
Peptone	Roth
Phenol	Roth
Potassiumdihydrogenphosphate	Fluka
Sodiumacetate	Merck
Sodiumcitrate	Roth
N,N,N‘,N‘-Tetraethylmethylenediamin (TEMED)	Serva
Tris-(hydroxymethyl)aminomethane	Gerbu
Urea	Gerbu
Xylenecyanol blue (XCB)	Serva
Yeast extract	Gerbu

All other chemicals (not listed above) were purchased from Sigma, Gerbu or Life Technologies and had a purity grade “pro analysis”.

6.2 Radioisotopes

[γ-^{32}P] ATP	Hartmann Analytic and PerkinElmer
[5’-^{32}P] pCp	Hartmann Analytic and PerkinElmer

6.3 Size markers

1 kb DNA ladder	New England Biolabs
2 Log DNA ladder	New England Biolabs
Broad range prestained Protein Ladder (6-175 kDa)	New England Biolabs

6.4 Enzymes

Calf Intestinal Alkaline Phosphatase (CIAP)	MBI Fermentas
DNase I	Promega, Ambion
Pfu polymerase	Promega, MBI Fermentas and our lab
Pyrophosphatase	Roche
Restriction endonucleases	MBI Fermentas and New England Biolabs
Taq polymerase	MBI Fermentas and our lab
Thermoscript	Invitrogen, Promega
T1 nuclease	Gibco BRL
T4 DNA ligase	Gibco BRL, Invitrogen and MBI Fermentas
T4 Polynucleotide kinase	MBI Fermentas
T4 RNA ligase	MBI Fermentas
T7 RNA polymerase (Y639F)	our lab
Turbo DNase	Ambion
VentR® (exo-) DNA polymerase	New England Biolabs

6.5 Equipment

Agarose gel chamber	Biorad, Mini Sub Cell
Autoclave	Systec V95
Electroporator	Biorad, Gene Pulser Xcell, PC- and CE-module
Gel documentation system	Cybertech, CS1 with Mitsubishi Video Copy Processor; Biostep, GelSystem MINI
Hand-monitor	Berthold, LB 1210 B
Heating blocks	Techne, Dri-Block DB-3D; Biometra, TB1
Incubator	Memmert BE400
Imager cassettes	Fuji Film, Bas cassette 4043, Rego, 35,6x43,2cm
Magnetic stirrers	Heidolph, MR 2002
Power supply	Pharmacia, EPS 3500; Bio Rad, Power Supply160/1.6 (Power Pac 3000); Apelex, PS 9009T
PAA-gel chamber	Custom-made, University of Lübeck
PCR cycler	Biometra, TGradient Thermocycler
pH-Meter	WTW, pH Level 1
Phosphoimager	Raytest, Bio-Imaging Analyser BAS 1000 (Fujifilm); FLA 3000, (Fujifilm)

Pipettes	Gilson-Pipetman, P20, P200, P1000 Abimed, P2
Protein Gel chamber	Mini Protean 3 cell, Biorad
Quartz cuvette	Hellma 104-QS, 105.202, 115B-QS, 105
Mixer	IKA, Vibrax-VXR; Eppendorf,
Thermomixer	5436, Thermomixer comfort
Shaking incubator	GFL 3033
Spectrophotometer	Hewlett Packard, Photometer 8453; Varian, Cary 50 Conc; Thermo Spectronic, Biomate 3
Software	PCBas/Aida Image Analyser v.3.45, Corel Graphics Suite; GraFit 3.0; Microsoft Office; Pymol, Delano, W.L. 2002 Vector NTI®, Invitrogen
Speedvac	Heto vacuum centrifuge
Scintillation counters	Perkin Elmer, Wallac WINSPECTRAL a/b 1414 Liquid Scintillation Counter; Packard, Tricarb 2000CA
Centrifuges	Heraeus, Biofuge pico, biofuge fresco; Sigma, Typ 112; Eppendorf, centrifuge 5810R, minispin plus Stratagene, PicoFuge

6.6 Abbreviations and Units

A_{260}	absorption at 260 nm
A	Adenosine
Amp	Ampicillin
APS	Ammonium peroxodisulfat
Bp	base pair(s)
BPB	Bromophenol blue
BSA	Bovine serum albumine
C	cytosine
C5	protein subunit of *E. coli* RNase P
cam	Chloramphenicol
C_{end}	end concentration
cpm	counts per minute
Da	dalton
DNA	deoxyribonucleic acid
DNase	deoxyribonuclease
dNTP	deoxynucleoside triphosphates
DTT	dithiothreitol
E	extinction
ε	molar extinction coefficient
EDTA	Ethylenediamine tetraacedic acid

EGTA	Ethylene glycol tetraacetic acid
EP	native *E. coli rnpB* promoter
Fig.	Figure
g	gram
G	guanosine
h	hour(s)
HEPES	N-2-Hydroxyethylpiperazin-N'-2-ethane sulfonic acid
IPTG	Isopropyl-β-D-thiogalactopyranosid
kbp	kilo base pairs
l	liter
LB	Luria-Bertani
M	molar [mol/l]
mA	milliampere
MBq	Megabecquerel
min	Minute
MOPS	3-Morpholinopropanesulfonic acid
MW	Molecular weight
nt(s)	Nucleotide(s)
NTP	Ribonucleosidtriphosphate
p.a.	pro analysis
PAA	Polyacrylamide
PAGE	Polyacrylamid gel elektrophoresis
PCR	Polymerase chain reaction
pmol	Picomol
P Protein	Protein subunit of RNase P
P RNA	RNA subunit of RNase P
RNA	ribonucleic acid
RNase	ribonuclease
rpm	rounds per minute
SDS	natriumdodecylsulfat
s	second
T	thymine
TBE	Tris-Borat-EDTA Buffer
TEMED	N,N,N,N,-Tetramethylethylendiamin
T_m	melting temperature
Tris	Tris-hydroxymethylaminomethan
(p)tRNA	(precursor) transfer RNA
U	Unit(s) (unit for enzyme activity)
U	Uridine
wt	wild-type
XCB	Xylene cyanol blue

7 Acknowledgements

I would like to express my sincere gratitude to all those who give me the possibility to complete this thesis.

Especially, I would like to thank…

… Prof. Dr. Roland K. Hartmann for giving me the opportunity to work in his research group and excellent scientific supervision of my work, and for his continuous encouragement and support. He introduced me into the wonders and frustrations of scientific research.

… Dr. Dagmar K. Willkomm for much knowledge and valuable advice about the project, biochemical experiments, and all computer aspects. Her inspiring suggestions helped me keep going with my work.

… Dr. Barbara Wegscheid, Dr. Michal Marszalkowski, and Dominik Helmecke for guiding me in a few useful RNA experiments.

… Dr. Simona Cuzic-Feltens, Dr. Heike Wünnenberg, Dr. Markus Gößringer, Dr. Arnold Grünweller, Dr. Michael Weber, and Andreas Ratje for their kind help and good suggestions during my study.

… Katja Hütte for her generous and efficient help in official matters.

… my dear colleagues of Hartmann group who create such a friendly work environment.

… all members of Kirsebom group, especially Prof. Dr. Leif A. Kirsebom and Shiying Wu, for their nice discussion and assistance during my short visit.

… all members of IRTG graduate school for the pleasant time we shared.

… all my friends for their precious friendship which kept me moving forward.

Last but not least

… my family for their love and encouragement.

… my husband Zhiguo for his everlasting support and understanding.

8 Publications arising from this work

Articles

Dan Li, Dagmar K. Willkomm, Leif A. Kirsebom, Roland K. Hartmann (in preparation) Improvements of human RNase P RNA (H1 RNA) activity are limited by the RNA's global instability

Dan Li, Dagmar K. Willkomm, Roland K. Hartmann (2009) Minor changes largely restore catalytic activity of archaeal RNase P RNA from *Methanothermobacter thermoautotrophicus*. Nucleic Acids Research, **37** (1), 231-242.

Dan Li, Dagmar K. Willkomm, Astrid Schön, Roland K. Hartmann (2007) RNase P of *Cyanophora paradoxa cyanelle*: A plastid ribozyme. Biochimie, **89**, 1528-1538.

Oral presentations

Dan Li, Dagmar K. Willkomm, Roland K. Hartmann (2009) Insights into archaeal & eukaryal RNase P RNA structure and function by a retro-evolution approach. RNA club, Frankfurt, Germany, February 18.

Dan Li, Dagmar K. Willkomm, Roland K. Hartmann (2008) Retro-evolution of Ribonuclease P RNA. Spring-Meeting and Workshop "Protein-nucleic acid interactions" of the International Research Training Group Gießen/Marburg-Moscow (DFG/RFBR-found), Schloß Rauischholzhausen, Germany, March 9-12 .

Dan Li, Dagmar K. Willkomm, Roland K. Hartmann (2007) Retro-evolution of RNase P RNA. Workshop "Protein-nucleic acid interactions" of the International Research Training Group Gießen/Marburg-Moscow (DFG/RFBR-found), Suzdal, Russia, June 20-24 .

Posters

Dan Li, Dagmar K. Willkomm, Roland K. Hartmann (2008) Minor changes largely restore catalytic activity of archaeal RNase P RNA from *Methanothermobacter thermoautotrophicus*. RNA Society Meeting 2008, Berlin, Germany, July 28 - Aug 03.

Dan Li, Dagmar K. Willkomm, Roland K. Hartmann (2007) Retro-evolution of Ribonuclease P RNA. The 22nd tRNA workshop, Uppsala, Sweden, November 1-6.

Dan Li, Dagmar K. Willkomm, Roland K. Hartmann (2006) "Retro-evolution" of RNase P. The 4th meeting of GBM study section 'RNA Biochemistry', Kassel, Germany, October 12-15.

9 Curriculum vitae

Li, Dan

Date of birth	09.11.1978
Place of birth	Guizhou, P. R. China
Nationality	Chinese
2007	Short visit in group of Prof. Dr. Leif A. Kirsebom, Department of Cell & Molecular Biology, Biomedical Center, Uppsala University, Sweden, found by NordForsk
2006-2009	Member of International Research Training Group "Enzymes and Multienzyme Complexes acting on Nucleic Acids" (GRK 1384), found by DFG
2005-2009	PhD work Institute of Pharmaceutical Chemistry, Philipps-University Marburg Adviser: Prof. Dr. Roland K. Hartmann
2004	Master degree of Medicinal Chemistry Thesis: Synthesis of 23-Hydroxybetulinic Acid Derivatives and Studies on Their Anti-tumor Activities Adviser: Prof. Dr. Xiaoming Wu
2000	Bachelor degree
1996-2004	China Pharmaceutical University, Nanjing
1993-1996	Senior High School, Duyun
1990-1993	Junior High School, Changshun
1985-1990	Primary School, Changshun

10 Selbstständigkeitserklärung

Ich versichere, dass ich meine Dissertation

Insights into RNase P RNA structure and function by a retro-evolution approach

selbstständig, ohne unerlaubte Hilfe angefertigt und mich dabei keiner anderen als der von mir ausdrücklich bezeichneten Quellen und Hilfen bedient habe.

Die Dissertation wurde in der jetzigen oder einer ähnlichen Form noch an keiner anderen Hochschule eingereicht und hat noch keinen sonstigen Prüfungszwecken gedient.

(Ort/Datum) (Unterschrift mit Vor- und Zuname)